

RADIATION DAMAGE IN ROCK-FORMING MINERALS

by

ROBERT EARL SCOTT

B.S., Massachusetts Institute of Technology
(1976)

SUBMITTED IN PARTIAL FULFILLMENT
OF THE REQUIREMENTS FOR THE
DEGREE OF

MASTER OF SCIENCE

at the

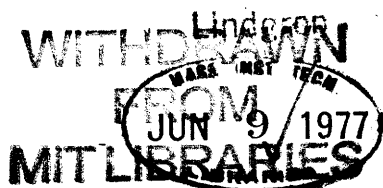
MASSACHUSETTS INSTITUTE OF TECHNOLOGY

May, 1977

Signature of Author.....
Department of Earth and Planetary Sciences, May 12, 1977

Certified by.....
Thesis Supervisor

Accepted by.....
Chairperson, Departmental Committee on Theses



ACKNOWLEDGEMENTS

My utmost thanks to Dr. Robert L. Huguenin for his suggestion of the topic, invaluable advice, great willingness, continued encouragement and considerable time he gave me.

My gratitude to Professor Roger G. Burns for taking me on as one of his advisees during the absence of Professor Thomas B. McCord.

Thanks are also due to Professor Robert L. Coble for his comments, suggestions, advice and efforts in providing me with invaluable information.

I am very grateful to the Remote Sensing Laboratory for providing me with financial support in the form of research assistantship.

My thanks are extended to Ms. Kristine L. Andersen for her advice, enthusiasm and encouragement throughout my studies.

Finally, my utmost praise to my dear friends: Gary S. Isaacs, Jean Harrison, Colin Gardinier and Adrian Middleton whose patience, continuous encouragement and great understanding were immeasurable.

But my warmest and greatest thanks goes to my father, mother, brother, sisters, my niece Sharon and God, without whom life would have no meaning.

To all of the above individuals and to all whom I might have omitted; I offer my sincere thanks.

To
my
cousin,
the late Leonard Charles Mosley

RADIATION DAMAGE IN ROCK-FORMING MINERALS

by

ROBERT EARL SCOTT

Submitted to the Department of Earth and Planetary Sciences
on May 12, 1977, in partial fulfillment of the requirements
for the Degree of Master of Science

ABSTRACT

The apparent absence of metal coatings, produced by solar-wind sputtering, on lunar samples indicates that the solar wind does not modify the soils to the extent predicted by laboratory studies. This suggests that the sputtering efficiency of the solar wind is somehow decreased in the lunar environment.

The model for backward sputtering of metals and oxides has been reviewed. The predicted sputtering yields of metals and oxides in comparison with the experimental yield values turns out to differ by at least a factor of 3 or better. For example, the predicted yield for Cu and Fe at 1.85keV are 0.014 and 0.035, respectively, and the experimental values are 0.03 and 0.009, respectively.

The sputtering yields of metals and oxides, obtained from modified theories of sputtering by Sigmund and Kelly, are used in conjunction with the solar wind plasma-lunar surface magnetic field interaction model to estimate the sputtering rates. The predicted order of enrichment of metals in lunar soils is in very good agreement with the order of enrichment determined from ESCA studies of lunar samples.

The interaction of the lunar surface magnetic fields with the solar-wind protons has been reviewed. The solar-wind protons are predicted to be completely stopped off at the Apollo 16 landing site, and their mean kinetic energies are reduced at other sites. At the Apollo 12 landing site, for example, the protons lose about 30-80% of their nominal (1keV) incident kinetic energy. The loss in proton energy by interaction with compressed magnetic fields reduces substantially the sputtering efficiency of the solar wind. The unexpected low abundances of metal surface coatings can now possibly be explained.

THESIS SUPERVISOR: Roger G. Burns
TITLE: Professor of Geochemistry

TABLE OF CONTENTS

TITLE PAGE.....	1
ACKNOWLEDGEMENTS.....	2
ABSTRACT.....	4
TABLE OF CONTENTS.....	5
LIST OF FIGURES AND TABLES.....	7
INTRODUCTION.....	15
I. BACKWARD SPUTTERING OF METALS AND OXIDES BY HYDROGEN IONS.....	16
A. Theory of Sputtering.....	16
B. Sputtering Yields of Metals for Protons at Normal Incidence.....	26
C. Variation of Sputtering Yield with Angle of Incidence for Metals.....	30
D. Velocity Distribution of Sputtered Atoms.....	33
E. Sputtering Yields of Oxides for Protons at Normal Incidence.....	36
F. Variation of Sputtering Yield with Angle of Incidence for Metal Oxides.....	38
G. Velocity Distribution of Sputtered Molecules.....	39
II. SPUTTERING EFFECTS ON THE LUNAR SURFACE.....	41
A. Lunar Magnetic Field.....	41
B. Reduction of the Mean Kinetic Energy of Solar-Wind Protons at the Lunar Surface by Magnetic Field Interaction.....	42
C. Fraction of Sputtered Atoms that Escape from the Moon.....	43
D. Fraction of Sputtered Molecules that Escape from the Moon.....	45
III. PREFERENTIAL SPUTTERING: METHOD FOR PREDICTING THE ORDER OF ENRICHMENT OF METALS.....	46
IV. SUMMARY.....	48
APPENDIX I.....	51
APPENDIX II.....	68
REFERENCES.....	72
TABLES.....	74

FIGURES.....110

LIST OF FIGURES AND TABLES

I. FIGURES

1.	Geometry of Sputtering Calculation.....	18
2.	Factor α in Eq.(25) for protons and deuterons incident on a heavy target.....	27
2a.	Variation of the sputtering yield with angle of incidence for Ar^+ ions incident on poly- crystalline copper.....	34
3.	Sputtering yields for H^+ ions incident on aluminum.....	111
4.	Sputtering yields for H^+ ions incident on aluminum.....	112
5.	Sputtering yields for H^+ ions incident on calcium.....	113
6.	Sputtering yields for H^+ ions incident on calcium.....	114
7.	Sputtering yields for H^+ ions incident on chromium.....	115
8.	Sputtering yields for H^+ ions incident on chromium.....	116
9.	Sputtering yields for H^+ ions incident on copper.....	117
10.	Sputtering yields for H^+ ions incident on copper.....	118
11.	Sputtering yields for H^+ ions incident on gold.....	119
12.	Sputtering yields for H^+ ions incident on gold.....	120
13.	Sputtering yields for H^+ ions incident on iron.....	121
14.	Sputtering yields for H^+ ions incident on iron.....	122
15.	Sputtering yields for H^+ ions incident on magnesium.....	123
16.	Sputtering yields for H^+ ions incident on magnesium.....	124
17.	Sputtering yields for H^+ ions incident on manganese.....	125
18.	Sputtering yields for H^+ ions incident on manganese.....	126
19.	Sputtering yields for H^+ ions incident on nickel.....	127
20.	Sputtering yields for H^+ ions incident on nickel.....	128
21.	Sputtering yields for H^+ ions incident on oxygen.....	129
22.	Sputtering yields for H^+ ions incident on oxygen.....	130

23.	Sputtering yields for H ⁺ ions incident on potassium.....	131
24.	Sputtering yields for H ⁺ ions incident on potassium.....	132
25.	Sputtering yields for H ⁺ ions incident on silver.....	133
26.	Sputtering yields for H ⁺ ions incident on silver.....	134
27.	Sputtering yields for H ⁺ ions incident on silicon.....	135
28.	Sputtering yields for H ⁺ ions incident on silicon.....	136
29.	Sputtering yields for H ⁺ ions incident on sodium.....	137
30.	Sputtering yields for H ⁺ ions incident on sodium.....	138
31.	Sputtering yields for H ⁺ ions incident on titanium.....	139
32.	Sputtering yields for H ⁺ ions incident on titanium.....	140
33.	Sputtering yields for H ⁺ ions incident on zinc.....	141
34.	Sputtering yields for H ⁺ ions incident on zinc.....	142
35.	Variation of the sputtering yield with angle of incidence for H ⁺ ions on aluminum.....	143
36.	Variation of the sputtering yield with angle of incidence for H ⁺ ions on calcium.....	144
37.	Variation of the sputtering yield with angle of incidence for H ⁺ ions on chromium.....	145
38.	Variation of the sputtering yield with angle of incidence for H ⁺ ions on copper.....	146
39.	Variation of the sputtering yield with angle of incidence for H ⁺ ions on gold.....	147
40.	Variation of the sputtering yield with angle of incidence for H ⁺ ions on iron.....	148
41.	Variation of the sputtering yield with angle of incidence for H ⁺ ions on magnesium.....	149
42.	Variation of the sputtering yield with angle of incidence for H ⁺ ions on manganese.....	150
43.	Variation of the sputtering yield with angle of incidence for H ⁺ ions on nickel.....	151
44.	Variation of the sputtering yield with angle of incidence for H ⁺ ions on potassium.....	152
45.	Variation of the sputtering yield with angle of incidence for H ⁺ ions on silver.....	153
45a.	Variation of the sputtering yield with angle of incidence for H ⁺ ions on sodium.....	154

46.	Variation of the sputtering yield with angle of incidence for H ⁺ ions on titanium.....	155
47.	Variation of the sputtering yield with angle of incidence for H ⁺ ions on zinc.....	156
48.	Velocity distribution of ejected atoms for H ⁺ ions incident on aluminum.....	157
49.	Velocity distribution of ejected atoms for H ⁺ ions incident on calcium.....	158
50.	Velocity distribution of ejected atoms for H ⁺ ions incident on chromium.....	159
51.	Velocity distribution of ejected atoms for H ⁺ ions incident on copper.....	160
52.	Velocity distribution of ejected atoms for H ⁺ ions incident on gold.....	161
53.	Velocity distribution of ejected atoms for H ⁺ ions incident on iron.....	162
54.	Velocity distribution of ejected atoms for H ⁺ ions incident on magnesium.....	163
55.	Velocity distribution of ejected atoms for H ⁺ ions incident on manganese.....	164
56.	Velocity distribution of ejected atoms for H ⁺ ions incident on nickel.....	165
57.	Velocity distribution of ejected atoms for H ⁺ ions incident on potassium.....	166
58.	Velocity distribution of ejected atoms for H ⁺ ions incident on silicon.....	167
59.	Velocity distribution of ejected atoms for H ⁺ ions incident on silver.....	168
60.	Velocity distribution of ejected atoms for H ⁺ ions incident on sodium.....	169
61.	Velocity distribution of ejected atoms for H ⁺ ions incident on titanium.....	170
62.	Velocity distribution of ejected atoms for H ⁺ ions incident on zinc.....	171
63.	Sputtering yields for H ⁺ ions incident on Al ₂ O ₃	172
64.	Sputtering yields for H ⁺ ions incident on CaO.....	173
65.	Sputtering yields for H ⁺ ions incident on FeO.....	174
66.	Sputtering yields for H ⁺ ions incident on Fe ₂ O ₃	175
67.	Sputtering yields for H ⁺ ions incident on Fe ₃ O ₄	176
68.	Sputtering yields for H ⁺ ions incident on MgO.....	177
69.	Sputtering yields for H ⁺ ions incident on MnO.....	178

70.	Sputtering yields for H ⁺ ions incident on TiO ₂	179
71.	Variation of the sputtering yield with angle of incidence for H ⁺ ions on Al ₂ O ₃	180
72.	Variation of the sputtering yield with angle of incidence for H ⁺ ions on CaO.....	181
73.	Variation of the sputtering yield with angle of incidence for H ⁺ ions on FeO.....	182
74.	Variation of the sputtering yield with angle of incidence for H ⁺ ions on Fe ₂ O ₃	183
75.	Variation of the sputtering yield with angle of incidence for H ⁺ ions on Fe ₂ O ₃	184
76.	Variation of the sputtering yield with angle of incidence for H ⁺ ions on MgO.....	185
77.	Variation of the sputtering yield with angle of incidence for H ⁺ ions on MnO.....	186
78.	Variation of the sputtering yield with angle of incidence for H ⁺ ions on TiO ₂	187
79.	Velocity distribution of ejected molecules for H ⁺ ions incident on Al ₂ O ₃ ,.....	188
80.	Velocity distribution of ejected molecules for H ⁺ ions incident on CaO.....	189
81.	Velocity distribution of ejected molecules for H ⁺ ions incident on FeO.....	190
82.	Velocity distribution of ejected molecules for H ⁺ ions incident on Fe ₂ O ₃ ,.....	191
83.	Velocity distribution of ejected molecules for H ⁺ ions incident on Fe ₃ O ₄	192
84.	Velocity distribution of ejected molecules for H ⁺ ions incident on MgO.....	193
85.	Velocity distribution of ejected molecules for H ⁺ ions incident on MnO.....	194
86.	Velocity distribution of ejected molecules for H ⁺ ions incident on TiO ₂ ,.....	195

II. TABLES

1.	Effective depth of origin of sputtered atoms.....	24
2.	Reduced nuclear stopping cross section s _n (ε) for Thomas-Fermi interaction.....	25
3.	Calculated a ₁₂ , E* and U ₀ for various targets.....	28
4.	Averages over the range distribution.....	31
5.	Calculated <ΔX ² >/<X> ² and <Y ² >/<X> ² for various targets.....	32
6.	Calculated E _T , V _p , and E _p for aluminum bombarded by H ⁺ ions.....	75

7. Calculated \bar{E}_T , V_p , and E_p for calcium bombarded by H^+ ions.....	75
8. Calculated \bar{E}_T , V_p , and E_p for chromium bombarded by H^+ ions.....	76
9. Calculated \bar{E}_T , V_p , and E_p for copper bombarded by H^+ ions.....	76
10. Calculated \bar{E}_T , V_p , and E_p for gold bombarded by H^+ ions.....	77
11. Calculated \bar{E}_T , V_p , and E_p for iron bombarded by H^+ ions.....	77
12. Calculated \bar{E}_T , V_p , and E_p for manganese bombarded by H^+ ions.....	78
13. Calculated \bar{E}_T , V_p , and E_p for magnesium bombarded by H^+ ions.....	78
14. Calculated \bar{E}_T , V_p , and E_p for nickel bombarded by H^+ ions.....	79
15. Calculated \bar{E}_T , V_p , and E_p for potassium bombarded by H^+ ions.....	79
16. Calculated \bar{E}_T , V_p , and E_p for silicon bombarded by H^+ ions.....	80
17. Calculated \bar{E}_T , V_p , and E_p for silver bombarded by H^+ ions.....	80
18. Calculated \bar{E}_T , V_p , and E_p for sodium bombarded by H^+ ions.....	81
19. Calculated \bar{E}_T , V_p , and E_p for titanium bombarded by H^+ ions.....	81
20. Calculated \bar{E}_T , V_p , and E_p for zinc bombarded by H^+ ions.....	82
20a. Calculated \bar{E}_T , V_p , and E_p for oxygen bombarded by H^+ ions.....	82
21. Sputtering yield of oxides for H_2^+ and H_3^+ ions at normal incidence.....	83
22. Sputtering yield of oxides for H^+ ions at normal incidence.....	83

23.	Tabulation of the moments $\langle \Delta X^2 \rangle / \langle X \rangle^2$ and $\langle Y^2 \rangle / \langle X \rangle^2$ for oxides.....	84
24.	Molecular weight and binding energy of metal oxides.....	85
25.	Calculated E_T , V_p , and E_p for Al_2O_3 , bombarded by H^+ ions.....	86
26.	Calculated E_T , V_p , and E_p for CaO , bombarded by H^+ ions.....	86
27.	Calculated E_T , V_p , and E_p for FeO , bombarded by H^+ ions.....	87
28.	Calculated E_T , V_p , and E_p for Fe_2O_3 , bombarded by H^+ ions.....	87
29.	Calculated E_T , V_p , and E_p for Fe_3O_4 , bombarded by H^+ ions.....	88
30.	Calculated E_T , V_p , and E_p for MgO , bombarded by H^+ ions.....	88
31.	Calculated E_T , V_p , and E_p for MnO , bombarded by H^+ ions.....	89
32.	Calculated E_T , V_p , and E_p for TiO_2 , bombarded by H^+ ions.....	89
33.	Average chemical composition of lunar surface regolith.....	90
34.	Summary of lunar remanent magnetic field.....	91
35.	The ratio of the solar-wind plasma pressure to total magnetic field pressure.....	92
36.	Estimate of the sputtering rates at the lunar surface.....	93
37.	Calculated F_T and F_p for aluminum, bombarded by H^+ ions.....	95
38.	Calculated F_T and F_p for calcium, bombarded by H^+ ions.....	95
39.	Calculated F_T and F_p for chromium, bombarded by H^+ ions.....	95
40.	Calculated F_T and F_p for copper, bombarded by H^+ ions.....	96
	bombarded by H^+ ions.....	96

41. Calculated F_T and F_p for gold bombarded by H^+ ions.....	97
42. Calculated F_T and F_p for iron bombarded by H^+ ions.....	97
43. Calculated F_T and F_p for magnesium bombarded by H^+ ions.....	98
44. Calculated F_T and F_p for manganese bombarded by H^+ ions.....	98
45. Calculated F_T and F_p for nickel bombarded by H^+ ions.....	99
46. Calculated F_T and F_p for potassium bombarded by H^+ ions.....	99
47. Calculated F_T and F_p for silicon bombarded by H^+ ions.....	100
48. Calculated F_T and F_p for silver bombarded by H^+ ions.....	100
49. Calculated F_T and F_p for sodium bombarded by H^+ ions.....	101
50. Calculated F_T and F_p for titanium bombarded by H^+ ions.....	101
51. Calculated F_T and F_p for zinc bombarded by H^+ ions.....	102
52. Calculated F_T and F_p for oxygen bombarded by H^+ ions.....	102
53. Calculated F_T and F_p for Al_2O_3 bombarded by H^+ ions.....	103
54. Calculated F_T and F_p for CaO bombarded by H^+ ions.....	103
55. Calculated F_T and F_p for FeO bombarded by H^+ ions.....	104
56. Calculated F_T and F_p for Fe_2O_3 bombarded by H^+ ions.....	104

57.	Calculated F_T and F_p for Fe_3O_4	
	bombarded by H^+ ions.....	105
58.	Calculated F_T and F_p for MgO	
	bombarded by H^+ ions.....	105
59.	Calculated F_T and F_p for MnO	
	bombarded by H^+ ions.....	106
60.	Calculated F_T and F_p for TiO_2	
	bombarded by H^+ ions.....	106
61.	Sputtering rates at Moon under solar-wind bombardment.....	107
62.	Comparison of $\Delta H_s(M)$ and $\Delta H_D(O)$ for some ele- ments occurring in lunar soils.....	109

INTRODUCTION

For many years the apparent absence of metal coatings, produced by solar-wind sputtering, on the lunar surface has been the subject of controversy. According to Hapke et al. [1975], the lunar fines are enriched in metallic Fe relative to the lunar crystalline rocks. The rocks typically have on the order of 0.1% Fe, while the fines contain about 0.5% Fe, much of which is in the superparamagnetic size range ($<100\text{\AA}$). Surfaces of many of the grains in the fines are coated with an amorphous layer about 0.1 μm thick and are enriched in Fe. However, there is some conflicting evidence concerning the Fe. Both the fraction of grains containing Fe and the degree of Fe enrichment are correlated with the albedo. The fines are deficient in oxygen relative to the crystalline rocks, although the extent to which this is due to the excess Fe or due to a separate phenomenon is not clear. This suggests that the sputtering efficiency of the solar-wind protons is somehow decreased in the lunar environment.

In this thesis, sputtering yields of metal/oxide targets by hydrogen ions are computed from modified theories of sputtering by Sigmund [1969] and Kelly [1973], respectively. The interaction of solar-wind plasma with localized surface magnetic fields and their effect on the sputtering efficiency of solar-wind protons near the lunar surface is discussed. The effects of sputtering on the composition of lunar surface materials are discussed, and the order of enrichment of metals in lunar surface materials is considered.

I. BACKWARD SPUTTERING OF METALS AND OXIDES BY HYDROGEN IONS

In the energy range 1eV to 2keV, very little experimental data on the sputtering yield, $S(\text{atoms/ion})$, of metals and oxides by hydrogen ions is available. Grølund and Moore [1960] used electromagnetically analyzed ionic beams from a radiofrequency source to study the sputtering yield for hydrogen ions normally incident on Ag atoms at energies from 2 to 12keV. KenKnight and Wehner [1964] obtained sputtering yield data for hydrogen molecular ions normally incident on Be, Al, Ti, V, Fe, Co, Ni, Cu, Zr, Mo, Pd, Ag, Ta, W, Re, Ir, Pt, and Au at 7keV by drilling holes in thin target foils with magnetically separated hydrogen beams (H_2^+ and H_3^+). Wehner et al. [1964a] obtained yield data for metals (Cu, Fe) at 1.85keV and Oxides (Al_2O_3 , $\text{TiO}_{1.86}$, $\text{FeO}_{1.5}$, Fe_2O_3 , SiO_2) at $\sim 7.0\text{keV}$ with the mass separation method. The results for protons can be inferred from the data provided by KenKnight and Wehner [1964] and Wehner et al. [1964a] since the hydrogen atoms sputter independently.

It will be the object of the following section to review a theoretical model for sputtering developed by Sigmund [1969]. We will show that although the theory applies only to ions with masses much greater than that of hydrogen, an approximation can be made that will alleviate this matter.

A. Theory of Sputtering

According to Sigmund [1969], the sputtering of a metal target by energetic ions or recoil atoms is assumed to result from cas-

cades of atomic collisions. The sputtering is calculated under the assumption of random slowing down in an infinite medium. An intergrodifferential equation for the yield is developed from the general Boltzmann transport equation given by Eq.(1)

$$-\frac{1}{v} \frac{\partial}{\partial t} G(x, \vec{v}_0, \vec{v}, t) - \eta \frac{\partial}{\partial x} G(x, \vec{v}_0, \vec{v}, t) = N \int d\sigma [G(x, \vec{v}_0, \vec{v}, t) - G(x, \vec{v}_0, \vec{v}', t) - G(x, \vec{v}_0, \vec{v}'', t)] \quad (1)$$

where $v = |\vec{v}|$ \equiv magnitude of arbitrary velocity vector of an atom in a plane $x=0$ at a time $t=0$,
 N \equiv density of target atoms
 $d\sigma$ \equiv differential cross section [= $d\sigma(\vec{v}, \vec{v}', \vec{v}'')$
 $= k(\vec{v}, \vec{v}', \vec{v}'') d^3 v' d^3 v''$],
 $G(x, \vec{v}_0, \vec{v}, t) d^3 v_0 dx$ \equiv average number of atoms moving at time t in layer (x, dx) with velocity ($v_0, d^3 v_0$),
 v_0 \equiv velocity of atoms in a plane at time t ,
 v' \equiv velocity of scattered particle,
 v'' \equiv velocity of recoiling atom,
 η \equiv v_x/v .

The sputtering yield for backward sputtering of a metal target with a plane surface at $x=0$ (see fig.1) is then

$$S = \int d^3 v_0 |v_{0x}| \int_0^\infty dt G(0, \vec{v}_0, \vec{v}, t) \quad (2)$$

where the integration over $d^3 v_0$ extends over all \vec{v}_0 with negative x components large enough to overcome surface binding forces.

Multiplying Eq.(1) by dt and integrating over the interval $(0, \infty)$ we have

$$-\frac{1}{v} \delta(x) \delta(\vec{v} - \vec{v}_0) - \eta \frac{\partial}{\partial x} F(x, \vec{v}_0, v) = N \int d\sigma [F(x, \vec{v}_0, \vec{v}) - F(x, \vec{v}_0, \vec{v}') - F(x, \vec{v}_0, \vec{v}'')] \quad (3)$$

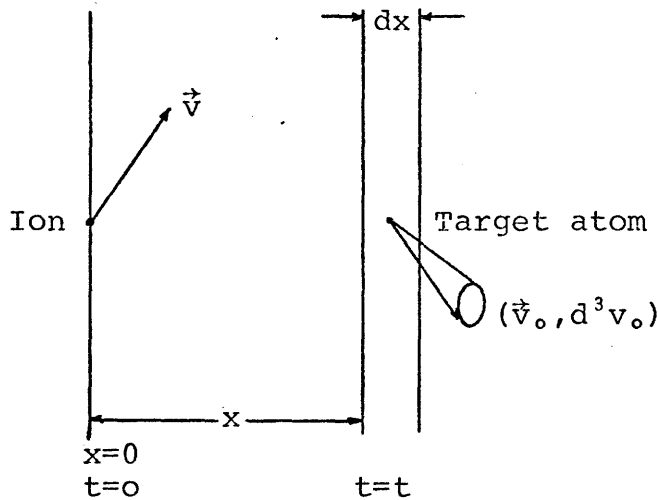


Fig. 1. Geometry of Sputtering calculation. [From Sigmund, 1969].

$$\text{where } F(x, \vec{v}_0, \vec{v}) = \int_0^\infty G(x, \vec{v}_0, v) dt$$

$F(x, \vec{v}_0, \vec{v}) | v_{ox} | d^3 v_0 \equiv$ total number of atoms that penetrate the plane x with a velocity $(\vec{v}_0, d^3 v_0)$ during the development of the collision cascade

$$G(x, \vec{v}_0, \vec{v}, t=0) = \delta(x) \delta(\vec{v} - \vec{v}_0) \equiv \text{one starting particle}$$

and $G(x, \vec{v}_0, \vec{v}, \infty) = 0$ since all starting particles have slowed down below any finite velocity v_0 .

If we consider only backward sputtering and introduce the function

$$H(x, \vec{v}) = \int d^3 v_0 | v_{ox} | F(x, \vec{v}_0, \vec{v})$$

with

$$\eta_0 = v_{ox}/v \leq 0$$

$$E_0 = M_2 v_0^2/2 \geq U(\eta_0)$$

M_2 mass of the metal target atom

where $U(\eta_0)$ is the surface binding energy that, in general, depends on the direction of ejection, characterized by the direction cosine η_0 , Eq. (3) takes the following form

$$\delta(x) \int \frac{|v_0 x|}{v} \delta(\vec{v} - \vec{v}_0) d^3 v_0 - \eta \frac{\partial}{\partial x} H(x, \vec{v}) = N \int d\sigma [H(x, \vec{v}) - H(x, \vec{v}') - H(x, \vec{v}'')] \quad (4)$$

Introducing the function

$$\Theta(\xi) = \begin{cases} 1 & \text{for } \xi > 0 \\ 0 & \text{for } \xi < 0 \end{cases}$$

and satisfying the condition $E_0 = M_2 v_0^2 / 2 \geq U(\eta_0)$ and $\eta_0 = v_0 x / v_0 \leq 0$, Eq. (4) can be rewritten as

$$-\delta(x) \eta \Theta(-\eta) \Theta(E - U(\eta)) - \eta \frac{\partial}{\partial x} H(x, \vec{v}) = N \int d\sigma [H(x, \vec{v}) - H(x, \vec{v}') - H(x, \vec{v}'')] \quad (5)$$

By introducing energy instead of velocity variables, we finally obtain

$$\begin{aligned} -\delta(x) \eta \Theta(-\eta) \Theta(E - U(\eta)) - \eta \frac{\partial}{\partial x} H(x, E, \eta) \\ = N \int d\sigma [H(x, E, \eta) - H(x, E', \eta') - H(x, E'', \eta'')] \end{aligned} \quad (6)$$

where E' , η' , E'' and η'' are the energies and directional cosines with respect to the x -axis of the scattered and recoiling particle respectively.

The sputter yield is given by

$$S(E, \eta) = H(x=0, E, \eta). \quad (7)$$

Expanding H in terms of the Legendre polynomials ($P_\ell(\eta)$) we have

$$H(x, E, \eta) = \sum_{\ell=0}^{\infty} (2\ell+1) H_\ell(x, E) P_\ell(\eta) \quad (8)$$

Multiplying Eq. (6) by $P_\ell(\eta)$ and integrating over all possible $\eta (\eta \leq 0)$ we find that

$$\begin{aligned} \delta(x) Q_\ell(E) - \frac{\partial}{\partial x} [l H_{\ell-1}(x, E) + (l+1) H_{\ell+1}(x, E)] \\ = (2l+1) N \int d\sigma [H_\ell(x, E) - P_\ell(\cos \phi') H_\ell(x, E') \\ - P_\ell(\cos \phi'') H_\ell(x, E'')] \end{aligned} \quad (9)$$

where $Q_\ell(E) = \frac{2l+1}{2} \int_{-1}^0 (-\eta) d\eta \Theta(E - U(\eta)) P_\ell(\eta)$ (10)

ϕ' \equiv laboratory scattering angle of scattered atom
 ϕ'' \equiv laboratory scattering angle of recoiling atom.

If we multiply Eq. (9) by $x^n (n=0, 1, 2, 3, \dots)$, integrate over all possible x , and introduce the moment integral

$$H_\ell^n(E) = \int_{-\infty}^{+\infty} x^n H_\ell(x, E) dx \quad (11)$$

we have

$$\begin{aligned} \delta_{no} Q_\ell(E) - n [l H_{\ell-1}^{n-1}(E) + (l+1) H_{\ell+1}^{n-1}(E)] - (2l+1) N \int d\sigma [H_\ell^n(E) \\ - P_\ell(\cos \phi') H_\ell^n(E') - P_\ell(\cos \phi'') H_\ell^n(E'')] \end{aligned} \quad (12)$$

with $\delta_{no} \equiv \int_{-\infty}^{+\infty} \delta(x) x^n dx$

If we separate elastic from inelastic (electronic) collisions using a method proposed by Lindhard et al. [1963], Eq. (12) becomes

$$\delta_{n0} Q_\ell(E) - n [l H_{\ell-1}^{n-1}(E) + (l+1) H_{\ell+1}^{n-1}(E)] = (2l+1) N S_e(E) \frac{d}{dE} H_\ell^n(E) \\ + (2l+1) N \int_{T=0}^E d\sigma(E, T) [H_\ell^n(E) - P_\ell(\cos \phi') H_\ell^n(E-T) - P_\ell(\cos \phi'') H_\ell^n(T)] \quad (13)$$

where

$$S_e \equiv \text{electronic stopping cross section}, \\ d(E, T) \equiv \text{differential cross section for elastic scattering}, \\ \cos \phi' \equiv (1-T/E)^{1/2} + (M_2/M_1)(T/E)(1-T/E)^{-1/2}/2, \\ \cos \phi'' \equiv (T/T_m)^{1/2}, \\ T_m \equiv [4M_1 M_2 / (M_1 + M_2)^2] E \equiv \text{maximum recoil energy}, \\ M_1 \equiv \text{mass of ion}.$$

For $n=0$ Eq. (13) yields

$$Q_\ell(E) = (2l+1) N \int_{T=0}^E d\sigma(E, T) [H_\ell^0(E) - P_\ell(\cos \phi') H_\ell^0(E-T) - P_\ell(\cos \phi'') H_\ell^0(T)] \quad (14)$$

where it is assumed that $S_e(E)=0$. With $d\sigma(E, T) = C N E^{-m} T^{-1-m} dT$, ($0 \leq m \leq 1$) the following expressions are given for the source terms in Eq. (10)

$$Q_0(E) = \frac{1}{4} (1 - U_0/E) \quad (15a)$$

$$Q_1(E) = \frac{1}{2} [-1 + (U_0/E)^{3/2}] \quad (15b)$$

$$Q_2(E) = \frac{5}{16} [1 + 2U_0/E - 3(U_0/E)^2], \quad (15c)$$

$$Q_3(E) = \frac{7}{4} [- (U_0/E)^{3/2} + (U_0/E)^{5/2}] \quad (15d)$$

where we have used the identity $U(n_0) = U_0/n_0^2$. For $E < U_0$, the source term takes on the following value

$$Q_\ell^0(E) = 0$$

and $H_\ell^0(E) = 0$.

The following expressions for the leading terms of an asymptotic expansion, in powers of E , of the moment $H_0^o(E)$ is given below.

$$16a) \quad H_0^o(E) \sim \frac{1}{\Psi(1) - \Psi(1-m)} \frac{m}{1-2m} \frac{E}{8NCU_0^{1-2m}} + \frac{1}{-1/m - B(-m, 2m)} \frac{E^{2m}}{8NC}$$

$$16b) \quad H_1^o(E) \sim \frac{-1}{\Psi(1) - \Psi(1-m)} \frac{m}{1-4m} \frac{E^{1/2}}{4NCU_0^{1/2-2m}} + \frac{1}{1/m + 2/(1+2m) + B(-m, 3/2+2m)} \frac{E^{2m}}{6NC}$$

$$16c) \quad H_2^o(E) \sim - \frac{1}{1/m + 3/(1+m) + 3B(-m, 2+2m) + 2B(1-m, 2m)} \frac{E^{2m}}{8NC}$$

where $B(\xi, \eta) \equiv$ Beta function = $\Gamma(\xi)\Gamma(\eta)/\Gamma(\xi+\eta)$
 $\Psi(\xi) \equiv$ Digamma function = $d/d\xi(\ln\Gamma(\xi))$

For $m=0$ Eqs. (16a-16d) take the following form (see Appendix I)

$$H_0^o(E) \sim \frac{1}{8\Psi'(1)} \frac{E}{NC_0U_0} \quad (17a)$$

$$H_1^o(E) \sim \frac{1}{4\Psi'(1)} \frac{E^{1/2}}{NC_0U_0^{1/2}} \quad (17b)$$

$$H_2^o(E) \sim 0 \quad (17c)$$

with $\Psi'(\xi) = d/d\xi(\Psi(\xi))$, $\Psi'(1) = \pi^2/6$

$$C_0 = \pi\lambda_0 a^2/2$$

where $\lambda_0 = 24$ (18)

$$a = 0.219\text{\AA}.$$

The moment $H_0^o(E)$ is the leading term at all energies $E \gg U$. and it has the asymptotic form given by Eq. (17a). The moment $H_0^o(E)$ is the integral of $H_0(x, E)$ over all x . It determines the number of atoms penetrating a plane at an arbitrary position x with a certain minimum energy when there is a homogeneous isotropic source of recoiling atoms throughout an infinite medium.

Since $H_0^o(E)$ is proportional to E , for elastic scattering, E

in Eq.(17a) is replaced by $\nu(E)$, so that Eq.(17a) takes the form

$$H_0^*(E) = \frac{1}{8\psi'(1)} \frac{\nu(E)}{NC_0U_0} \quad (19)$$

where $\nu(E)/E$ is the fraction of the energy that is not lost to ionization during the slowing down process.

Using the expression

$$\int_{-\infty}^{\infty} dx F(x, E, \gamma) = \nu(E)$$

and Eqs.(8,11 and 18), Eq.(19) can be rewritten as

$$H(x, E, \gamma) = \frac{3}{4\pi^2} \frac{F(x, E, \gamma)}{NC_0U_0} \quad (20)$$

where $\Delta x = 3/4NC_0$ is the expression for the effective depth of origin of sputtered atoms. The effective sputterind depth Δx is given for a few metals and metal oxides in Table 1.

The sputtering yield of a metal target for normally incident ions is given by

$$S(E) = \Lambda \alpha N S_n(E) \quad (21)$$

where $S_n(E) = [1/(1-m)]C\gamma^{1-m} E^{1-2m}$ is the elastic stopping power of the ion, α is the factor that depends only on m and M_2/M_1 and $\Lambda = (3/4\pi^2)(1/NC_0U_0)$.

If the energy of the impinging ion, E , is less than some limiting energy

Metal	$\Delta X (\text{\AA})$	Oxide	$\Delta X (\text{\AA})$
Al	15.4	Al_2O_3	10.4
Ag	3.9	CaO	12.4
Au	2.1	Cr_2O_3	8.0
Ca	26.7	FeO	7.2
Cr	5.8	Fe_2O_3	7.9
Cu	4.8	Fe_3O_4	8.0
Fe	5.3	MgO	11.6
K	48.1	MnO	7.7
Mg	23.9	TiO_2	9.8
Mn	5.7		
Na	42.7		
Ni	4.7		
Si	17.9		
Ti	9.1		
Zn	5.8		

Table 1. Effective depth of origin of sputtered atoms.

$$E^* = \left(\frac{3\lambda_{1/3}}{2\lambda_0} \right)^{3/2} \frac{M_1 + M_2}{M_2} \left(\frac{a_{12}}{a} \right)^3 \frac{Z_1 Z_2 e^2}{a_{12}} \quad (22)$$

with

$$\begin{aligned} \lambda_{1/3} &= 1.309 \\ a &= 0.219 \text{\AA} \\ a_0 &= \text{Bohr radius} = 0.529 \text{\AA} \\ a_{12} &= 0.8853(Z_1^{2/3} + Z_2^{2/3})^{-1/2} \\ Z_1 &\equiv \text{atomic number of ion} \\ Z_2 &\equiv \text{atomic number of metal target atom} \end{aligned}$$

the elastic stopping power assumes the following form

$$S_n(E) = C_0 T_m. \quad (23)$$

For $E > E^*$, in the elastic collision region, Eq. (23) becomes

$$S_n(E) = 4\pi Z_1 Z_2 e^2 a_{12} [M_1 / (M_1 + M_2)] s_n(\epsilon) \quad (24)$$

where $\epsilon = [M_2 E / (M_1 + M_2)] / [Z_1 Z_2 e^2 / a_{12}]$ and $s_n(\epsilon)$ is the universal function tabulated in Table 2.

ϵ	$s_n(\epsilon)$	ϵ	$s_n(\epsilon)$
0.002	0.120	0.4	0.405
0.004	0.154	1.0	0.356
0.01	0.211	2.0	0.291
0.02	0.261	4.0	0.214
0.04	0.311	10	0.128
0.1	0.372	20	0.0813
0.2	0.403	40	0.0493

Table 2. Reduced nuclear stopping cross section $s_n(\epsilon)$ for Thomas-Fermi interaction. [From Sigmund, 1969].

Utilizing the expressions given by Eqs. (23 and 24), Eq. (21) can be written in its final form,

$$S(E) = (3/4\pi^2) \alpha T_m / U_0. \quad E < E^* \quad (25)$$

$$S(E) = \frac{0.0420 \cdot \alpha \cdot 4\pi Z_1 Z_2 e^2 a_{12} [M_1/(M_1+M_2)] S_n(\epsilon)}{U_0 \text{Å}^2} \quad E > E^* \quad (25)$$

Expression (25) holds only for $M_1 \gtrsim M_2$. In the case of proton sputtering $M_1 \ll M_2$. This implies that expression (25) is invalid unless the parameter α is improved by a method described in the next section.

B. Sputtering Yields of Metals for Protons at Normal Incidence

Before calculating the yield curves of metals, we have to make a decision concerning the parameter α shown in figure 2 and the surface binding condition.

Figure 2 shows α as a function of ϵ for protons and deuterons. The curves are rough estimates. In order to improve α , we scaled it to the sputtering yield value of Ag for normally incident H^+ at 2keV provided by Grolund and Moore [1960]. We found that a better estimate of α is given by the following expression

$$\alpha' = \alpha/2.$$

For metals, the surface binding energy U_0 is equal to the measured sublimation energy.

In Table 3, we have computed a_{12} , E^* and listed the sublimation energy (U_0), the atomic number (Z_2) and the mass (M_2) of the following metals: Al, Ca, Cr, Cu, Au, Fe, Mg, Ni, K, Ag, Na, Ti and Zn.

From Eq.(25) and the data provided by Fig.(2) , Tables 2 and 3, the yield curves were calculated for the metals listed in Table 3 (see Figures 3-34).

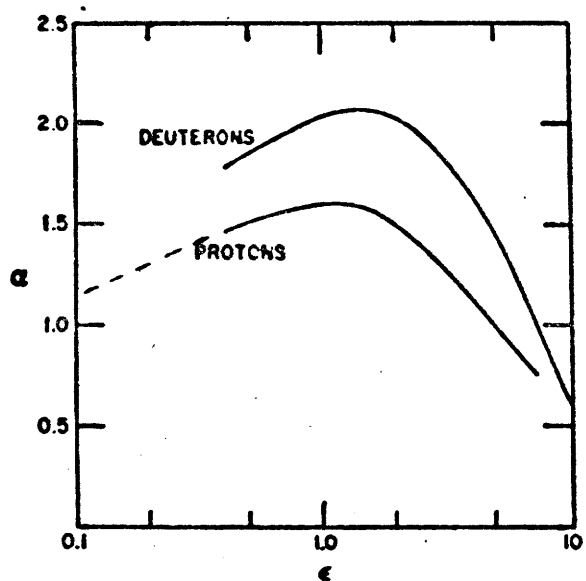


Fig. 2. Factor α in Eq.(25) for protons and deuterons incident on a heavy target. [From Sigmund, 1969].

Metal	a_{12} (Å)	E^* (eV)	U_0 (eV/atom) ¹	Z_2	M_2 (amu)
Al	0.1833	13.5	3.34	13	26.98154
Ca	0.1619	17.3	1.825	20	40.08
Cr	0.1535	18.5	4.10	24	51.996
Cu	0.1450	19.9	3.50	29	63.546
Au	0.1063	28.8	3.78	79	196.9665
Fe	0.1498	19.1	4.29	26	55.847
Mg	0.1875	14.1	1.53	12	24.312
Mn	0.1516	18.8	2.98	25	54.938
Ni	0.1465	19.8	4.435	28	58.71
K	0.1644	30.0	0.941	19	39.09
Ag	0.1251	23.8	2.96	47	107.868
Si	0.1795	15.0	4.64	14	28.086
Na	0.1921	13.6	1.13	11	22.9898
Ti	0.1575	18.0	4.855	22	47.9
Zn	0.1435	20.3	1.35	30	65.38

Table 3. Calculated a_{12} , E^* , and U_0 for various targets.¹From C. Kittel [1976]

Grølund and Moore [1960] reports yield values for H^+ ions incident on Ag targets (see Fig. 26). The predicted sputtering yields are slightly larger than Grolund and Moore's reported values by a factor of ~ 1.3 . The agreement with theory is surprisingly good.

KenKnight and Wehner [1964] reports yield data for light ions (H_2^+ , H_3^+) incident on Al, Au, Fe, Ni, and Ti at 7keV, and on Cu at energies from 1 to 5keV. The results for protons were deduced from the data provided by KenKnight and Wehner [see Figs.(4, 10, 12, 14, 20, 26 and 30)]. The predicted sputtering yields differ from KenKnight and Wehner's reported values by a factor which ranges from 1.04 for Cu to 2.9 for Fe.

Wehner [1964] reports yield values for H^+ ions on Fe and Cu targets at 1.85keV [see figs.(10,14)]. The predicted sputtering yields in this case differ from the reported values by a factor of 2.1 for Cu and 3.9 for Fe.

The agreement between theoretical and experimental values at low energies are not as good for Fe as it was in the case of Ag and Cu. This discrepancy can be explained as follows:

- 1) The assumption of random slowing down and of binary collisions may break down at low energies. There may be a small contribution from focused collision sequences. The quantitative effect on the sputtering yield will depend on the target.
- 2) The uncertainty of the low-energy cross section, as defined

by $d\sigma = C_0 dT/T$, affects the numerical factor in front of Eq.(20), the value of C_0 (that may depend on the target), and the dependence on U_0 .

3) The surface binding condition $U(n_0) = U_0/n_0^2$ affects the numerical factor in front of Eq.(20); the value of U_0 is not known from first principles but determines the magnitude of the yield.

4) The assumption of a plane surface may influence the magnitude of the yield. So long as surface roughness is on a scale that is small compared to the dimensions of the cascades, its effect on the sputtering yield will often average out. Surface roughness on a large scale, however, will tend to increase the yield. The quantitative effect depends on the geometry and can be estimated when the shape of the surface is known.

5) The assumption of an infinite medium may also affect the flux of low-energy recoils. [Sigmund, 1969]

There is no way of estimating the uncertainty in the theoretical sputtering yield values from the above points, but from comparison of both theoretical and experimental data one has to expect an uncertainty of at least a factor of 2 and in some cases 3.

C. Variation of Sputtering Yield with Angle of Incidence for Metals

In Section I.B. we reported sputtering yield values for normally incident hydrogen ions. It appears most reasonable to consider the variation of the sputtering yield with the angle of in-

cidence.

According to Sigmund [1969], the dependence of the sputtering yield $S(E, \eta)$ on the angle of incidence, η , can be estimated by the following expression

$$\frac{S(E, \eta)}{S(E, 1)} = (\eta^2 + (1-\eta^2) \frac{\langle Y^2 \rangle}{\langle \Delta X^2 \rangle})^{-1/2} \exp \left[\frac{\langle X \rangle^2}{2 \langle \Delta X^2 \rangle} (1 + \frac{\eta^2}{1-\eta^2} \frac{\langle \Delta X^2 \rangle}{\langle Y^2 \rangle})^{-1} \right] \quad (26)$$

where $S(E, 1)$ is the yield for perpendicular incidence. The moments $\langle X \rangle$, $\langle \Delta X^2 \rangle$, and $\langle Y^2 \rangle$ were tabulated by Sigmund and Sanders [1967] and are given in Table 4.

M_2/M_1	$\frac{\langle X \rangle}{E/NC_1}$	$\frac{\langle \Delta X^2 \rangle}{\langle X \rangle^2}$	$\frac{\langle Y^2 \rangle}{\langle X \rangle^2}$	$\frac{\langle XY^2 \rangle}{\langle X \rangle \langle Y^2 \rangle}$	$\frac{\langle \Delta X^3 \rangle}{\langle X \rangle^3}$
1/10	0.842	0.058	0.018	1.07	0.007
1/4	0.577	0.125	0.044	1.16	0.021
1/2	0.453	0.195	0.089	1.20	0.043
1	0.369	0.275	0.176	1.20	0.079
2	0.297	0.409	0.343	1.16	0.135
4	0.229	0.170	0.674	1.12	0.221
10	0.153	1.684	1.671	1.07	0.345

Table 4. Averages over the range distribution. $M_1 \neq M_2$.
 $d\sigma_1 = C_1 E^{1/2} T^{3/2} dT$. [From Sigmund and Sanders, 1967].

The values of $\langle \Delta X^2 \rangle / \langle X \rangle^2$ and $\langle Y^2 \rangle / \langle X \rangle^2$ for $M_2/M_1 > 10$ were computed by fitting the best straight line of the form $y=ax+b$ and a power curve of the form $y=ax^b$, respectively, to the data points given in Table 4 [see Table 5 and Appendix II].

Inserting the values of $\langle \Delta X^2 \rangle / \langle X \rangle^2$ and $\langle Y^2 \rangle / \langle X \rangle^2$ into Eq. (26), we obtain the variation of yield with η [see Figs. (35-47)]. According to Sigmund [1969], the sputtering yield goes through a

Metal	M_2/M_1	$\langle \Delta x^2 \rangle / \langle x \rangle^2$	$\langle Y^2 \rangle / \langle x \rangle^2$
Al	26.8	4.363	4.409
Ca	39.8	6.437	6.505
Cr	51.6	8.320	8.397
Cu	63.0	10.139	10.218
Au	195.4	31.263	31.098
Fe	55.4	8.926	9.005
Mg	24.1	3.932	3.972
Mn	54.5	8.782	8.861
Ni	58.2	9.373	9.452
K	38.8	6.277	6.344
Si	27.9	4.538	4.587
Ag	107.0	17.159	17.201
Na	22.8	3.725	3.761
Ti	47.5	7.666	7.740
Zn	64.9	10.442	10.521

Table 5. Calculated $\langle \Delta x^2 \rangle / \langle x \rangle^2$ and $\langle Y^2 \rangle / \langle x \rangle^2$ for various targets.

maximum at very oblique incidence and approaches zero for $\theta=90^\circ$. This maximum cannot be explained on the basis of the assumption of an infinite medium. There will be a certain glancing angle at which the repulsive action of the surface atoms is strong enough to prevent the ions from penetrating into the metal target, and this angle will be a function of the structure of the target's surface.

Dupp and Scharmann [1966], Cheney and Pitkin [1965], and Colombie [1964] reported values of the ratio $S(E,\eta)/S(E,1)$ for Ar^+ ion incident on polycrystalline copper (see Fig. 2a). The agreement between theoretical prediction and experimental data is quite good for $\theta \leq 70^\circ$.

D. Velocity Distribution of Sputtered Atoms

In a later section we will be concerned with the fraction of atoms that escape the Moon by natural sputtering. To calculate this we need the velocity distribution of sputtered atoms.

The average energy \bar{E}_T transferred to a target atom by a collision with an energetic ion is given by the following expression

$$\bar{E}_T = [2M_1 M_2 / (M_1 + M_2)^2] E_i \quad (27)$$

where E_i is the energy of the impinging ion. The number of atoms ejected from the target, having a velocity between v and $v+dv$, is given by the expression below

$$f dv = 2\pi N \left(\frac{3M_2}{\pi \bar{E}_T} \right)^{1/2} v^2 \exp[-3M_2 v^2 / 4\bar{E}_T] \exp[-3E_b / 2\bar{E}_T] dv \quad (28)$$

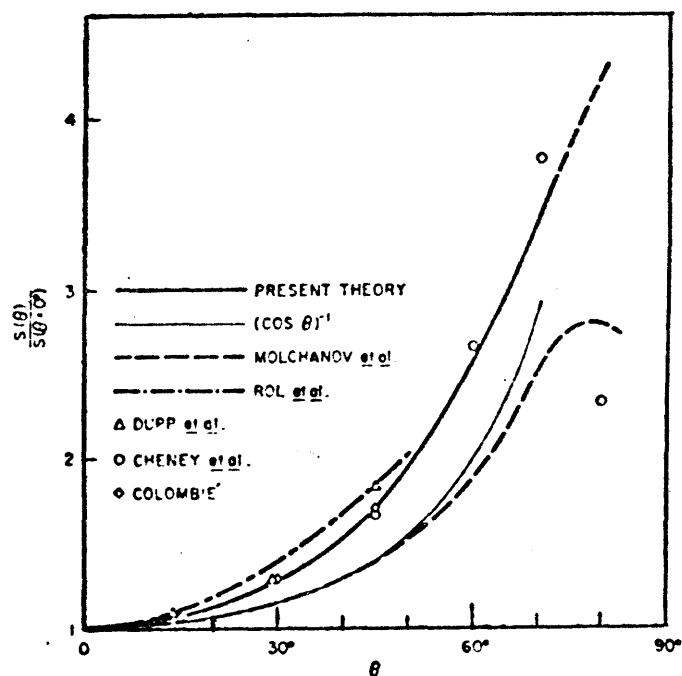


Fig. 2a. Variation of the sputtering yield with angle of incidence for Ar^+ ions incident on polycrystalline copper. Thick solid curve: Eq.(26); thin solid curve: $1/\cos \theta$. [From Sigmund, 1969].

where f is known as the Maxwell-Boltzmann distribution function and E_b is the surface binding energy of the target. The most probable velocity, v_p , of the recoil atoms can be obtained by finding the velocity at which the function f has a maximum value. It is given by the equation

$$df/dv = 0. \quad (29)$$

From Eq. (28) we obtain

$$2\pi N \left(\frac{3M_2}{\pi \bar{E}_T} \right)^{3/2} \exp[-3E_b/2\bar{E}_T] \frac{d}{dv} [v^2 \exp(-3M_2 v^2/4\bar{E}_T)] = 0$$

$$\frac{d}{dv} [v^2 \exp(-3M_2 v^2/4\bar{E}_T)] = 0$$

$$2v \exp[-3M_2 v^2/4\bar{E}_T] - v^2 (3M_2/4\bar{E}_T) 2v \exp[-3M_2 v^2/4\bar{E}_T] = 0$$

$$[1 - v^2 (3M_2/4\bar{E}_T)] = 0$$

Therefore

$$\begin{aligned} v_p &= 2\sqrt{\bar{E}_T / 3M_2} \\ E_p &= M_2 v_p^2 / 2 \end{aligned} \quad (30)$$

In Tables 6-20, v_p , E_p and \bar{E}_T are tabulated for various targets.

The velocity distribution, df/dv , of the recoil atoms ejected can be obtained by differentiating the Maxwell-Boltzmann distribution function f with respect to the velocity v . It is given by the following equation,

$$\frac{df}{dv} = 4\pi \left(\frac{3M_2}{\pi E_T}\right)^{3/2} v \left(1 - \frac{3M_2}{4E_T} v^2\right) \exp[-3E_b/2E_T] \exp[-3M_2 v^2/4E_T] \quad (31)$$

Substitution of the values for M_2 , E_b abd E_T into Eq. (31) gives us the velocity distribution for various targets [see Figs. (48-62)]. Note that the velocity distribution of the sputtered atoms peak heavily at very small velocities (3-9 km/sec) in comparison with the velocities of the incident protons [$(1.4-4.4) \times 10^2$ km/sec].

E. Sputtering Yields of Oxides for Protons at Normal Incidence

The sputtering behavior of oxides is different from that of metals. According to Kelly and Lam [1973], the sputtering behavior of oxides is in some cases "normal" in the sense of following Sigmund's theory of collisional sputtering. In other cases the behavior is "abnormal", in that the collisional sputtering is supplemented by thermal sputtering or by oxygen sputtering.

The collisional sputtering yield of oxides cannot be explained by Sigmund's theory. Instead, two approximations were used: One is to use Eq. (25) with the mean atomic weight of the oxide substituted; while the other is to use Eq. (25) in a form which is weighted for the mole fractions of metal and oxygen,

$$S = X_{\text{METAL}} S(M_{\text{METAL}}) + X_{\text{oxygen}} S(M_{\text{oxygen}}) \quad (32)$$

where $X = [(A/E)] / [(A/E) + (100-A)/B]$,
 $A \equiv$ weighted percent of solute,
 $B \equiv$ molecular weight of solvent,
 $E \equiv$ molecular weight of solute.

The sputtering yields are tabulated with the aid of Figs.(3-34).

The results are shown in Figs.(63-70).

Wehner [1964] reports yield values for light ions (H_2^+ , H_3^+) incident on Al_2O_3 , TiO_2 , FeO , Fe_2O_3 and SiO_2 at 6-7keV [Table 21]. The results for protons were deduced from the data in Table 21 [see Table 22]. The predicted sputtering yields differ from Wehner's reported values by a factor of 2 except in the case of SiO_2 , which differs by a factor of 8.4. This discrepancy may be accounted for by oxygen sputterind and/or thermal sputtering.

Wehner et al. [1963] studied the effects of H^+ bombardment of Al_2O_3 , CuO , Cu_2O , FeO , Fe_2O_3 , and various rock powders at a temperature of 300°C. The results can be summarized as follows:

1) The surface of many materials, after sufficient bombardment, becomes covered with a brittle crust in which individual dust particles become cemented together by sputtered atoms. In Al_2O_3 only very little or very fragile crusting is observed. The crust is thicker in more loosely packed places or materials.

2) The surface layer of many compounds becomes enriched with metal atoms. Black CuO is first converted into red Cu_2O before becoming covered with a very porous Cu layer. The red Fe_2O_3 converts into Fe_3O_4 , then to ferromagnetic FeO , and finally Fe metal traces appear on the surface. The reduction to a composition richer in metal and the formation of a "metal black" causes a darkening of the surface in most cases. In the process of breaking up mol-

ecules under bombardment and of sputtering atoms back and forth, oxygen atoms are more likely to escape from the surface than metal atoms.

3) As previously noted for metal oxides, whenever a crust is formed it has a fibrous structure with closely spaced needles and spires and deep small holes all aligned in the direction of the ion bombardment. The predominance of microscopically very steep walls is evidenced by the fact that the surface looks rather dark when viewed in isotropic light, but becomes shiny when illuminated and viewed from the same oblique angle.

Another effect of sputtering the oxides with hydrogen ions is that water molecules can form by implantation of H^+ and incipient formation of OH. The water molecules can be driven from the target by thermally heating the oxide or bombarding it with ultraviolet radiation [R.L. Huguenin, personal communication].

F. Variation of Sputtering Yield with Angle of Incidence for Metal Oxides

The procedure for estimating the dependence of the sputtering yield, $S(E,\eta)$, on the angle of incidence η in the case of oxides is quite similar to that used in the case of metals. Recalling Eq.(26) we have

$$\frac{S(E,\eta)}{S(E,1)} = (\eta^2 + (1-\eta^2) \frac{\langle Y^2 \rangle}{\langle \Delta x^2 \rangle})^{-1/2} \exp \left[\frac{\langle x \rangle^2}{2\langle \Delta x \rangle} (1 + \frac{\eta^2}{1-\eta^2} \frac{\langle \Delta x^2 \rangle}{\langle Y^2 \rangle})^{-1} \right]$$

The necessary moments are tabulated in Table 23. Using the infor-

mation provided by Table 23 we obtained an estimate of the dependence of the sputtering yield on the angle of incidence [see Figs. (71-78)] and we note that for heavier oxides (Fe_3O_4) the difference between $S(E, \eta)$ for normal incidence and grazing incidence is small in comparison with the lighter oxides (MgO, CaO).

G. Velocity Distribution of Sputtered Molecules

In a later section we will be concerned with the order of enrichment of oxides in the lunar material. In order to calculate the fraction of oxides which remain in the surface, we need to calculate the escape velocity of oxides which are representative of the lunar surface.

Utilizing the information provided by Table 24 and Eqs.(27 and 30) we are able to compute v_p , E_p as well as \bar{E}_T for metal oxides (see Tables 25-32). Substitution of the values for M_2 , E_b and E_T into Eq.(31) yields the velocity distributions [see Figs. (79-86)]. Note that at $E_i=1\text{keV}$ the velocity distribution of the sputtered molecules peaks heavily at $v=(1-2\text{km/sec})$ for the heavier oxides and at $v=(3-4\text{km/sec})$ for the lighter ones. Statistically more light than heavy molecules should be given sufficient energy to escape the solid during sputtering, therefore MgO would be sputtered in preference to Fe_3O_4 . The collisional sputtering model indicates that the major oxides should be enriched in proportion to their molecular weights and predicts the following order of enrichment: $\text{Fe}_3\text{O}_4 > \text{Fe}_2\text{O}_3 > \text{Al}_2\text{O}_3 > \text{TiO}_2 > \text{FeO} > \text{MnO} > \text{CaO} > \text{MgO}$. As we

will discuss in a later section, the actual order of enrichment observed is $\text{Al}_2\text{O}_3 > \text{FeO} > \text{CaO} > \text{MgO} > \text{TiO}_2$ for Lunar Maria and $\text{Al}_2\text{O}_3 > \text{CaO} > \text{MgO} > \text{FeO} > \text{TiO}_2$ for Lunar Highlands [Taylor, 1975] (see Table 33). There is no explanation, at the writing of this thesis, for the discrepancy in the ordering of TiO_2 .

II. SPUTTERING EFFECTS ON THE LUNAR SURFACE

The lunar surface is continually bombarded by intense solar radiation. The surface is unprotected by an atmosphere or strong magnetic field; thus solar illumination is unattenuated at all wavelengths and high energy protons and other ions are allowed to reach the surface. Laboratory studies of the interaction of the solar wind with the surface indicate that the optical properties and composition of the soil should have been greatly modified. One of the predicted modifications is that the soil particles should be coated with metallic Fe, produced by solar-wind sputtering. When lunar samples were returned to the earth, metal coatings were not found. The apparent absence of metal coatings indicates that the solar wind does not modify the soils to the predicted extent.

In Section B, I will show that the solar-wind protons are reduced in energy by interaction with surface magnetic fields; thus their sputtering efficiency is greatly reduced. If this is true, then the observed low abundances of metal surface coatings can be at least in part explained.

A. Lunar Magnetic Field

The magnetic fields associated with the electrical currents produced by electromagnetic excitation of the Moon were measured at the Apollo landing sites. Steady remanent magnetic fields were measured on the lunar surface at the Apollo 12, 14, 15 and 16 landing sites by a surface magnetometer. Table 34 gives the magnitudes of the remanent fields at these sites.

Lin et al. [1976] were able to measure lunar surface magnetic fields down to a spatial scale of 7km by the electron reflection method. The area observed extends from 15°E to 50°E longitude at ~5°S latitude. The field strengths range up to ~ $10^2\gamma$, averaged over the resolution element (see Table 34).

B. Reduction of the Mean Kinetic Energy of Solar-Wind Protons at the Lunar Surface by Magnetic Field Interaction

According to Scott [1976], the streaming solar-wind plasma has a magnetic field associated with it, which exerts a magnetic 'pressure' on the remanent magnetic fields associated with the lunar surface. This pressure acts to compress the surface field. If the local surface field is strong enough, it can stop the wind before it reaches the surface, i.e. a bow shock is formed. A weaker field would not stop the wind, but would reduce its incident energy at the surface.

In order to determine to what extent the protons are slowed by the magnetic field compression, it is necessary to determine the strengths of the local remanent fields. Steady remanent fields have been measured at nine surface sites during the Apollo 12, 14, 15 and 16 missions and also in the region located at ~5°S latitude, 15°E-50°E longitude.

The ratio of the plasma pressure to the total magnetic pressure is expressed as

$$\beta = n_p m_p v_s^2 / (B_{st}^2 / 8\pi) \quad (33)$$

where $B_{st} = B_s + \Delta B$ is the total surface compressed field,

and

$B_s \equiv$ steady remanent field,
 $B \equiv B_A - (B_E + B_S)$,
 $B_A \equiv$ total surface field,
 $B_E \equiv$ extralunar field measured by Explorer 35,
 $v_s \equiv$ solar wind velocity (4.376×10^2 km/sec),
 $n_p \equiv$ proton density,
 $m_p \equiv$ proton mass.

The values for $\beta \leq 1$ implies that the steady remanent field is compressed to the stagnation magnitude required to stand off the solar wind. $\beta \geq 1$ implies that the steady remanent field is not compressed to the stagnation magnitude required to stand off the solar-wind plasma (see Table 35).

The compressed remanent field reduces the mean energy and velocity of the protons at one site by as much as 459 eV and 1.1×10^2 km/sec, respectively. Such reduction in incident proton energies would substantially reduce the sputtering efficiency of the protons.

In order to arrive at a reliable estimate of the sputtering rates on the lunar surface, the flux, incident energy of the proton and the sputtering yields of lunar soils have to be known. Assuming a flux of 4×10^8 protons/cm² sec [Formisano and Moreno, 1971] and using the data in Table 35 and Figs. (3-34 and 63-70), an estimate of the sputtering rates on the lunar surface is obtained (see Table 36).

C. Fraction of Sputtered Atoms that Escape from the Moon

In order to obtain an estimate of the amount of material lost from the Moon (metal coatings, oxides), we have to compute the

fraction of sputtered atoms/molecules with velocities greater than the lunar escape velocity ($v_e = 2.4 \text{ km/sec}$).

The fraction of sputtered atoms with velocities greater than the lunar escape velocity can be determined by integrating fdv from $v=v_e$ to $v=+\infty$. It is given by the equation

$$F_T = \int_{v_e}^{\infty} 2\pi \left(\frac{3M_2}{\pi \bar{E}_T} \right)^{3/2} v^2 \exp[-3M_2 v^2/4\bar{E}_T] \exp[-3E_b/2\bar{E}_T] dv \quad (34)$$

This gives

$$\begin{aligned} F_T &= \int_0^{\infty} 2\pi \left(\frac{3M_2}{\pi \bar{E}_T} \right)^{3/2} v^2 \exp[-3M_2 v^2/4\bar{E}_T] \exp[-3E_b/2\bar{E}_T] dv \\ &\quad - \int_0^{v_e} 2\pi \left(\frac{3M_2}{\pi \bar{E}_T} \right)^{3/2} v^2 \exp[-3M_2 v^2/4\bar{E}_T] \exp[-3E_b/2\bar{E}_T] dv \\ F_T &= \exp[-3E_b/2\bar{E}_T] \left(1 - \int_0^{v_e} 2\pi \left(\frac{3M_2}{\pi \bar{E}_T} \right)^{3/2} v^2 \exp[-3M_2 v^2/4\bar{E}_T] dv \right) \end{aligned} \quad (35)$$

The change of variable $v = [(\zeta+1)/2]v_e$ converts Eq. (35) to

$$F_T = \exp[-3E_b/2\bar{E}_T] \left(1 - 2\pi \left(\frac{3M_2}{\pi \bar{E}_T} \right)^{3/2} \int_{-1}^1 \left[\left(\frac{\zeta+1}{2} \right) v_e \right]^2 \exp\left\{-3M_2 \left[\left(\frac{\zeta+1}{2} \right) v_e \right]^2 / 4\bar{E}_T \right\} d\zeta \right)$$

Eq. (36) may be approximated by the following expression

$$F_T \approx \exp[-3E_b/2\bar{E}_T] \left(1 - 2\pi \left(\frac{\gamma}{\pi} \right)^{3/2} \sum_{k=1}^n A_k f(x_k) \right) \quad (36)$$

with

$$\begin{aligned} \gamma &= 3M_2/\bar{E}_T \\ x_k &\equiv \text{Gaussian arguments} \\ A_k &\equiv \text{Gaussian weights} \end{aligned}$$

and $f(x_k) = \left[\left(\frac{x_k+1}{2} \right) v_e \right]^2 \exp\left[-\gamma \left(\left(\frac{x_k+1}{2} \right) v_e \right)^2 / 4 \right]$

Because velocities of the sputtered atoms depend on their masses as well as the surface binding energy of the target being

bombarded, larger fractions of the lighter species will escape the lunar surface. According to Cassidy and Hapke [1975], the probable fraction of sputtered atoms lost, F_p , is assumed to be $0.5F_T$ since it is assumed that half of the atoms will have a velocity component in the downward direction (see Tables 37-52).

D. Fraction of Sputtered Molecules that Escape from the Moon

The fraction of sputtered molecules with velocities greater than the lunar escape velocity were calculated (see Tables 53-60). Comparison of the fraction F_T for metal oxides and their corresponding metals indicates that F_T is a strong function of E_b as well as M_2 . This suggests that there would be some preferential retention of heavy oxides with high binding energies. The predicted order of enrichment using surface binding energies as well as molecular weights is: $\text{Fe}_2\text{O}_3 > \text{Fe}_3\text{O}_4 > \text{Al}_2\text{O}_3 > \text{FeO} > \text{MnO} > \text{TiO}_2 > \text{CaO} > \text{MgO}$. This order tends to be in better agreement with the order observed.

III. PREFERENTIAL SPUTTERING: METHOD FOR PREDICTING THE ORDER OF ENRICHMENT OF METALS

The escape rate (amount of material lost by the Moon) may be estimated by multiplying the sputtering yield of metals/oxides by the probable fraction lost, F_p (see Table 61).

The order of enrichment of metals in the lunar surface material, however, can be best explained by a thermodynamic model proposed by Pillinger et al. [1976].

According to Pillinger et al. [1976], the transfer of momentum concept is a good initial working hypothesis for the prediction of the order of enrichment, but because it does not take into consideration the nature of the bonding between atoms, it cannot completely explain preferential sputtering either for lunar materials or two element compounds. They found that preferential sputtering will occur to give a metal when: $\Delta H_s(M)$ [sublimation energy of the metal] $> \Delta H_D(O)/y$ (the heat of dissociation/oxygen atom) or when $\Delta H_s(M)/[\Delta H_D(O)/y] > 1$. The values of $\Delta H_s(M)$, $\Delta H_D(O)/y$ and $\Delta H_s(M)/[\Delta H_D(O)/y]$ are given in Table 62.

The thermodynamic model explains much more satisfactorily the data obtained from the lunar samples. Of the major elements only iron would be converted to metal; titanium by virtue of its conversion to lower oxides, e.g. Ti_2O_3 , would also be enriched relative to oxygen. The calculated preferential sputtering factors gives the order of enrichment: $Fe > Ti > Si > Al > Ca > Mg$ which agrees with the order of enrichment observed during surface analysis by ESCA [Housley and Grant, 1975] and our predicted order of enrichment

(see Table 61).

IV. SUMMARY

The model for backward sputtering of metals/oxides as proposed by Sigmund [1969] and Kelly [1973], respectively, has been reviewed.

Sigmund's theory is valid only for $M_1 \geq M_2$. In order to apply Sigmund's theory to proton sputtering ($M_1 \ll M_2$), we have therefore had to consider an approximation. The quantity α , which depends only on M_2/M_1 , was improved by substituting experimental S values into the analytical S deduced by Sigmund [1969].

The predicted sputtering yields of metals/oxides, in comparison with the experimental yield values, turns out to differ by at least a factor of 3 or better. For example, the predicted values for Cu and Fe at 1.85keV are 0.014 and 0.035, respectively, and the experimental values are 0.03 and 0.009, respectively.

The sputtering yields of metals/oxides, obtained from modified theories of sputtering by Sigmund and Kelly, are used in conjunction with the solar wind plasma- lunar surface magnetic field interaction model to estimate the sputtering rates at the lunar surface.

The interaction of the lunar surface magnetic fields with the solar-wind protons has been reviewed. According to the magnetic compression model, the streaming solar-wind plasma has a magnetic field associated with it, which exerts a magnetic 'pressure' on the remanent magnetic fields associated with the lunar surface. This pressure compresses the surface field. If the local surface field is strong enough, it can stop the wind before

it reaches the surface, i.e. a bow shock is formed. A weaker field would not stop the solar wind, but would reduce its incident energy at the surface.

The solar-wind protons are predicted to be completely stood-off at the Apollo 16 landing site, and their mean kinetic energies reduced at other sites. At the Apollo 12 landing site, for example, the protons lose about 30-80% of their nominal (1keV) incident energies [Scott, 1976].

The loss in proton energy by interaction with compressed magnetic fields can have a substantial effect on the sputtering efficiency of the solar wind. When high energy solar-wind ions impact lunar soil, the kinetic energy is converted to thermal energy. Since the protons are small ($\sim 10^{-9}$ cm.) in comparison to grains in the lunar soil, the thermal energy is confined to a region of atomic dimensions, and dissociation (sputtering) occurs. The number of atoms dissociated per incident ion (sputtering yield) is simply dependent on the ion energy.

Sputtering rates fall off precipitously with reductions in incident ion energies. From the data of Wehner [1963] and others it appears that a minimum ion energy of near 20-50eV is required for sputtering to occur. The loss of 30-80% in the ion energy at the Apollo 12 landing site should reduce substantially the sputtering efficiency. Sputtering efficiencies at other regions of the Moon will similarly be low; thus the unexpected low abundances of metal surface coatings predicted to have been produced by sput-

tering can now be possibly explained.

Laboratory work is needed to determine the dependence of sputtering yield on incident ion energies for lunar-like soils, in order to test the proposed interaction model.

APPENDIX I

Solutions of the Integral Equation Governing the Sputtering Yield of Polycrystalline Targets

In Section I.A. we analyzed the integral equation

$$S = \int d^3 v_0 |v_{0x}| \int_0^\infty dt G(0, \vec{v}_0, \vec{v}, t)$$

that determines the number of atoms that have sufficient energy to overcome the surface binding forces of the target. The solutions given were asymptotically exact in the limit of high ion energy. In this section the above integral equation will be analyzed with the aid of a method proposed by Robinson [1963; 1968].

The average number of atoms moving in a layer (x, dx) at time t with velocity $(\vec{v}_0, d^3 v_0)$ is represented by the function

$$G(x, \vec{v}_0, \vec{v}, t) d^3 v_0 dx \quad (I.1)$$

The number of atoms with velocity $(\vec{v}_0, d^3 v_0)$ penetrating the layer x in a time interval dt is given by

$$G(x, \vec{v}_0, \vec{v}, t) d^3 v_0 |v_{0x}| dt \quad (I.2)$$

where $v_{0x} \equiv$ the x -component of \vec{v}_0 .

The sputtering yield for backward sputtering of a solid with a plane surface at $x=0$ is given by

$$S = \int d^3 v_0 |v_{0x}| \int_0^\infty dt G(0, \vec{v}_0, \vec{v}, t) \quad (I.3)$$

where the integration over $d^3 v_0$ extends over all \vec{v}_0 with negative x -components large enough to overcome surface binding forces.

In an isotropic and homogeneous target, the function

$G(x, \vec{v}_0, \vec{v}, t)$ will satisfy the Boltzmann's equation

$$-\frac{1}{v} \frac{\partial}{\partial t} G(x, \vec{v}_0, \vec{v}, t) - \eta \frac{\partial}{\partial x} G(x, \vec{v}_0, \vec{v}, t) = N \int d\sigma [G(x, \vec{v}_0, \vec{v}, t) - G(x, \vec{v}_0, \vec{v}', t) - G(x, \vec{v}_0, \vec{v}'', t)] \quad (I.4)$$

Consider a particle initially at $x=0$ moving at $t=0$. After a time $t=\delta t$, it may or may not have made a collision. The probability of making or not making a collision is given by

$$G(x, \vec{v}_0, \vec{v}, t) = N v \delta t \int d\sigma [G(x, \vec{v}_0, \vec{v}', t) + G(x, \vec{v}_0, \vec{v}'', t) + [(1 - N v \delta t \int d\sigma) G(x - \eta v \delta t, \vec{v}_0, \vec{v}, t - \delta t)]] \quad (I.5)$$

where the first term on the right-hand side of Eq.(I.5) expresses the probability of making a collision and the second term is the probability for not making a collision.

Let $G(\delta t) = G(x - \eta v \delta t, \vec{v}_0, \vec{v}, t - \delta t)$ and $\chi = x - \eta v \delta t$, $\tau = t - \delta t$

Therefore

$$G(\delta t) = G(\chi, \vec{v}_0, \vec{v}, \tau)$$

$$\frac{dG(\delta t)}{d\delta t} = \frac{\partial G}{\partial \chi} \frac{d\chi}{d\delta t} + \frac{\partial G}{\partial \vec{v}_0} \frac{d\vec{v}_0}{d\delta t} + \frac{\partial G}{\partial \vec{v}} \frac{d\vec{v}}{d\delta t} + \frac{\partial G}{\partial \tau} \frac{d\tau}{d\delta t} \quad (I.6)$$

and since $[d\chi/d\delta t] = -\eta v$, $[d\vec{v}_0/d\delta t] = [d\vec{v}/d\delta t] = 0$, $[d\tau/d\delta t] = -1$

$$G'(\delta t) = -\eta v \frac{\partial G}{\partial \chi} - \frac{\partial G}{\partial \tau}$$

$$G'(0) = -\eta v \frac{\partial G}{\partial \chi} - \frac{\partial G}{\partial \tau} \quad (I.7)$$

The Taylor series expansion for $G(\delta t)$ is

$$G(\delta t) = G(0) + G'(0)\delta t + \frac{G''(0)}{2!} (\delta t)^2 + \dots + \frac{G^{(n)}(0)}{n!} (\delta t)^n + \dots$$

or

$$G(x - \eta v \delta t, \vec{v}_0, \vec{v}, t - \delta t) = G(x, \vec{v}_0, \vec{v}, t) - (\eta v \frac{\partial G}{\partial x} + \frac{\partial G}{\partial t}) \delta t + \dots \quad (I.8)$$

Substituting Eq. (I.8) into Eq. (I.5) we have

$$\begin{aligned} G(x, \vec{v}_0, \vec{v}, t) &= N v \delta t \int d\sigma [G(x, \vec{v}_0, \vec{v}', t) + G(x, \vec{v}_0, \vec{v}'', t)] \\ &\quad + (1 - N v \delta t \int d\sigma) [G(x, \vec{v}_0, \vec{v}, t) - (\eta v \frac{\partial G}{\partial x} + \frac{\partial G}{\partial t}) \delta t] \end{aligned} \quad (I.9)$$

$$\begin{aligned} G(x, \vec{v}_0, \vec{v}, t) &= N v \delta t \int d\sigma [G(x, \vec{v}_0, \vec{v}', t) + G(x, \vec{v}_0, \vec{v}'', t)] \\ &\quad + \cancel{G(x, \vec{v}_0, \vec{v}, t)} - (\eta v \frac{\partial G}{\partial x} + \frac{\partial G}{\partial t}) \delta t \\ &\quad - N v \delta t \int d\sigma G(x, \vec{v}_0, \vec{v}, t) + N v \delta t^2 \int d\sigma (\eta v \frac{\partial G}{\partial x} + \frac{\partial G}{\partial t}) \end{aligned} \quad (I.10)$$

Neglecting the last term on the right-hand side of Eq. (I.10) we obtain

$$\begin{aligned} (\eta v \frac{\partial G}{\partial x} + \frac{\partial G}{\partial t}) \delta t &= N v \delta t \int d\sigma [G(x, \vec{v}_0, \vec{v}', t) + G(x, \vec{v}_0, \vec{v}'', t)] \\ &\quad - N v \delta t \int d\sigma G(x, \vec{v}_0, \vec{v}, t) \end{aligned}$$

and

$$-\eta \frac{\partial G}{\partial x} - \frac{1}{v} \frac{\partial G}{\partial t} = N \int d\sigma [G(x, \vec{v}_0, \vec{v}, t) - G(x, \vec{v}_0, \vec{v}', t) - G(x, \vec{v}_0, \vec{v}'', t)] \quad (I.11)$$

Now we introduce the function

$$F(x, \vec{v}_0, \vec{v}) = \int_0^\infty G(x, \vec{v}_0, \vec{v}) dt \quad (I.12)$$

where $F(x, \vec{v}_0, \vec{v}) | v_{ox} | dv$ is the total number of atoms that penetrate the plane x with a velocity $(\vec{v}_0, d^3 v_0)$. $F(x, \vec{v}_0, \vec{v})$ satisfies

an equation that follows from Eq. (I.4) by integration over t .

Rewriting Eq. (I.4)

$$-\frac{1}{v} \frac{\partial}{\partial t} G(x, \vec{v}_0, v, t) - \eta \frac{\partial}{\partial x} G(x, \vec{v}_0, \vec{v}, t) = N \int d\sigma [G(x, \vec{v}_0, \vec{v}, t) - G(x, \vec{v}_0, \vec{v}', t) - G(x, \vec{v}_0, \vec{v}'', t)]$$

multiplying through by dt and integrating we have

$$-\frac{1}{v} \int_0^\infty \frac{\partial}{\partial t} G(x, \vec{v}_0, \vec{v}, t) dt - \eta \int_0^\infty \frac{\partial}{\partial x} G(x, \vec{v}_0, \vec{v}, t) dt = N \int d\sigma \left[\int_0^\infty G(x, \vec{v}_0, \vec{v}, t) dt - \int_0^\infty G(x, \vec{v}_0, \vec{v}', t) dt - \int_0^\infty G(x, \vec{v}_0, \vec{v}'', t) dt \right] \quad (I.13)$$

Utilizing expression (I.12), Eq. (I.13) assumes the form

$$-\frac{1}{v} G(x, \vec{v}_0, \vec{v}, t) \Big|_0^\infty - \eta \frac{\partial}{\partial x} F(x, \vec{v}_0, \vec{v}) = N \int d\sigma [F(x, \vec{v}_0, \vec{v}) - F(x, \vec{v}_0, \vec{v}') - F(x, \vec{v}_0, \vec{v}'')] \quad (I.14)$$

$$-\frac{1}{v} \delta(x) \delta(\vec{v} - \vec{v}_0) - \eta \frac{\partial}{\partial x} F(x, \vec{v}_0, \vec{v}) = N \int d\sigma [F(x, \vec{v}_0, \vec{v}) - F(x, \vec{v}_0, \vec{v}') - F(x, \vec{v}_0, \vec{v}'')] \quad (I.15)$$

where we have made the assumption that

$$G(x, \vec{v}_0, \vec{v}, t=0) = \delta(x) \delta(\vec{v} - \vec{v}_0) \quad (I.16)$$

represents one starting particle, and

$$G(x, \vec{v}_0, \vec{v}, \infty) = 0 \quad (I.17)$$

since at $t=\infty$ all atoms have slowed down below any finite velocity

v_0 .

Considering only backward sputtering and introducing the function

$$H(x, v) = \int d^3 v_0 |v_{0x}| F(x, \vec{v}_0, \vec{v}) \quad (I.18)$$

where

$$\begin{aligned} n_0 &= v_{0x}/v \leq 0, \\ E_0 &= M_2 v_0^2/2 \geq U(n_0), \\ M_2 &\equiv \text{mass of target atom}, \\ U(n_0) &\equiv \text{surface binding energy}. \end{aligned} \quad (I.19)$$

$H(x, \vec{v})$ represents the sputtering yield of a target atom for the case that the source is at $x=0$ and the sputtered surface in the plane x . Recalling Eq. (I.15)

$$\frac{1}{v} \delta(x) \delta(\vec{v} - \vec{v}_0) - \eta \frac{\partial}{\partial x} F(x, \vec{v}_0, \vec{v}) = N \int d\sigma [F(x, \vec{v}_0, \vec{v}) - F(x, \vec{v}_0, \vec{v}') - F(x, \vec{v}_0, \vec{v}'')] \quad (I.20)$$

and multiplying it by $|v_{0x}|$, integrating over \vec{v}_0 we have

$$\begin{aligned} \int \frac{|v_{0x}|}{v} \delta(x) \delta(\vec{v} - \vec{v}_0) d^3 v_0 - \eta \int \frac{\partial}{\partial x} |v_{0x}| F(x, \vec{v}_0, \vec{v}) d^3 v_0 \\ = N \int d\sigma \int d^3 v_0 [|v_{0x}| \{F(x, \vec{v}_0, \vec{v}) - F(x, \vec{v}_0, \vec{v}') - F(x, \vec{v}_0, \vec{v}'')\}] \end{aligned} \quad (I.21)$$

$$\begin{aligned} \delta(x) \int \frac{|v_{0x}|}{v} \delta(\vec{v} - \vec{v}_0) d^3 v_0 - \eta \frac{\partial}{\partial x} \int |v_{0x}| F(x, \vec{v}_0, \vec{v}) d^3 v_0 \\ = N \int d\sigma \int d^3 v_0 [|v_{0x}| \{F(x, \vec{v}_0, \vec{v}) - F(x, \vec{v}_0, \vec{v}') - F(x, \vec{v}_0, \vec{v}'')\}] \end{aligned} \quad (I.22)$$

$$\delta(x) \int \frac{|v_{0x}|}{v} \delta(\vec{v} - \vec{v}_0) d^3 v_0 - \eta \frac{\partial}{\partial x} H(x, v) = N \int d\sigma [H(x, v) - H(x, \vec{v}')] - H(x, \vec{v}'') \quad (I.23)$$

Introducing the function

$$\begin{aligned}\Theta(\xi) &= 1 \text{ for } \xi > 0 \\ &= 0 \text{ for } \xi < 0\end{aligned}$$

and satisfying the condition given by expression (I.19), Eq.(I.23) can be rewritten as

$$\begin{aligned}-\delta(x)\eta\Theta(-\eta)\Theta(E-U(\eta)) - \eta \frac{\partial}{\partial x} H(x, \vec{v}) &= N \int d\sigma [H(x, \vec{v}) - \\ &\quad - H(x, \vec{v}') - H(x, \vec{v}'')].\end{aligned}\tag{I.24}$$

In a random medium $H(x, \vec{v})$ is a function of x , v , and η , the directional cosine, but not on the azimuth of \vec{v} with respect to the x -axis. Introduction of energy, E , instead of velocity variables, we have

$$\begin{aligned}-\delta(x)\eta\Theta(-\eta)\Theta(E-U(\eta)) - \eta \frac{\partial}{\partial x} H(x, E, \eta) &\\ = N \int d\sigma [H(x, E, \eta) - H(x, E', \eta') - H(x, E'', \eta'')]\end{aligned}\tag{I.25}$$

where E' , η' , E'' and η'' are the energies and directional cosines with respect to the x -axis of the scattered and recoiling particle, respectively.

The sputter yield is given by

$$S(E, \eta) = H(x=0, E, \eta).\tag{I.26}$$

Expanding H in terms of Legendre polynomials we have

$$H(x, E, \eta) = \sum_{\ell=0}^{\infty} (2\ell+1) H_\ell(x, E) P_\ell(\eta) \quad (I.27)$$

where $P_\ell(\eta)$ are Legendre polynomials.

Eq. (I.25) is multiplied by $P_\ell(\eta)$ and integrate over η with the condition $\eta \leq 0$.

$$\begin{aligned} & \int_{-1}^1 -\delta(x)\eta \Theta(-\eta) \Theta(E-U(\eta)) P_\ell(\eta) d\eta - \int_{-1}^1 \eta \frac{\partial}{\partial x} H(x, E, \eta) P_\ell(\eta) d\eta \\ &= N \int d\sigma \left[\int_{-1}^1 \{ H(x, E, \eta) - H(x, E', \eta') - H(x, E'', \eta'') \} P_\ell(\eta) d\eta \right] \end{aligned} \quad (I.28)$$

$$\begin{aligned} & \int_{-1}^1 -\delta(x)\eta \Theta(-\eta) \Theta(E-U(\eta)) P_\ell(\eta) d\eta - \int_{-1}^1 \eta \frac{\partial}{\partial x} \sum_{\ell} (2\ell+1) H_\ell(x, E) P_\ell(\eta) P_\ell(\eta) d\eta \\ &= N \int d\sigma \left[\int_{-1}^1 \left\{ \sum_{\ell} H_\ell(x, E) P_\ell(\eta) P_\ell(\eta) - \sum_{\ell} H_\ell(x, E') P_\ell(\eta) P_\ell(\eta') \right. \right. \\ & \quad \left. \left. - \sum_{\ell} H_\ell(x, E'') P_\ell(\eta) P_\ell(\eta'') \right\} d\eta \right] \end{aligned} \quad (I.29)$$

Using the following relation between the $P_\ell(\eta)$'s

$$(2\ell+1) \eta P_\ell(\eta) = (\ell+1) P_{\ell+1}(\eta) + \ell P_{\ell-1}(\eta) \quad (I.30)$$

the following equation is obtained.

$$\begin{aligned} & \int_{-1}^1 -\delta(x)\eta \Theta(-\eta) \Theta(E-U(\eta)) P_\ell(\eta) d\eta - \int_{-1}^1 \frac{\partial}{\partial x} \sum_{\ell=0}^{\infty} \left[(2\ell+1) \left\{ \frac{\ell+1}{2\ell+1} H_{\ell+1}(x, E) \right. \right. \\ & \quad \left. \left. + \frac{\ell}{2\ell+1} H_{\ell-1}(x, E) \right\} P_\ell(\eta) P_\ell(\eta) d\eta \right. \\ &= N \int d\sigma \left[(2\ell+1) \int_{-1}^1 \left\{ \sum_{\ell=0}^{\infty} H_\ell(x, E) P_\ell(\eta) P_\ell(\eta) - H_\ell(x, E') P_\ell(\eta) P_\ell(\eta') \right. \right. \\ & \quad \left. \left. - H_\ell(x, E'') P_\ell(\eta) P_\ell(\eta'') \right\} d\eta \right] \end{aligned} \quad (I.31)$$

Using the following relations

$$\int_{-1}^1 P_\ell(\eta) P_\ell(\eta) d\eta = \frac{2}{2\ell+1} \quad (I.32)$$

$$\frac{2l+1}{2} \int_{-1}^1 H(x, E, \eta) P_l(\eta) d\eta = H_l(x, E) \quad (I.32)$$

the above equation becomes

$$\begin{aligned} & \int_{-1}^1 -\delta(x)\eta \Theta(-\eta) \Theta(E-U(\eta)) P_l(\eta) d\eta - \left(\frac{2}{2l+1}\right) \frac{\partial}{\partial x} \left\{ (l+1) H_{l+1}(x, E) + l H_{l-1}(x, E) \right\} \\ &= N \int d\sigma \left[(2l+1) \left(\frac{2}{2l+1}\right) H_l(x, E) - \left(\frac{2l+1}{2}\right) H_l(x, E') P_l(\eta') \int_{-1}^1 P_l(\eta) d\eta \right. \\ & \quad \left. - \left(\frac{2l+1}{2}\right) H_l(x, E'') P_l(\eta'') \int_{-1}^1 P_l(\eta) d\eta \right] \end{aligned} \quad (I.33)$$

$$\begin{aligned} & \frac{2l+1}{2} \int_{-1}^1 -\delta(x)\eta \Theta(-\eta) \Theta(E-U(\eta)) P_l(\eta) d\eta - \frac{\partial}{\partial x} \left\{ (l+1) H_{l+1}(x, E) + l H_{l-1}(x, E) \right\} \\ &= (2l+1) N \int d\sigma \left[H_l(x, E) - H_l(x, E') P_l(\eta') \left(\frac{2l+1}{2}\right) \int_{-1}^1 P_l(\eta) d\eta \right. \\ & \quad \left. - H_l(x, E'') P_l(\eta'') \left(\frac{2l+1}{2}\right) \int_{-1}^1 P_l(\eta) d\eta \right] \end{aligned} \quad (I.34)$$

Using the relation

$$\int_0^1 P_l(\eta) d\eta = \begin{cases} 1 & l=0 \\ 0 & l=2, 4, 6, \dots \\ (-1)^{(l-1)/2} \frac{(l-1)!}{2^l (\frac{l+1}{2})! (\frac{l-1}{2})!} & l=1, 3, 5, \dots \end{cases} \quad (I.35)$$

Eq. (I.34) has the final form

$$\begin{aligned} & \delta(x) Q_l(E) - \frac{\partial}{\partial x} [l H_{l-1}(x, E) + (l+1) H_{l+1}(x, E)] \\ &= (2l+1) N \int d\sigma [H_l(x, E) - P_l(\cos \phi') H_l(x, E') - P_l(\cos \phi'') H_l(x, E'')] \end{aligned} \quad (I.36)$$

where

$$Q_l(E) = \frac{2l+1}{2} \int_{-1}^1 (-\eta) d\eta \Theta(E-U(\eta)) P_l(\eta) \quad (I.37)$$

and

ϕ' ≡ laboratory scattering angle of scattered atom,
 ϕ'' ≡ laboratory scattering angle of recoiling atom.

Introducing the moment

$$H_\ell^n(E) = \int_{-\infty}^{\infty} x^n H_\ell(x, E) dx \quad (I.38)$$

multiplying Eq. (I.36) by x^n and integrating we have

$$\begin{aligned} Q_\ell(E) \int_{-\infty}^{\infty} \delta(x) x^n dx - \frac{\partial}{\partial x} \left[\int_{-\infty}^{\infty} \ell x^n H_{\ell-1}(x, E) dx + \int_{-\infty}^{\infty} (\ell+1) x^n H_{\ell+1}(x, E) dx \right] \\ = (2\ell+1) N \int d\sigma \left[\int_{-\infty}^{\infty} x^n H_\ell(x, E) dx - \int_{-\infty}^{\infty} P_\ell(\cos \phi') x^n H_\ell(x, E') dx - \right. \\ \left. - \int_{-\infty}^{\infty} P_\ell(\cos \phi'') x^n H_\ell(x, E'') dx \right] \quad (I.39) \end{aligned}$$

$$\begin{aligned} Q_\ell(E) \int_{-\infty}^{\infty} \delta(x) x^n dx - n \left[\int_{-\infty}^{\infty} \ell x^{n-1} H_{\ell-1}(x, E) dx + \int_{-\infty}^{\infty} (\ell+1) x^{n-1} H_{\ell+1}(x, E) dx \right] \\ = (2\ell+1) N \int d\sigma \left[\int_{-\infty}^{\infty} x^n H_\ell(x, E) dx - \int_{-\infty}^{\infty} x^n H_\ell(x, E') P_\ell(\cos \phi') dx - \right. \\ \left. - \int_{-\infty}^{\infty} x^n H_\ell(x, E'') P_\ell(\cos \phi'') dx \right] \quad (I.40) \end{aligned}$$

With

$$\int_{-\infty}^{\infty} \delta(x) x^n dx = \delta_{n0}$$

we have

$$\begin{aligned} \delta_{n0} Q_\ell(E) - n \left[\ell H_{\ell-1}^{n-1}(E) + (\ell+1) H_{\ell+1}^{n-1}(E) \right] = (2\ell+1) N \int d\sigma \left[H_\ell^n(E) - \right. \\ \left. - H_\ell^n(E') P_\ell(\cos \phi') - H_\ell^n(E'') P_\ell(\cos \phi'') \right] \quad (I.41) \end{aligned}$$

The terms which include the elastic and inelastic (electronic) collisions can be separated by using the method given by Lindhard

et al. [1963]. This yields

$$(I.42) \quad \delta_{n0} Q_\ell(E) - n [\ell H_{\ell-1}^{n-1}(E) + (\ell+1) H_{\ell+1}^{n-1}(E)] = (2\ell+1) S_e(E) \frac{d}{dE} H_\ell^n(E) \\ + (2\ell+1) N \int_{T=0}^E d\sigma(E, T) [H_\ell^n(E) - H_\ell^n(E-T) P_\ell(\cos \phi') - H_\ell^n(T) P_\ell(\cos \phi'')]$$

where $S_e(E)$ is the electronic stopping cross section, $d\sigma(E, T)$ is the differential cross section for elastic scattering, T is the recoil energy, and

$$\begin{aligned} \cos \phi' &= (1-T/E)^{1/2} + [(1-M_2/M_1)(T/E)(1-T/E)^{-1/2}]/2 \\ \cos \phi'' &= (T/T_m)^{1/2} \\ T_m &= \gamma E \\ \gamma &= 4M_1 M_2 / (M_1 + M_2)^2 \\ M_1 &\equiv \text{mass of incident ion} \end{aligned} \quad (I.43)$$

For $n=0$ Eq. (I.41) becomes

$$Q_\ell(E) = (2\ell+1) N \int_{T=0}^E d\sigma(E, T) [H_\ell^0(E) - P_\ell(\cos \phi') H_\ell^0(E-T) - P_\ell(\cos \phi'') H_\ell^0(T)] \quad (I.44)$$

An especially useful approximation of $d\sigma$ (Thomas-Fermi cross section) is the power approximation, where

$$d\sigma = CE^{-m} T^{-1-m} dT$$

and m is a number between 0 and 1. Eq. (I.44) becomes

$$\begin{aligned} Q_\ell(E) &= (2\ell+1) N C E^{-m} \int_0^E \frac{dT}{T^{1+m}} [H_\ell^0(E) - P_\ell((1-T/E)^{1/2} + (1-M_2/M_1)(T/E)(1-T/E)^{-1/2})/2 \cdot \\ &\quad \times H_\ell^0(E-T) - P_\ell((T/T_m)^{1/2}) H_\ell^0(T)] \end{aligned} \quad (I.45)$$

for $M_1=M_2$ we have

$$Q_\ell(E) = (2\ell+1) NCE^{-m} \int_0^E dT/T^{1+m} [H_\ell^0(E) - P_\ell((1-T/E)^{1/2}) H_\ell^0(E-T) - P_\ell((T/E)^{1/2}) H_\ell^0(T)]$$

where we assumed $S_e(E)=0$.

Now we proceed to solve the integral given by Eq. (I.44). We use the procedure which has been described by Robinson [1965; 1968]. Rewriting Eq. (I.44) we have

$$Q_\ell(E) = (2\ell+1) \int_0^E d\sigma(E,T) [H_\ell^0(E) - P_\ell((1-T/E)^{1/2}) H_\ell^0(E-T) - P_\ell((T/E)^{1/2}) H_\ell^0(T)]$$

Let's consider the case for $\ell=0$. The above equation takes the following form

$$Q_0(E) = \int_0^E d\sigma(E,T) [H_0^0(E) - H_0^0(E-T) - H_0^0(T)]$$

where we have made use of the relation

$$P_0(\eta) = 1.$$

With the Thomas-Fermis cross section approximated by the power approximation

$$d\sigma(E,T) = CNE^{-m} T^{-1-m} dT \quad (I.46)$$

we have

$$Q_0(E) = CNE^{-m} \int_0^E \frac{dT}{T^{1+m}} [H_0^0(E) - H_0^0(E-T) - H_0^0(T)] \quad (I.47)$$

$H_0^0(E) \equiv$ the integral of $H_0(x,E)$ over all x ; i.e. determines the number of atoms penetrating a plane at an arbitrary position x with a certain minimum energy, when there is a homogeneous isotropic source of recoiling atoms throughout an infinite medium.

$$H_o^o(E) = \begin{cases} 0 & \text{for } E > U_o \\ 1 & \text{for } U_o < E < 2U_o \end{cases} \quad (I.48)$$

U_o being the surface binding energy. With m fixed Robinson calculated the asymptotic solution

$$H_o^o(E) \sim \xi(m) \frac{E}{2U_o} \quad \text{for } U >> 2U_o \quad (I.49)$$

with

$$\xi(m) = 2(2^m - 1)/[\Psi(1) - \Psi(1-m)]$$

where $\xi=1$ at $m=-1$ (hard-sphere scattering), $\xi=(12/\pi^2)\ln 2=0.84$ at $m=0$ and $\xi=0$ at $m=1$.

If m in Eq. (I.49) is a function of E [$m=m(E)$], the function $H_o^o(E)$ is nonlinear over most of the energy range. For fixed m we have

$$\begin{aligned} \frac{\delta E}{E} &= \frac{1}{E} \int_0^E \frac{dE'}{S(E')} \int_0^{U_o} CE'^{(1-m)} T^{-1-m} T dT \\ &= \frac{1}{E} \int_0^E \frac{dE'}{\frac{1}{1-m} CE'^{(1-2m)}} \int_0^{U_o} CE'^{(1-m)} T^{-m} dT \\ &= \frac{1}{CE} \left[\frac{(1-m)}{2m} E'^{2m} \right]_0^E \cdot CE'^{(1-m)} \left[\frac{T^{(1-m)}}{(1-m)} \right]_0^{U_o} \\ &= \frac{1}{E} \left(\frac{1}{2m} \right) E^{2m} \cdot E^{-m} \cdot U_o^{(1-m)} \\ &= \frac{1}{2m} \left[\frac{U_o}{E} \right]^{(1-m)} \quad (I.50) \end{aligned}$$

where

$$S(E) = \int_0^E d\sigma(E, T) = \frac{1}{1-m} CE^{1-2m}$$

is the elastic stopping power. From Eq. (I.50) we see that $\delta E/E$ increases with m . In the keV region and below where $m \lesssim 0.5$, $\delta E/E$

will always be $\ll 1$ for $E \gg U_0$. This shows that m in the expression $\xi(m)$ cannot be determined by Eq. (I.50). Therefore we replace Eq. (I.50) by

$$m = m(2U_0). \quad (I.51)$$

If $\xi = \xi[m(2U_0)]$ is inserted into Eq. (I.49), $H_o^*(E)$ becomes linear for $E \gg 2U_0$. It is possible to obtain Eq. (I.49) if the power m in the cross section, Eq. (I.50) is allowed to vary from step to step. First we consider one single step

$$\begin{aligned} m(E) &= m_0 \text{ for } 2U_0 \leq E \leq U_1 \\ &= m_1 \text{ for } E > U_1 \end{aligned} \quad (I.52)$$

where $m_1 > m_0$ and $E \gg 2U_0$. For $E \leq E_1$, we can utilize the exact solution given by Robinson [1965; 1968]. For $m = m_0$.

$$H_o^*(E) = \frac{1}{2\pi i} \frac{1}{NC} \int_{a-i\infty}^{a+i\infty} ds \left(\frac{E}{2U_0}\right)^s \frac{k(s, m_0)}{F(s, m_0)} \quad (I.53)$$

where

$$F(s, m) = 1 - \frac{\Gamma(s) \Gamma(1-m)}{\Gamma(s-m)} \quad (I.54)$$

$$k(s, m) = \frac{1-2^m}{s} + \frac{s-m}{s} [2^s B_{1/2}(s, 1-m) - B(s, 1-m)] \quad (I.55)$$

$$C = \frac{1}{2} \pi \lambda_m a_{22}^2 (zz_2^2 e^2/a_{22})^{2m} \quad (I.56)$$

and a is some arbitrary real number > 1 . $B(s, 1-m)$ and $B_{1/2}(s, 1-m)$ are the Beta and incomplete Beta functions, respectively. The integrand in Eq. (I.53) has singularities at roots s_i of the equa-

tion $F(s_1, m) = 0$ and $s_0 = 1$, $-1 < s_1 < 0$, $-2 < s_2 < -1$, etc.

With

$$F(s_1, m_0) = 0$$

we have

$$\frac{\Gamma(s) \Gamma(1-m_0)}{\Gamma(s-m_0)} = 1$$

$$\Gamma(s) = \Gamma(s-m_0)/\Gamma(1-m_0) \quad (I.57)$$

Using Sterling's formula we have

$$\Gamma(z) \sim e^{-z} z^{z-1/2} (2\pi)^{1/2} \left[1 + \frac{1}{12z} + \frac{1}{288z^2} - \frac{139}{51840z^3} - \frac{571}{2488320z^4} \right] + \dots$$

$$\therefore \Gamma(1-m) \sim e^{m-1} (1-m)^{(1-m)-1/2} (2\pi)^{1/2} \left[1 + \frac{1}{12(1-m)} + \frac{1}{288(1-m)^2} - \frac{139}{51840(1-m)^3} \right] + \dots$$

$$\Gamma(s-m) \sim e^{m-s} (s-m)^{(s-m)-1/2} (2\pi)^{1/2} \left[1 + \frac{1}{12(s-m)} + \frac{1}{288(s-m)^2} - \frac{139}{51840(s-m)^3} \right] + \dots$$

$$\begin{aligned} \Gamma(s) &= \frac{\Gamma(s-m)}{\Gamma(1-m)} = \frac{e^{m-s} (s-m)^{(s-1/2-m)}}{e^{m-1} (1-m)^{(1/2-m)}} \frac{(2\pi)^{1/2} \left[1 + \frac{1}{12(s-m)} \right]}{(2\pi)^{1/2} \left[1 + \frac{1}{12(1-m)} \right]} \\ &\approx e^{1-s} \frac{(s-m)^{(s-1/2-m)} \left[1 + \frac{1}{12(s-m)} \right]}{(1-m)^{(1/2-m)} \left[1 + \frac{1}{12(1-m)} \right]} \end{aligned}$$

$$e^{-s} s^{s-1/2} (2\pi)^{1/2} \left[1 + \frac{1}{12s} \right] = e^{1-s} \frac{(s-m)^{(s-1/2-m)} \left[1 + \frac{1}{12(s-m)} \right]}{(1-m)^{(1/2-m)} \left[1 + \frac{1}{12(1-m)} \right]} \quad (I.58)$$

For $s_0=1$ we have from Eq.(I.58) that

$$\begin{aligned} e^{-1} (2\pi)^{1/2} [1 + \frac{1}{12}] &\approx e^0 \\ 1 &= \frac{\sqrt{2\pi}}{e} [1 + 1/12] \\ 1 &\approx (0.9990) \end{aligned}$$

so that $s_0=1$ is one root of Eq.(I.57). The poles of the function $k(s, m_0)$ in Eq.(I.53) are cancelled by the poles of the denominator so that the integrand is regular outside the real axis. The path of integration C_1 (Fig.A.1) can be transformed to C_2 that encloses the real axis for $s \leq 1$ in the positive direction. Utilizing the residue

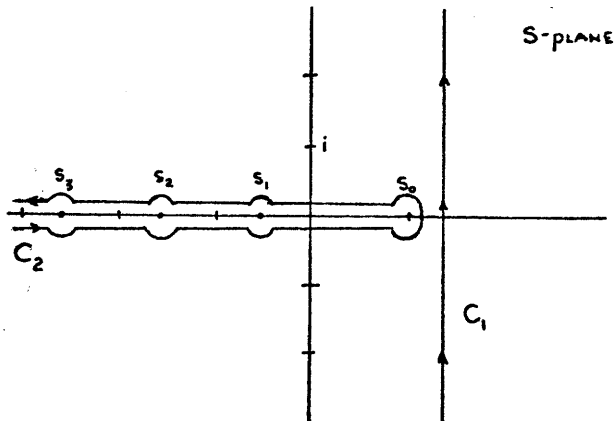


Fig. A.1

theorem $(\oint_C f(z) dz = 2\pi i \sum_{k=1}^n \text{Res } f(a_k))$ we have

$$H_o^o(E) = \sum_{i=0}^{\infty} A_i (E/2u_o)^{s_i} (1/NC) \quad (I.59)$$

where

$$H_o^*(E) = \sum_{i=0}^{\infty} \frac{\frac{1-2^m}{s_i} + \frac{s_i-m_0}{s_i} [2^{s_i} B_{1/2}(s_i, 1-m_0) - B(s_i, 1-m_0)]}{\Psi(s_i - m_0) - \Psi(s_i)} \left(\frac{E}{2U_0}\right)^{s_i} \frac{1}{NC} \quad (I.60)$$

$$A_i = \frac{k(s_i, m_0)}{\Psi(s_i - m_0) - \Psi(s_i)} ; \quad \Psi(x) = \frac{d}{dx} \ln \Gamma(x) \quad (I.61)$$

For $i=0$, $s_0=1$ Eq. (I.60), takes the following form

$$H_o^*(E) = \frac{(1-2^m) + (1-m_0) [B_{1/2}(1, 1-m_0) - B(1, 1-m_0)]}{\Psi(1-m_0) - \Psi(1)} \left(\frac{E}{2U_0}\right) \frac{1}{NC}$$

$$H_o^*(E) = \frac{1-2^m}{\Psi(1-m_0) - \Psi(1)} - \frac{(1-m_0) [B_{1/2}(1, 1-m_0) - B(1, 1-m_0)]}{\Psi(1-m_0) - \Psi(1)} \left(\frac{E}{2U_0}\right) \frac{1}{NC}$$

$$= \frac{1-2^m}{\Psi(1-m_0) - \Psi(1)} - \frac{(1-m_0) [\Gamma(1)\Gamma(1-m_0)/\Gamma(2-m_0)]}{2[\Psi(1-m_0) - \Psi(1)]} \left(\frac{E}{2U_0}\right) \frac{1}{NC}$$

$$= \frac{1-2^m}{\Psi(1-m_0) - \Psi(1)} - \frac{(1-m_0) \left[\frac{\Gamma(1)\Gamma(1-m_0)}{(1-m_0)\Gamma(1-m_0)} \right]}{2[\Psi(1-m_0) - \Psi(1)]} \left(\frac{E}{2U_0}\right) \frac{1}{NC}$$

$$= \frac{1-2^m}{\Psi(1-m_0) - \Psi(1)} - \frac{\frac{1}{2}}{[\Psi(1-m_0) - \Psi(1)]} \left(\frac{E}{2U_0}\right) \frac{1}{NC}$$

$$= \frac{\frac{1}{2} - 2^m}{\Psi(1-m_0) - \Psi(1)} \left(\frac{E}{2U_0}\right) \frac{1}{NC}$$

For $m=0$, i.e. $E < E_1$, we obtain (using L'Hopital's Rule)

$$H_o^*(E) = \frac{\ln 2}{2\Psi'(1)} \frac{E}{NCU_0} \quad (I.62)$$

Now we wish to calculate $\Psi'(1)$. We have

$$\left[\frac{d}{d\xi} \Psi(\xi) \right]_{\xi=1} = \left\{ \frac{d}{d\xi} [\Psi(\xi+1)] \right\}_{\xi=0}$$

$$\begin{aligned}
 \left[\frac{d}{d\xi} \Psi(1+\xi) \right]_{\xi=0} &= \left[\sum_{k=1}^{\infty} (k+\xi)^{-2} \right]_{\xi=0} \\
 &= \sum_{k=1}^{\infty} k^{-2} \\
 &= \pi^2/6
 \end{aligned}$$

Eq. (I.62) takes the form

$$H_0 = 3\ln 2/\pi^2 [E/N C_0 U_0] \quad (I.63)$$

Eq. (I.63) differs from Eq. (17a) by a factor of $1/4\ln 2$. The difference occurs because in our analysis of the integral equation using Robinson's method, we solved the equation for $E \geq 2U_0$. On the otherhand Sigmund solved the equation for $E \geq U_0$.

APPENDIX II

CURVE FITTINGA. Linear Least Square Fit

In Section I.C., the values of $\langle \Delta X^2 \rangle / \langle X \rangle^2$ and $\langle Y^2 \rangle / \langle X \rangle^2$ were computed by the method of least squares for $M_2/M_1 > 10$, since Sigmund and Sanders [1967] only computed values for $0.1 \leq M_2/M_1 \leq 10$. In this section we will explain the technique of linear regression by the method of least squares.

First we will illustrate the simplest kind of least squares fit, that which is often called a simple linear regression. We will fit a straight line

$$y = a_0 + a_1 x \quad (\text{II.1})$$

to the data points in Table 4. The moment $\langle \Delta X^2 \rangle / \langle X \rangle^2$ is plotted as a function of M_2/M_1 . The least squares coefficients are determined from the set of N data points (x_i, y_i) in the following manner. The function to be minimized is:

$$f(a_0, a_1) = \sum_{i=1}^N [y(x_i) - y_i]^2 \quad (\text{II.2})$$

$$= \sum_{i=1}^N [a_0 + a_1 x_i - y_i]^2 \quad (\text{II.3})$$

Differentiating, we obtain the two normal equations

$$\frac{\partial f}{\partial a_0} = \sum_i 2(a_0 + a_1 x_i - y_i) = 0 \quad (\text{II.4})$$

$$\frac{\partial f}{\partial a_1} = \sum_i 2(a_0 + a_1 x_i - y_i) x_i = 0 \quad (\text{II.5})$$

or

$$a_0 N + a_1 \sum x_i = \sum y_i \quad (\text{II.6})$$

$$a_0 \sum x_i + a_1 \sum x_i^2 = \sum x_i y_i \quad (\text{II.7})$$

Using Cramer's rule

$$a_0 = \frac{\begin{vmatrix} \sum y_i & \sum x_i \\ \sum x_i y_i & \sum x_i^2 \end{vmatrix}}{\begin{vmatrix} N & \sum x_i \\ \sum x_i & \sum x_i^2 \end{vmatrix}} \quad a_1 = \frac{\begin{vmatrix} N & \sum y_i \\ \sum x_i & \sum x_i y_i \end{vmatrix}}{\begin{vmatrix} N & \sum x_i \\ \sum x_i & \sum x_i^2 \end{vmatrix}} \quad (\text{II.8})$$

Finally, we obtain the expressions for the least squares coefficients in terms of sums of the x_i and y_i :

$$a_0 = \frac{\sum y_i \sum x_i - \sum x_i y_i \sum x_i}{N \sum x_i^2 - (\sum x_i)^2} \quad (\text{II.9})$$

$$a_1 = \frac{N \sum x_i y_i - \sum x_i \sum y_i}{N \sum x_i^2 - (\sum x_i)^2} \quad (\text{II.10})$$

where

$$\begin{aligned} x &= M_2/M_1 \\ y &= \langle \Delta X^2 \rangle / \langle X \rangle^2 \end{aligned}$$

The quality of the least squares fit to the data points provided is given by the expression

$$r^2 = \frac{[N \sum x_i y_i - \sum x_i y_i]^2}{N [N \sum x_i^2 - (\sum x_i)^2] [N \sum y_i^2 - (\sum y_i)^2]} \quad (\text{II.11})$$

The value of r^2 will lie between 0 and 1. The closer r^2 is to 1, the better the fit.

Least-squaring the data provided by Table 4 we find that $a_0=0.15955$, $a_1=0.08686$ and $r^2=0.99800$.

II. Power Curve Fit

We will fit a power curve

$$y = a_0 x^{a_1} \quad (a_0 > 0) \quad (\text{II.12})$$

to the data points in Table 4. The moment $\langle y^2 \rangle / \langle x \rangle^2$ is plotted as a function of M_2/M_1 . By writing Eq. (II.12) as

$$\ln y = a_1 \ln x + \ln a_0 \quad (\text{II.13})$$

the problem can be solved as a linear regression problem. Using the same procedure of Section I we find that

$$a_1 = \frac{N \sum (\ln y_i) \sum (\ln x_i) - (\sum \ln x_i)(\sum \ln y_i)}{N \sum (\ln x_i)^2 - (\sum \ln x_i)^2} \quad (\text{II.14})$$

$$a_0 = \exp \left[\frac{1}{N} \left(\sum \ln y_i - a_1 \sum \ln x_i \right) \right] \quad (\text{II.15})$$

where

$$\begin{aligned} x &= M_2/M_1 \\ y &= \langle y^2 \rangle / \langle x \rangle^2 \end{aligned}$$

and

$$r^2 = \frac{[N \sum (\ln x_i)(\ln y_i) - (\sum \ln x_i)(\sum \ln y_i)]^2}{N [N \sum (\ln x_i)^2 - (\sum \ln x_i)^2][N \sum (\ln y_i)^2 - (\sum \ln y_i)^2]} \quad (\text{II.16})$$

Fitting a power curve to the data points provided by Table 4 find that $a_0=0.17381$, $a_1=0.98330$ and $r^2=0.99997$. [Hewlett-Packard HP-25 Applications Programs, 1975].

REFERENCES

1. Cassidy, W., and B. Hapke, Effects of darkening on surfaces of airless bodies, Science, 172, 716-718, 1971.
2. Cheney, K.B., and E.T. Pitkin, J. Appl. Phys., 36, 3542, 1965.
3. Colombie', N., Thesis, University of Toulouse, 1964 (unpublished).
4. Dyal, P., C.W. Parkin, and W.D. Daily, Surface magnetometer experiments: Internal properties and lunar field interactions with the solar plasma, Proc. Lunar Sci. Conf. 3rd., 2287-2307, 1972.
5. Dupp, G. and A. Scharmann, Z. Physik, 194, 448, 1966.
6. Formisano, V., and G. Moreno, Rivista del Nuovo Cimento, 1, 365, 1971.
7. Grølund, F., and W.J. Moore, Sputtering of silver by light ions with energies from 2 to 12keV, The Journal of Chemical Physics, 32, 1540-1545, 1960.
8. Hapke, B., W. Cassidy and E. Wells, Effects of vapor-phase deposition processes on the optical, chemical, and magnetic properties of the lunar regolith, The Moon, 13, 339-353, 1975.
9. Housley, R.M. and R.M. Grant, ESCA studies of lunar surface chemistry, Proc. Sixth Lunar Sci. Conf., 3269-3275, 1975.
10. Kelly, R. and N.Q. Lam, The sputtering of oxides part I: A survey of the experimental results, Radiation Effects, 19, 39-47, 1973.
11. KenKnight, C.E. and G.K. Wehner, Sputtering of metals by hydrogen ions, Journal of Applied Physics, 35, 322-326, 1964.
12. Kittel, C., Introduction to Solid State Physics, John Wiley & Sons, Inc., New York, 1976, p.78.
13. Lin, R.P., K.A. Anderson, R.E. McGuire, and J.E. McCoy, Fine scale lunar surface magnetic fields detected by the electron reflection method, Lunar Science VII: Revised Abstracts of Papers Presented at the Seventh Lunar Science Conference, 492-494, 1976.
14. Lindhard, J., V. Nielsen, M. Scharff, and P.V. Thomsen, Integral equations governing radiation effects (Notes on atomic collisions, II), Matematisk-fysiske Meddelelser udgivet af Det Kongelige Danske Videnskabernes Selskab, Bind 33, 1-42, 1963.

15. Lindhard, J., M. Scharff and H.E. Schiøtt, Range concepts and heavy ion ranges (Notes on atomic collisions, II), Matematisk-fysiske Meddelelser udgivet af Det Kongelige Danske Videnskabernes Selskab, Bind 33, nr. 14, 1-42, 1963.
16. Molchanov, V.A. and V.G. Tel'kovskii, Dokl. Akad. Nauk SSSR, 136, 801, 1961 [English transl.: Soviet Physics - Doklady, 6, 137, 1961].
17. Robinson, M.T., The influence of the scattering law on the radiation damage displacement cascade, Philosophical Magazine, 12, 741-765, 1965.
18. Robinson, M.T., The influence of the scattering law on the radiation damage displacement cascade. II, Philosophical Magazine, 17, 639-642, 1968.
19. Rol, P.K., J.M. Fluit, and J. Kistemaker, Physica, 26, 1000, 1960.
20. Scott, R.E., Thesis, Massachusetts Institute of Technology, 1976 (unpublished).
21. Sigmund, P. and J.B. Sanders, in Proceedings of the International Conference on "Application of Ion Beams to Semiconductor Technology," edited by P. Glotin (Editions Ophrys, Paris, 1967), p.228.
22. Sigmund, P., Theory of sputtering.I. Sputtering yield of amorphous and polycrystalline targets, Physical Review, 184, 383-416, 1969.
23. Taylor, R.S., Lunar Science: A Post-Apollo View, Pergamon Press, Inc., New York, 1975.
24. Wehner, G.K., Sputtering effects on the moon's surface, General Mills Third Quarterly Status Report Covering Period 25 October 1963 to 24 January 1964 (unpublished).
25. Wehner, G.K., D.L. Rosenberg and C.E. KenKnight, Investigation of sputtering effects on the moon's surface, General Mills Fourth Quarterly Status Report Covering Period 25 January 1964a to 24 April 1964a (unpublished).

TABLES

Energy of Incident H ⁺ (eV)	\bar{E}_T (eV)	v _p (km/sec)	E _p (eV)
1000	69.4	18.2	46.3
900	62.5	17.3	41.7
800	55.5	16.3	37.0
700	48.6	15.2	32.4
600	41.7	14.1	27.8
500	37.7	12.9	23.1
400	27.8	11.5	18.5
300	20.8	10.0	13.9
200	13.9	8.1	9.3
100	6.9	5.8	4.6
50	3.5	4.1	2.3
10	0.7	1.8	0.5
1	0.1	0.6	0.05

Table 6. Calculated \bar{E}_T , v_p, and E_p for aluminum bombarded by H⁺

Energy of Incident H ⁺ (eV)	\bar{E}_T (eV)	v _p (km/sec)	E _p (eV)
1000	47.9	12.4	31.9
900	43.1	11.8	28.7
800	38.3	11.1	25.5
700	33.5	10.4	22.3
600	28.7	9.6	19.1
500	23.9	8.8	16.0
400	19.1	7.8	12.8
300	14.4	6.8	9.6
200	9.5	5.5	6.4
100	4.7	3.9	3.2
50	2.4	2.8	1.6
10	0.5	1.2	0.3
1	0.05	0.4	0.03

Table 7. Calculated \bar{E}_T , v_p, and E_p for calcium bombarded by H⁺

Energy of Incident H ⁺ (eV)	\bar{E}_T (eV)	v _p (km/sec)	E _p (eV)
1000	37.4	9.6	24.9
900	33.6	9.1	22.4
800	29.8	8.6	19.9
700	26.1	8.0	17.4
600	22.4	7.4	14.9
500	18.7	6.8	12.5
400	14.9	6.1	10.0
300	11.2	5.3	7.5
200	7.5	4.3	5.0
100	3.7	3.0	2.5
50	1.9	2.1	1.3
10	0.4	0.9	0.3
1	0.04	0.3	0.03

Table 8. Calculated \bar{E}_T , v_p, and E_p for chromium bombarded by H⁺

Energy of Incident H ⁺ (eV)	\bar{E}_T (eV)	v _p (km/sec)	E _p (eV)
1000	30.7	7.9	20.5
900	27.7	7.5	18.5
800	24.6	7.1	16.4
700	21.5	6.6	14.4
600	18.4	6.1	12.3
500	15.4	5.6	10.3
400	12.3	5.0	8.2
300	9.2	4.3	6.2
200	6.1	3.5	4.1
100	3.1	2.5	2.1
50	1.5	1.8	1.0
10	0.3	0.8	0.2
1	0.03	0.2	0.02

Table 9. Calculated \bar{E}_T , v_p, and E_p for copper bombarded by H⁺

Energy of Incident H ⁺ (eV)	\bar{E}_T (eV)	v _p (km/sec)	E _p (eV)
1000	10.1	2.6	6.8
900	9.1	2.4	6.1
800	8.1	2.3	5.4
700	7.1	2.2	4.7
600	6.1	2.0	4.1
500	5.1	1.8	3.4
400	4.1	1.6	2.7
300	3.0	1.4	2.0
200	2.0	1.2	1.4
100	1.0	0.8	0.7
50	0.5	0.6	0.3
10	0.1	0.3	0.1
1	0.01	0.1	0.01

Table 10. Calculated \bar{E}_T , v_p, and E_p for gold bombarded by H⁺

Energy of Incident H ⁺ (eV)	\bar{E}_T (eV)	v _p (km/sec)	E _p (eV)
1000	34.8	8.9	23.2
900	31.3	8.5	20.9
800	27.9	8.0	18.6
700	24.4	7.5	16.3
600	20.9	6.9	13.9
500	17.4	6.3	11.6
400	13.9	5.7	9.3
300	10.4	4.9	7.0
200	7.0	4.0	4.6
100	3.5	2.8	2.3
50	1.7	2.0	1.2
10	0.3	0.9	0.2
1	0.04	0.3	0.03

Table 11. Calculated \bar{E}_T , v_p, and E_p for iron bombarded by H⁺

Energy of Incident H ⁺ (eV)	\bar{E}_T (eV)	v _p (km/sec)	E _p (eV)
1000	35.4	9.1	23.6
900	31.8	8.6	21.2
800	28.3	8.1	18.9
700	24.7	7.6	16.5
600	21.2	7.1	14.2
500	17.7	6.4	11.8
400	14.2	5.8	9.4
300	10.6	5.0	7.1
200	7.1	4.1	4.7
100	3.5	2.9	2.4
50	1.8	2.0	1.2
10	0.4	0.9	0.2
1	0.04	2.9	0.03

Table 12. Calculated \bar{E}_T , v_p, and E_p for manganese bombarded by H⁺

Energy of Incident H ⁺ (eV)	\bar{E}_T (eV)	v _p (km/sec)	E _p (eV)
1000	76.4	20.1	51.0
900	68.8	19.1	45.9
800	61.2	18.0	40.8
700	53.5	16.8	35.7
600	45.9	15.6	30.6
500	38.2	14.2	25.5
400	30.6	12.7	20.4
300	22.9	11.0	15.3
200	15.3	9.0	10.2
100	7.6	6.4	5.1
50	3.8	4.5	2.6
10	0.8	2.0	0.5
1	0.1	0.6	0.1

Table 13. Calculated \bar{E}_T , v_p, and E_p for magnesium bombarded by H⁺

Energy of Incident H ⁺ (eV)	\bar{E}_T (eV)	v _p (km/sec)	E _p (eV)
1000	33.2	8.5	22.1
900	29.9	8.1	19.9
800	26.5	7.6	17.7
700	23.2	7.1	15.5
600	19.9	6.6	13.3
500	16.6	6.0	11.1
400	13.3	5.4	8.9
300	10.0	4.7	6.6
200	6.6	3.8	4.4
100	3.3	2.7	2.2
50	1.7	1.9	1.1
10	0.3	0.9	0.2
1	0.03	0.3	0.02

Table 14. Calculated \bar{E}_T , v_p, and E_p for nickel bombarded by H⁺

Energy of Incident H ⁺ (eV)	\bar{E}_T (eV)	v _p (km/sec)	E _p (eV)
1000	49.0	12.7	32.7
900	44.1	12.1	29.4
800	39.2	11.4	26.1
700	34.3	10.6	22.9
600	29.4	9.8	19.6
500	24.5	9.0	16.3
400	19.6	8.0	13.1
300	14.7	7.0	9.8
200	9.8	5.7	6.5
100	4.9	4.0	3.3
50	2.5	2.8	1.6
10	0.5	1.3	0.3
1	0.05	0.4	0.04

Table 15. Calculated \bar{E}_T , v_p, and E_p for potassium bombarded by H⁺

Energy of Incident H^+ (eV)	\bar{E}_T (eV)	v_p (km/sec)	E_p (eV)
1000	66.9	17.5	44.6
900	60.2	16.6	40.3
800	53.5	15.7	35.7
700	46.8	14.6	31.2
600	40.1	13.6	26.8
500	33.4	12.4	22.3
400	26.8	11.1	17.8
300	20.1	9.6	13.4
200	13.4	7.8	8.9
100	6.7	5.5	4.5
50	3.3	3.9	2.2
10	0.7	1.8	0.5
1	0.07	0.6	0.1

Table 16. Calculated \bar{E}_T , v_p , and E_p for silicon bombarded by H^+

Energy of Incident H^+ (eV)	\bar{E}_T (eV)	v_p (km/sec)	E_p (eV)
1000	18.3	4.7	12.2
900	16.5	4.4	11.0
800	14.7	4.2	9.8
700	12.8	3.9	8.6
600	11.0	3.6	7.3
500	9.2	3.3	6.1
400	7.3	3.0	4.9
300	5.5	2.6	3.7
200	3.7	2.1	2.5
100	1.8	1.5	1.2
50	0.9	1.0	0.6
10	0.2	0.5	0.1
1	0.02	0.1	0.01

Table 17. Calculated \bar{E}_T , v_p , and E_p for silver bombarded by H^+

Energy of Incident H ⁺ (eV)	\bar{E}_T (eV)	v _p (km/sec)	E _p (eV)
1000	80.5	21.2	53.7
900	72.4	20.1	48.3
800	64.4	19.0	42.9
700	56.3	17.8	37.6
600	48.3	16.4	32.2
500	40.2	15.0	26.8
400	32.2	13.4	21.5
300	24.1	11.6	16.1
200	16.1	9.5	10.7
100	8.0	6.7	5.4
50	4.0	4.7	2.7
10	0.8	2.1	0.5
1	0.1	0.7	0.1

Table 18. Calculated \bar{E}_T , v_p, and E_p for sodium bombarded by H⁺

Energy of Incident H ⁺ (eV)	\bar{E}_T (eV)	v _p (km/sec)	E _p (eV)
1000	40.4	10.4	26.9
900	36.3	9.9	24.2
800	32.3	9.3	21.5
700	28.3	8.7	18.8
600	24.2	8.1	16.2
500	20.2	7.4	13.5
400	16.1	6.6	10.8
300	12.1	5.7	8.1
200	8.1	4.7	5.4
100	4.0	3.3	2.7
50	2.0	2.3	1.4
10	0.4	1.0	0.3
1	0.04	0.3	0.03

Table 19. Calculated \bar{E}_T , v_p, and E_p for titanium bombarded by H⁺

Energy of Incident H ⁺ (eV)	\bar{E}_T (eV)	v _p (km/sec)	E _p (eV)
1000	29.9	7.7	19.9
900	26.9	7.3	17.9
800	23.9	6.9	16.0
700	20.9	6.4	14.0
600	17.9	5.9	12.0
500	15.0	5.4	10.0
400	12.0	4.9	8.0
300	9.0	4.2	6.0
200	6.0	3.4	4.0
100	3.0	2.4	2.0
50	1.5	1.7	1.0
10	0.3	0.8	0.2
1	0.03	0.2	0.02

Table 20. Calculated \bar{E}_T , v_p, and E_p for zinc bombarded by H⁺

Energy of Incident H ⁺ (eV)	\bar{E}_T (eV)	v _p (km/sec)	E _p (eV)
1000	111.5	30.0	74.4
900	100.4	28.4	66.9
800	89.2	26.8	59.5
700	78.1	25.1	52.1
600	66.9	23.2	44.6
500	55.7	21.1	37.2
400	44.6	18.9	29.7
300	33.5	16.4	22.3
200	22.3	13.3	14.9
100	11.2	9.5	7.4
50	5.6	6.7	3.7
10	1.1	3.0	0.7
1	0.1	0.9	0.1

Table 20a. Calculated \bar{E}_T , v_p, and E_p for oxygen bombarded by H⁺

Oxide	keV	$10^3 S_{H_2^+}$	$10^3 S_{H_3^+}$	Comment
Al_2O_3	7.0	10.5	15.0	$x=1.86$ beam shift
	7.0	11.8	17.1	
TiO_x	6.0	7.5	12.9	$x=1.86$ beam shift
	6.5	7.5	10.6	
FeO_x	6.5	12.7	20.4	$x=1.86$
Fe_2O_3	7.0	9.4	12.8	uniformity (?)
SiO_2	7.5	83.0	92.0	

Table 21. Sputtering yield of oxides for H_2^+ and H_3^+ ions at normal incidence. [From Wehner, 1964].

Oxide	keV	$S_{H_2^+}^*$	$S_{H_2^+}$ (Eq. 32)
Al_2O_3	7.0	0.005	0.010
	7.0	0.006	0.010
TiO_x	6.0	0.004	0.013
	6.5	0.004	0.011
FeO_x	6.5	0.006	0.011
Fe_2O_3	7.0	0.005	0.013
SiO_2	7.5	0.042	0.005

Table 22. Sputtering yield of oxides for H_2^+ at normal incidence.

* Values for $S_{H_2^+}$ deduced from data given in Table 21.

Oxide	M_2/M_1	$\langle \Delta X^2 \rangle / \langle X \rangle^2$	$\langle Y^2 \rangle / \langle X \rangle^2$
Al_2O_3	101.2	16.227	16.278
Cao	55.6	8.964	9.043
FeO	71.3	11.461	11.538
Fe_2O_3	158.4	25.366	25.304
Fe_3O_4	229.7	36.740	36.462
MgO	40.0	6.468	6.536
MnO	70.4	11.317	11.394
TiO_2	79.3	12.735	12.808

Table 23. Tabulation of the moments $\langle \Delta X^2 \rangle / \langle X \rangle^2$ and $\langle Y^2 \rangle / \langle X \rangle^2$ for oxides.

Oxide	M_2 (amu)	E_b (eV)
Al_2O_3	101.96	10.0 ¹
CaO	56.08	8.4
FeO	71.85	13.1
Fe_2O_3	159.69	14.3
Fe_3O_4	231.54	13.8
MgO	40.31	7.9 ¹
MnO	70.94	10.6
TiO ₂	79.9	10.3 ¹

Table 24. Molecular weight and binding energy of metal oxides.
¹From Kelly and Lam [1973].

Energy of Incident H ⁺ (eV)	\bar{E}_T (eV)	v _p (km/sec)	E _p (eV)
1000	19.4	4.9	12.9
900	17.4	4.7	23.3
800	15.5	4.4	11.6
700	13.6	4.1	9.1
600	11.6	3.8	7.8
500	9.7	3.5	6.5
400	7.8	3.1	5.2
300	5.8	2.7	3.9
200	3.9	2.2	2.6
100	1.9	1.6	1.3
50	1.0	1.1	0.7
10	0.2	0.5	0.1
1	0.01	0.2	0.02

Table 25. Calculated \bar{E}_T , v_p, and E_p for Al₂O₃ bombarded by H⁺

Energy of Incident H ⁺ (eV)	\bar{E}_T (eV)	v _p (km/sec)	E _p (eV)
1000	34.7	8.9	23.1
900	31.2	8.5	20.8
800	27.8	8.0	18.5
700	24.3	7.5	16.2
600	20.8	6.9	13.9
500	17.3	6.3	11.6
400	13.9	5.6	9.3
300	10.4	4.9	6.9
200	6.9	4.0	4.6
100	3.5	2.8	2.3
50	1.7	2.0	1.2
10	0.3	0.9	0.2
1	0.04	0.3	0.03

Table 26. Calculated \bar{E}_T , v_p, and E_p for CaO bombarded by H⁺

Energy of Incident H ⁺ (eV)	\bar{E}_T (eV)	v _p (km/sec)	E _p (eV)
1000	27.3	7.0	18.2
900	24.6	6.6	16.4
800	21.8	6.3	14.6
700	19.1	5.8	12.7
600	16.4	5.4	10.9
500	13.6	4.9	9.1
400	10.9	4.4	7.3
300	8.2	3.8	5.5
200	5.5	3.1	3.6
100	2.7	2.2	1.8
50	1.4	1.6	0.9
10	0.3	0.7	0.2
1	0.03	0.2	0.02

Table 27. Calculated \bar{E}_T , v_p, and E_p for FeO bombarded by H⁺

Energy of Incident H ⁺ (eV)	\bar{E}_T (eV)	v _p (km/sec)	E _p (eV)
1000	12.5	3.1	8.3
900	11.2	3.0	7.5
800	10.0	2.8	6.7
700	8.7	2.7	5.8
600	7.5	2.5	5.0
500	6.2	2.2	4.2
400	5.0	2.0	3.3
300	3.7	1.7	2.5
200	2.5	1.4	1.7
100	1.2	1.0	0.8
50	0.6	0.7	0.4
10	0.1	0.3	0.1
1	0.01	0.1	0.01

Table 28. Calculated \bar{E}_T , v_p, and E_p for Fe₂O₃ bombarded by H⁺

Energy of Incident H ⁺ (eV)	\bar{E}_T (eV)	v _p (km/sec)	E _p (eV)
1000	8.6	2.2	5.8
900	7.8	2.1	5.2
800	6.9	2.0	4.6
700	6.0	1.8	4.0
600	5.2	1.7	3.5
500	4.3	1.5	2.9
400	3.5	1.4	2.3
300	2.6	1.2	1.8
200	1.7	1.0	1.2
100	0.9	0.7	0.6
50	0.4	0.5	0.3
10	0.1	0.2	0.1
1	0.01	0.1	0.01

Table 29. Calculated \bar{E}_T , v_p, and E_p for Fe₃O₄ bombarded by H⁺

Energy of Incident H ⁺ (eV)	\bar{E}_T (eV)	v _p (km/sec)	E _p (eV)
1000	47.6	12.3	31.8
900	42.8	11.7	28.6
800	38.1	11.0	25.4
700	33.3	10.3	22.2
600	28.6	9.6	19.0
500	23.8	8.7	15.9
400	19.0	7.8	12.7
300	14.3	6.8	9.5
200	9.5	5.5	6.4
100	4.8	3.9	3.2
50	2.4	2.8	1.6
10	0.5	1.2	0.3
1	0.05	0.4	0.03

Table 30. Calculated \bar{E}_T , v_p, and E_p for MgO bombarded by H⁺

Energy of Incident H ⁺ (eV)	\bar{E}_T (eV)	v _p (km/sec)	E _p (eV)
1000	27.6	7.1	18.4
900	24.9	6.7	16.6
800	22.1	6.3	14.7
700	19.3	5.9	12.9
600	16.6	5.5	11.1
500	13.8	5.0	9.2
400	11.1	4.4	7.4
300	8.3	3.9	5.5
200	5.5	3.2	3.7
100	2.8	2.2	1.8
50	1.4	1.6	0.9
10	0.3	0.7	0.2
1	0.03	0.2	0.02

Table 31. Calculated \bar{E}_T , v_p, and E_p for MnO bombarded by H⁺

Energy of Incident H ⁺ (eV)	\bar{E}_T (eV)	v _p (km/sec)	E _p (eV)
1000	24.6	6.3	16.4
900	22.1	6.0	14.8
800	19.7	5.6	13.1
700	17.2	5.3	11.5
600	14.8	4.9	9.8
500	12.3	4.5	8.2
400	9.8	4.0	6.6
300	7.4	3.4	4.9
200	4.9	2.8	3.3
100	2.5	2.0	1.6
50	1.2	1.4	0.8
10	0.2	0.6	0.2
1	0.03	0.2	0.02

Table 32. Calculated \bar{E}_T , v_p, and E_p for TiO₂ bombarded by H⁺

Oxide	Maria (wt %)	Highlands (wt %)
SiO ₂	45.4	45.5
TiO ₂	3.9	0.6
Al ₂ O ₃	14.9	24.0
FeO	14.1	5.9
MgO	9.2	7.5
CaO	11.8	15.9
Na ₂ O	0.6	0.6
K ₂ O	----	----

Table 33. Average chemical composition of Lunar Surface Regolith. [From Taylor, 1975].

Site	Coordinates		Field Magnitude (γ)
Apollo 12	3.2°S	23.4°W	38
Apollo 14			
Site A	3.2°S	17.2°W	103
Site C'	2.6°S	15.5°W	43
Apollo 15	26.1°N	3.7°E	3
Apollo 16			
ALSEP	8.9°S	15.5°E	234
Site 2	9.0°S	15.5°E	189
Site 5	9.1°S	15.5°E	112
Site 13	8.9°S	15.5°E	327
FRPS	9.0°S	15.5°E	113
Taylor Crater	16.0°E	4.5°S	20
Alfraganus Crater	19.0°E	5.0°S	83
M. Tranquilitatis	26.5°E	5.0°S	86
Toricelli R	29.0°E	6.0°S	30
Capella CA	36.0°E	6.5°S	85
Capella D	39.0°E	6.5°S	75
Gutenberg G	40.5°E	6.0°S	43
M. Fecunditatis	42.5°E	6.0°S	100

Table 34. Summary of Lunar remanent magnetic field. From [Dyal et al., 1972 and Lin et al., 1976].

Site	β	Final Velocity of H ⁺ (km/sec)	Final Energy of H ⁺ (eV)
Apollo 12	2.788	351.9	641.3
Apollo 14			
Site A	0.380	-561.8	1635.0
Site C'	2.178	323.1	540.7
Apollo 15	348.300	438.7	997.1
Apollo 16			
ALSEP	0.074	-1560.0	12600.0
Site 2	0.113	-1233.0	7872.0
Site 5	0.321	-639.0	2115.0
Site 13	0.038	-2221.0	25560.0
FRPS	0.315	-674.4	2171.0
Taylor Crater	10.070	417.0	900.6
Alfraganus Crater	0.584	-370.5	711.0
M. Tranquilitatis	0.544	-401.9	836.9
Toricelli R	4.464	387.2	776.4
Capella CA	0.557	-391.6	794.4
Capella D	0.716	-276.9	397.1
Gutenberg G	2.178	323.1	540.7
M. Fecunditatis	0.403	-535.2	1484.0

Table 35. The ratio of solar-wind plasma pressure to total magnetic field pressure.

Site	Oxide	[Sputtering Rate at Moon]		Metal	[Sputtering Rate at Moon]	
		Atoms/cm ² year	Å/year		Atoms/cm ² year	Å/year
Apollo 12	Al ₂ O ₃	0.91 x 10 ¹⁵	3.0	Al	0.69 x 10 ¹⁵	2.3
	CaO	1.61 "	5.3	Ca	1.14 "	3.8
	FeO	0.72 "	2.4	Cr	0.43 "	1.4
	MgO	1.33 "	4.4	Cu	0.41 "	1.4
	MnO	0.81 "	2.7	Fe	0.40 "	1.3
	TiO ₂	0.83 "	2.8	K	2.18 "	7.2
				Mg	1.61 "	5.3
				Mn	0.58 "	1.9
				Na	2.17 "	7.2
				Si	0.51 "	1.7
				Ti	0.38 "	1.3
Apollo 14 Site C' (Gutenberg G)	Al ₂ O ₃	0.91 x 10 ¹⁵	3.0	Al	0.69 x 10 ¹⁵	2.3
	CaO	1.60 "	5.3	Ca	1.11 "	3.7
	FeO	0.73 "	2.4	Cr	0.42 "	1.4
	MgO	1.33 "	4.4	Cu	0.44 "	1.5
	MnO	0.81 "	2.7	Fe	0.40 "	1.3
	TiO ₂	0.84 "	2.8	K	2.15 "	7.1
				Mg	1.59 "	5.3
				Mn	0.57 "	1.9
				Na	2.13 "	7.1
				Si	0.51 "	1.7
				Ti	0.37 "	1.2
Apollo 15	Al ₂ O ₃	0.85 x 10 ¹⁵	2.8	Al	0.72 x 10 ¹⁵	2.4
	CaO	1.59 "	5.3	Ca	1.19 "	3.9
	FeO	0.67 "	2.2	Cr	0.45 "	1.5
	MgO	1.29 "	4.3	Cu	0.32 "	1.1
	MnO	0.76 "	2.5	Fe	0.43 "	1.4
	TiO ₂	0.75 "	2.5	K	2.27 "	7.5
				Mg	1.64 "	5.5
				Mn	0.61 "	2.0
				Na	2.24 "	7.5
				Si	0.52 "	1.7
				Ti	0.40 "	1.3

Site	Oxide	[Sputtering Rate at Moon]		Metal	[Sputtering Rate at Moon]	
		Atoms/cm ² year	Å/year		Atoms/cm ² year	Å/year
Taylor Crater	Al ₂ O ₃	0.86 x 10 ¹⁵	2.9	Al	0.72 x 10 ¹⁵	2.4
	CaO	1.59 "	5.3	Ca	1.16 "	3.9
	FeO	0.68 "	2.3	Cr	0.45 "	1.5
	MgO	1.30 "	4.3	Cu	0.35 "	1.2
	MnO	0.78 "	2.6	Fe	0.42 "	1.4
	TiO ₂	0.77 "	2.6	K	2.23 "	7.4
				Mg	1.64 "	5.5
				Mn	0.61 "	2.0
				Na	2.21 "	7.3
				Si	0.52 "	1.7
				Ti	0.39 "	1.3
Toricelli R	Al ₂ O ₃	0.89 x 10 ¹⁵	2.9	Al	0.71 x 10 ¹⁵	2.4
	CaO	1.59 "	5.3	Ca	1.16 "	3.8
	FeO	0.71 "	2.4	Cr	0.44 "	1.5
	MgO	1.31 "	4.3	Cu	0.38 "	1.3
	MnO	0.76 "	2.6	Fe	0.41 "	1.4
	TiO ₂	0.79 "	2.6	K	2.22 "	7.4
				Mg	1.61 "	5.4
				Mn	0.59 "	2.0
				Na	2.18 "	7.3
				Si	0.52 "	1.7
				Ti	0.38 "	1.3

Table 36. Estimate of the sputtering rates at the lunar surface.

Energy of Incident H ⁺ (eV)	F _T	F _p
1000	0.929	0.465
900	0.921	0.461
800	0.912	0.456
700	0.899	0.450
600	0.883	0.442
500	0.871	0.436
400	0.830	0.415
300	0.778	0.389
200	0.685	0.343
100	0.463	0.232
50	0.207	0.104
10	0.0002	0.0001
1	0	0

Table 37. Calculated F_T, and F_p for aluminum bombarded by H⁺

Energy of Incident H ⁺ (eV)	F _T	F _p
1000	0.940	0.470
900	0.933	0.467
800	0.924	0.462
700	0.913	0.457
600	0.900	0.450
500	0.879	0.440
400	0.849	0.425
300	0.802	0.401
200	0.711	0.356
100	0.488	0.244
50	0.349	0.175
10	0.0002	0.0001
1	0	0

Table 38. Calculated F_T, and F_p for calcium bombarded by H⁺

Energy of Incident H ⁺ (eV)	F _T	F _p
1000	0.837	0.419
900	0.822	0.411
800	0.802	0.401
700	0.776	0.388
600	0.742	0.371
500	0.698	0.349
400	0.635	0.318
300	0.542	0.271
200	0.392	0.196
100	0.144	0.072
50	0.018	0.009
10	0	0
1	0	0

Table 39. Calculated F_T, and F_p for chromium bombarded by H⁺

Energy of Incident H ⁺ (eV)	F _T	F _p
1000	0.827	0.414
900	0.808	0.404
800	0.786	0.393
700	0.758	0.379
600	0.722	0.361
500	0.674	0.337
400	0.606	0.303
300	0.507	0.254
200	0.351	0.176
100	0.113	0.057
50	0.055	0.028
10	0	0
1	0	0

Table 40. Calculated F_T, and F_p for copper bombarded by H⁺

Energy of Incident H ⁺ (eV)	F _T	F _P
1000	0.363	0.182
900	0.319	0.160
800	0.272	0.136
700	0.219	0.110
600	0.164	0.082
500	0.109	0.055
400	0.058	0.029
300	0.020	0.010
200	0.002	0.001
100	0	0
50	0	0
10	0	0
1	0	0

Table 41. Calculated F_T, and F_P for gold bombarded by H⁺

Energy of Incident H ⁺ (eV)	F _T	F _P
1000	0.820	0.410
900	0.801	0.401
800	0.779	0.390
700	0.750	0.375
600	0.714	0.357
500	0.666	0.333
400	0.599	0.300
300	0.500	0.250
200	0.336	0.168
100	0.111	0.056
50	0.010	0.005
10	0	0
1	0	0

Table 42. Calculated F_T, and F_P for iron bombarded by H⁺

Energy of Incident H ⁺ (eV)	F _T	F _p
1000	0.969	0.485
900	0.966	0.483
800	0.961	0.481
700	0.956	0.478
600	0.948	0.474
500	0.939	0.470
400	0.923	0.462
300	0.898	0.449
200	0.849	0.425
100	0.714	0.357
50	0.497	0.249
10	0.021	0.011
1	0	0

Table 43. Calculated F_T, and F_p for magnesium bombarded by H⁺

Energy of Incident H ⁺ (eV)	F _T	F _p
1000	0.870	0.435
900	0.856	0.428
800	0.839	0.420
700	0.817	0.409
600	0.788	0.394
500	0.750	0.375
400	0.694	0.347
300	0.610	0.305
200	0.467	0.234
100	0.202	0.101
50	0.035	0.018
10	0	0
1	0	0

Table 44. Calculated F_T, and F_p for manganese bombarded by H⁺

Energy of Incident H ⁺ (eV)	F _T	F _P
1000	0.806	0.403
900	0.786	0.393
800	0.762	0.381
700	0.731	0.366
600	0.693	0.347
500	0.642	0.321
400	0.571	0.286
300	0.469	0.235
200	0.314	0.157
100	0.090	0.045
50	0.008	0.004
10	0	0
1	0	0

Table 45. Calculated F_T, and F_P for nickel bombarded by H⁺

Energy of Incident H ⁺ (eV)	F _T	F _P
1000	0.970	0.485
900	0.966	0.483
800	0.958	0.479
700	0.952	0.476
600	0.944	0.472
500	0.932	0.466
400	0.914	0.457
300	0.883	0.442
200	0.823	0.412
100	0.655	0.328
50	0.397	0.199
10	0.030	0.015
1	0	0

Table 46. Calculated F_T, and F_P for potassium bombarded by H⁺

Energy of Incident H ⁺ (eV)	F _T	F _p
1000	0.899	0.450
900	0.889	0.445
800	0.875	0.438
700	0.859	0.430
600	0.837	0.419
500	0.808	0.404
400	0.766	0.383
300	0.699	0.350
200	0.582	0.291
100	0.335	0.168
50	0.033	0.017
10	0	0
1	0	0

Table 47. Calculated F_T, and F_p for silicon bombarded by H⁺

Energy of Incident H ⁺ (eV)	F _T	F _p
1000	0.719	0.360
900	0.690	0.345
800	0.655	0.328
700	0.612	0.306
600	0.558	0.279
500	0.489	0.245
400	0.400	0.200
300	0.282	0.141
200	0.138	0.069
100	0.026	0.013
50	0.0001	0.00005
10	0	0
1	0	0

Table 48. Calculated F_T, and F_p for silver bombarded by H⁺

Energy of Incident H ⁺ (eV)	F _T	F _P
1000	0.978	0.489
900	0.976	0.488
800	0.973	0.487
700	0.968	0.484
600	0.964	0.482
500	0.955	0.478
400	0.945	0.473
300	0.927	0.464
200	0.890	0.445
100	0.785	0.393
50	0.603	0.302
10	0.058	0.029
1	0	0

Table 49. Calculated F_T, and F_P for sodium bombarded by H⁺

Energy of Incident H ⁺ (eV)	F _T	F _P
1000	0.827	0.414
900	0.810	0.405
800	0.788	0.394
700	0.761	0.381
600	0.727	0.364
500	0.680	0.340
400	0.616	0.308
300	0.521	0.261
200	0.371	0.186
100	0.130	0.065
50	0.015	0.008
10	0	0
1	0	0

Table 50. Calculated F_T, and F_P for titanium bombarded by H⁺

Energy of Incident H ⁺ (eV)	F _T	F _P
1000	0.915	0.458
900	0.905	0.453
800	0.892	0.446
700	0.876	0.438
600	0.854	0.427
500	0.824	0.412
400	0.780	0.390
300	0.709	0.355
200	0.579	0.290
100	0.300	0.150
50	0.073	0.037
10	0	0
1	0	0

Table 51. Calculated F_T, and F_P for zinc bombarded by H⁺

Energy of Incident H ⁺ (eV)	F _T	F _P
1000	0.966	0.483
900	0.962	0.481
800	0.956	0.478
700	0.950	0.475
600	0.942	0.471
500	0.931	0.466
400	0.915	0.458
300	0.888	0.444
200	0.836	0.418
100	0.697	0.349
50	0.481	0.241
10	0.026	0.013
1	0	0

Table 52. Calculated F_T, and F_P for oxygen bombarded by H⁺

Energy of Incident H ⁺ (eV)	F _T	F _p
1000	0.428	0.214
900	0.388	0.194
800	0.343	0.172
700	0.292	0.146
600	0.236	0.118
500	0.174	0.087
400	0.111	0.056
300	0.051	0.026
200	0.011	0.006
100	0	0
50	0	0
10	0	0
1	0	0

Table 53. Calculated F_T, and F_p for Al₂O₃ bombarded by H⁺

Energy of Incident H ⁺ (eV)	F _T	F _p
1000	0.686	0.343
900	0.657	0.329
800	0.623	0.312
700	0.581	0.291
600	0.531	0.266
500	0.466	0.233
400	0.383	0.192
300	0.276	0.138
200	0.142	0.071
100	0.019	0.010
50	0.0003	0.00015
10	0	0
1	0	0

Table 54. Calculated F_T, and F_p for CaO bombarded by H⁺

Energy of Incident H ⁺ (eV)	F _T	F _P
1000	0.474	0.237
900	0.435	0.218
800	0.391	0.196
700	0.341	0.171
600	0.284	0.142
500	0.220	0.110
400	0.149	0.075
300	0.078	0.039
200	0.021	0.011
100	0.0004	0.0002
50	0	0
10	0	0
1	0	0

Table 55. Calculated F_T, and F_P for FeO bombarded by H⁺

Energy of Incident H ⁺ (eV)	F _T	F _P
1000	0.138	0.069
900	0.110	0.055
800	0.082	0.041
700	0.056	0.028
600	0.034	0.017
500	0.017	0.009
400	0.006	0.003
300	0.001	0.0005
200	0	0
100	0	0
50	0	0
10	0	0
1	0	0

Table 56. Calculated F_T, and F_P for Fe₂O₃ bombarded by H⁺

Energy of Incident H ⁺ (eV)	F _T	F _P
1000	0.046	0.023
900	0.032	0.016
800	0.020	0.010
700	0.011	0.006
600	0.005	0.003
500	0.002	0.001
400	0.001	0.0005
300	0.0003	0.00015
200	0	0
100	0	0
50	0	0
10	0	0
1	0	0

Table 57. Calculated F_T, and F_P for Fe₃O₄ bombarded by H⁺

Energy of Incident H ⁺ (eV)	F _T	F _P
1000	0.776	0.388
900	0.754	0.377
800	0.727	0.364
700	0.694	0.347
600	0.653	0.327
500	0.599	0.300
400	0.526	0.263
300	0.423	0.212
200	0.272	0.136
100	0.072	0.036
50	0.005	0.0025
10	0	0
1	0	0

Table 58. Calculated F_T, and F_P for MgO bombarded by H⁺

Energy of Incident H ⁺ (eV)	F _T	F _p
1000	0.547	0.274
900	0.511	0.256
800	0.469	0.235
700	0.420	0.210
600	0.362	0.181
500	0.294	0.147
400	0.215	0.108
300	0.127	0.064
200	0.043	0.022
100	0.002	0.001
50	0	0
10	0	0
1	0	0

Table 59. Calculated F_T, and F_p for MnO bombarded by H⁺

Energy of Incident H ⁺ (eV)	F _T	F _p
1000	0.514	0.257
900	0.476	0.238
800	0.433	0.217
700	0.383	0.192
600	0.325	0.163
500	0.257	0.129
400	0.175	0.088
300	0.095	0.048
200	0.030	0.015
100	0.001	0.0005
50	0	0
10	0	0
1	0	0

Table 60. Calculated F_T, and F_p for TiO₂ bombarded by H⁺

Site	Oxide	[Loss Rate]		Metal	[Loss Rate]	
		Atoms/cm ² year	Å/year		Atoms/cm ² year	Å/year
Apollo 12	Al ₂ O ₃	0.12 x 10 ¹⁵	0.40	Al	0.31 x 10 ¹⁵	1.02
	CaO	0.45 "	1.48	Ca	0.52 "	1.71
	FeO	0.11 "	0.37	Cr	0.16 "	0.54
	MgO	0.45 "	1.98	Cu	0.15 "	0.50
	MnO	0.16 "	0.52	Fe	0.15 "	0.48
	TiO ₂	0.15 "	0.48	K	1.03 "	3.43
				Mg	0.77 "	2.54
				Mn	0.23 "	0.77
				Na	1.05 "	3.48
				Si	0.22 "	0.72
				Ti	0.14 "	0.49
Apollo 14 Site C' (Gutenberg G)	Al ₂ O ₃	0.09 x 10 ¹⁵	0.30	Al	0.30 x 10 ¹⁵	1.00
	CaO	0.40 "	1.31	Ca	0.49 "	1.64
	FeO	0.09 "	0.30	Cr	0.15 "	0.50
	MgO	0.42 "	1.34	Cu	0.15 "	0.51
	MnO	0.13 "	0.44	Fe	0.14 "	0.46
	TiO ₂	0.12 "	0.40	K	1.01 "	3.34
				Mg	0.75 "	2.49
				Mn	0.22 "	0.72
				Na	0.27 "	0.91
				Si	0.21 "	0.69
				Ti	0.13 "	0.43
Apollo 15	Al ₂ O ₃	0.18 x 10 ¹⁵	0.60	Al	0.33 x 10 ¹⁵	1.11
	CaO	0.55 "	1.81	Ca	0.49 "	1.86
	FeO	0.16 "	0.53	Cr	0.19 "	0.63
	MgO	0.50 "	1.66	Cu	0.13 "	0.44
	MnO	0.21 "	0.69	Fe	0.18 "	0.59
	TiO ₂	0.19 "	0.64	K	1.10 "	3.66
				Mg	0.80 "	2.64
				Mn	0.27 "	0.88
				Na	1.10 "	3.64
				Si	0.23 "	0.77
				Ti	0.17 "	0.55

Site	Oxide	[Loss Rate]		Metal	[Loss Rate]	
		Atoms/cm ² year	Å/year		Atoms/cm ² year	Å/year
Taylor Crater	Al ₂ O ₃	0.17 x 10 ¹⁵	0.55	Al	0.33 x 10 ¹⁵	1.10
	CaO	0.52 "	1.13	Ca	0.55 "	1.81
	FeO	0.15 "	0.49	Cr	0.19 "	0.63
	MgO	0.49 "	1.63	Cu	0.14 "	0.47
	MnO	0.20 "	0.66	Fe	0.17 "	0.55
	TiO ₂	0.18 "	0.61	K	1.08 "	3.59
				Mg	0.79 "	2.62
				Mn	0.26 "	0.87
				Na	1.08 "	3.57
				Si	0.23 "	0.77
				Ti	0.16 "	0.52
Toricelli R	Al ₂ O ₃	0.15 x 10 ¹⁵	0.49	Al	0.32 x 10 ¹⁵	1.07
	CaO	0.49 "	1.62	Ca	0.53 "	1.77
	FeO	0.14 "	0.45	Cr	0.18 "	0.58
	MgO	0.47 "	1.56	Cu	0.15 "	0.49
	MnO	0.17 "	0.58	Fe	0.16 "	0.53
	TiO ₂	0.17 "	0.55	K	1.06 "	3.53
				Mg	0.77 "	2.57
				Mn	0.25 "	0.82
				Na	1.06 "	3.52
				Si	0.23 "	0.75
				Ti	0.15 "	0.49

Table 61. Sputtering rates at Moon under solar-wind bombardment.

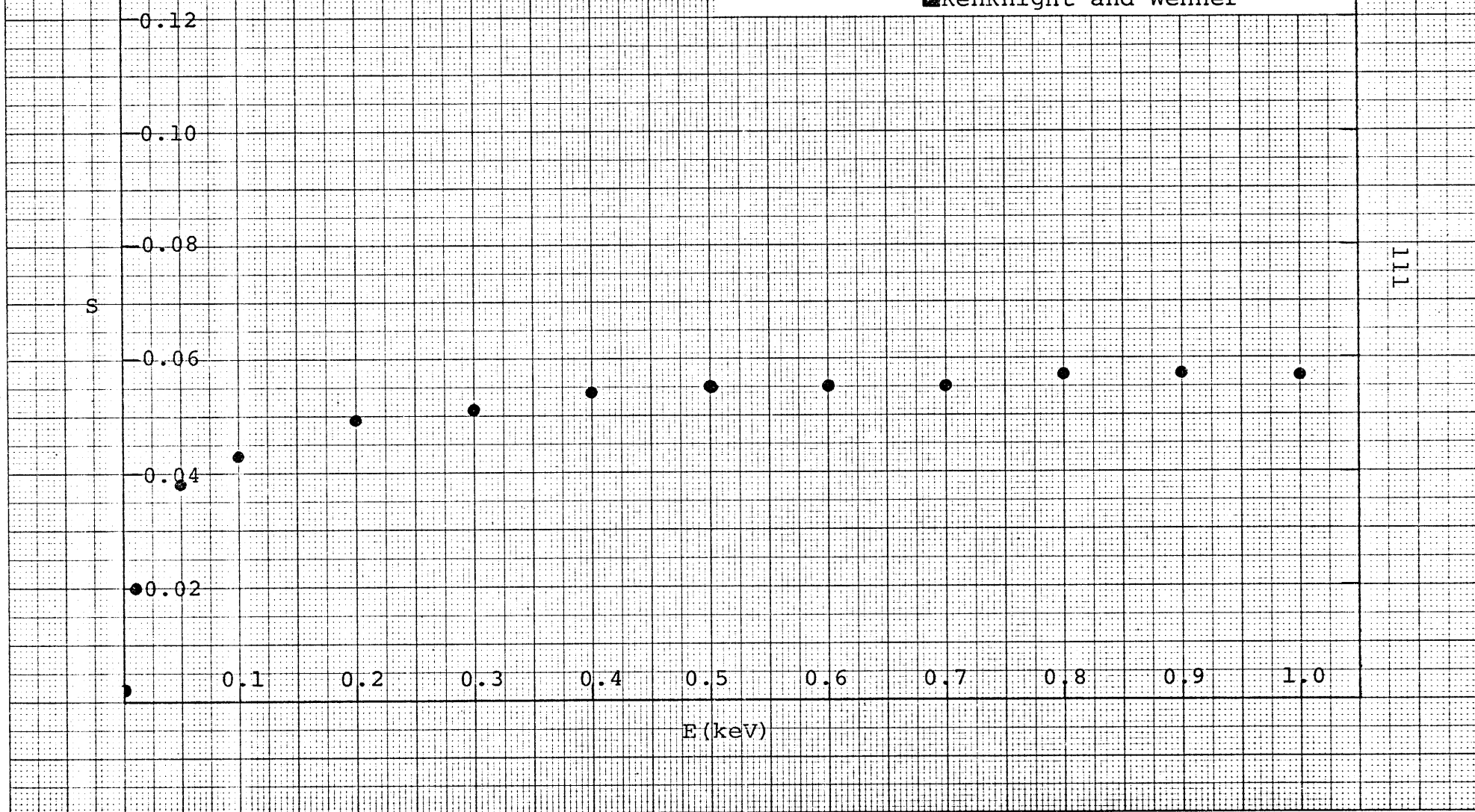
Oxide	$\Delta H_s(M)$	$\Delta H_D(O)/Y$	$\Delta H_s(M) / [\Delta H_D(O)/Y]$
Al_2O_3	76	134	0.57
CaO	36	151	0.24
FeO	84	64	1.31
MgO	33	145	0.23
SiO_2	87	104	0.84
TiO_2	106	114	0.93
Ti_2O_3	106	123	0.86
Ti_3O_5	106	117	0.91

Table 62. Comparison of $\Delta H_s(M)$ and $\Delta H_D(O)$ for some elements occurring in lunar soils. [From Pillinger et al., 1976].

FIGURES

Fig. 3. Sputtering yields for H^+ ions incident on aluminum [calculated from Eq.(25)].

■KenKnight and Wehner



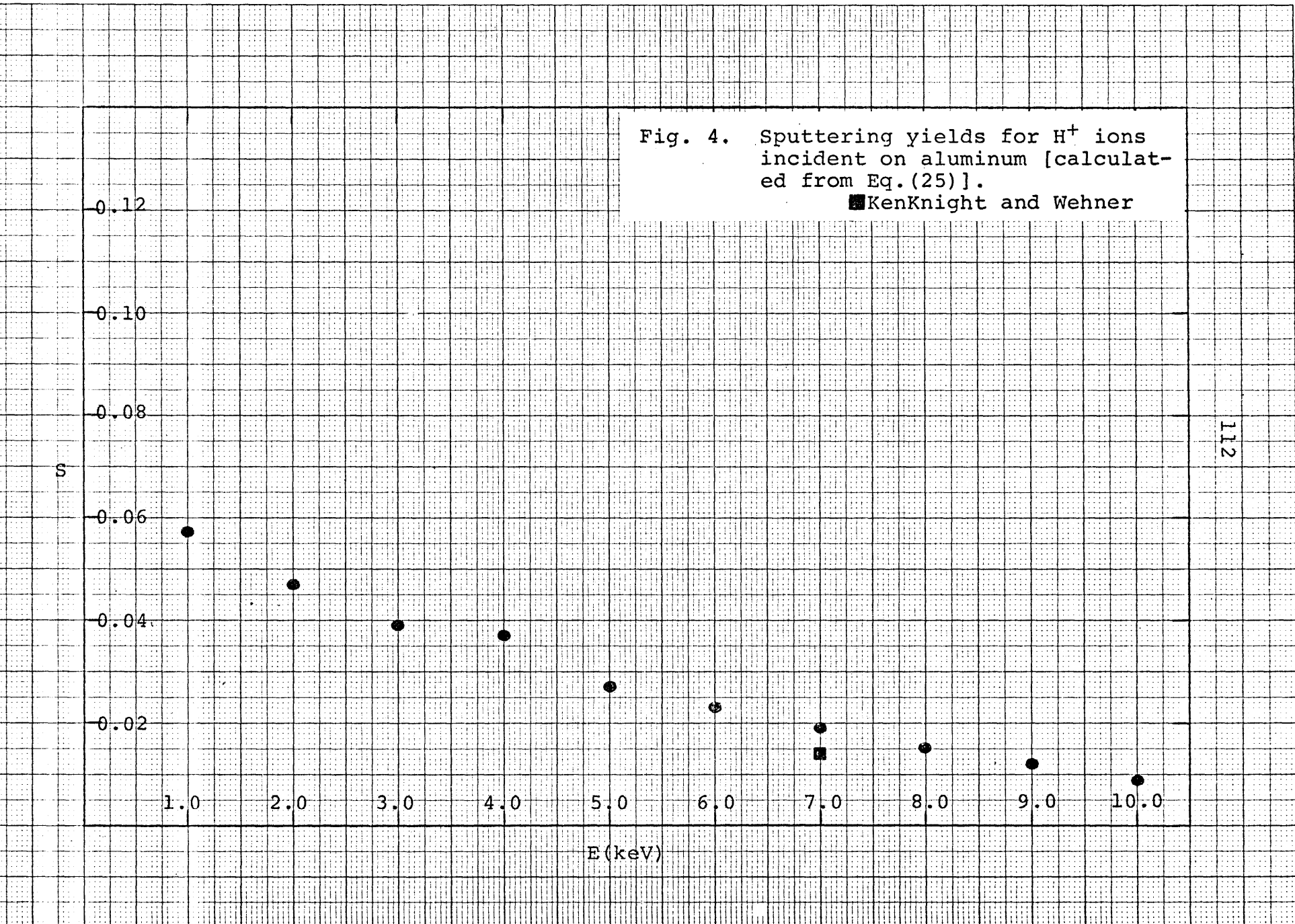


Fig. 4. Sputtering yields for H^+ ions incident on aluminum [calculated from Eq.(25)].

■ KenKnight and Wehner

Fig. 5. Sputtering yields for H^+ ions incident on calcium [calculated from Eq.(25)].

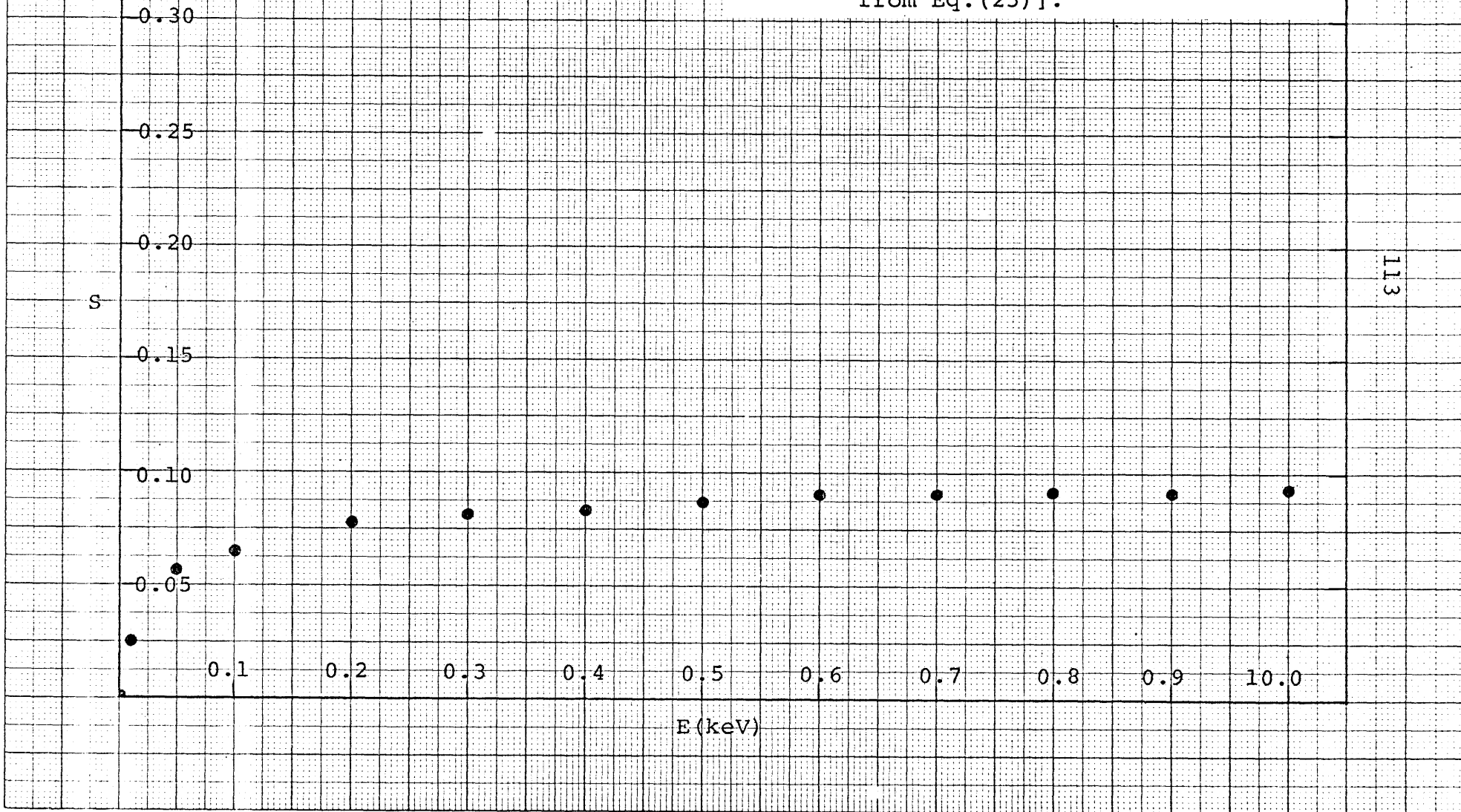


Fig. 6. Sputtering yields for H^+ ions incident on calcium [calculated from Eq.(25)].

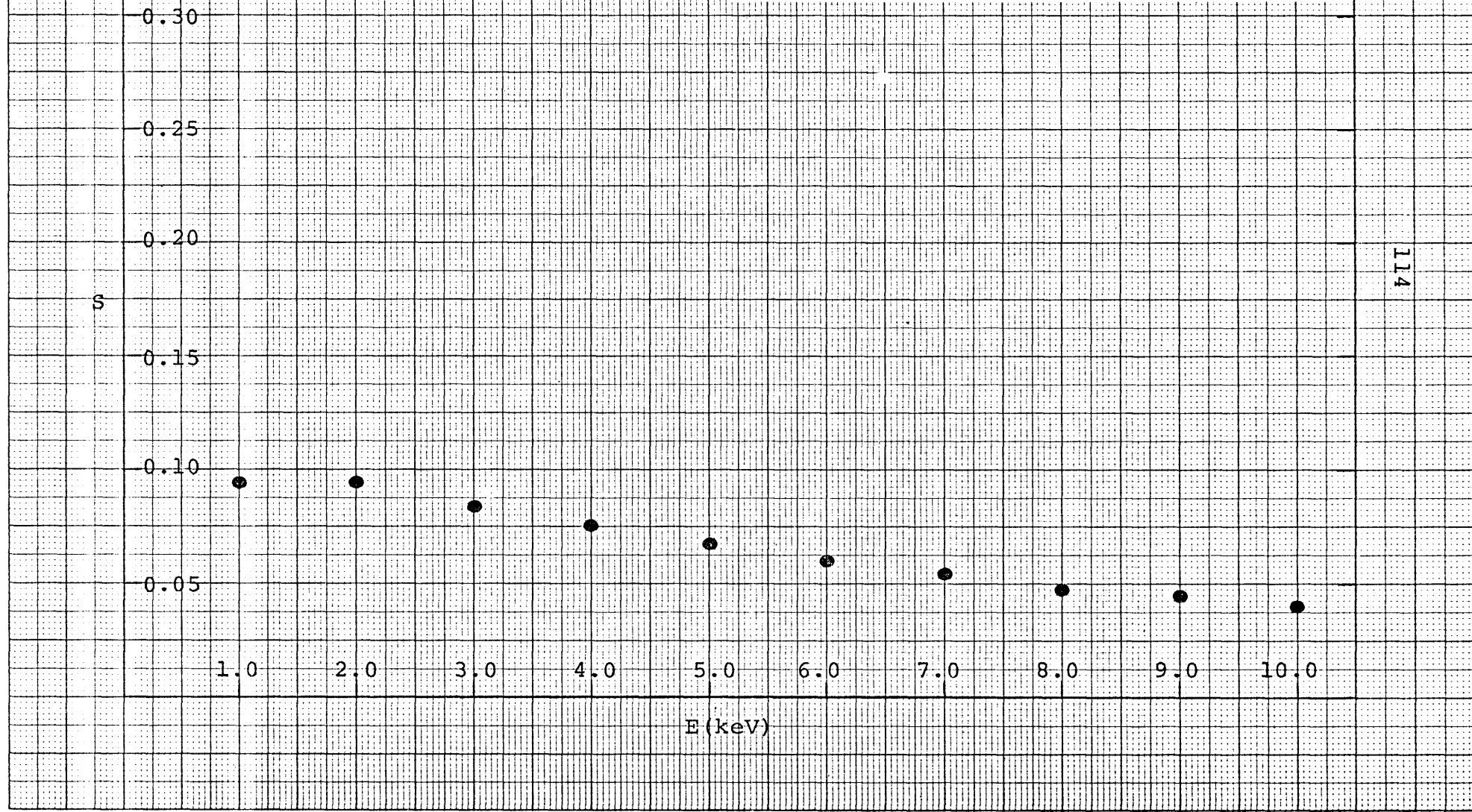


Fig. 7. Sputtering yields for H^+ ions incident on chromium [calculated from Eq. (25)].

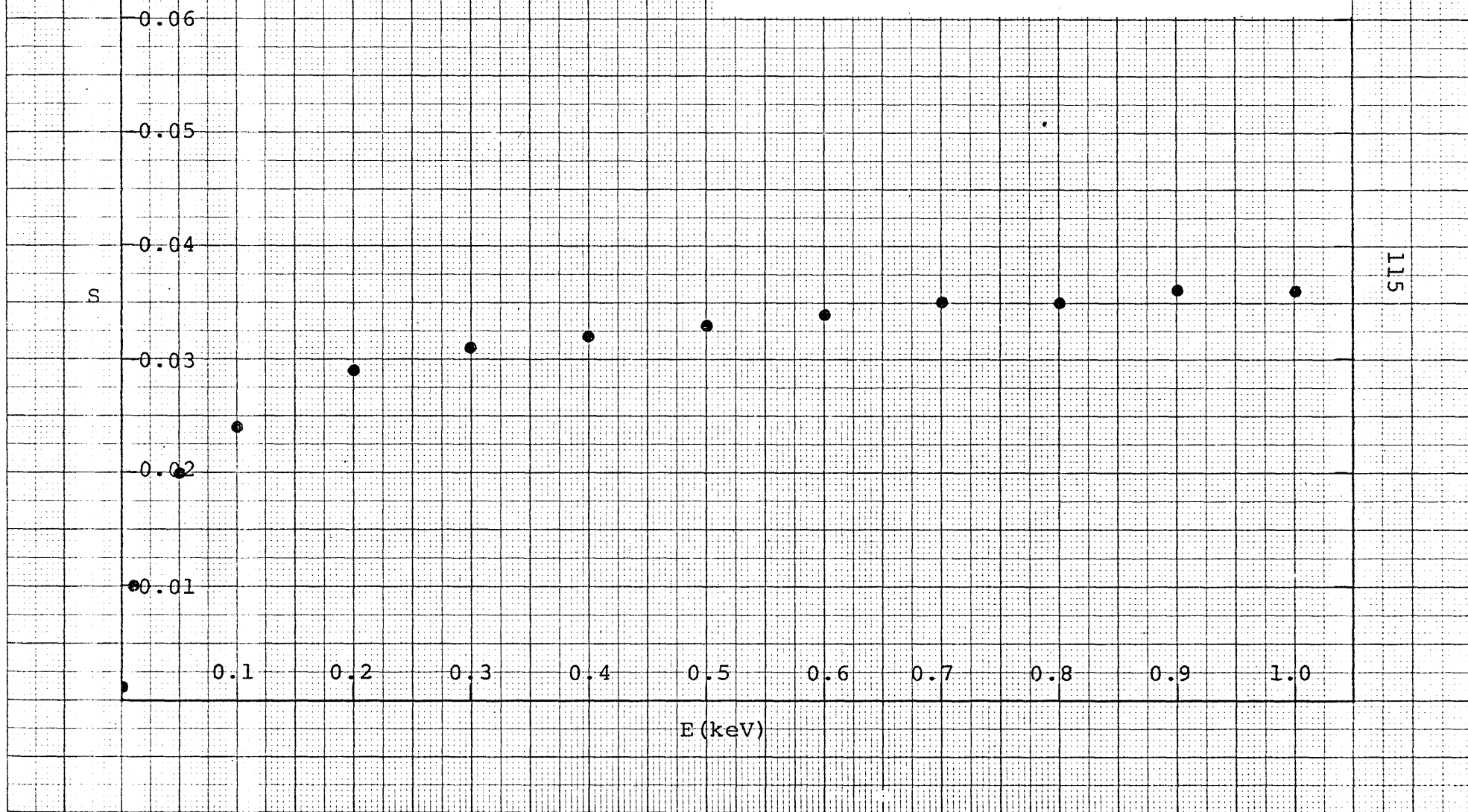


Fig. 8. Sputtering yields for H^+ ions incident on chromium [calculated from Eq.(25)].

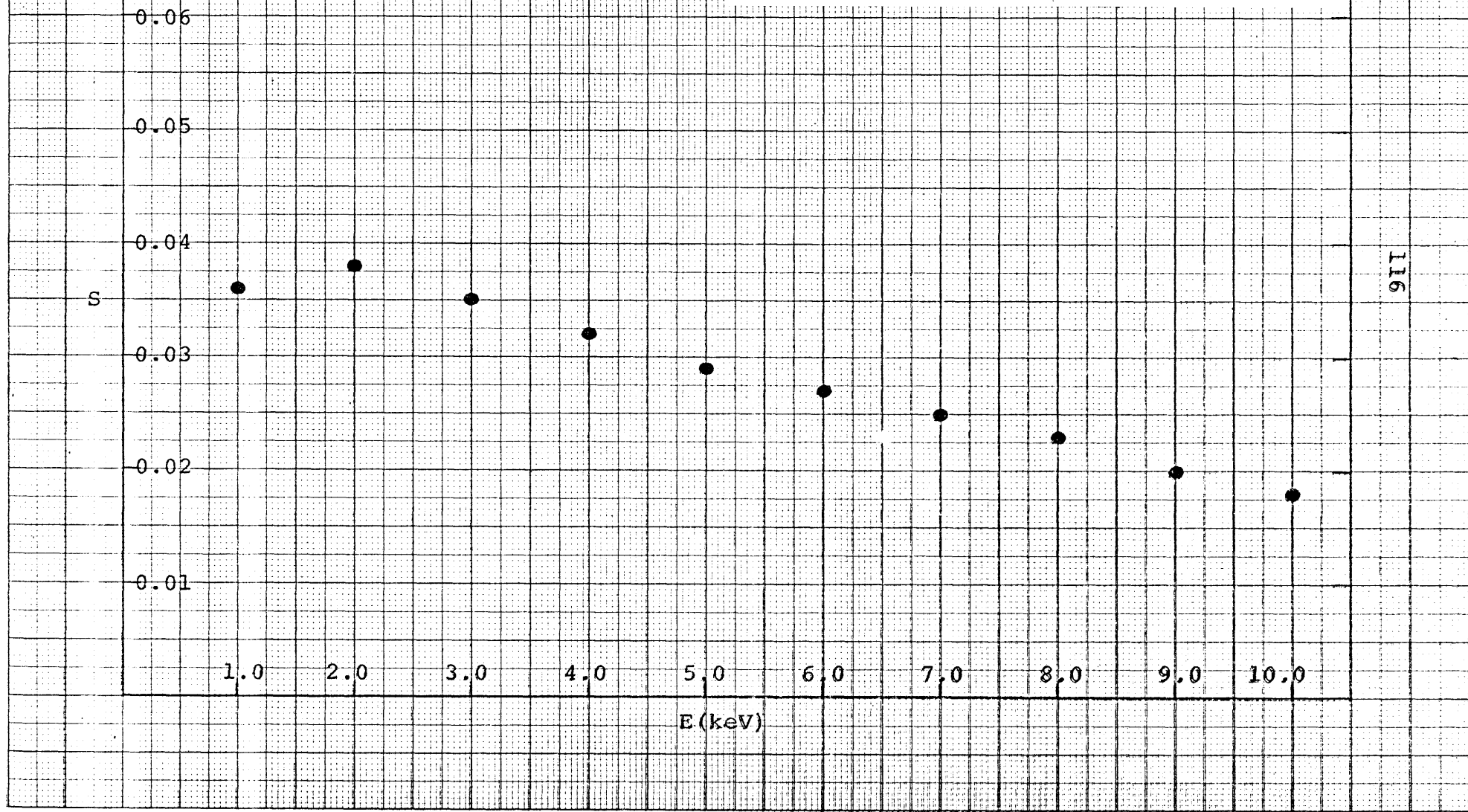


Fig. 9. Sputtering yields for H^+ ions incident on copper [calculated from Eq.(25)].

■KenKnight and Wehner

▲Wehner

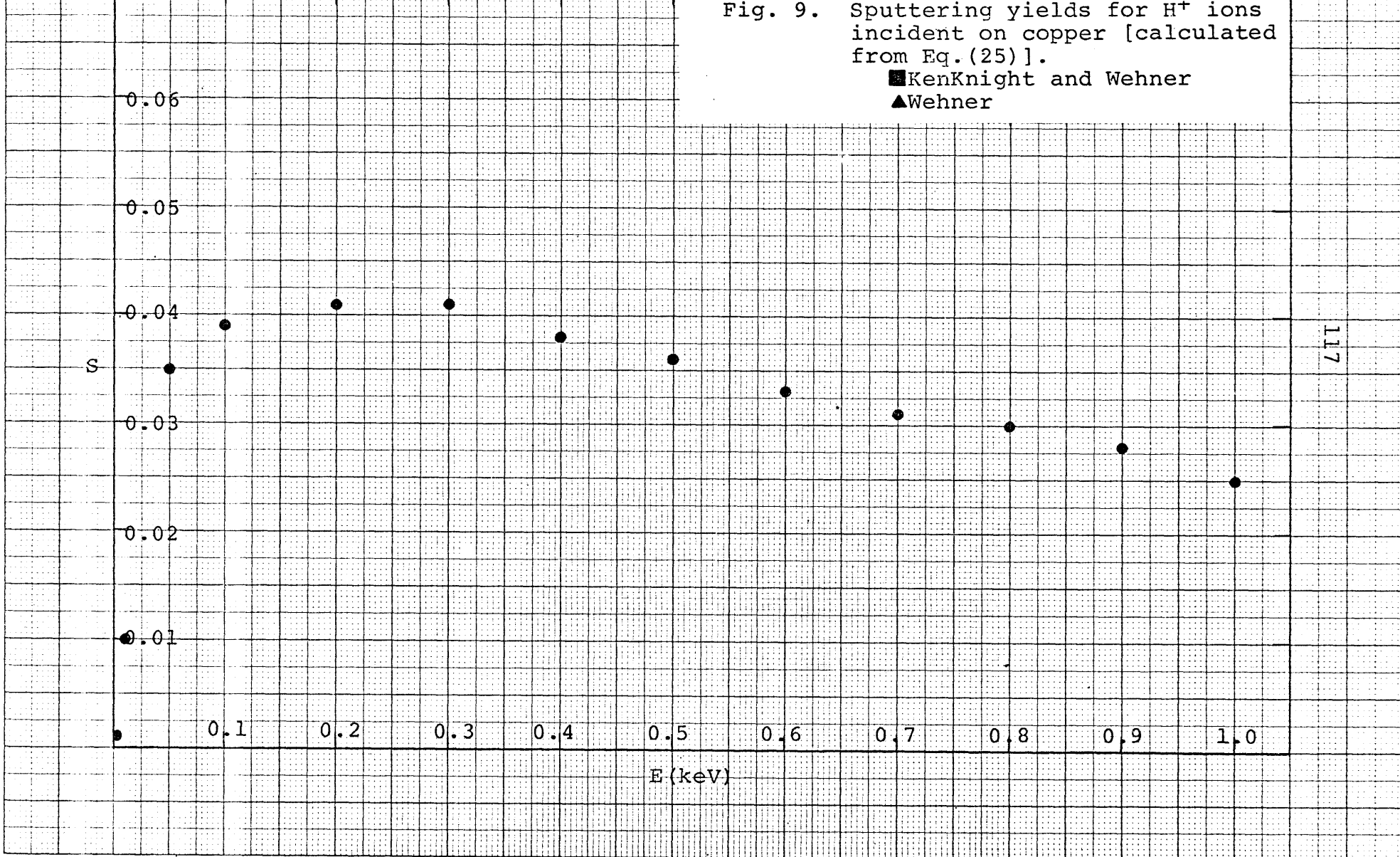


Fig. 10. Sputtering yields for H^+ ions incident on copper [calculated from Eq. (25)].

■ KenKnight and Wehner
▲ Wehner

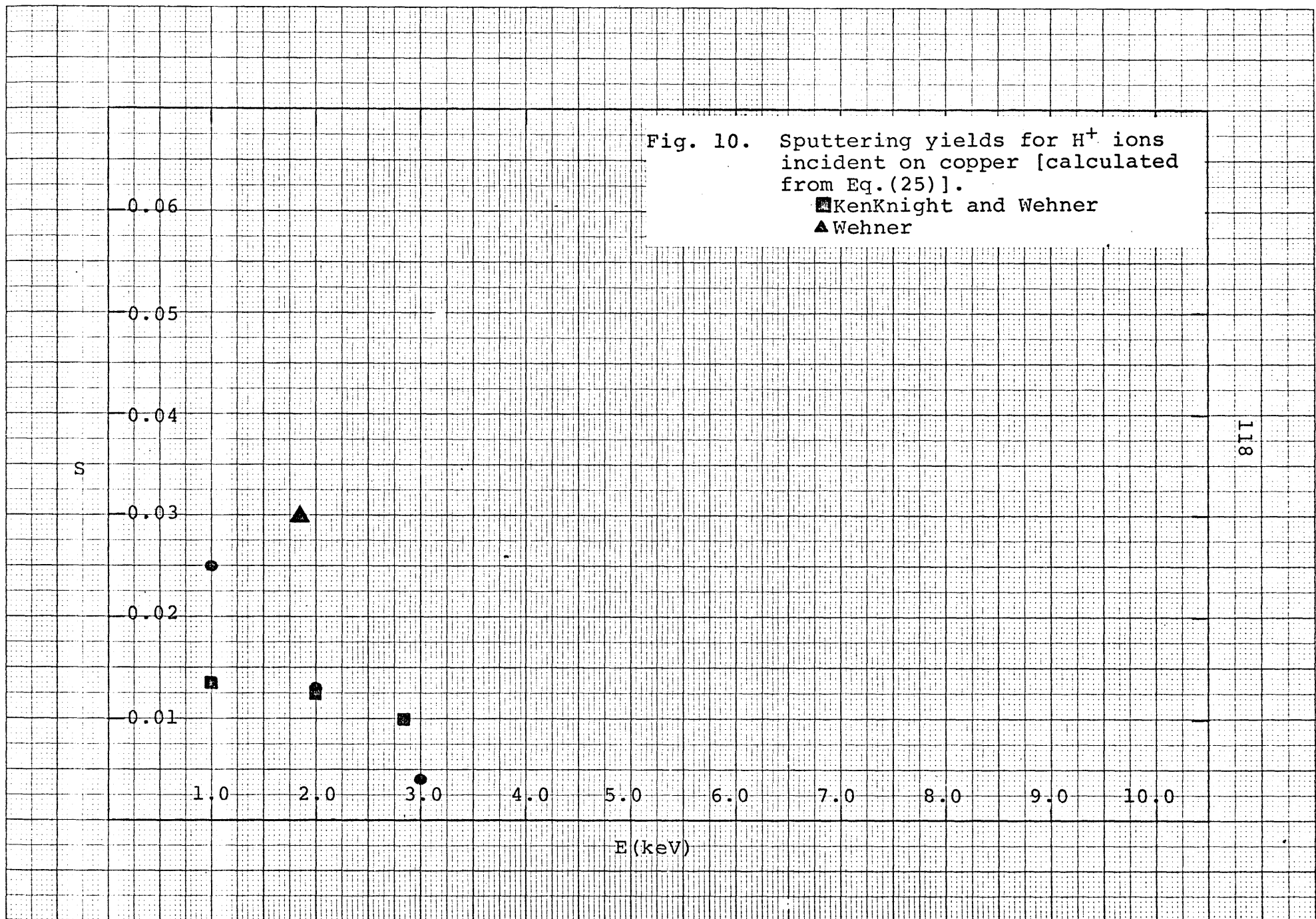


Fig. 11. Sputtering yields for H^+ ions incident on gold [calculated from Eq.(25)].

■ KenKnight and Wehner

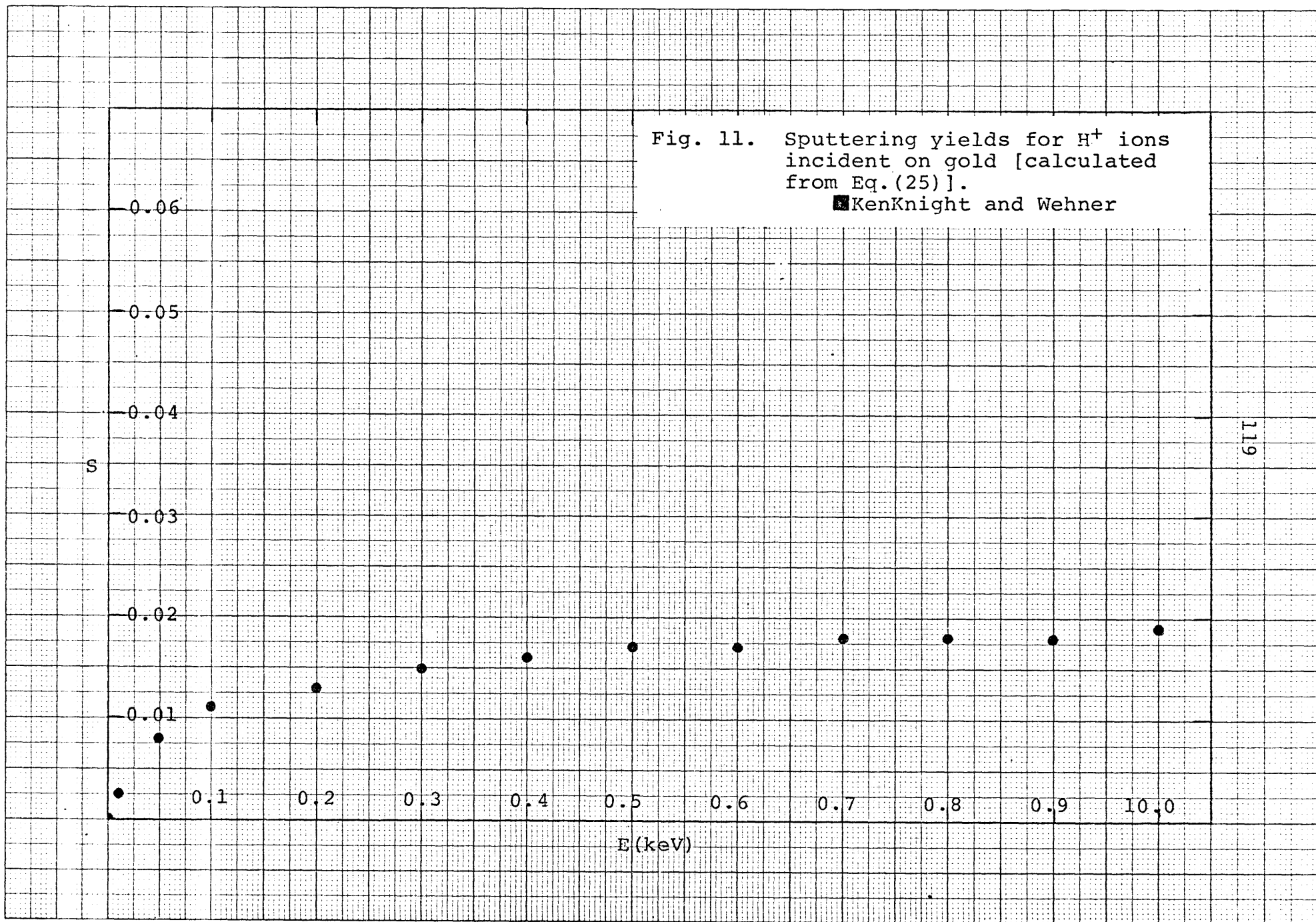


Fig. 12. Sputtering yields for H^+ ions incident on gold [calculated from Eq.(25)].

■ KenKnight and Wehner

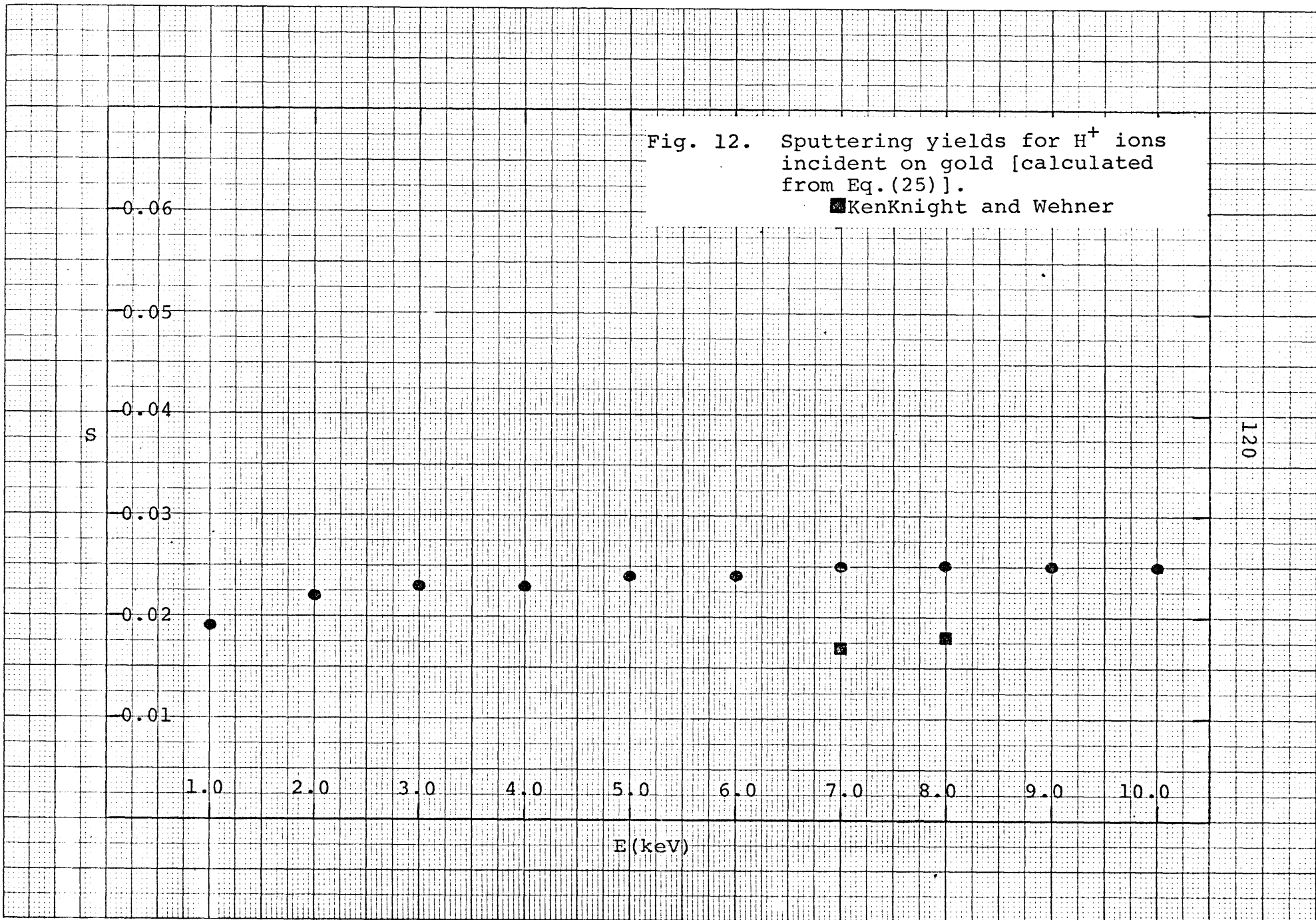


Fig. 13. Sputtering yields for H^+ ions incident on iron [calculated from Eq.(25)].

• Kenknight and Wehner

▲ Wehner

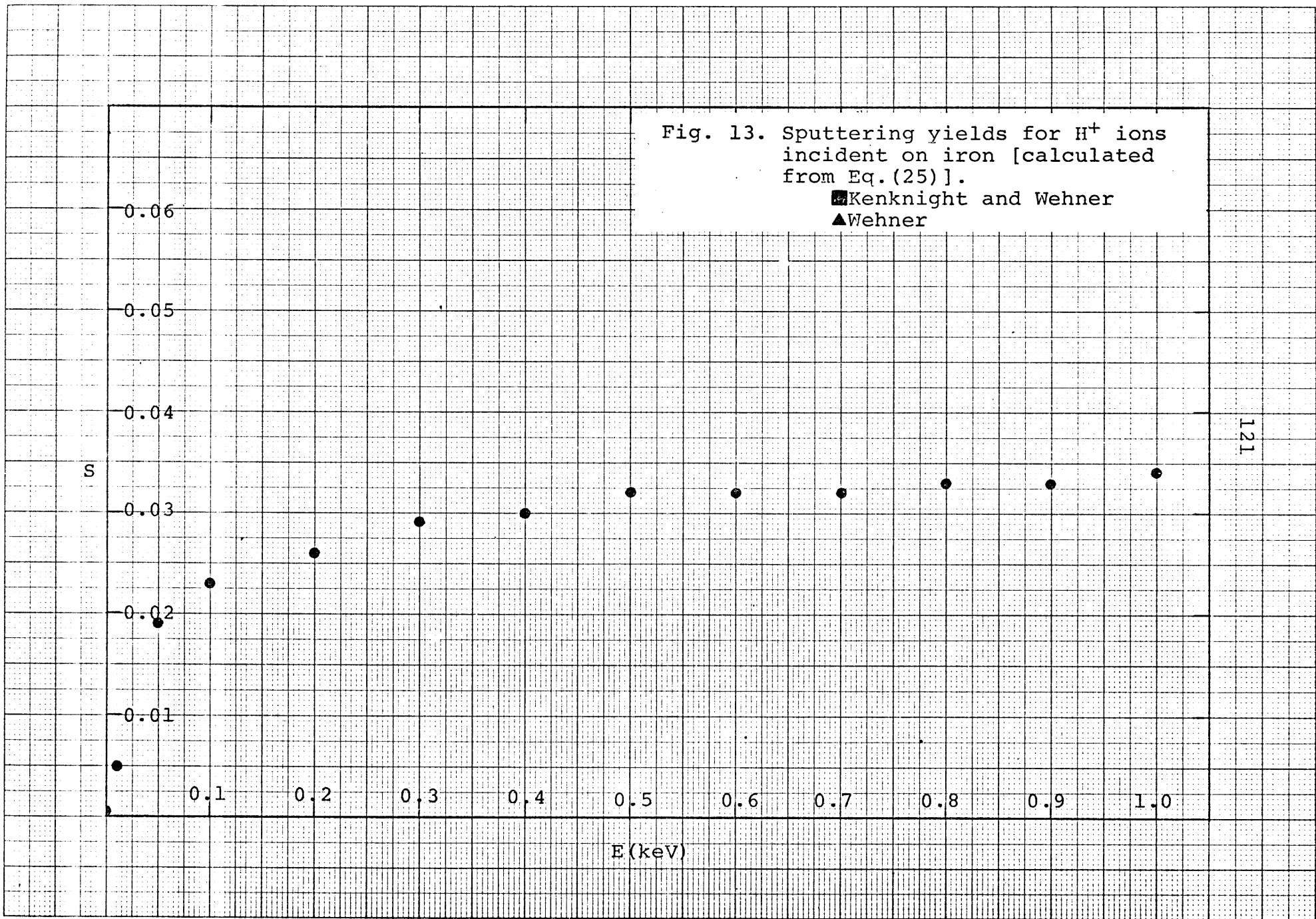


Fig. 14. Sputtering yields for H^+ ions incident on iron [calculated from Eq.(25)].

■ KenKnight and Wehner
▲ Wehner

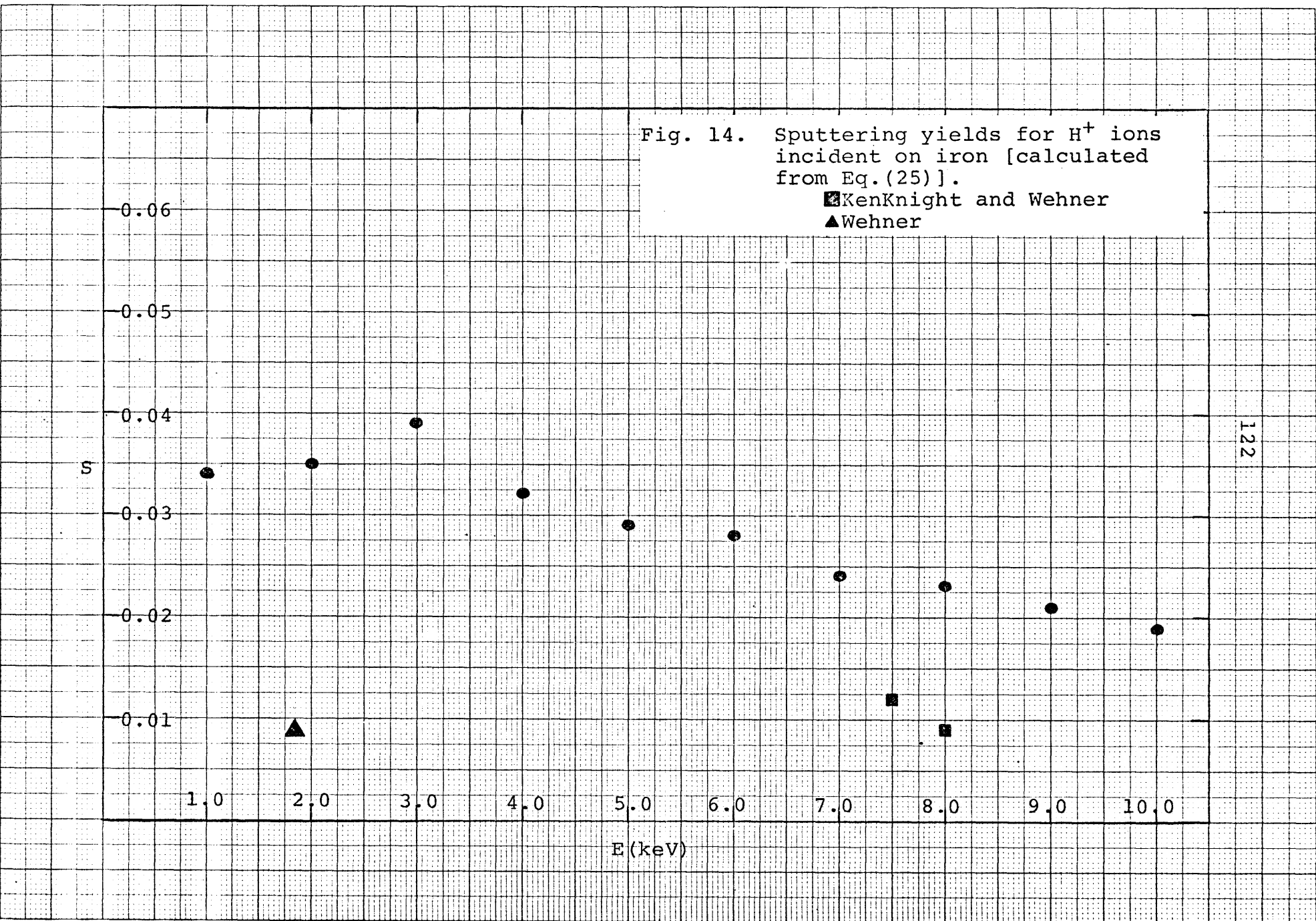


Fig. 15. Sputtering yields for H^+ ions incident on magnesium [calculated from Eq.(25)].

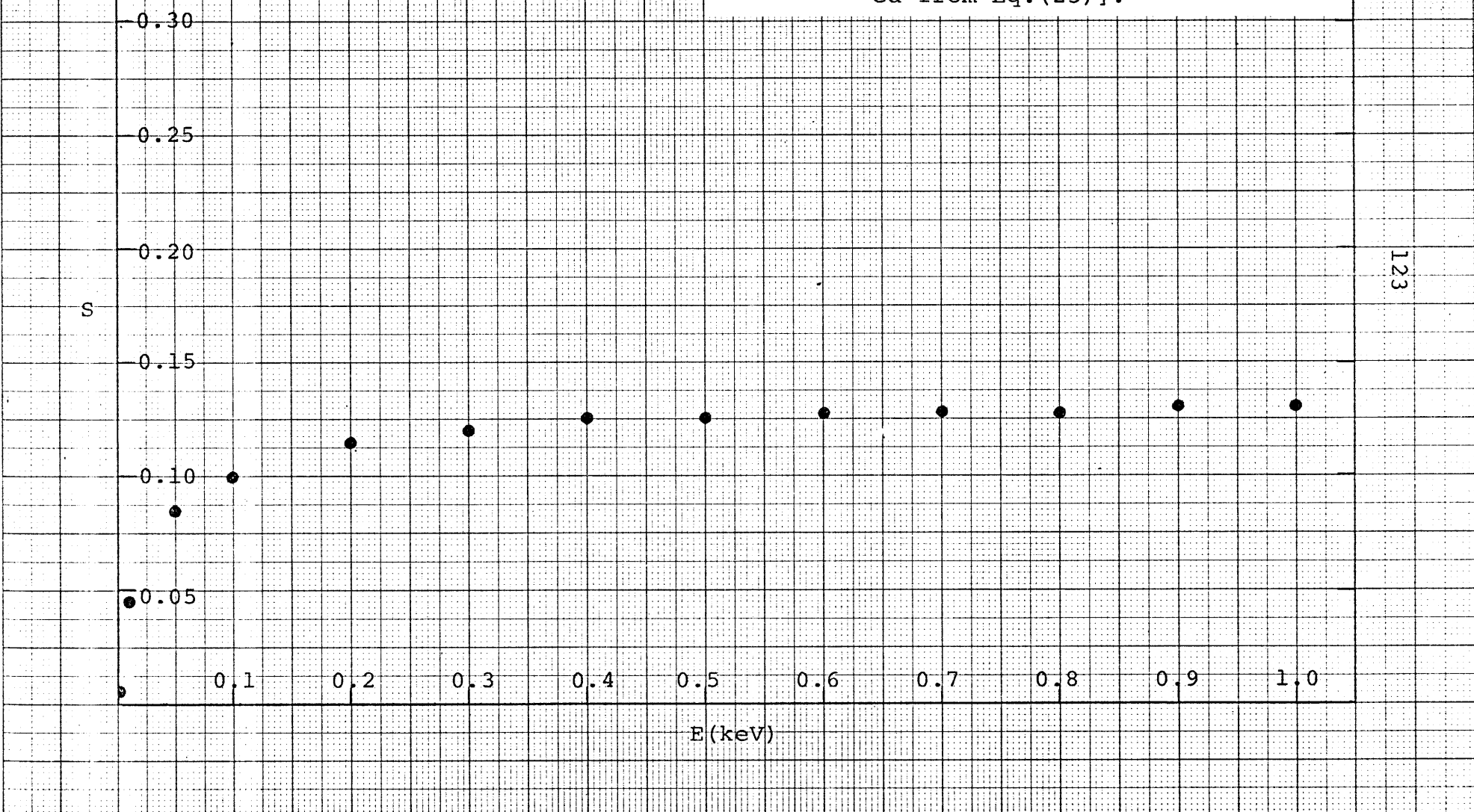


Fig. 16. Sputtering yields for H^+ ions incident on magnesium [calculated from Eq.(25)].

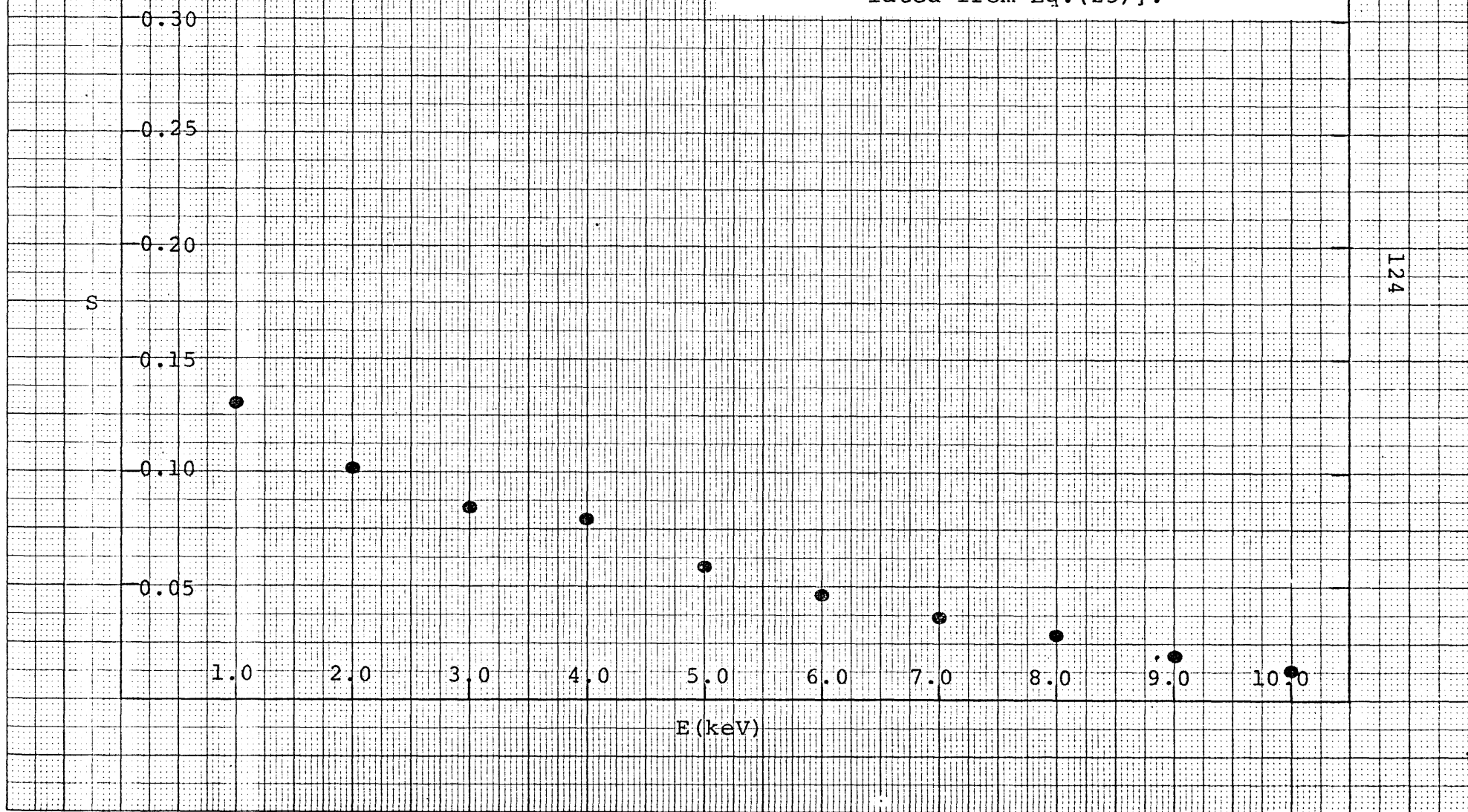


Fig. 17. Sputtering yields for H^+ ions incident on manganese [calculated from Eq. (25)].

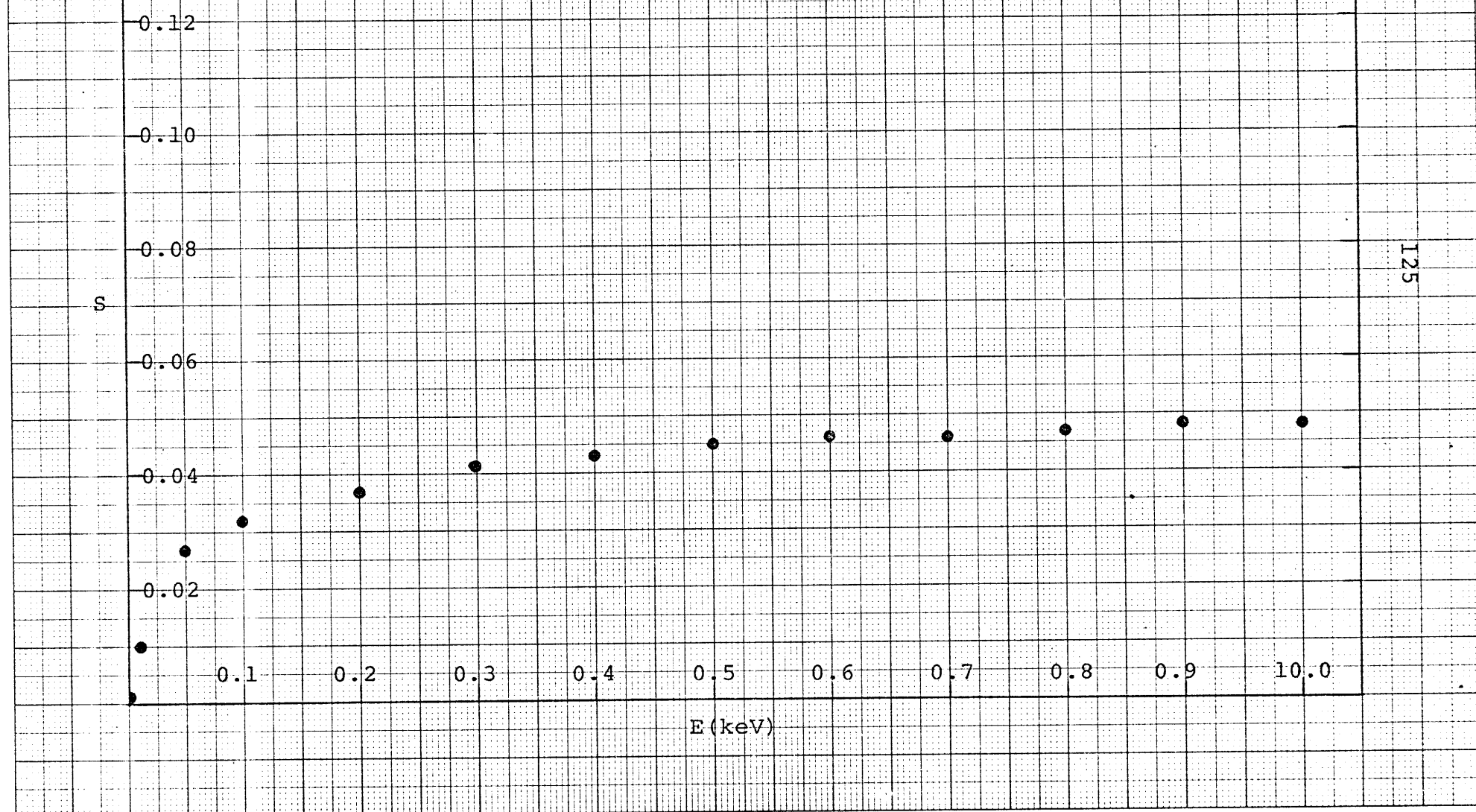


Fig. 18. Sputtering yields for H^+ ions incident on manganese [calculated from Eq.(25)].

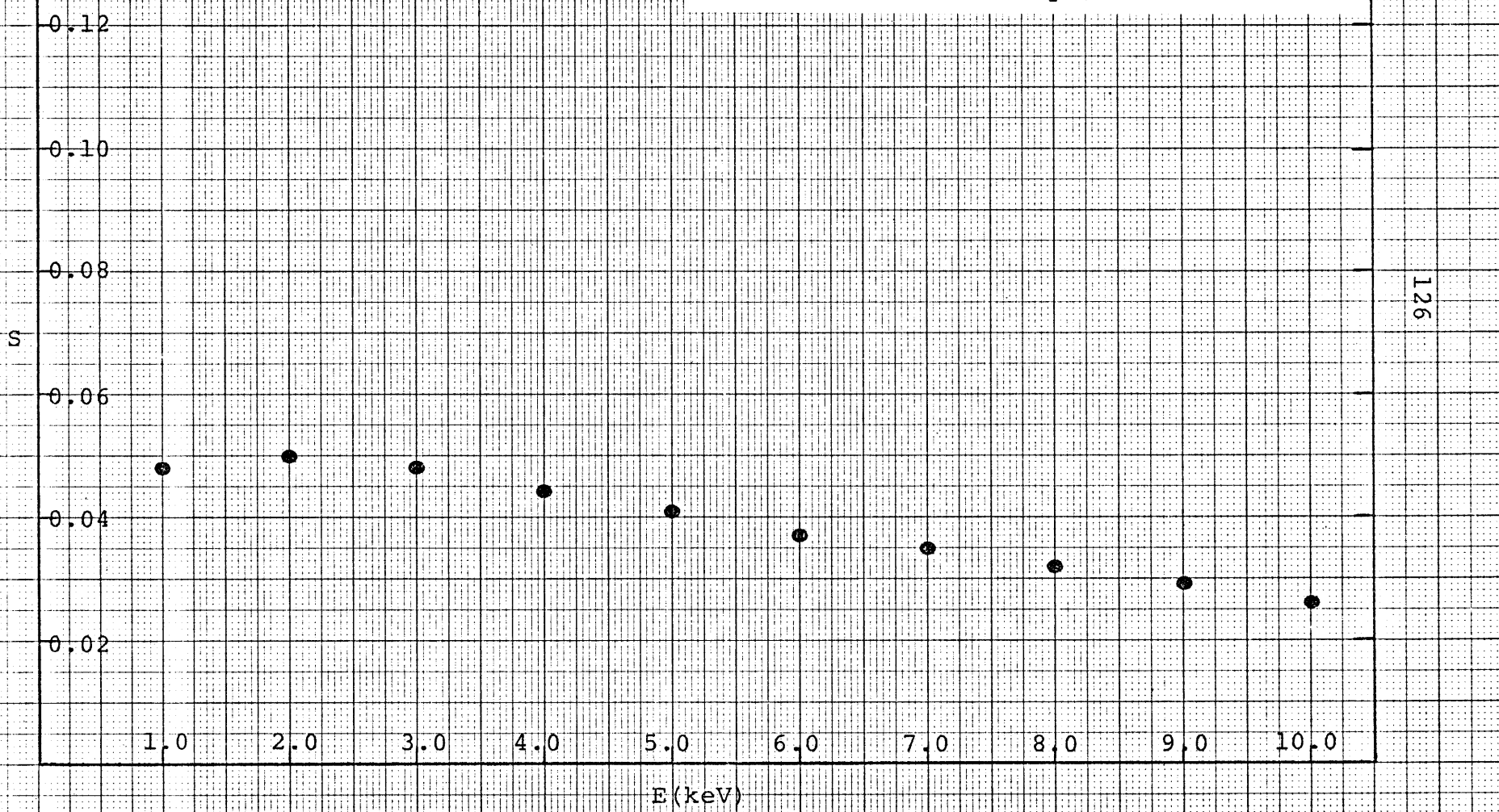


Fig. 19. Sputtering yields for H^+ ions incident on nickel [calculated from Eq. (25)].

■KenKnight and Wehner

127

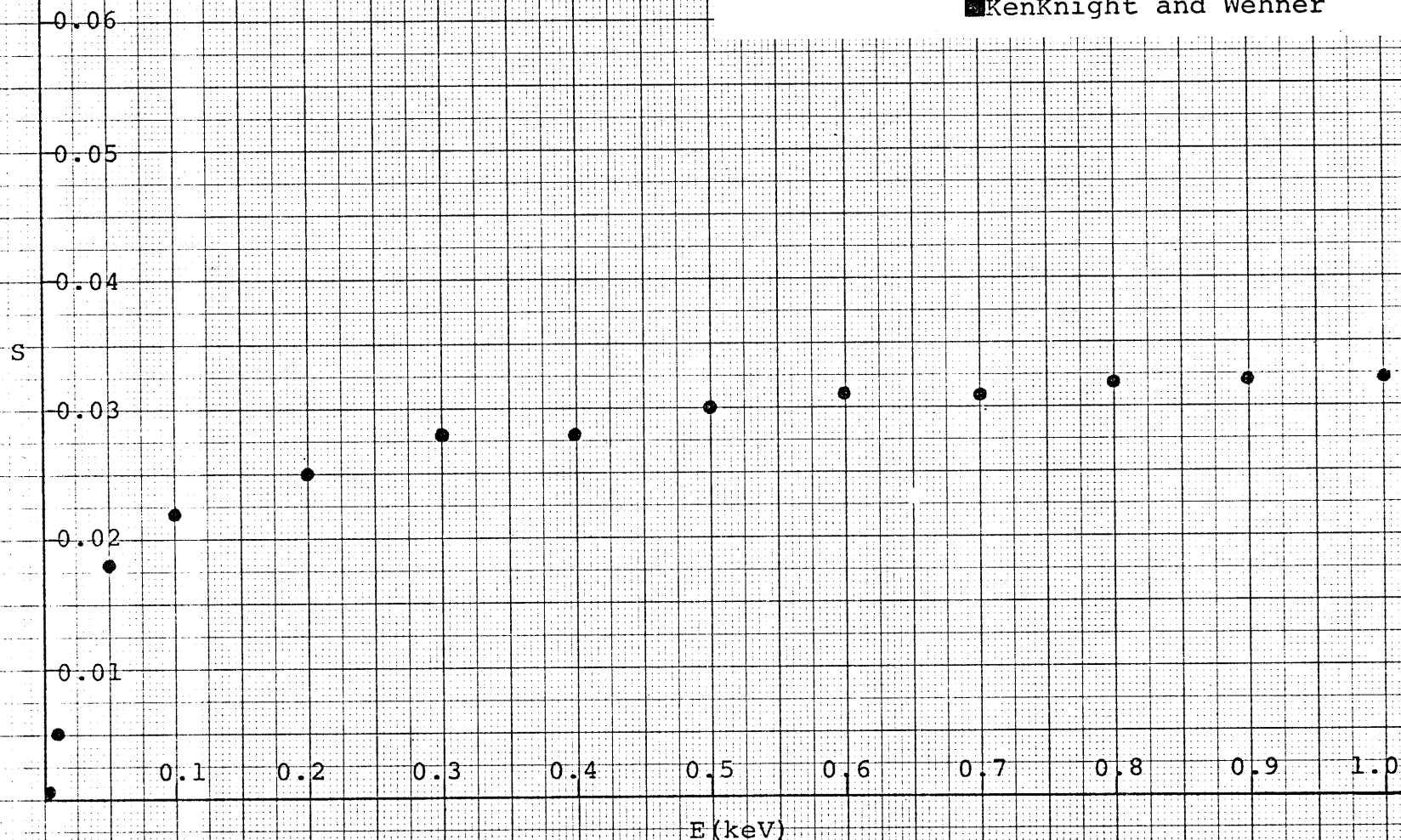


Fig. 20. Sputtering yields for H^+ ions incident on nickel [calculated from Eq. (25)].

■KenKnight and Wehner

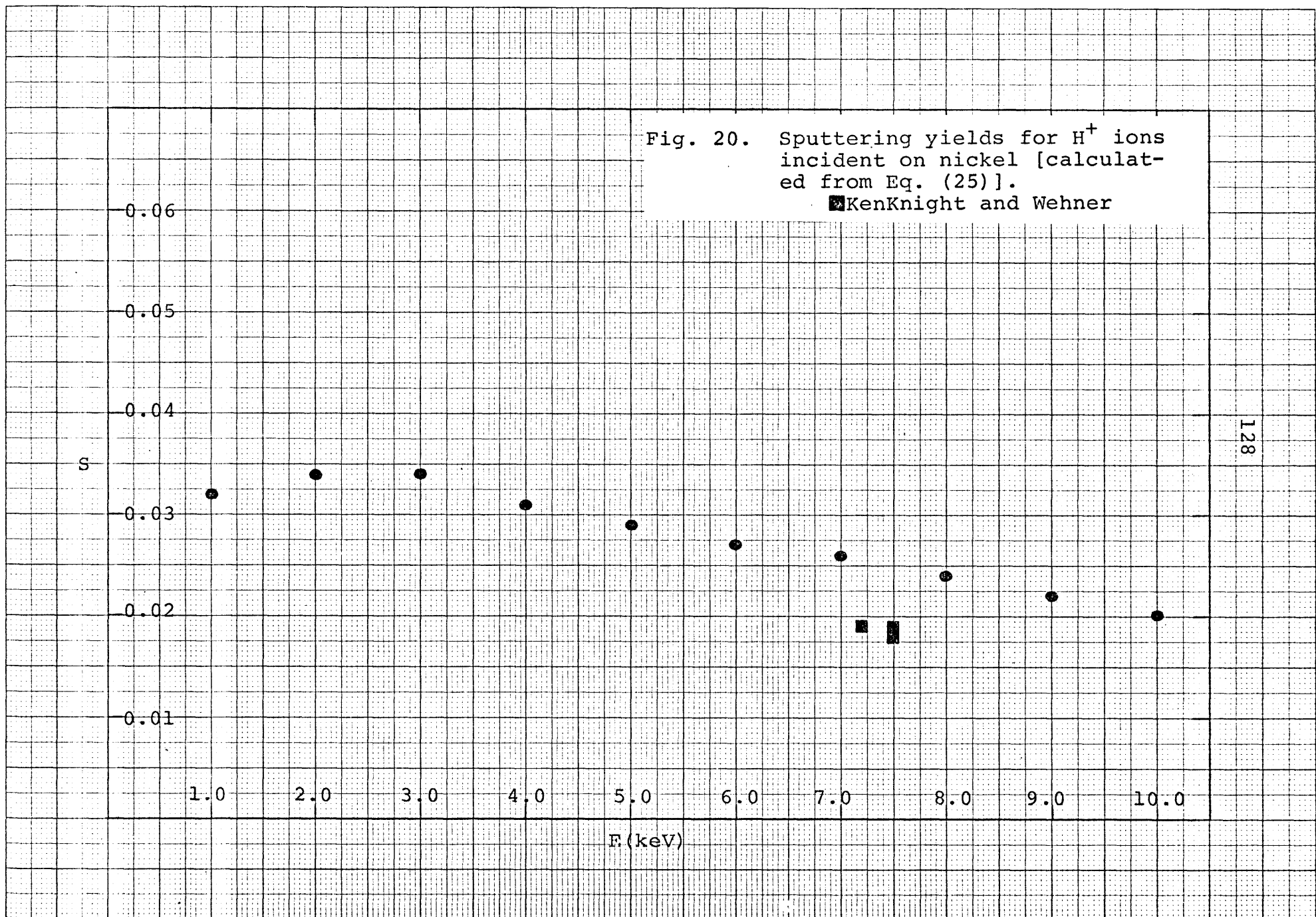


Fig. 21. Sputtering yields for H^+ ions incident on oxygen [calculated from Eq. (25)].

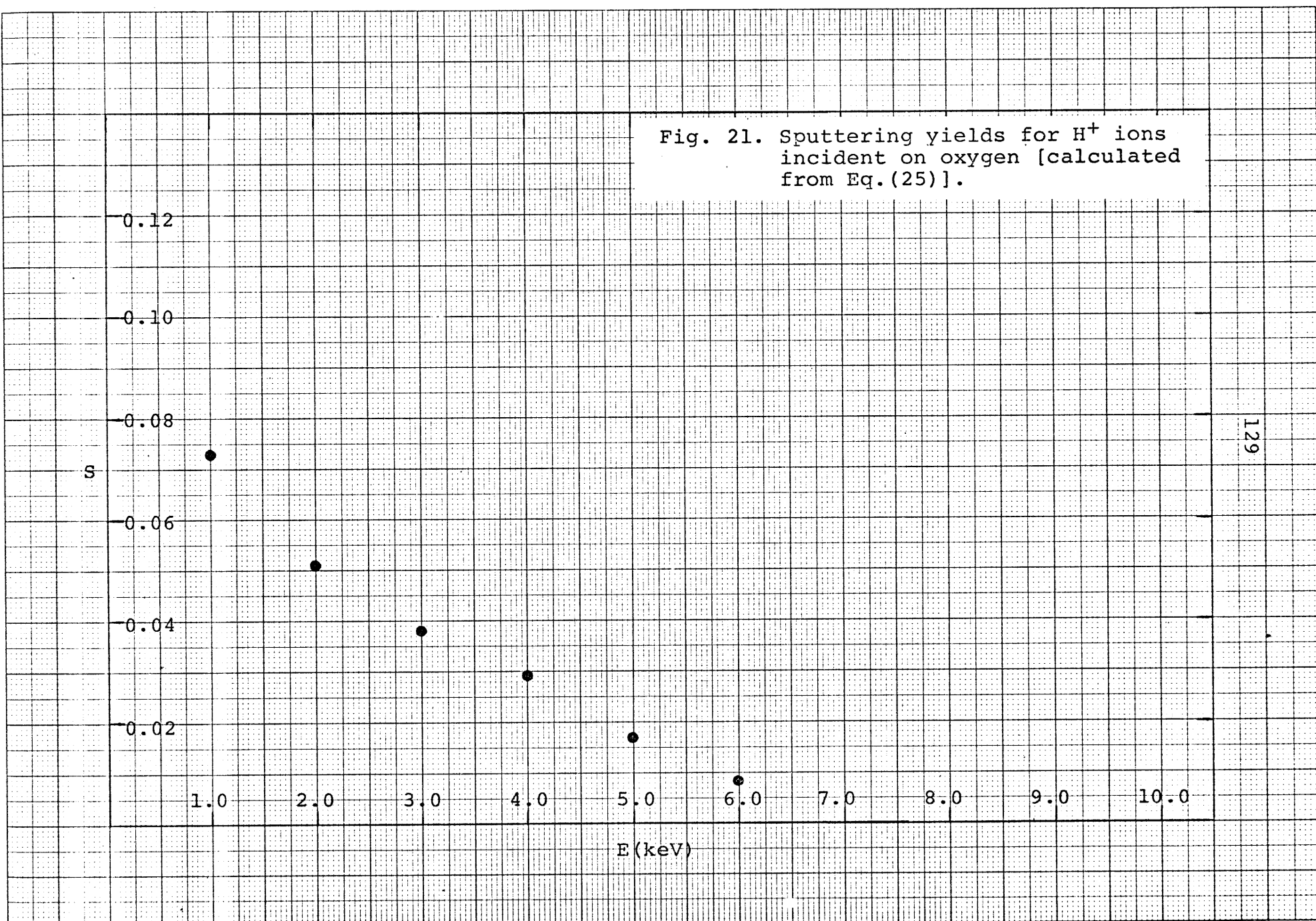


Fig. 22. Sputtering yields for H^+ ions incident on oxygen [calculated from Eq.(25)].

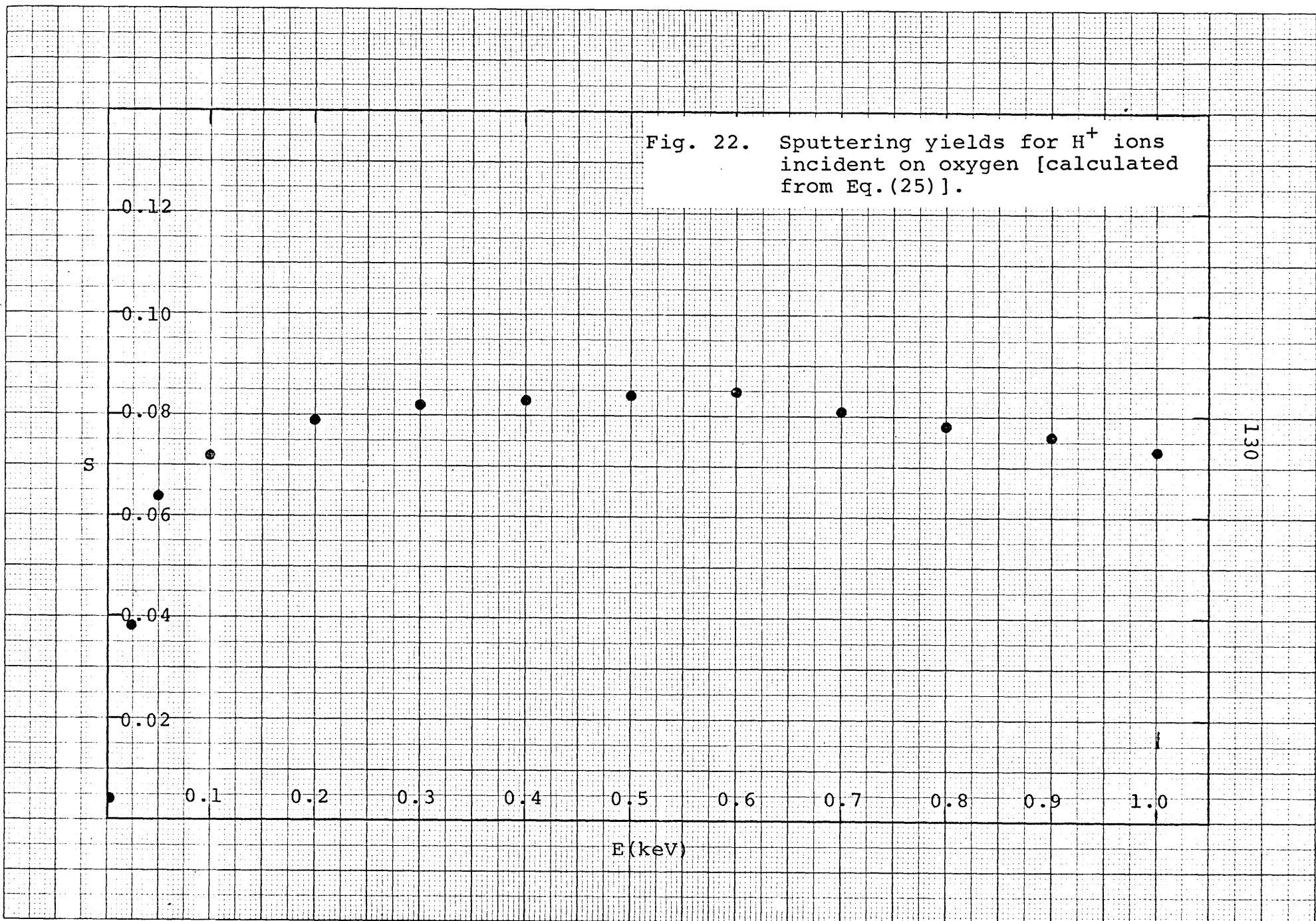


Fig. 23. Sputtering yields for H^+ ions incident on potassium [calculated from Eq. (25)].

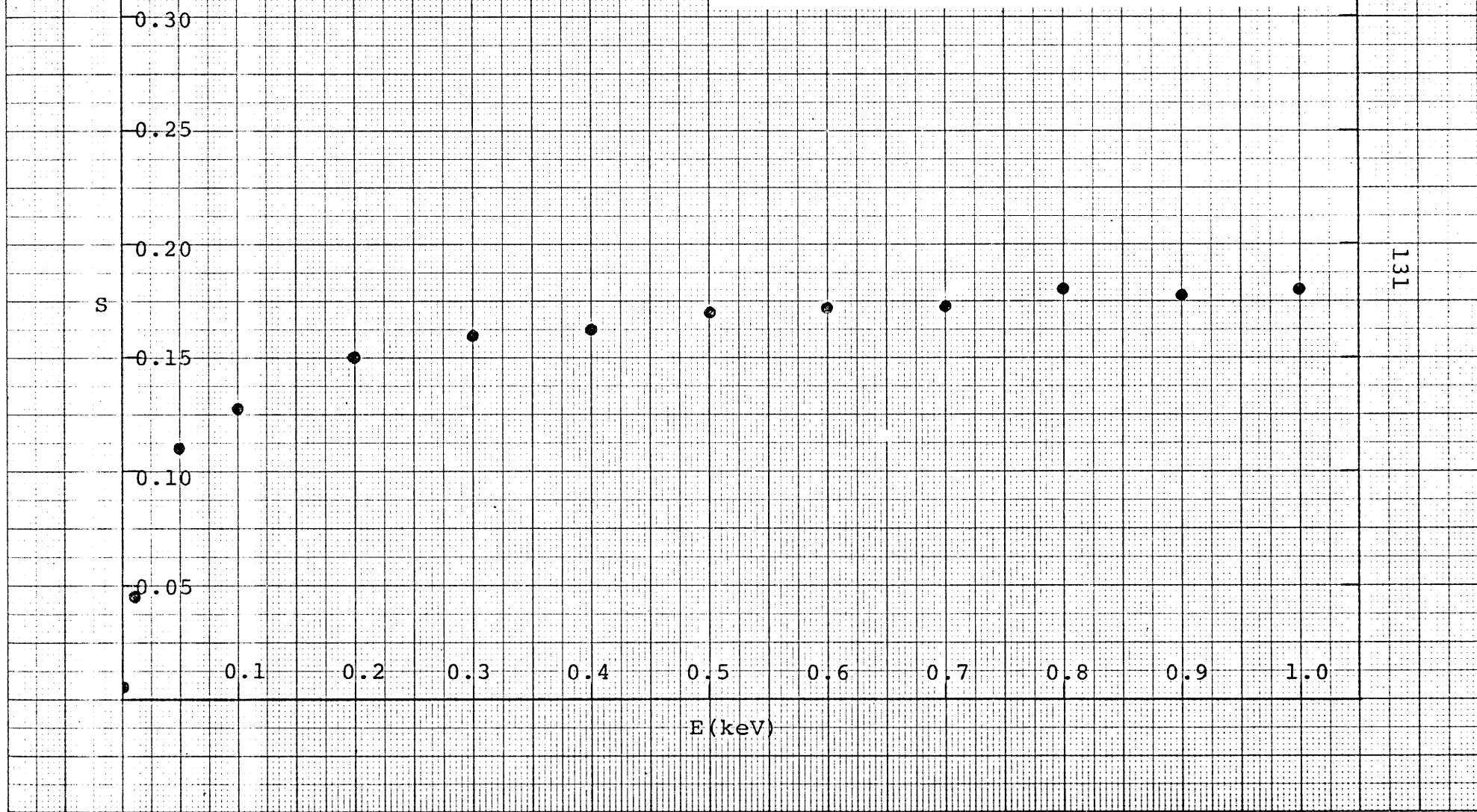


Fig. 24. Sputtering yields for H^+ ions incident on potassium [calculated from Eq. (25)].

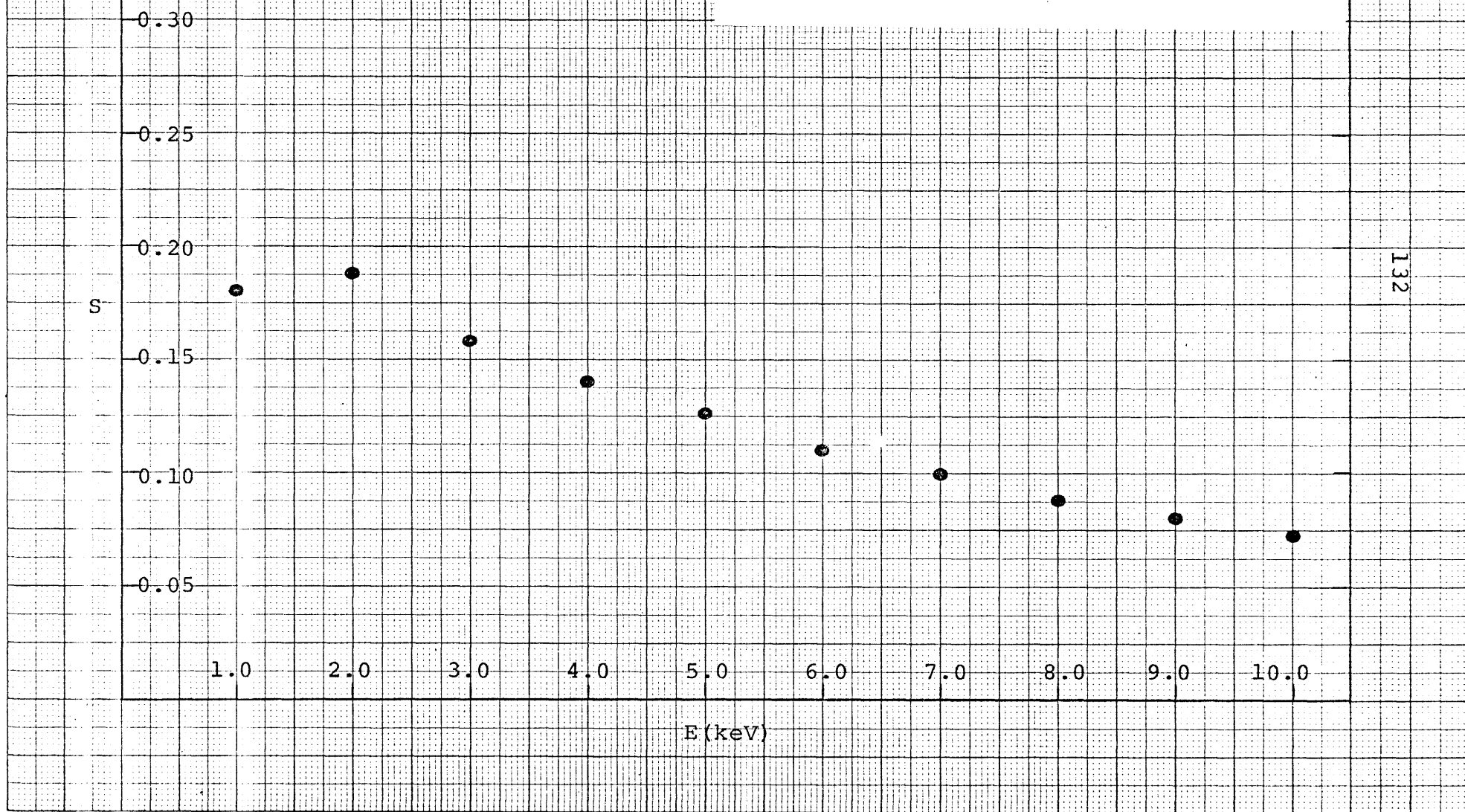


Fig. 25. Sputtering yields for H^+ ions incident on silver [calculated from Eq.(25)].

■ Grolund and Moore

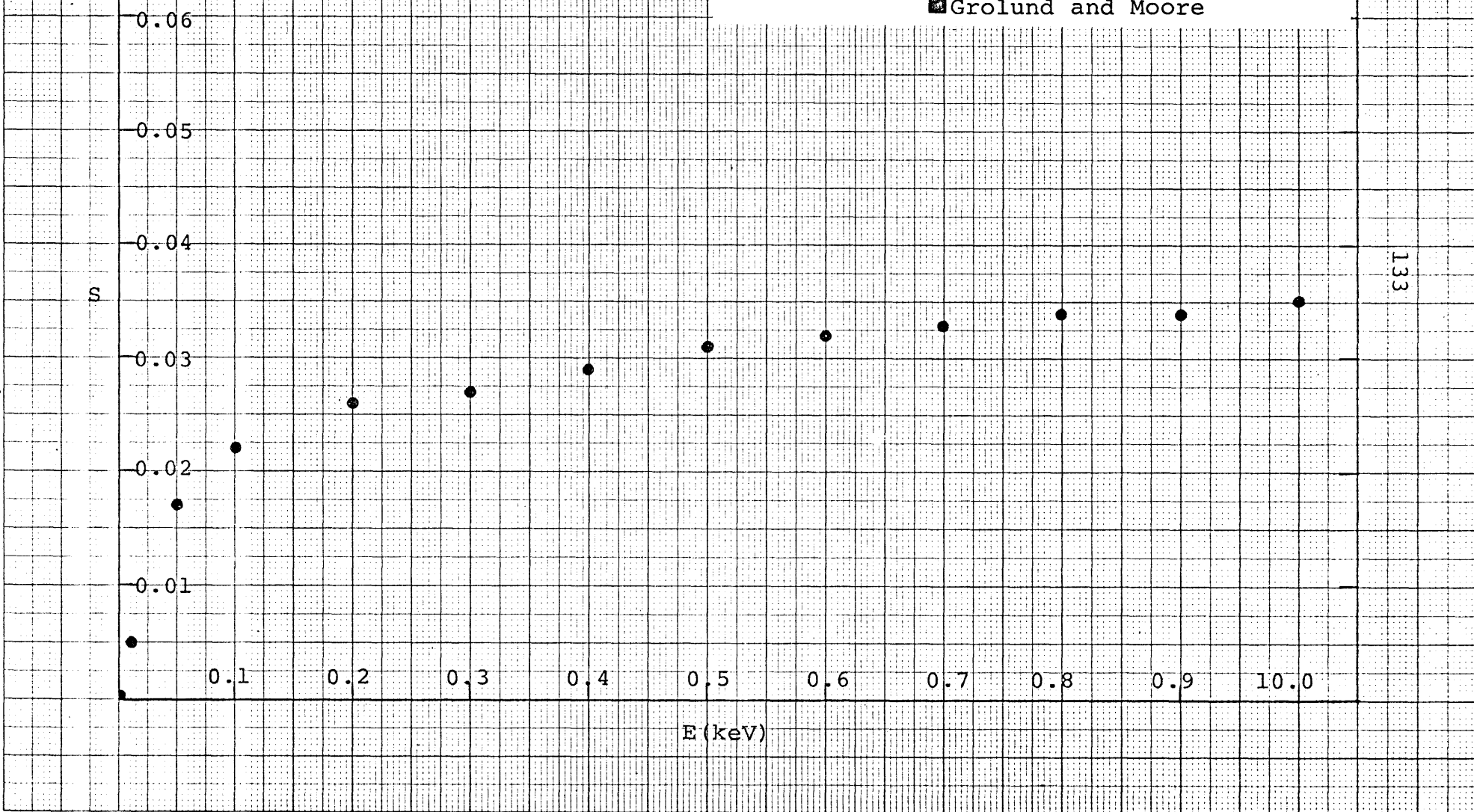


Fig. 26. Sputtering yields for H^+ ions incident on silver [calculated from Eq.(25)].

■ Grolund and Moore

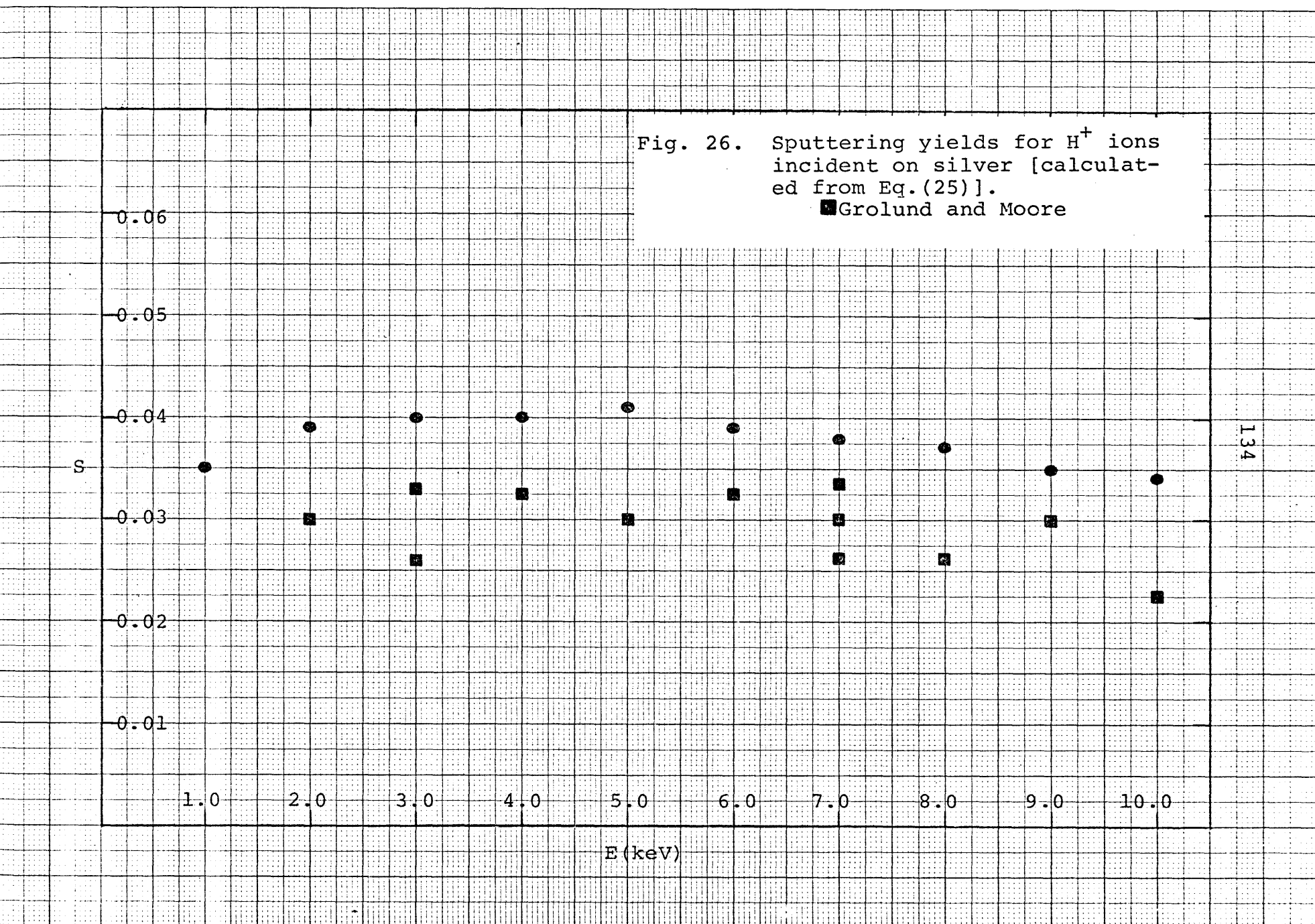


Fig. 27. Sputtering yields for H^+ ions incident on silicon [calculated from Eq.(25)].

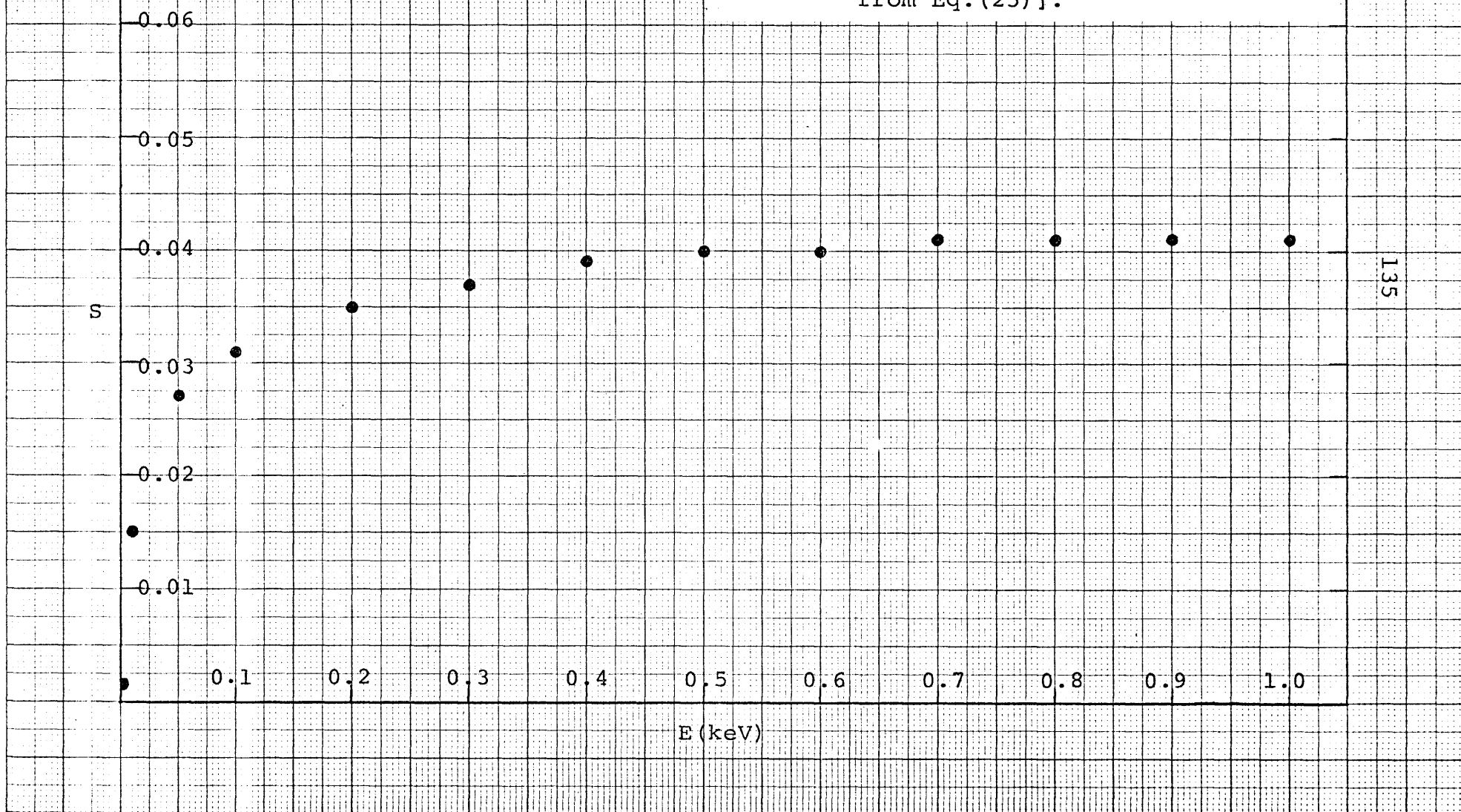


Fig. 28. Sputtering yields for H^+ ions incident on silicon [calculated from Eq. (25)].

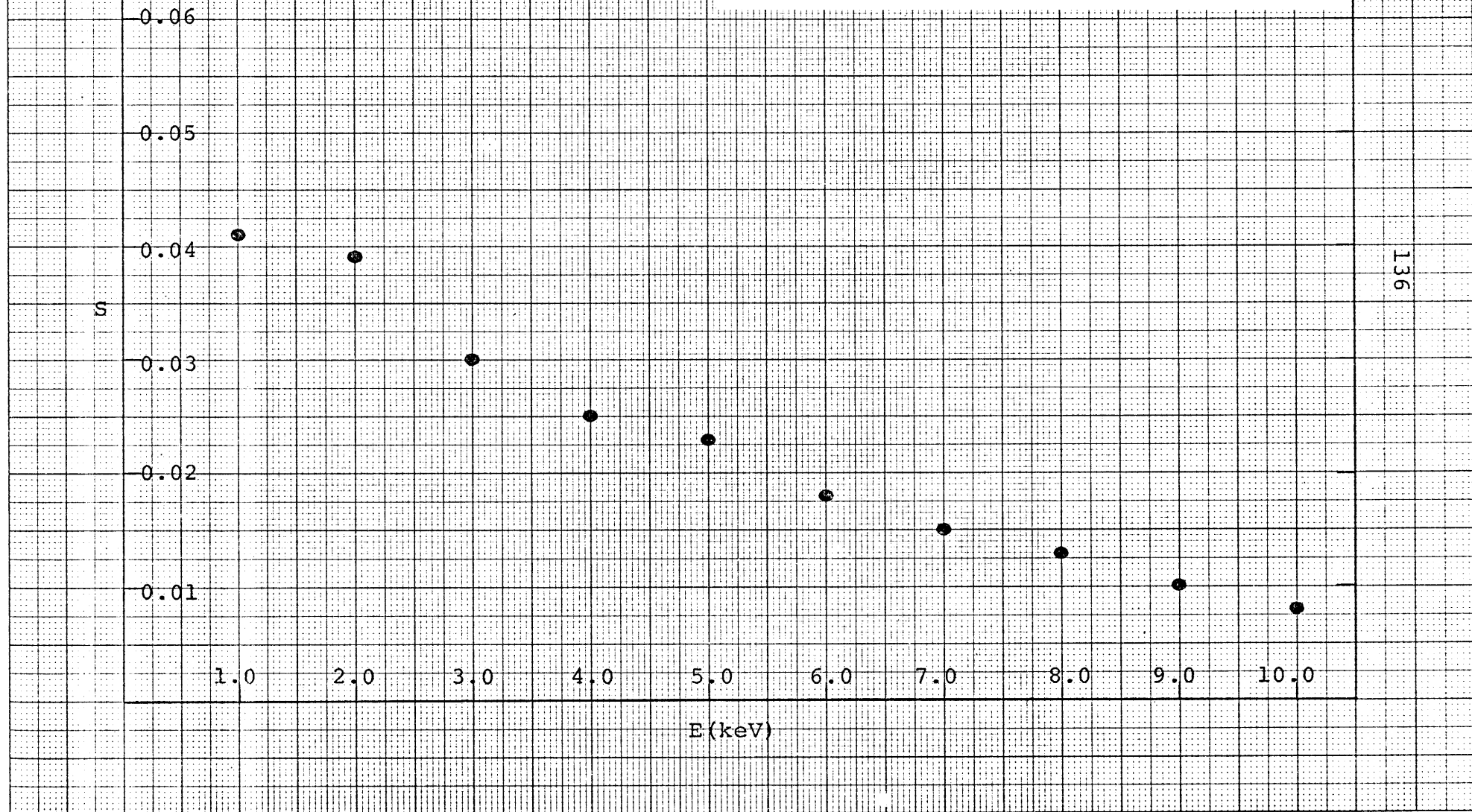


Fig. 29. Sputtering yields for H^+ ions incident on sodium [calculated from Eq. (25)].

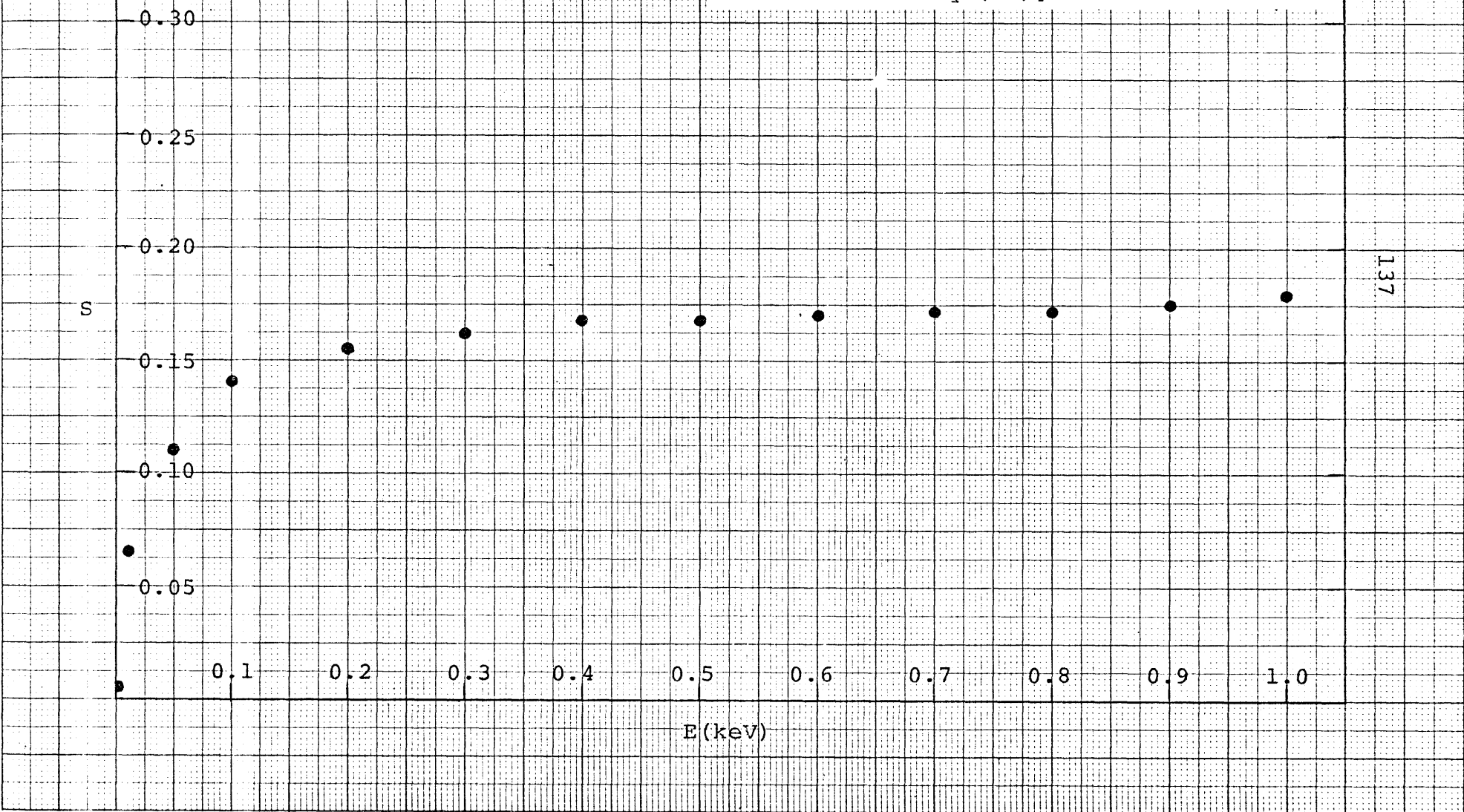


Fig. 30. Sputtering yields for H^+ ions incident on sodium [calculated from Eq. (25)].

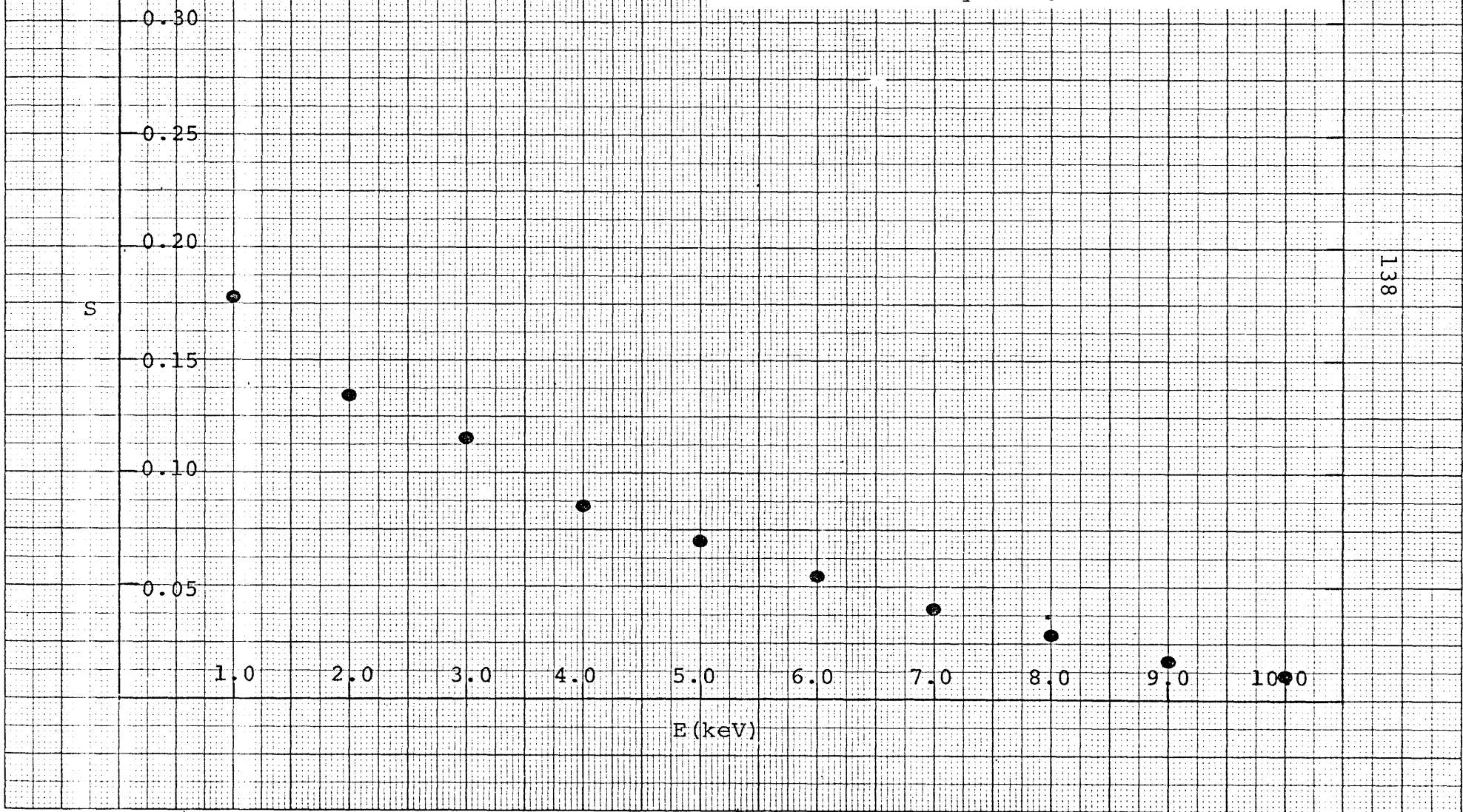
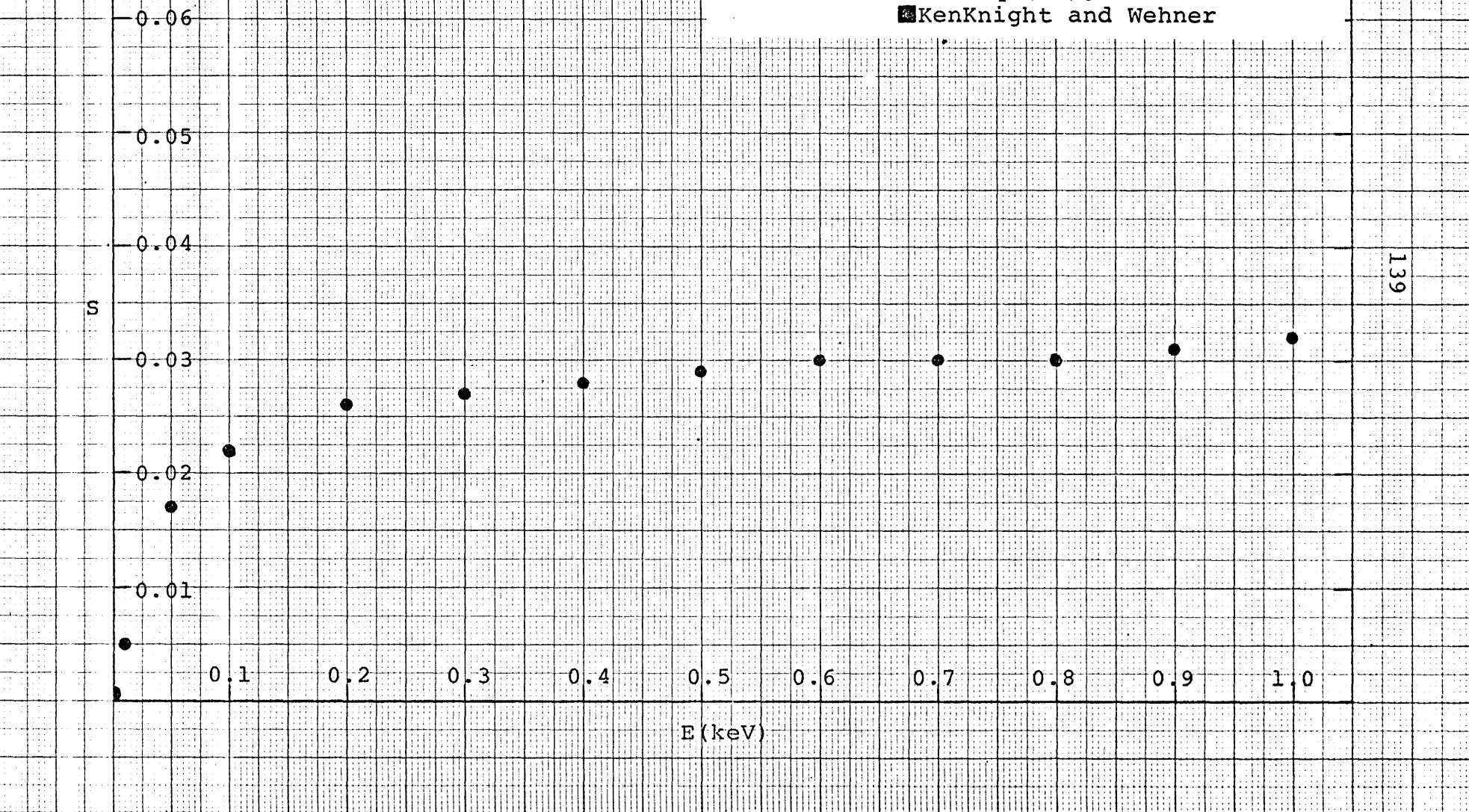


Fig. 31. Sputtering yields for H^+ ions incident on titanium [calculated from Eq.(25)].

KenKnight and Wehner



139

Fig. 32. Sputtering yields for H^+ ions incident on titanium [calculated from Eq. (25)].

■KenKnight and Wehner

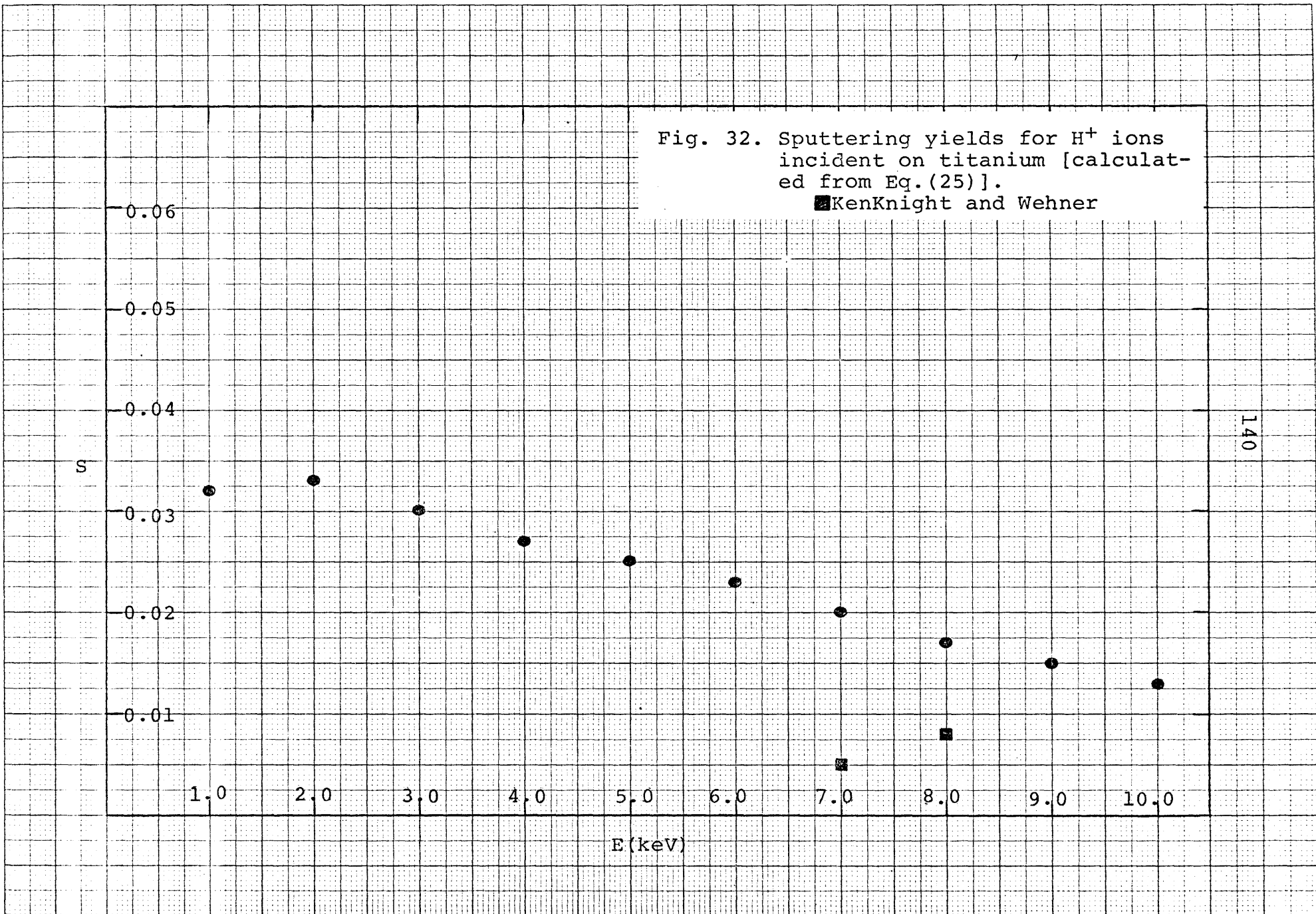


Fig. 33. Sputtering yields for H^+ ions incident on zinc [calculated from Eq.(25)].

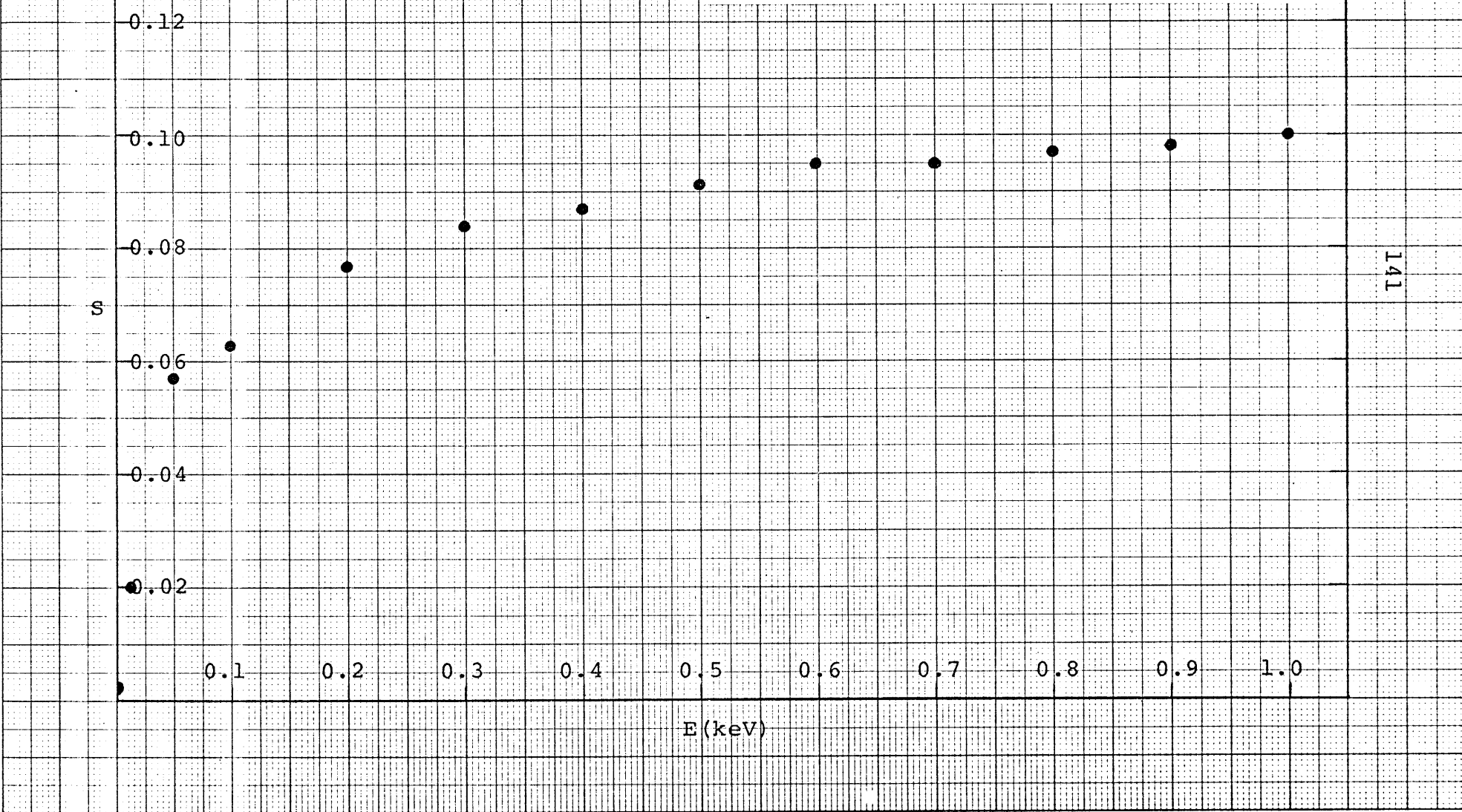


Fig. 34. Sputtering yields for H^+ ions incident on zinc [calculated from Eq. (25)].

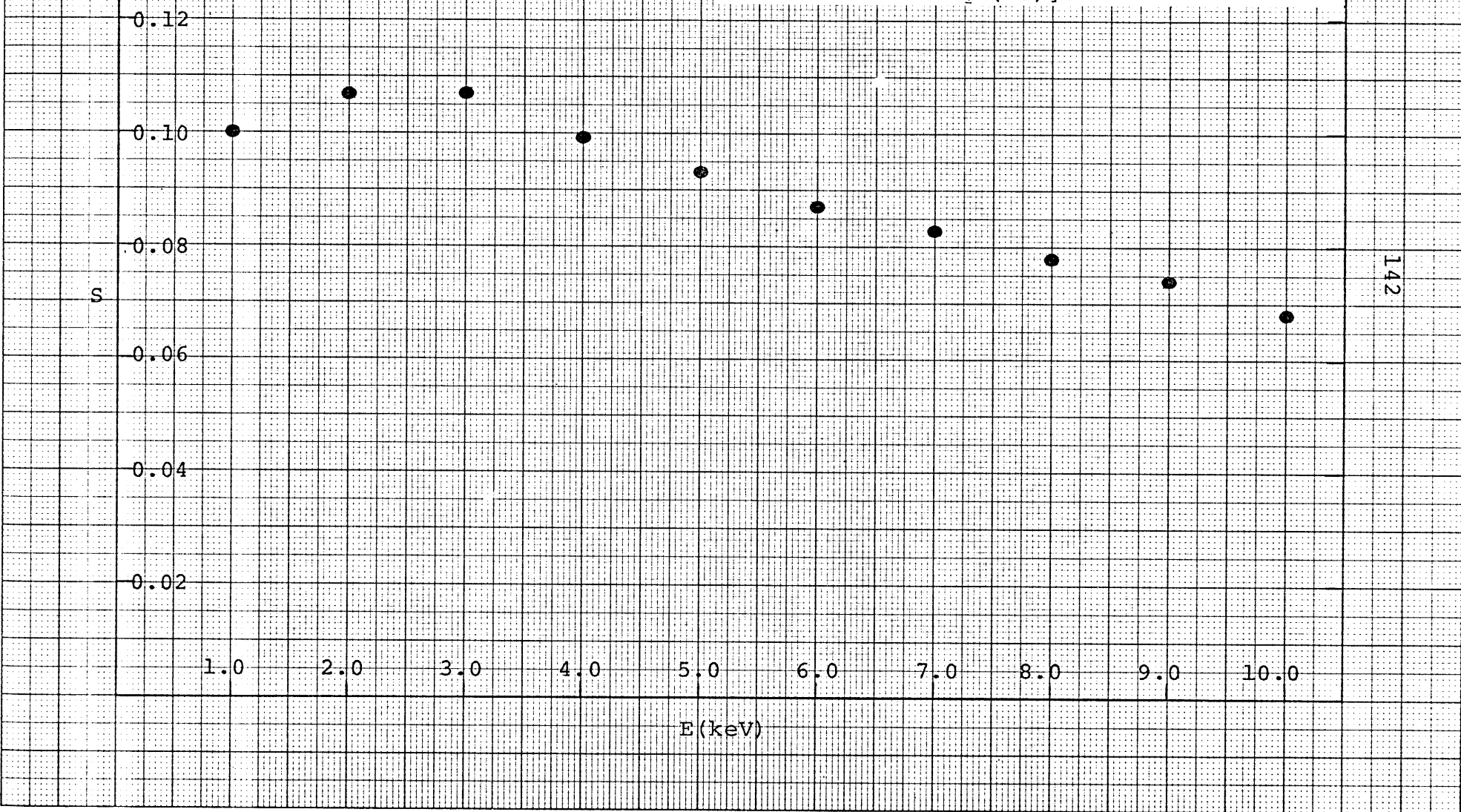


Fig. 35. Variation of the sputtering yield with angle of incidence for H^+ ions on aluminum [calculated from Eq. (26)].

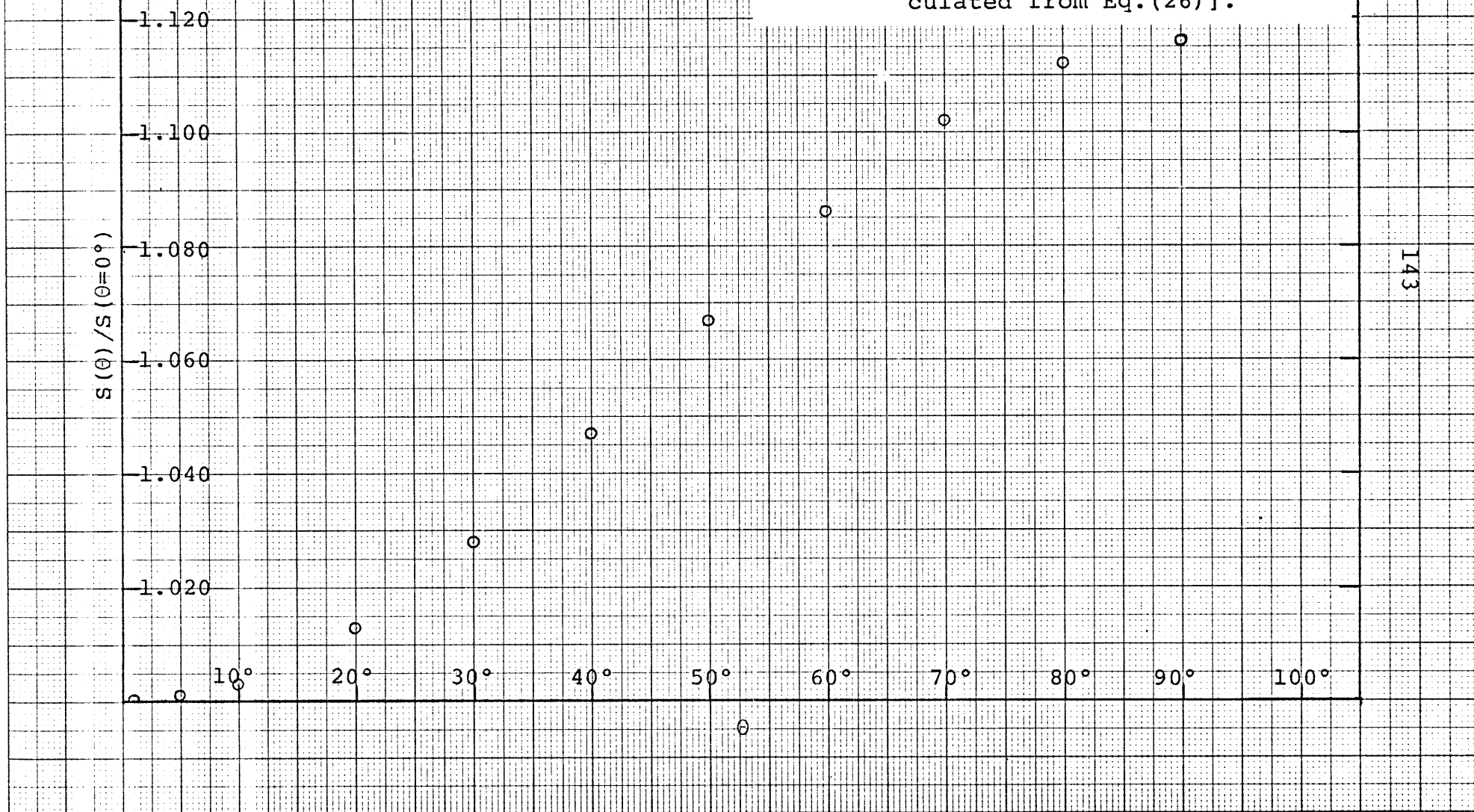


Fig. 36. Variation of the sputtering yield with angle of incidence for H^+ ions on calcium [calculated from Eq.(26)].

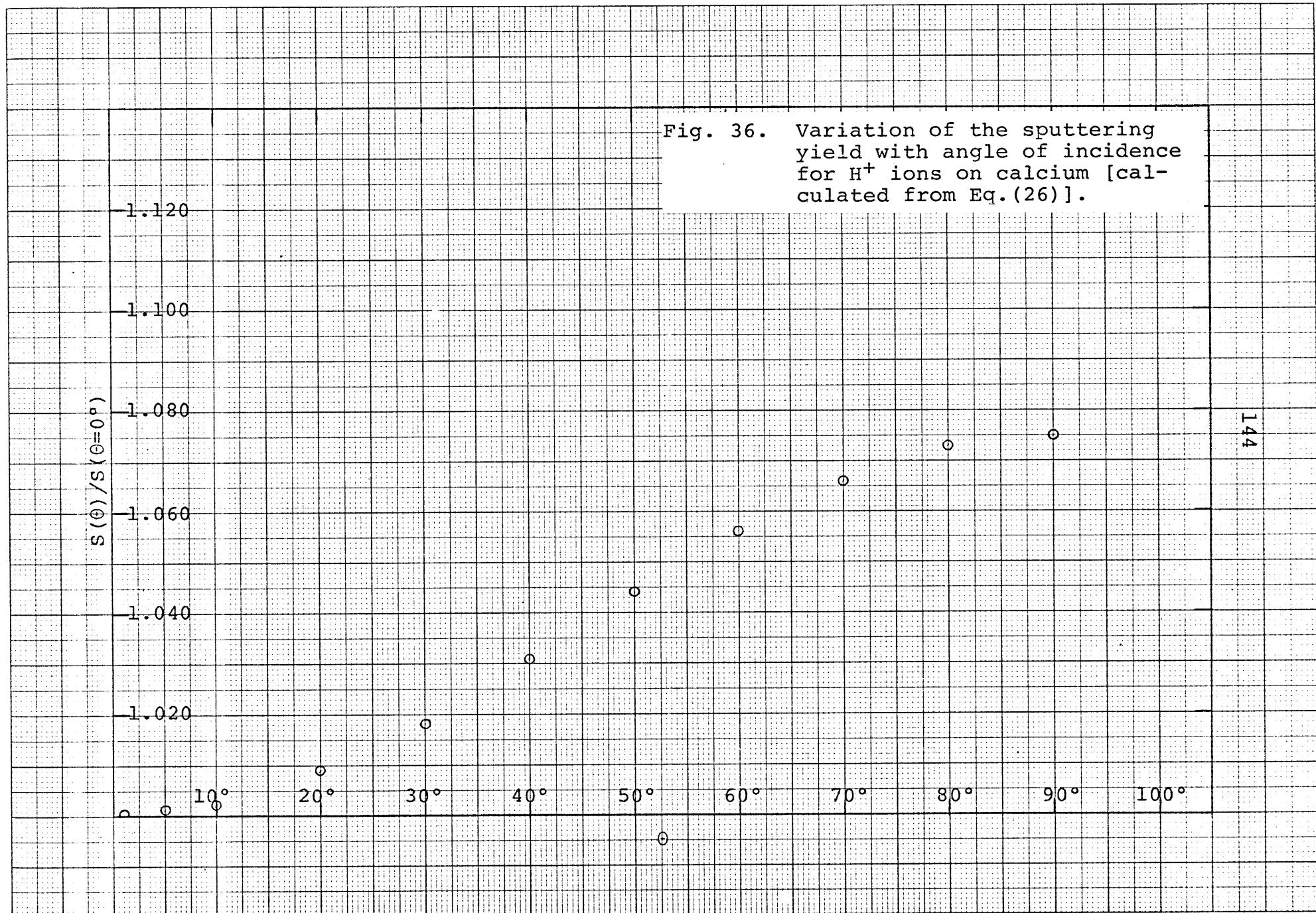


Fig. 37. Variation of the sputtering yield with angle of incidence for H^+ ions on chromium [calculated from Eq. (26)].

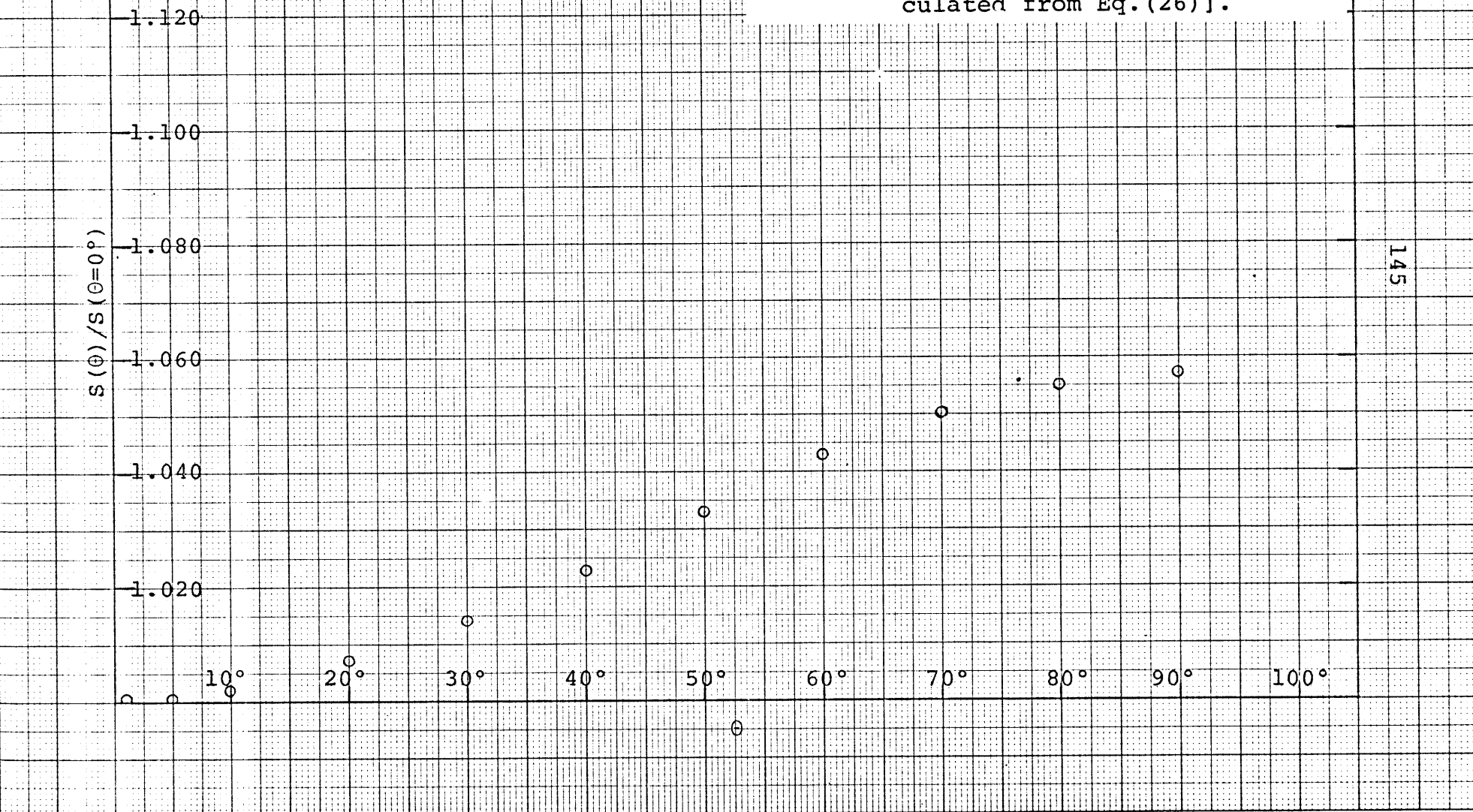
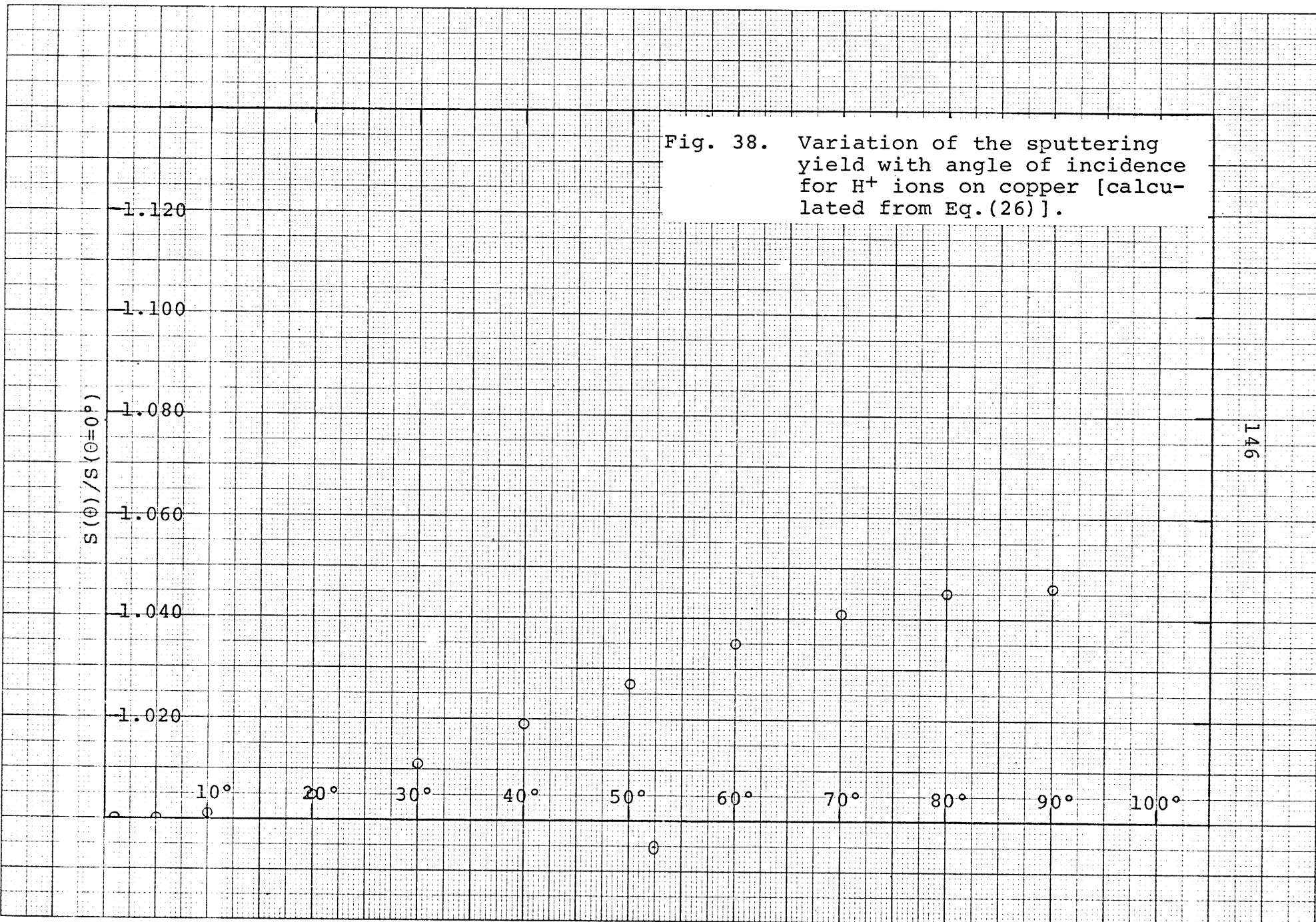


Fig. 38. Variation of the sputtering yield with angle of incidence for H^+ ions on copper [calculated from Eq. (26)].



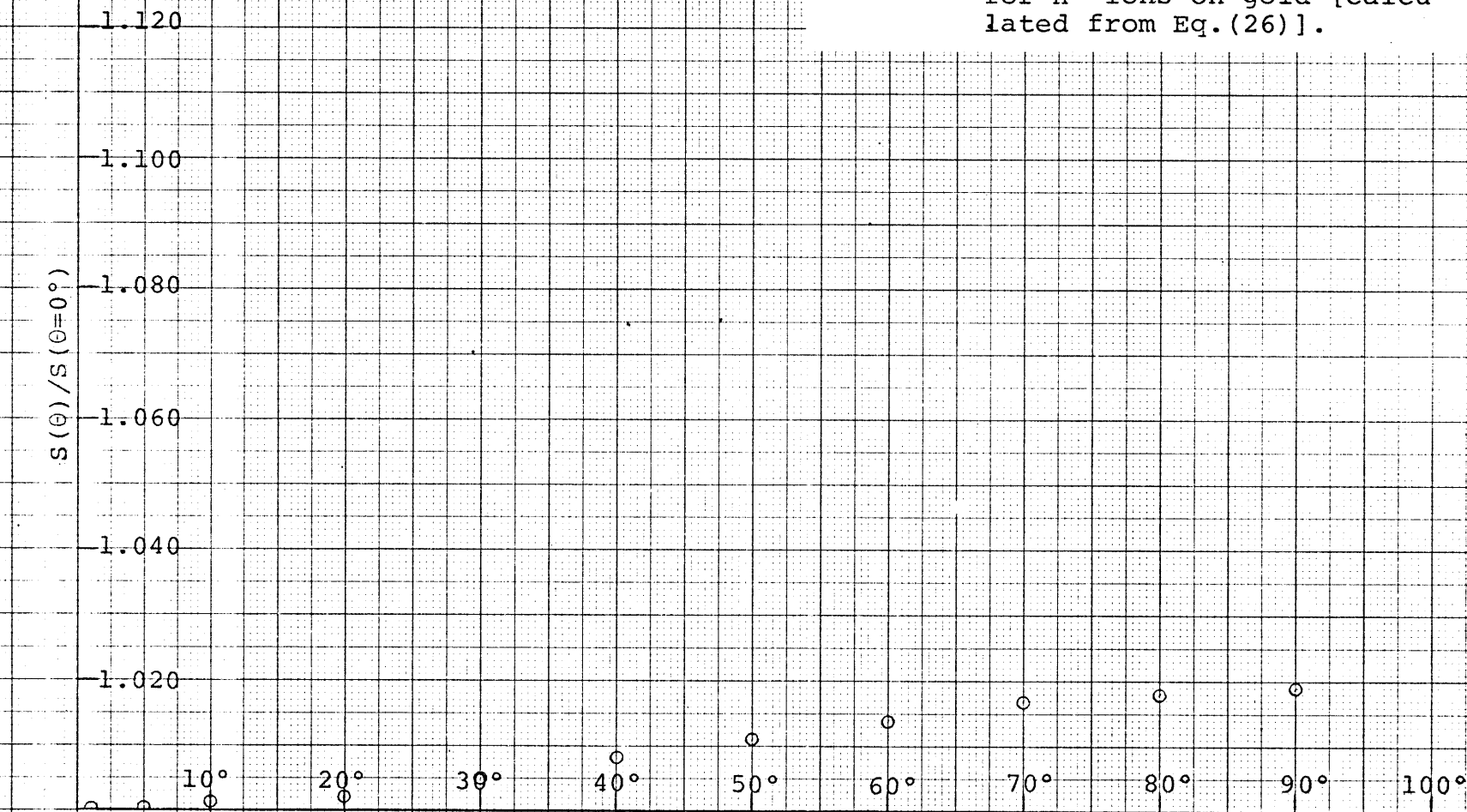


Fig. 39. Variation of the sputtering yield with angle of incidence for H^+ ions on gold [calculated from Eq. (26)].

147

Fig. 40. Variation of the sputtering yield with angle of incidence for H^+ ions on iron [calculated from Eq.(26)].

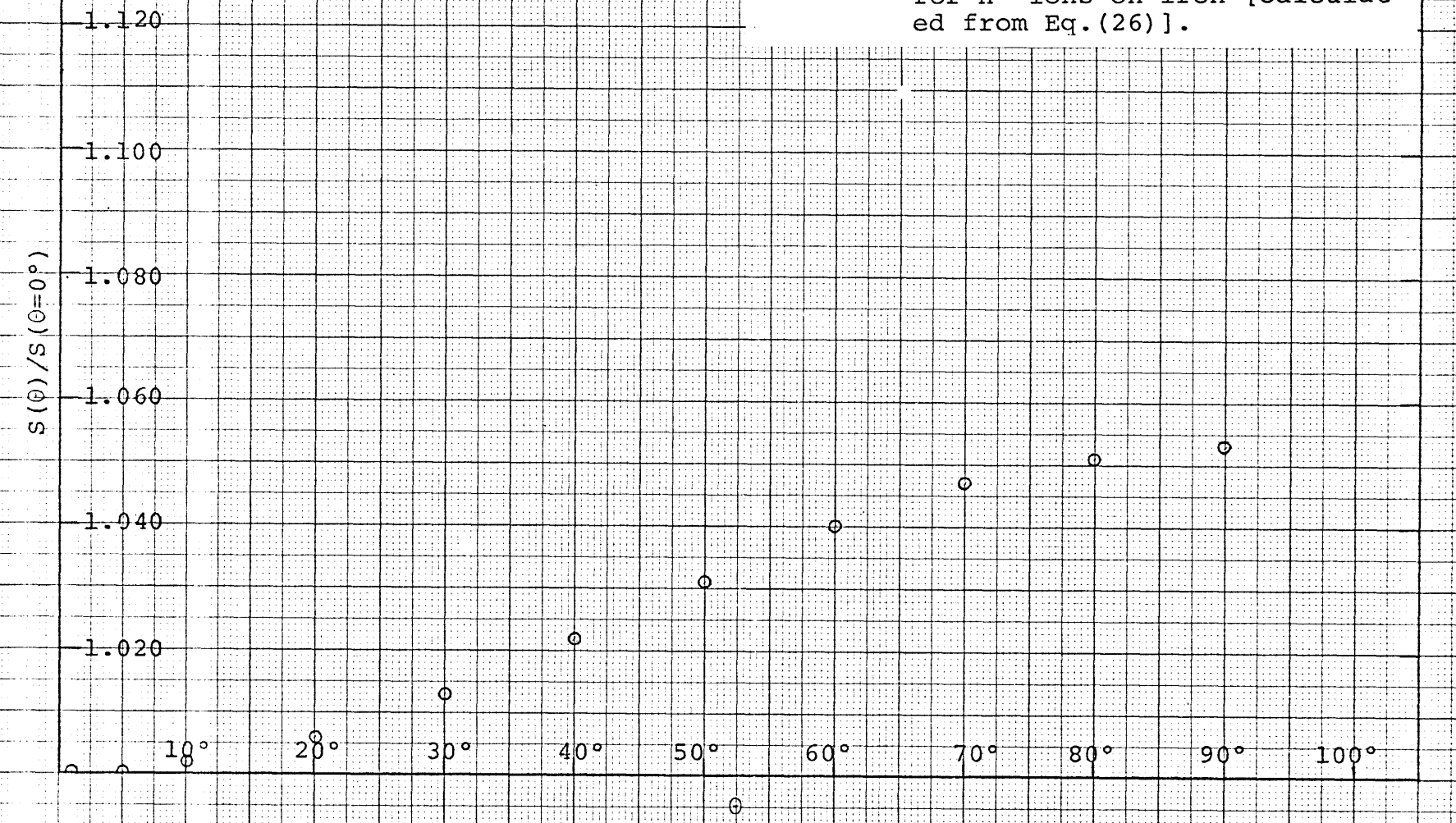


Fig. 41. Variation of the sputtering yield with angle of incidence for H^+ ions on magnesium [calculated from Eq. (26)].

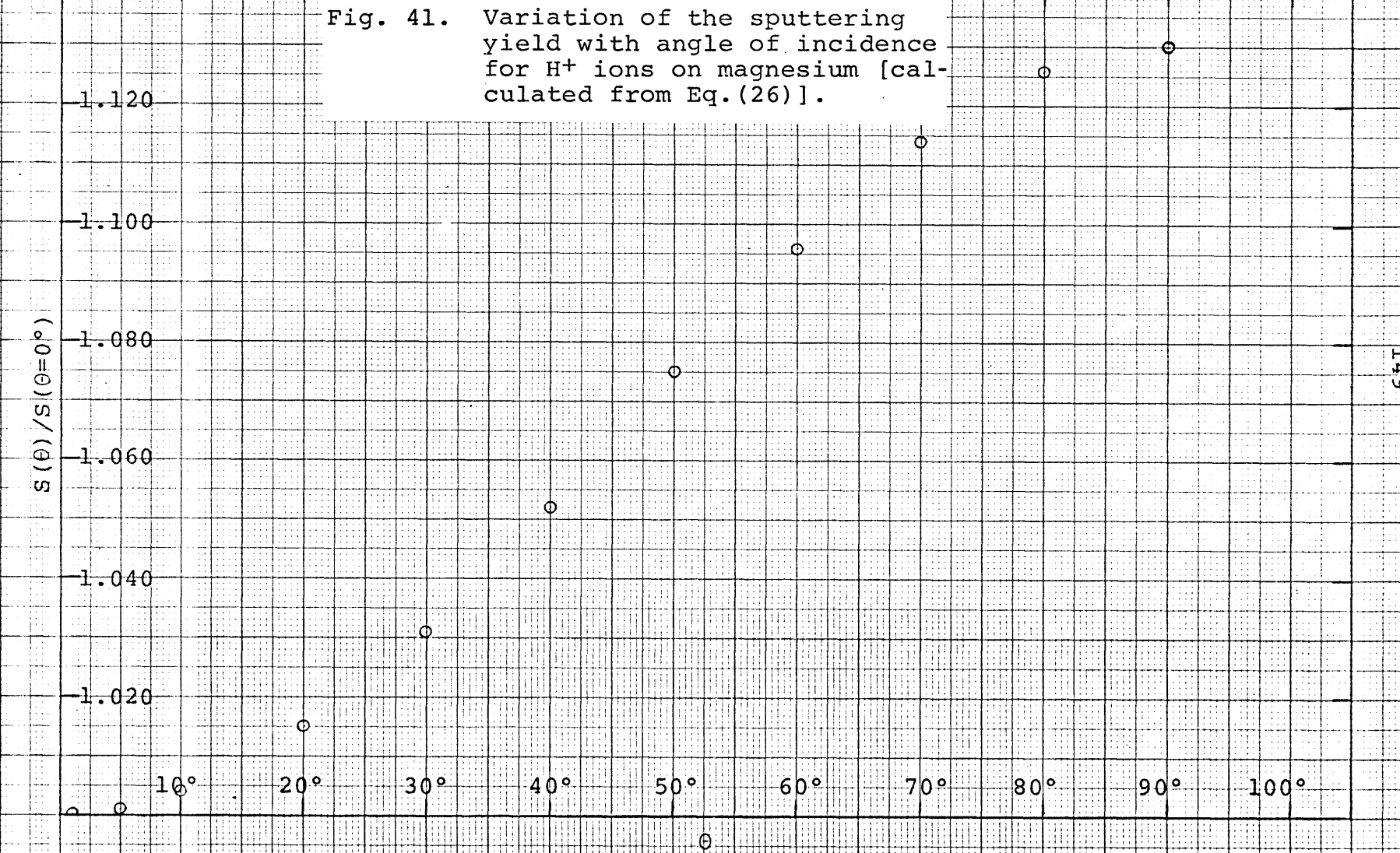


Fig. 42. Variation of the sputtering yield with angle of incidence for H^+ ions on manganese [calculated from Eq. (26)].

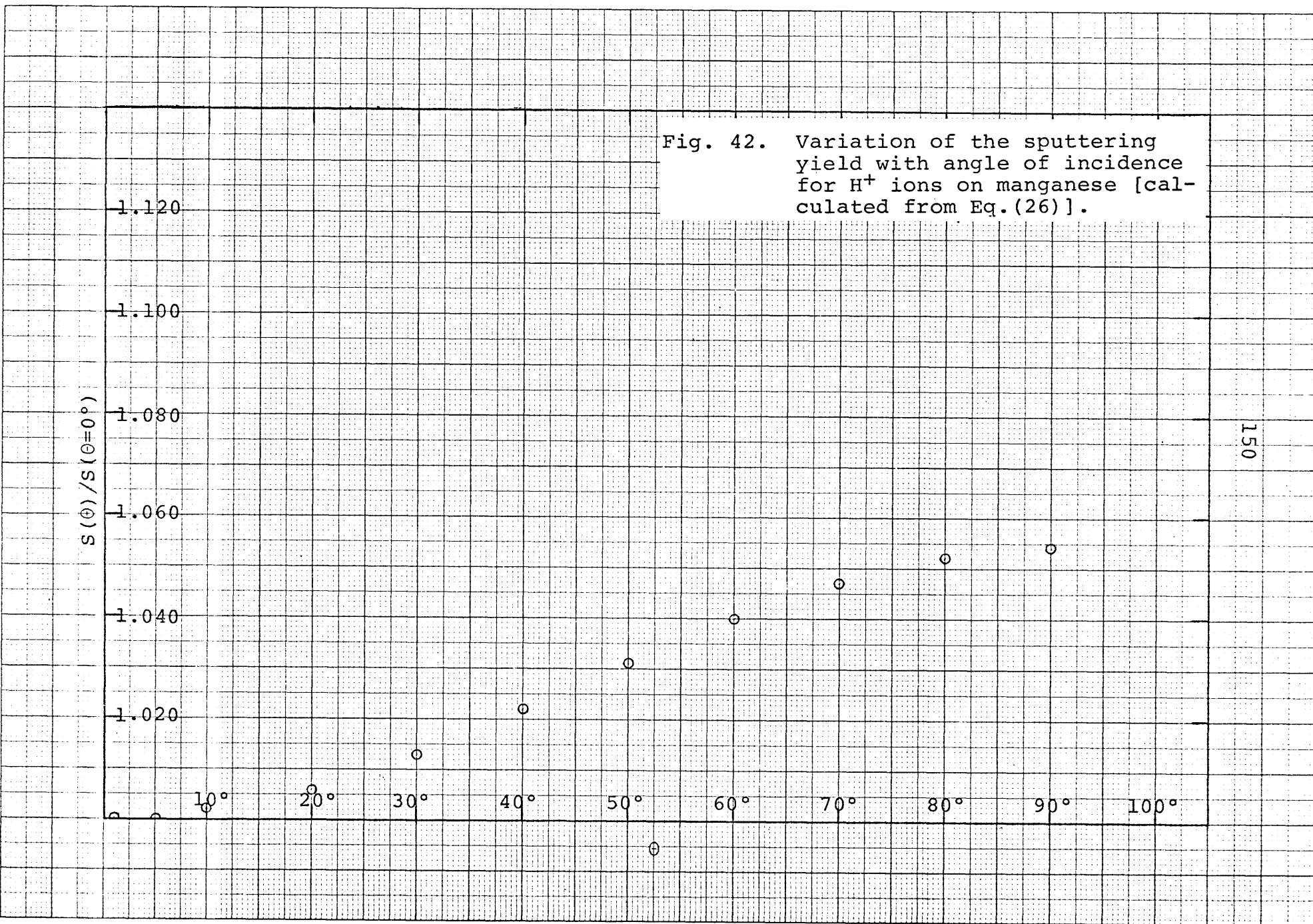
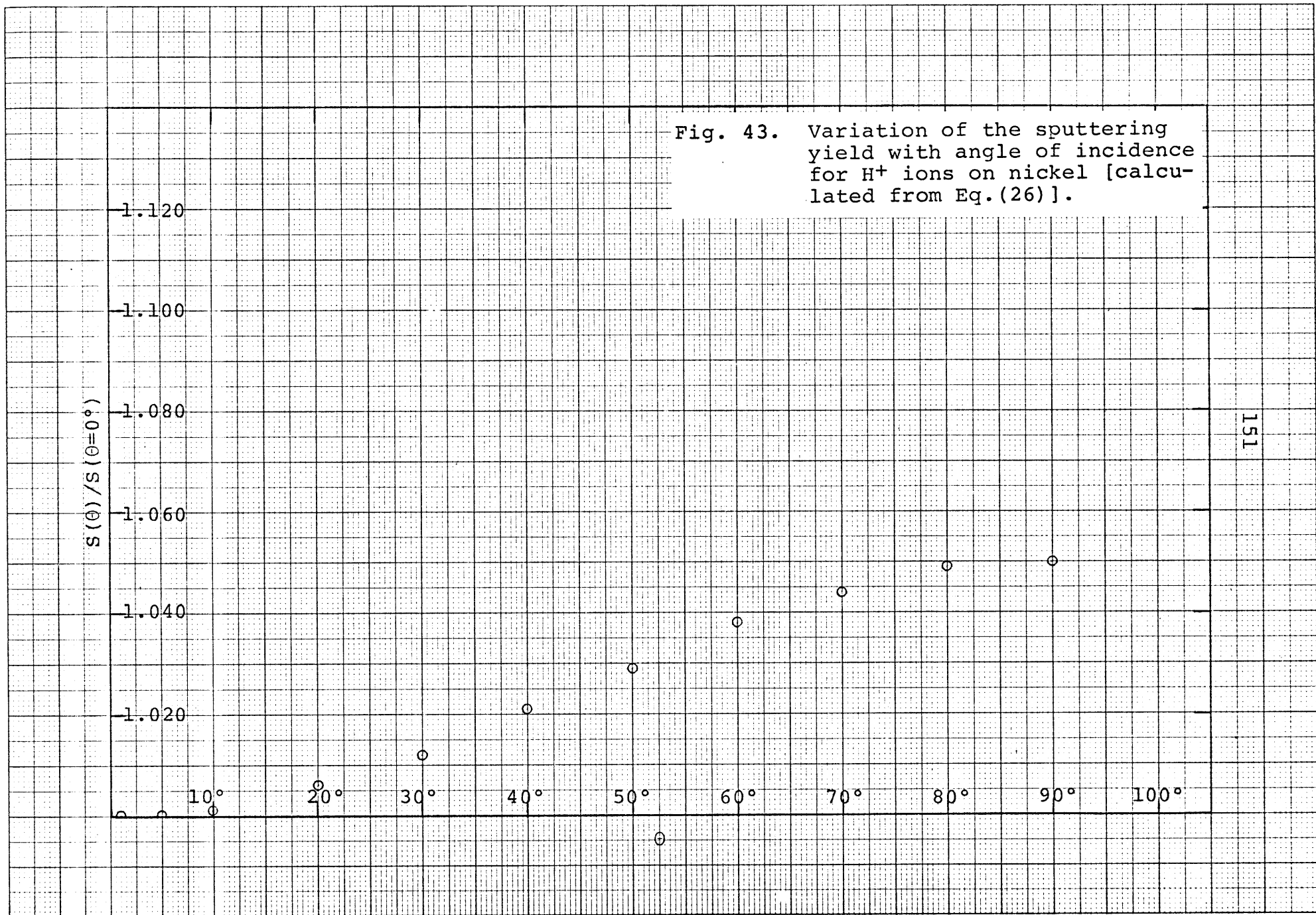


Fig. 43. Variation of the sputtering yield with angle of incidence for H^+ ions on nickel [calculated from Eq.(26)].



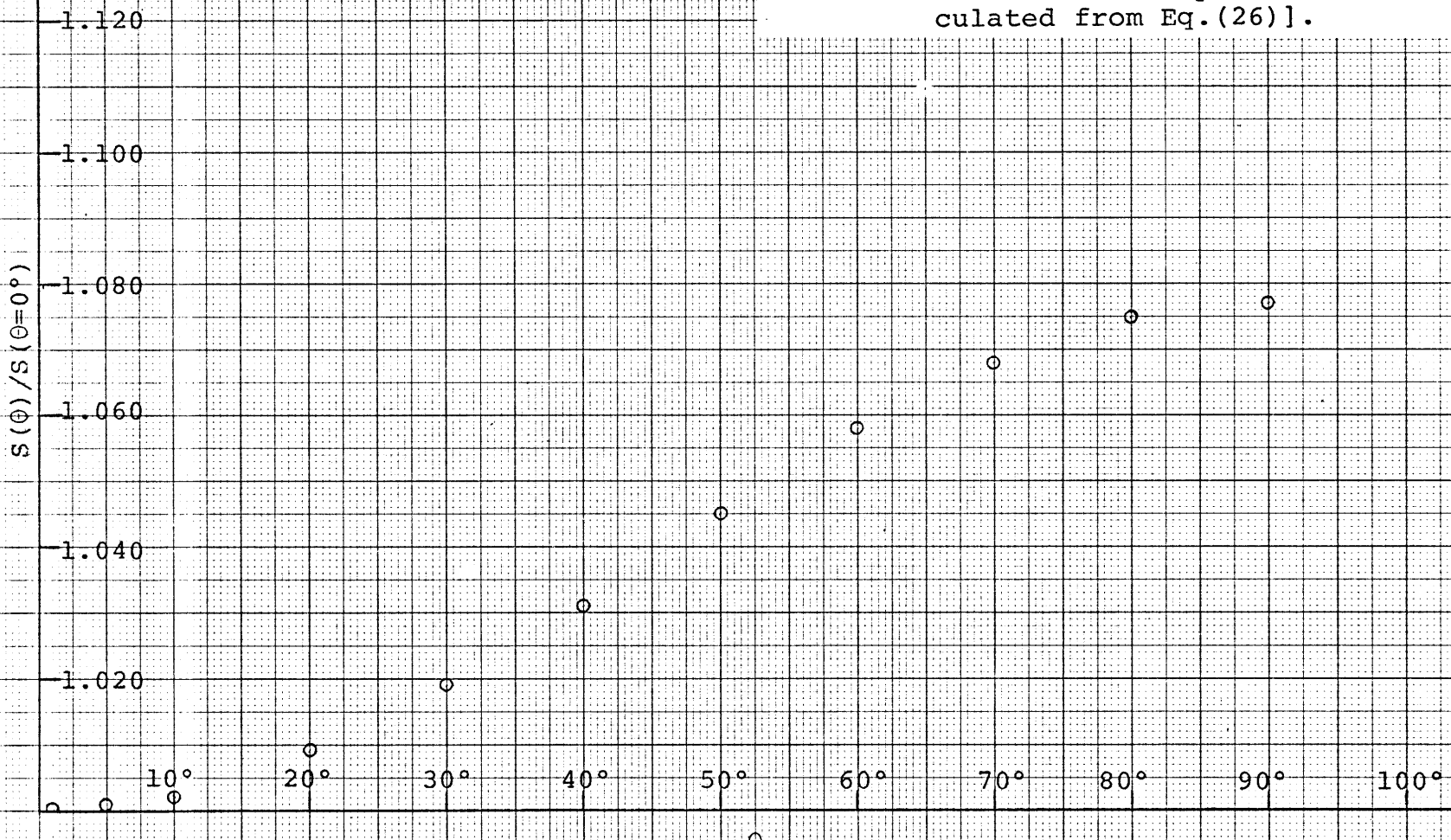


Fig. 44. Variation of the sputtering yield with angle of incidence for H^+ ions on potassium [calculated from Eq. (26)].

Fig. 45. Variation of the sputtering yield with angle of incidence for H^+ ions on silver [calculated from Eq. (26)].

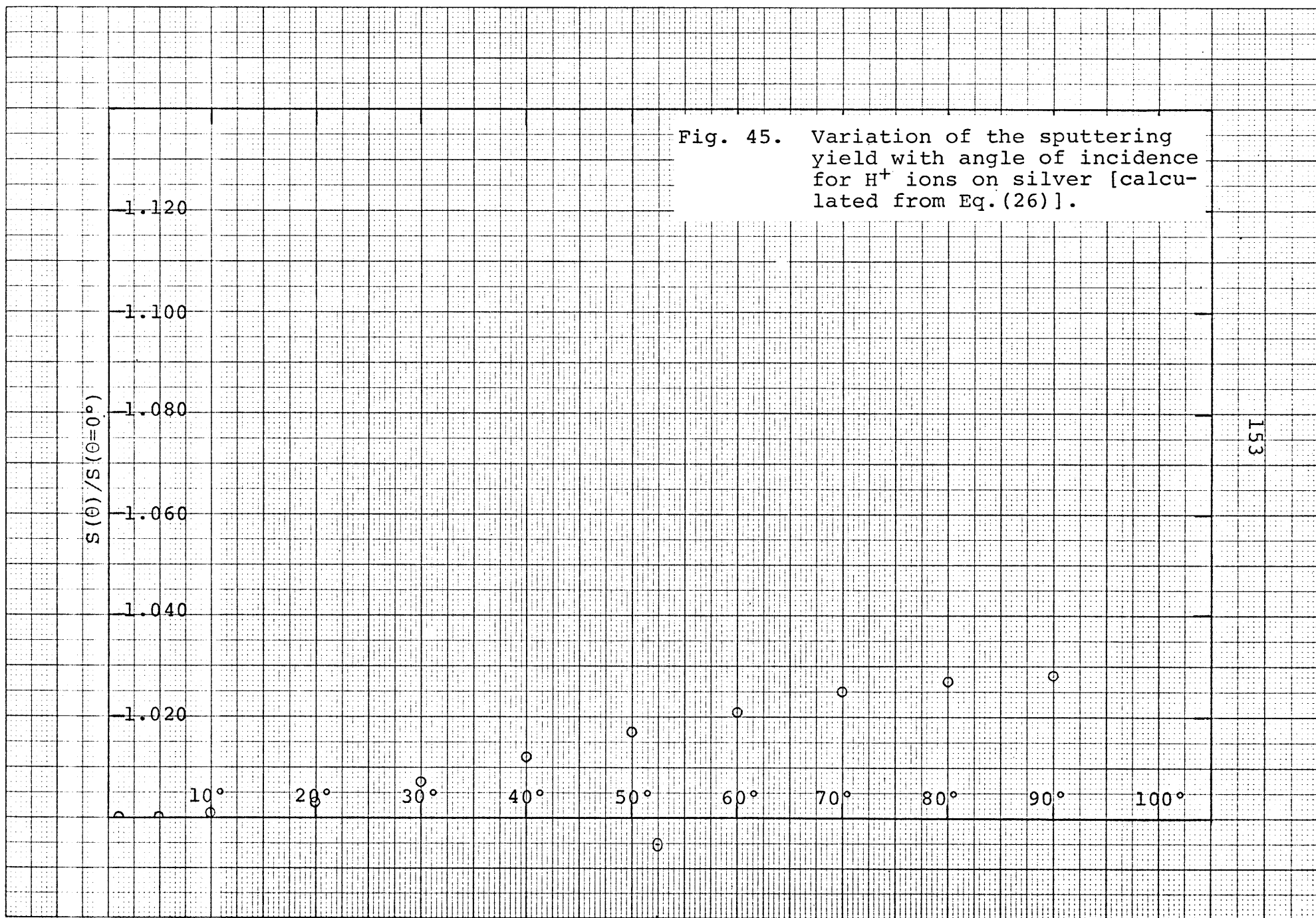


Fig. 45a. Variation of the sputtering yield with angle of incidence for H^+ ions on sodium [calculated from Eq.(26)].

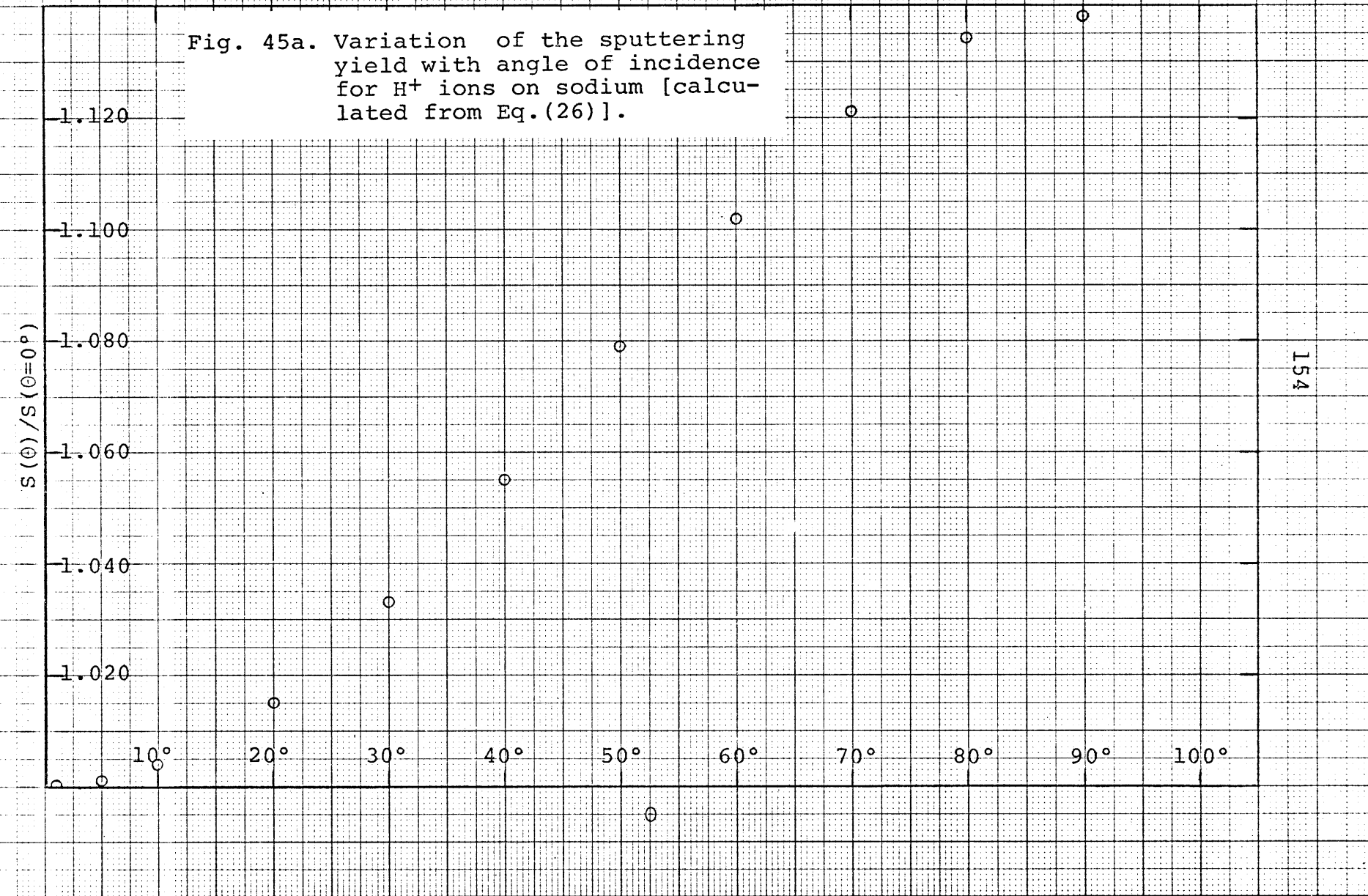
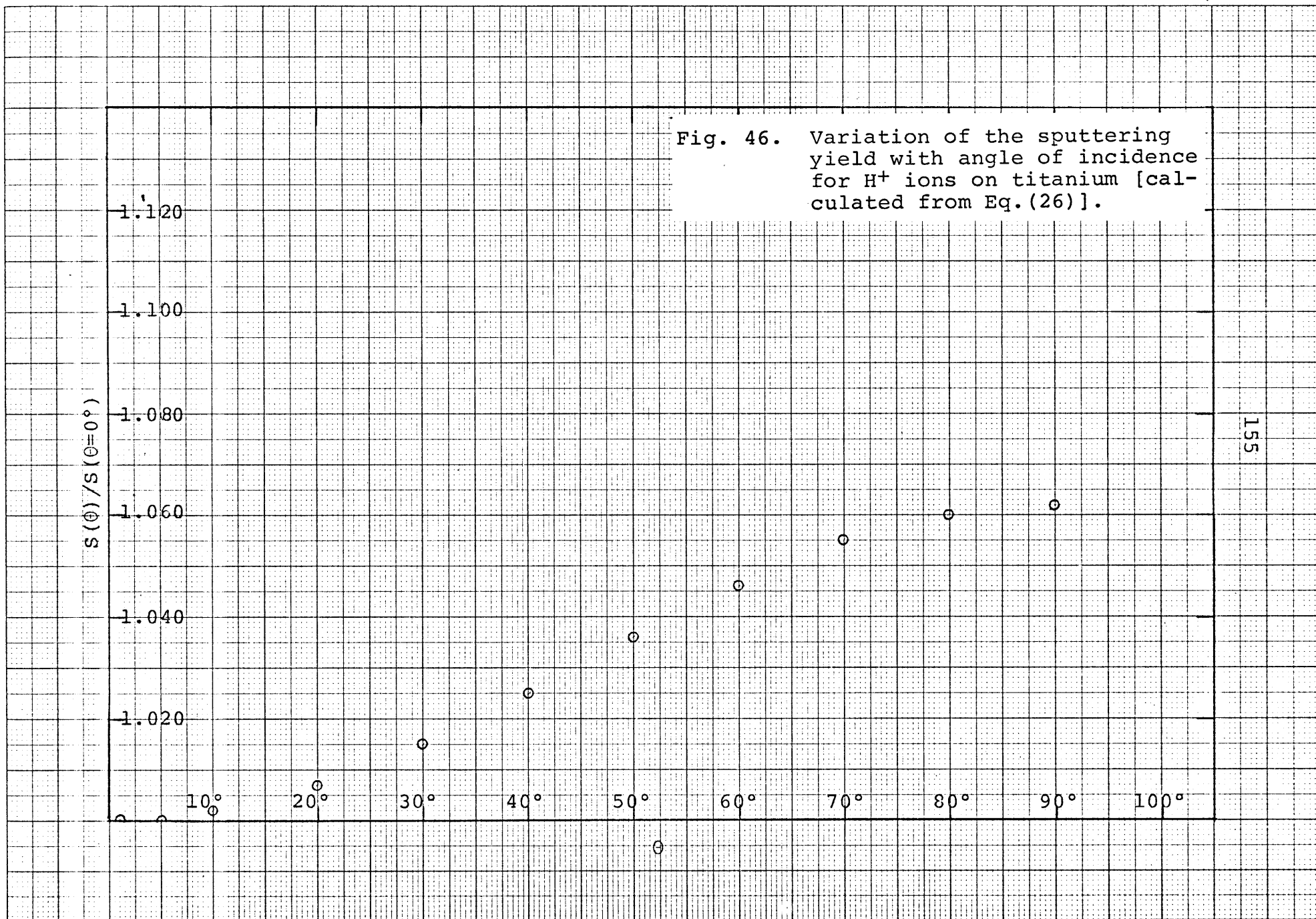


Fig. 46. Variation of the sputtering yield with angle of incidence for H^+ ions on titanium [calculated from Eq.(26)].



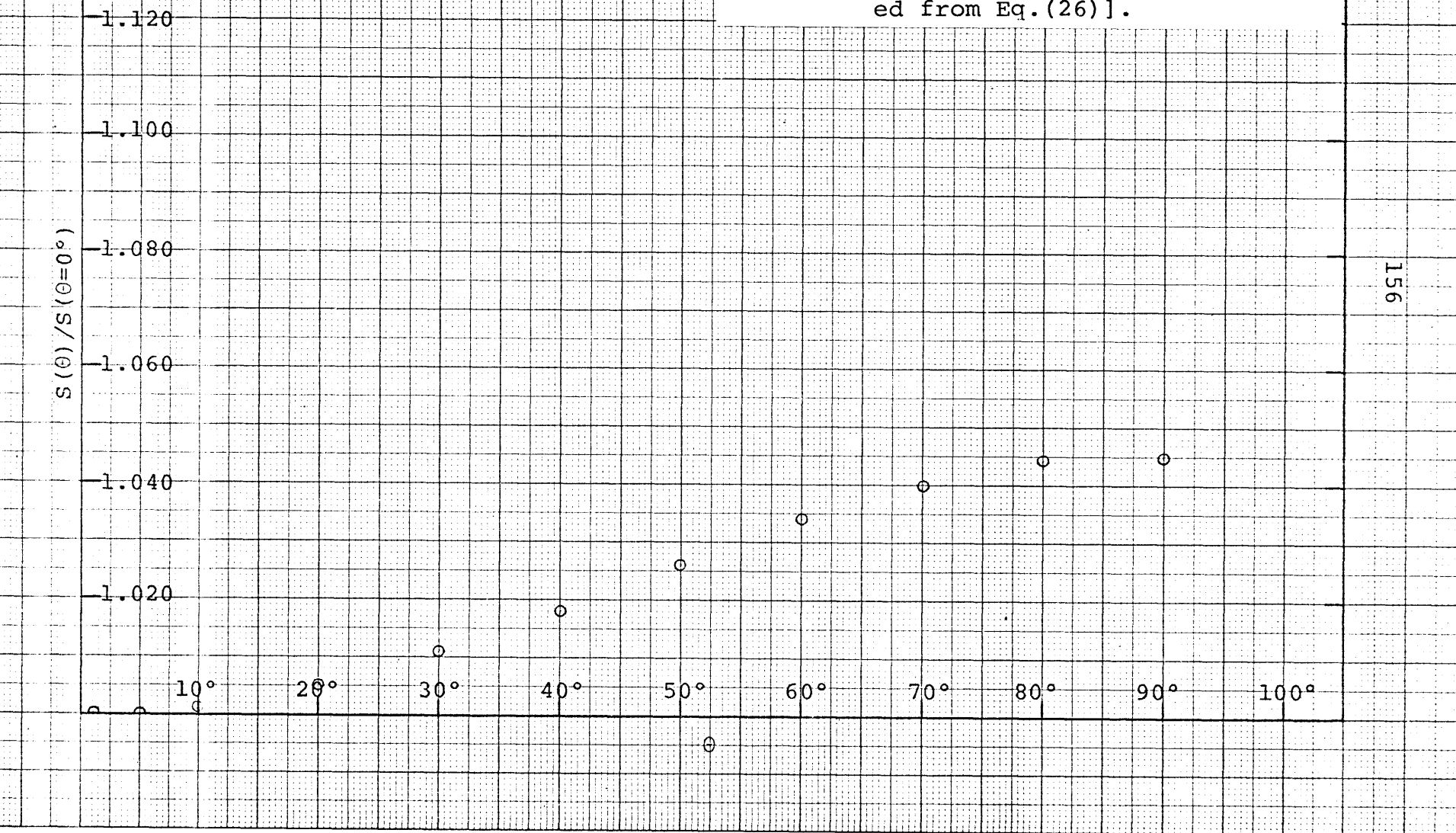
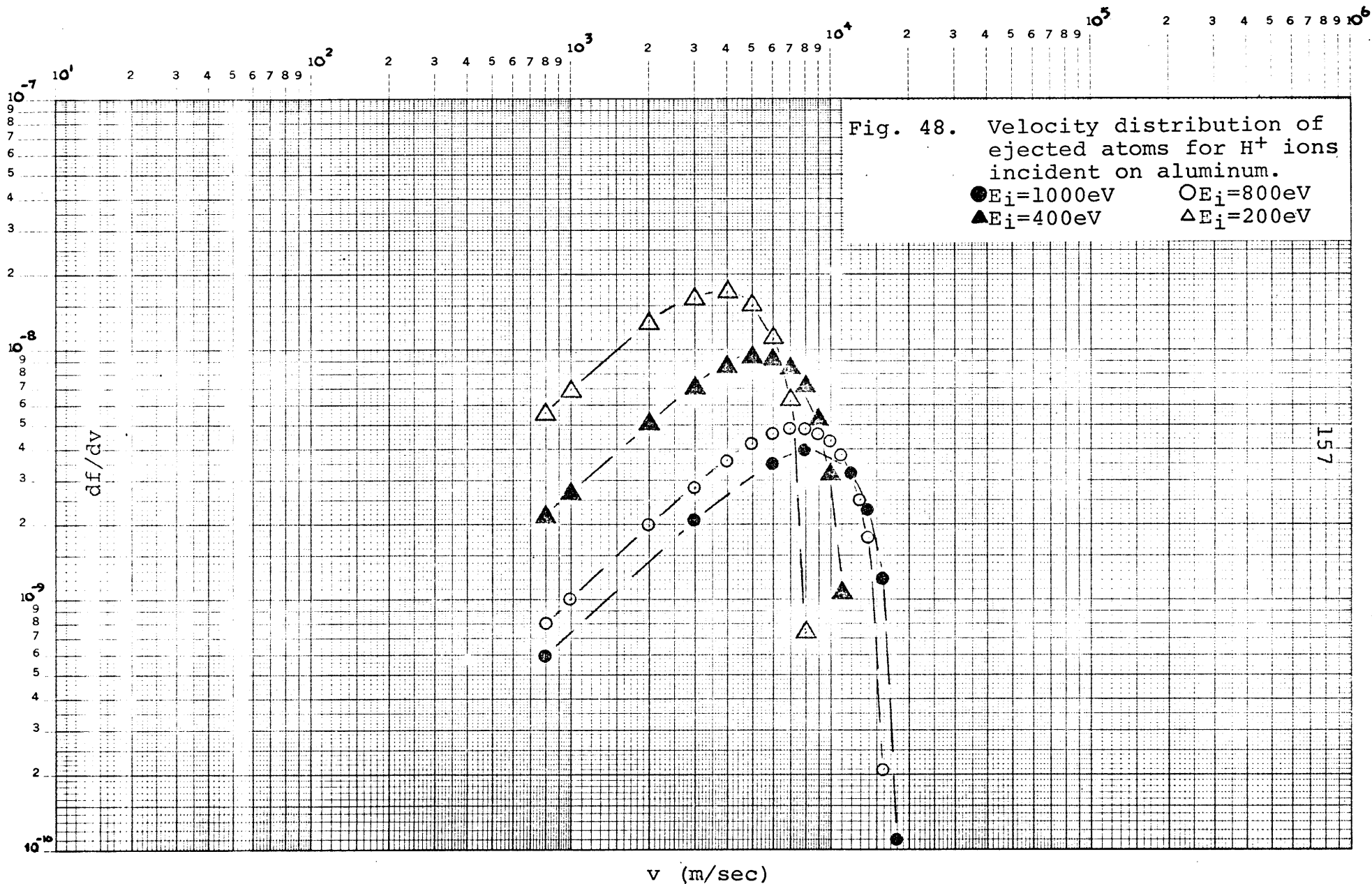
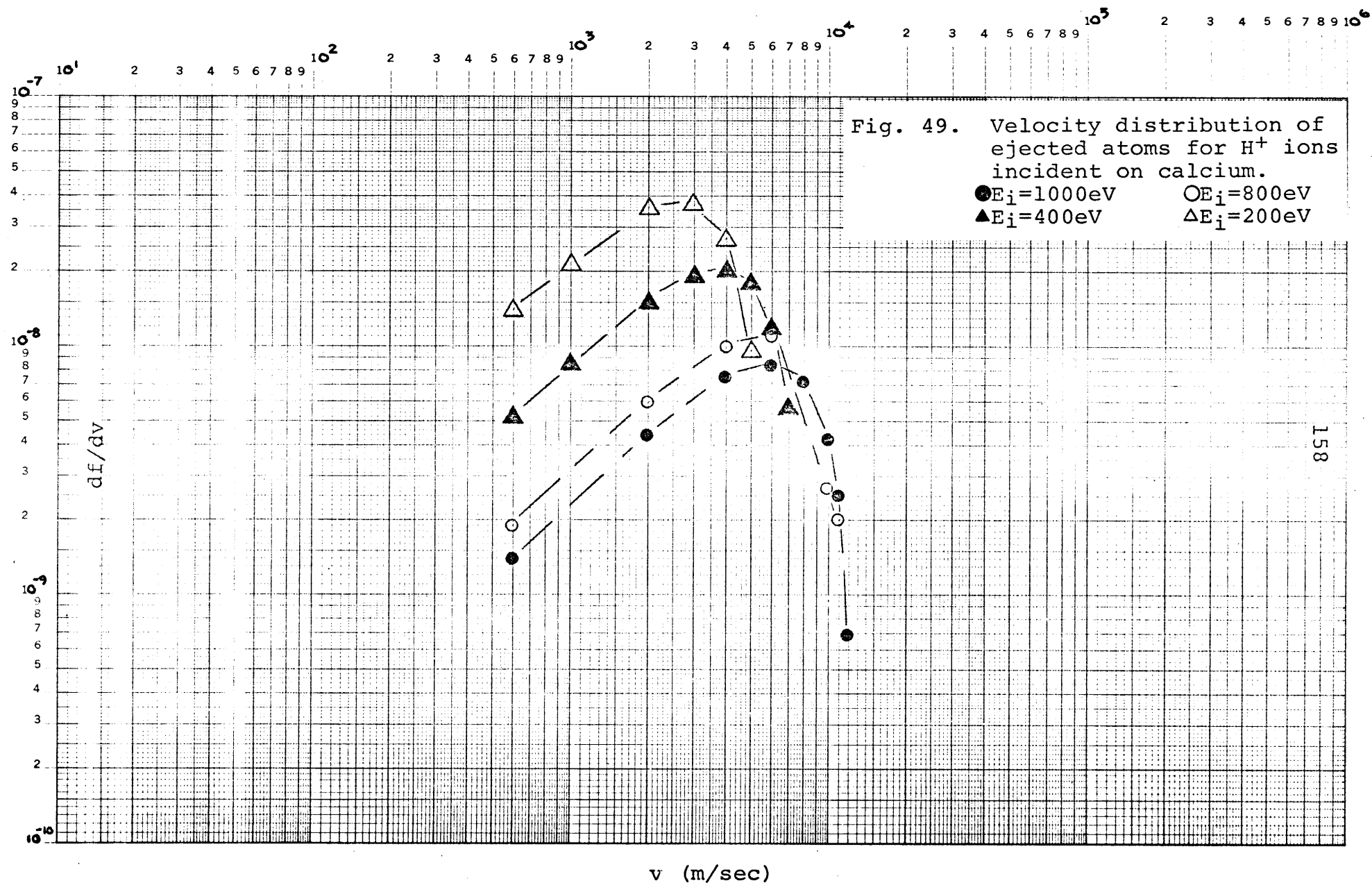
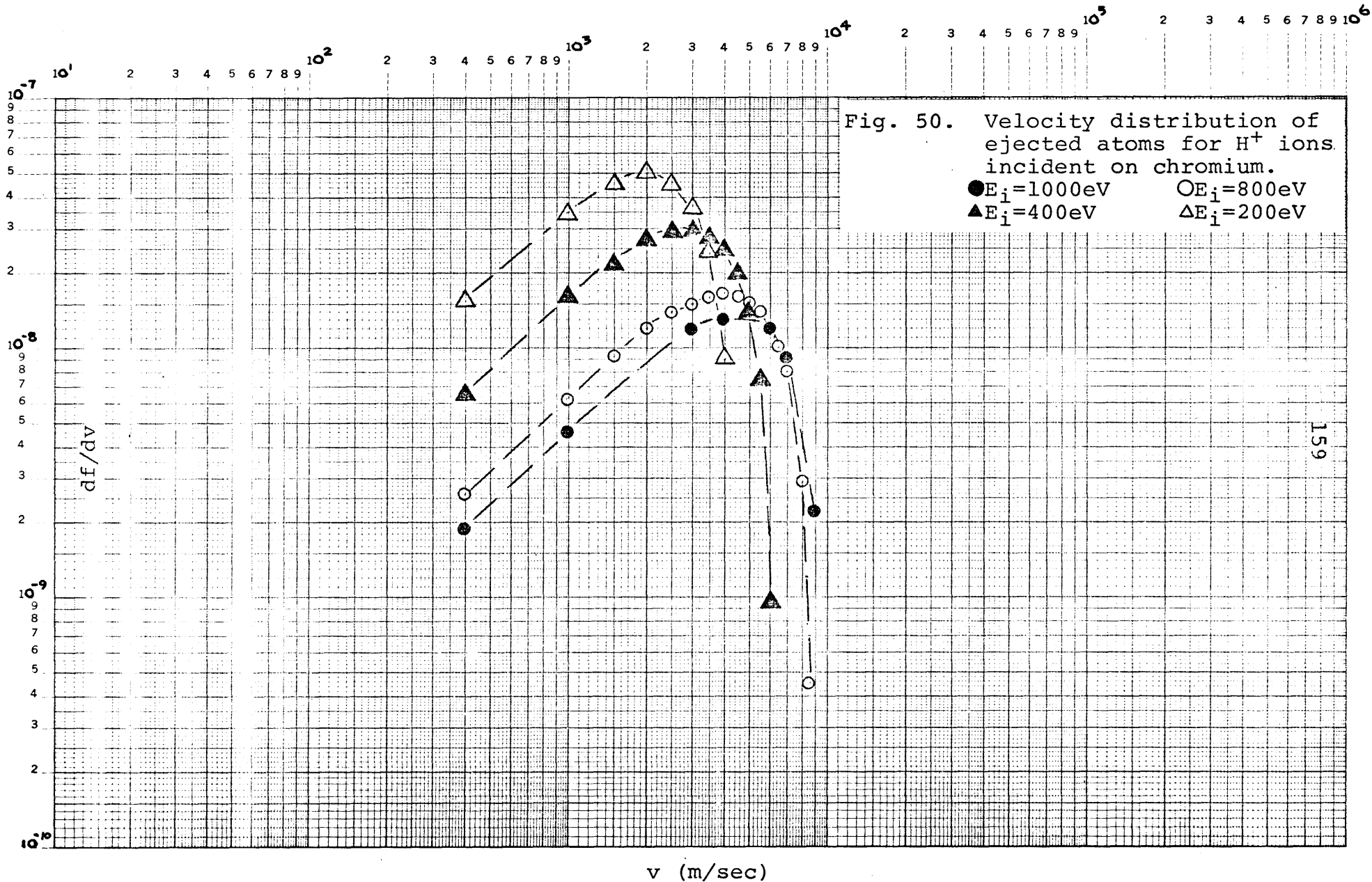


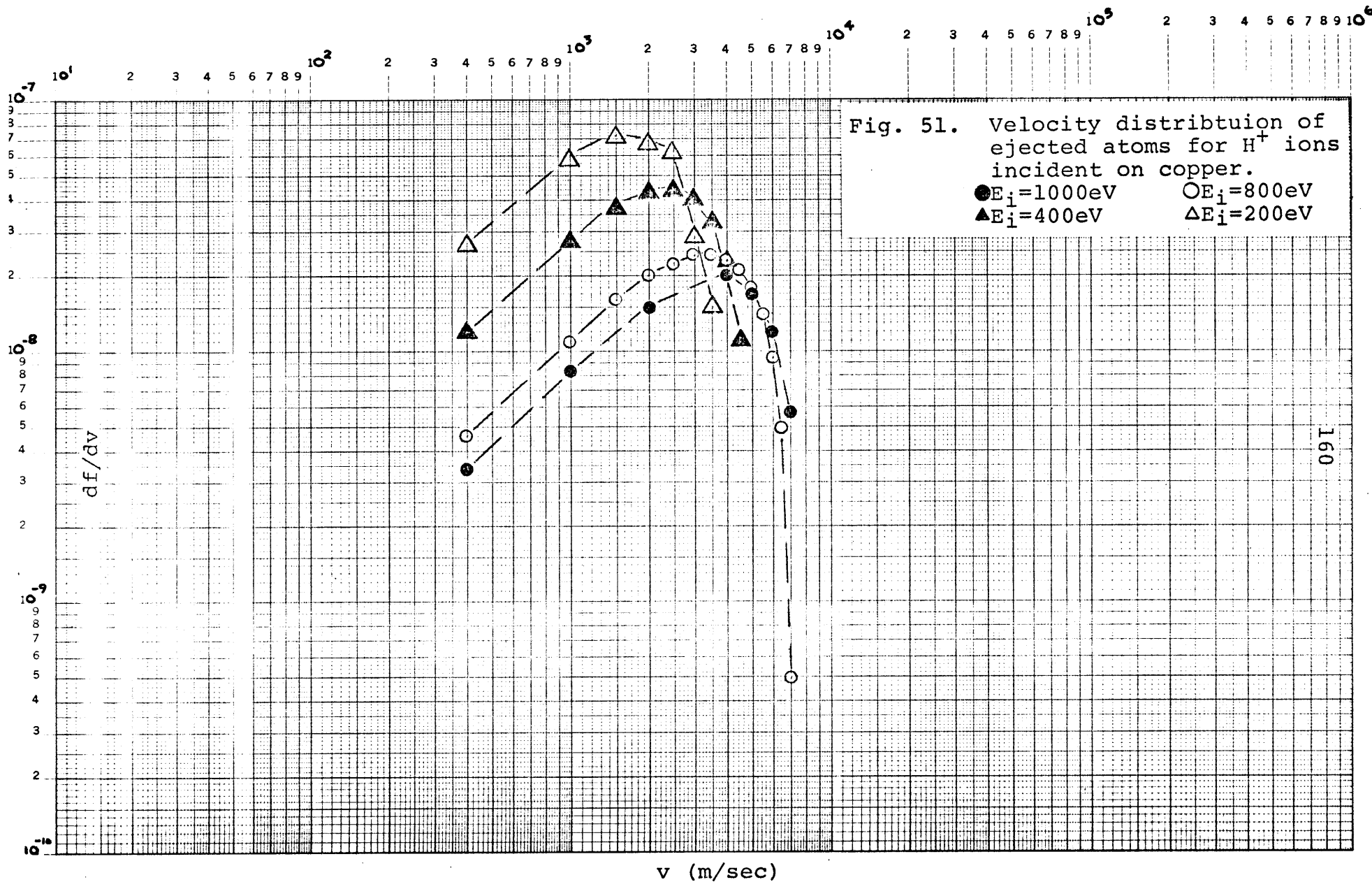
Fig. 47. Variation of the sputtering yield with angle of incidence for H^+ ions on zinc [calculated from Eq. (26)].

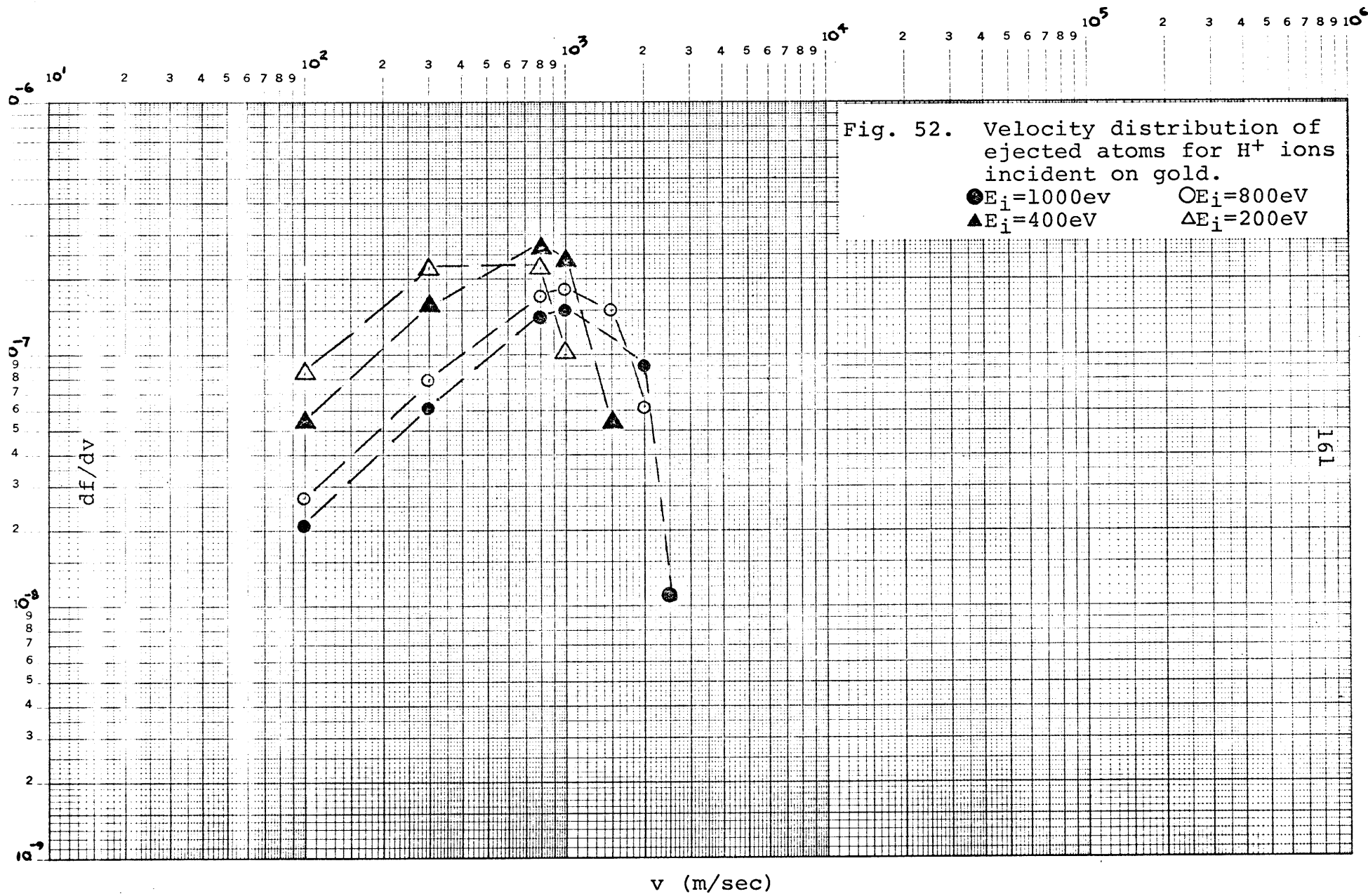
156

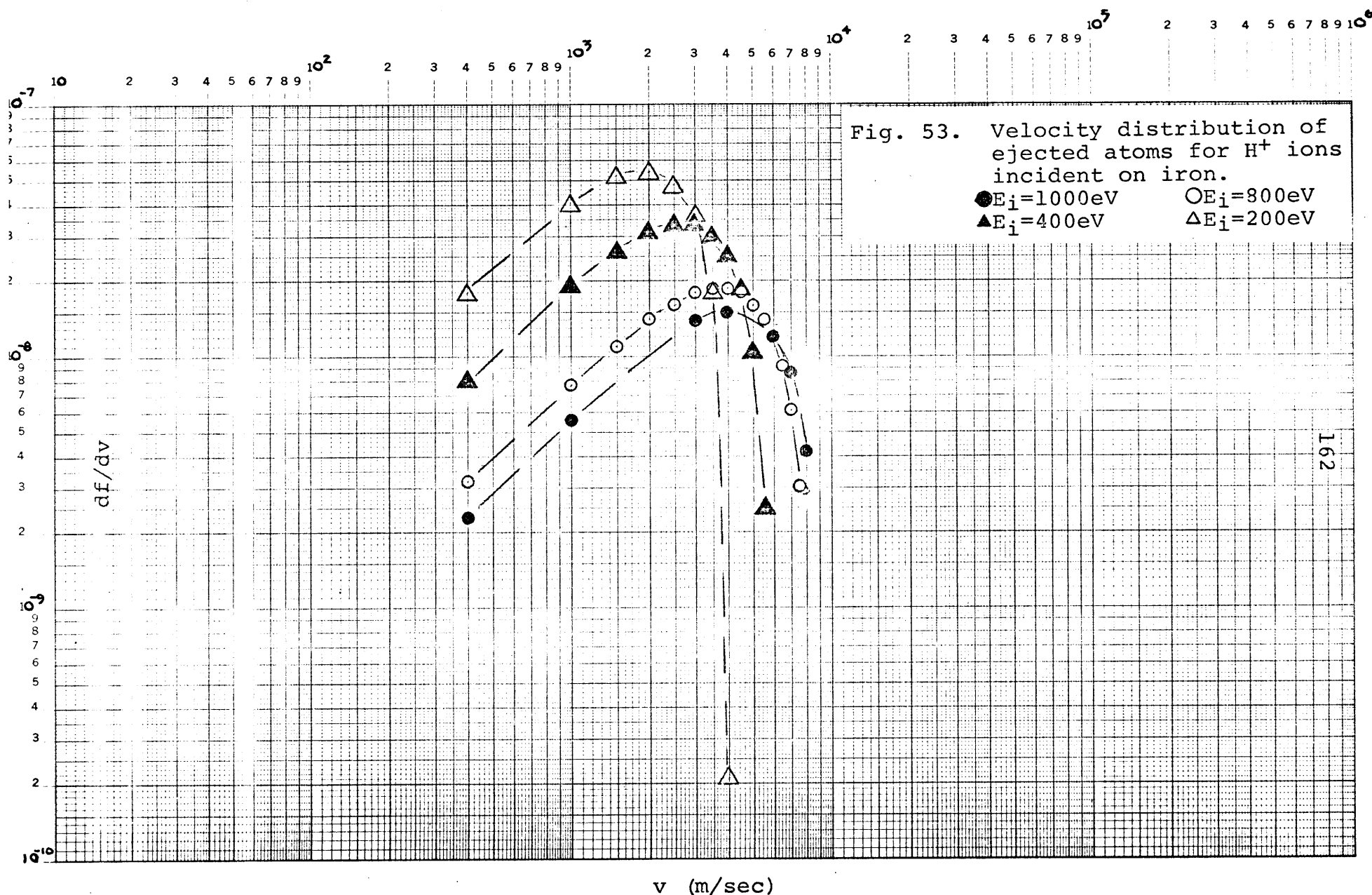


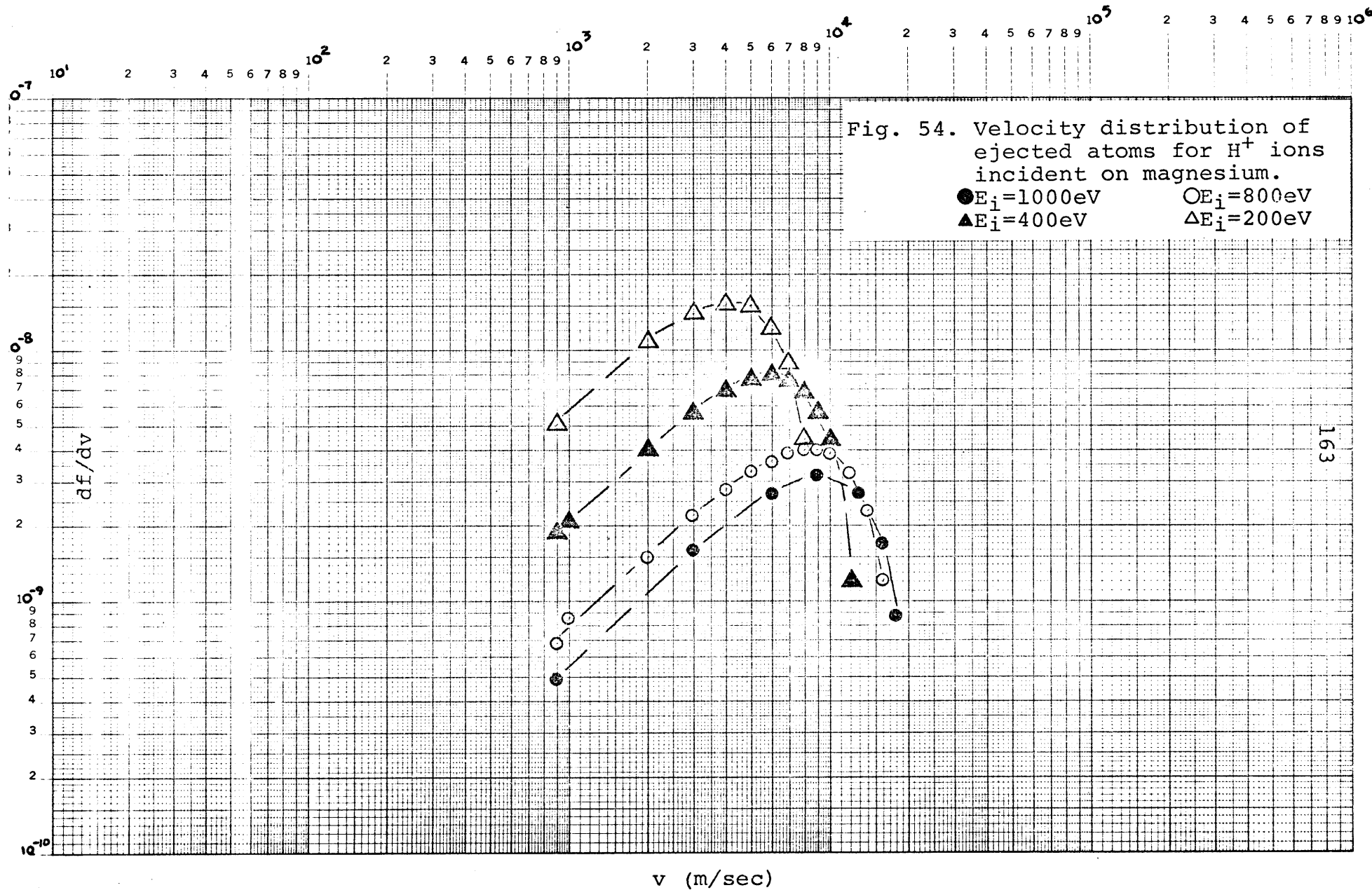


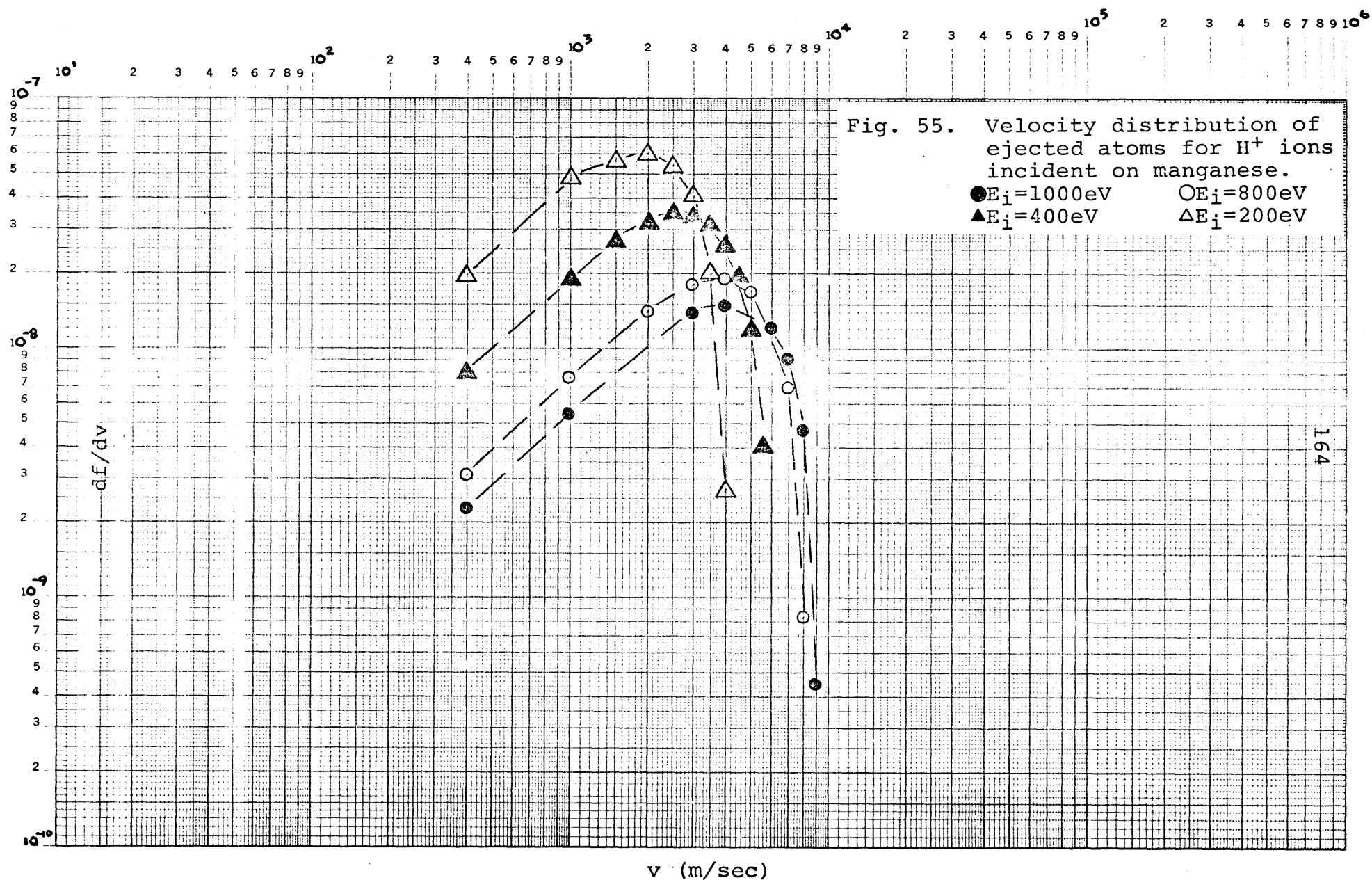


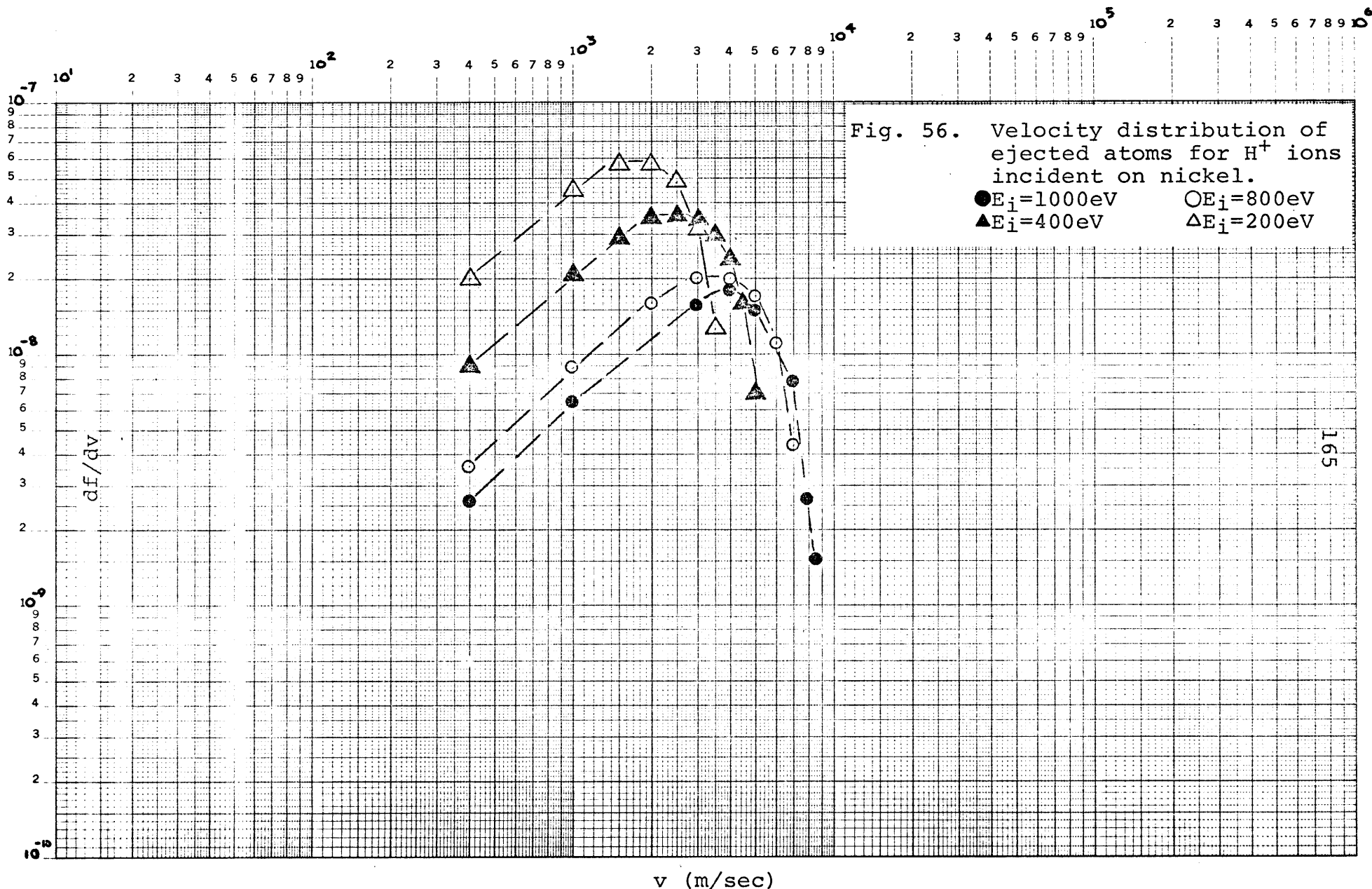












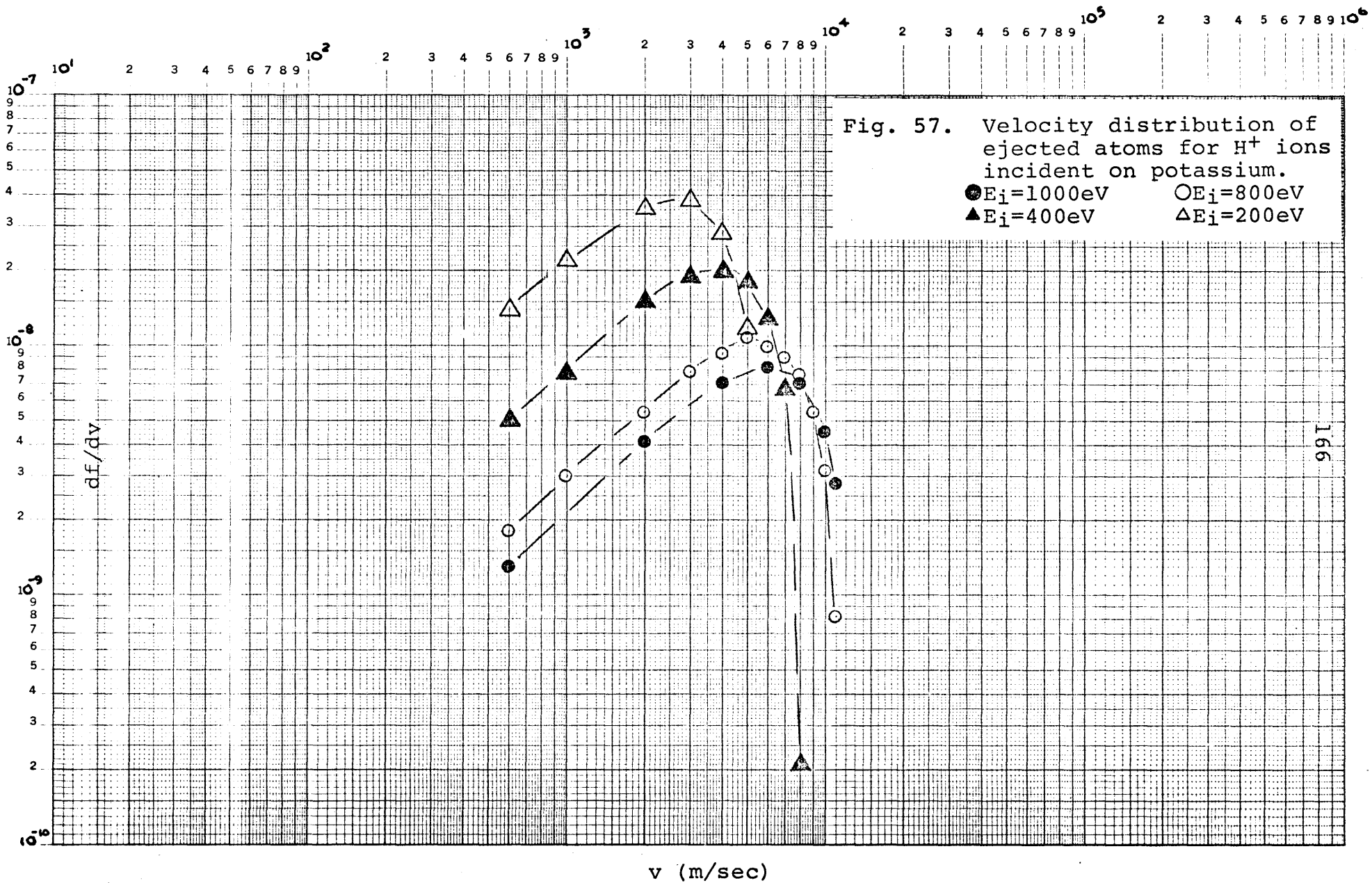
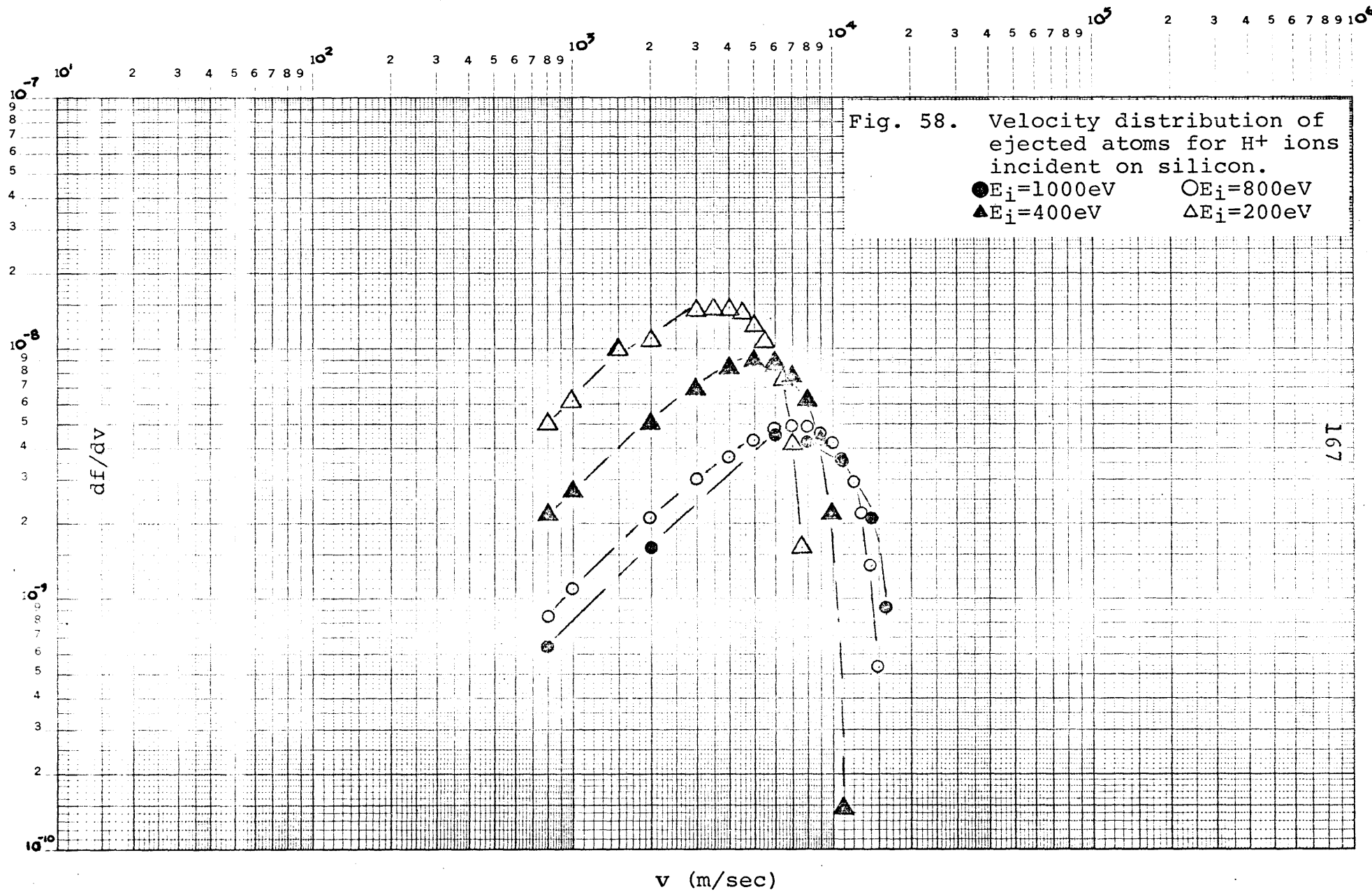
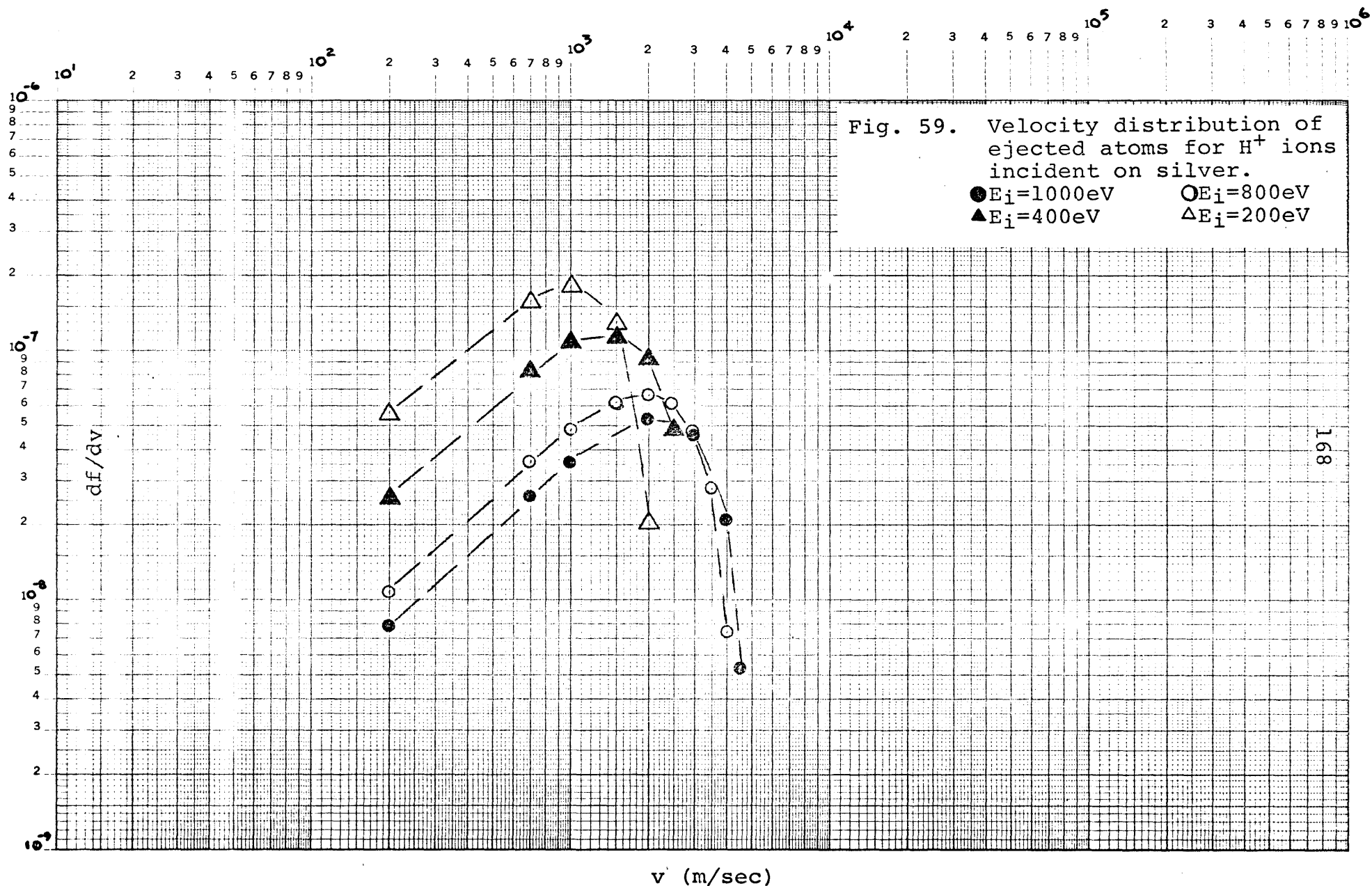


Fig. 57. Velocity distribution of ejected atoms for H^+ ions incident on potassium.

$\bullet E_i = 1000$ eV $\circ E_i = 800$ eV
 $\blacktriangle E_i = 400$ eV $\triangle E_i = 200$ eV





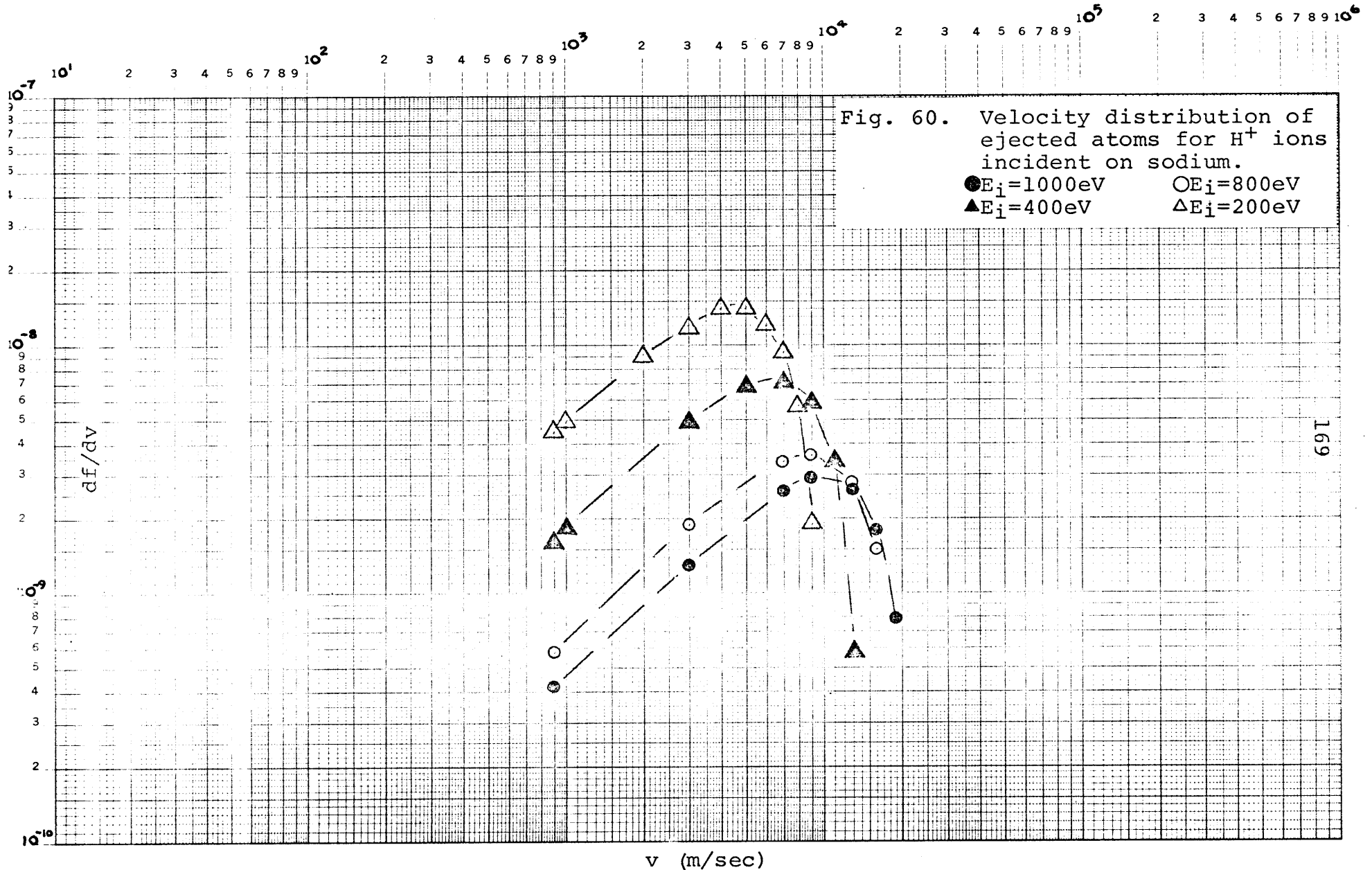
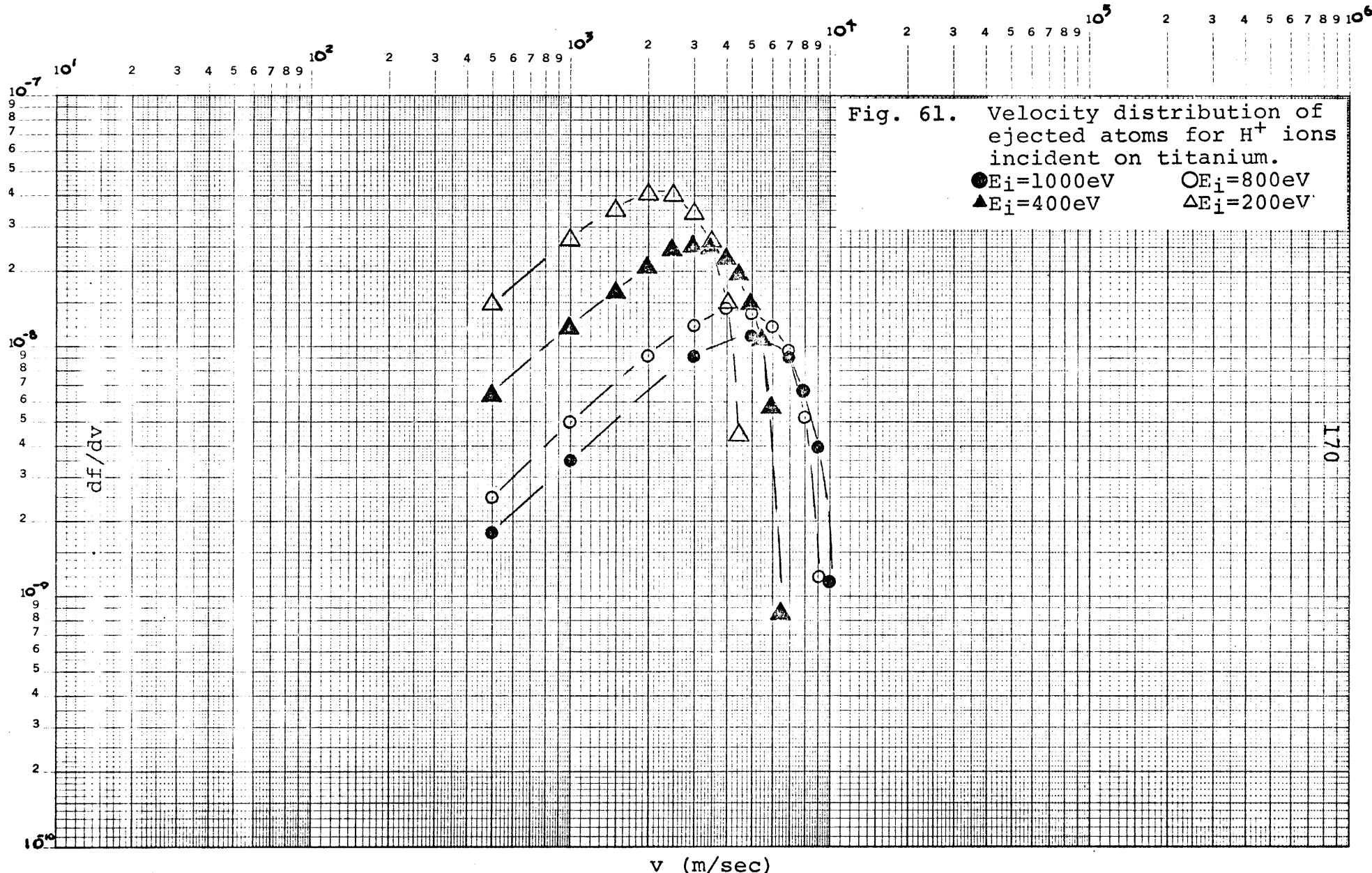


Fig. 60. Velocity distribution of ejected atoms for H^+ ions incident on sodium.

$\bullet E_i = 1000\text{eV}$ $\circ E_i = 800\text{eV}$
 $\blacktriangle E_i = 400\text{eV}$ $\triangle E_i = 200\text{eV}$



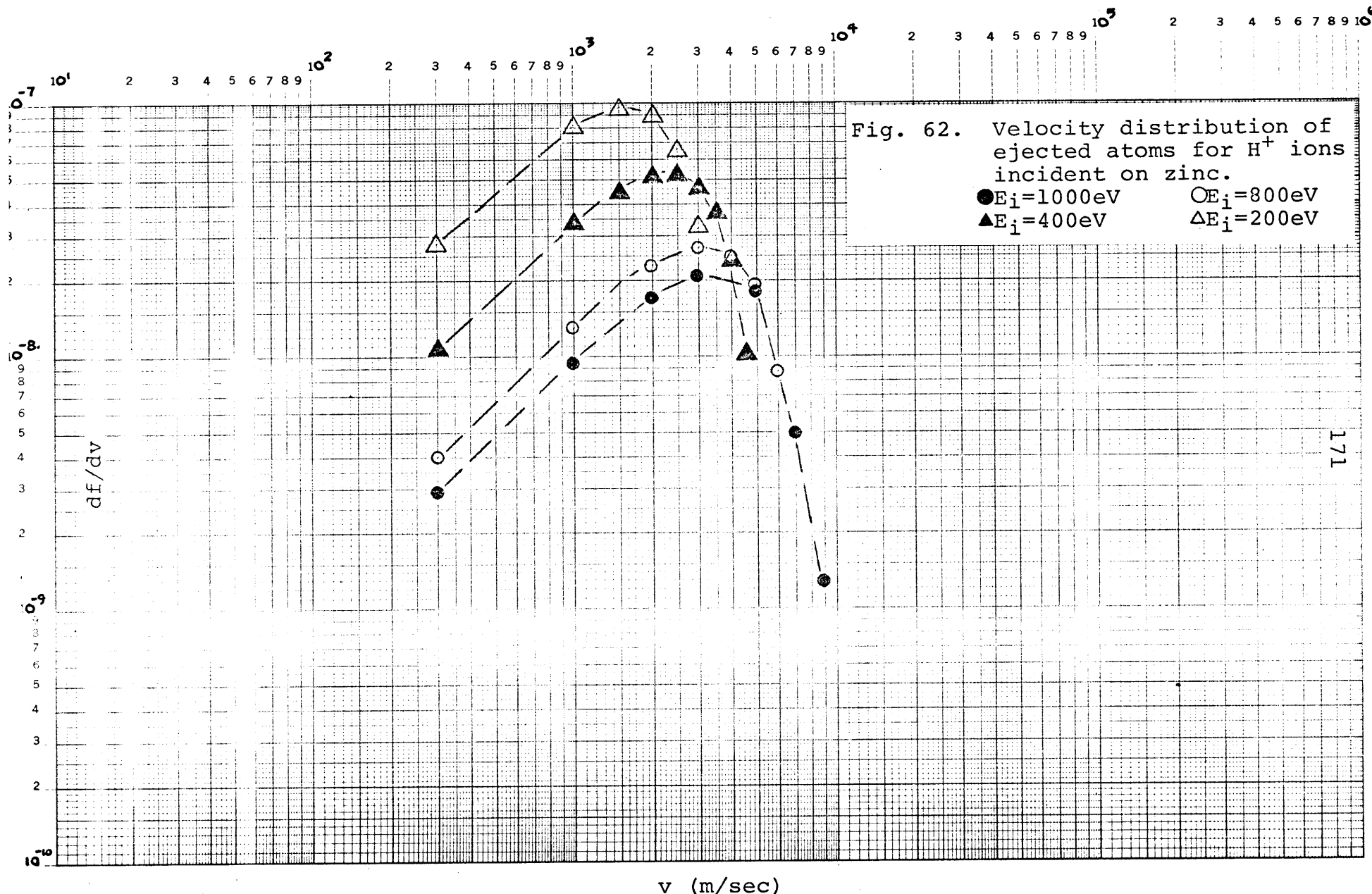


Fig. 63. Sputtering yields for H^+ ions incident on Al_2O_3 [calculated from Eq.(32)].

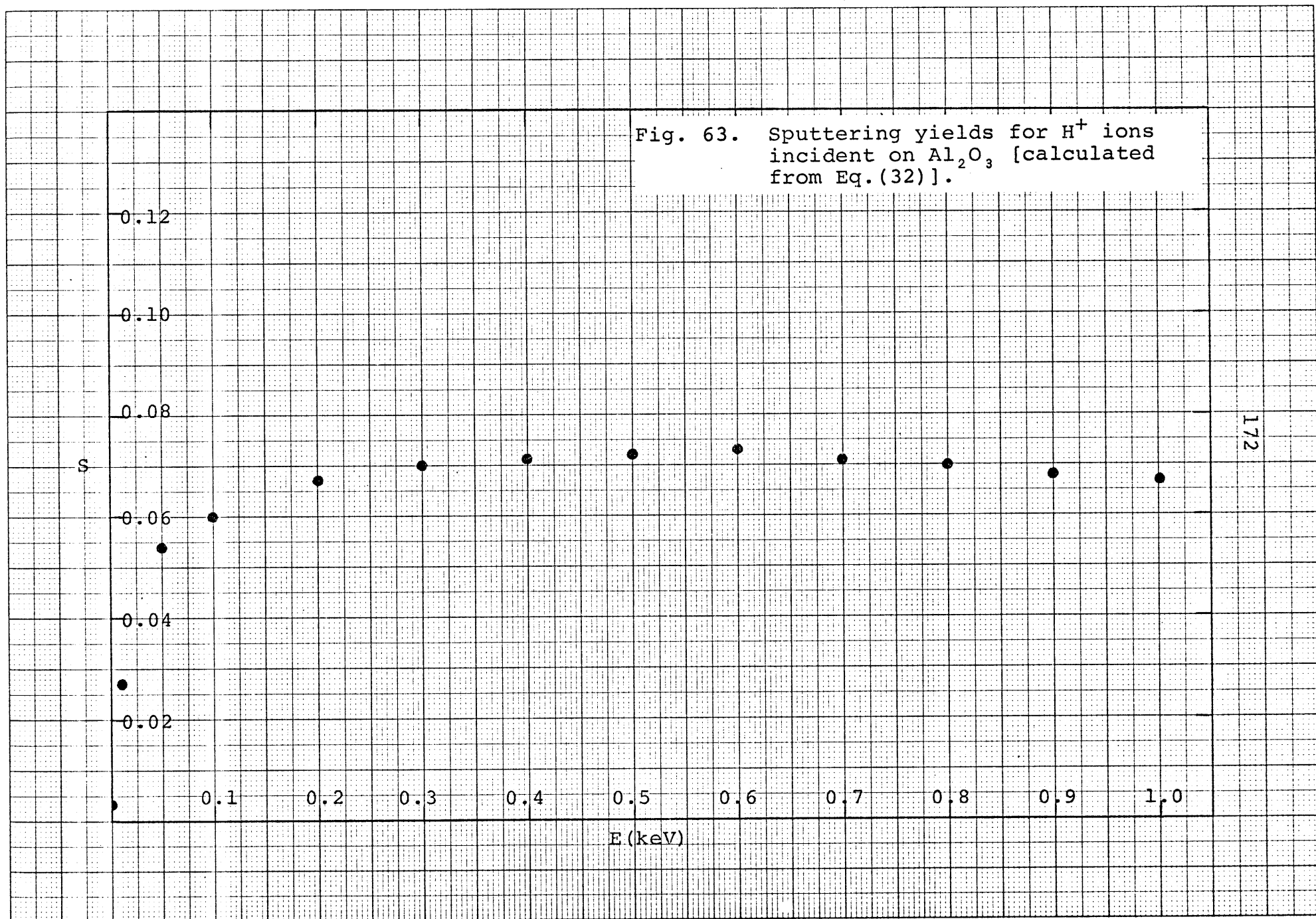
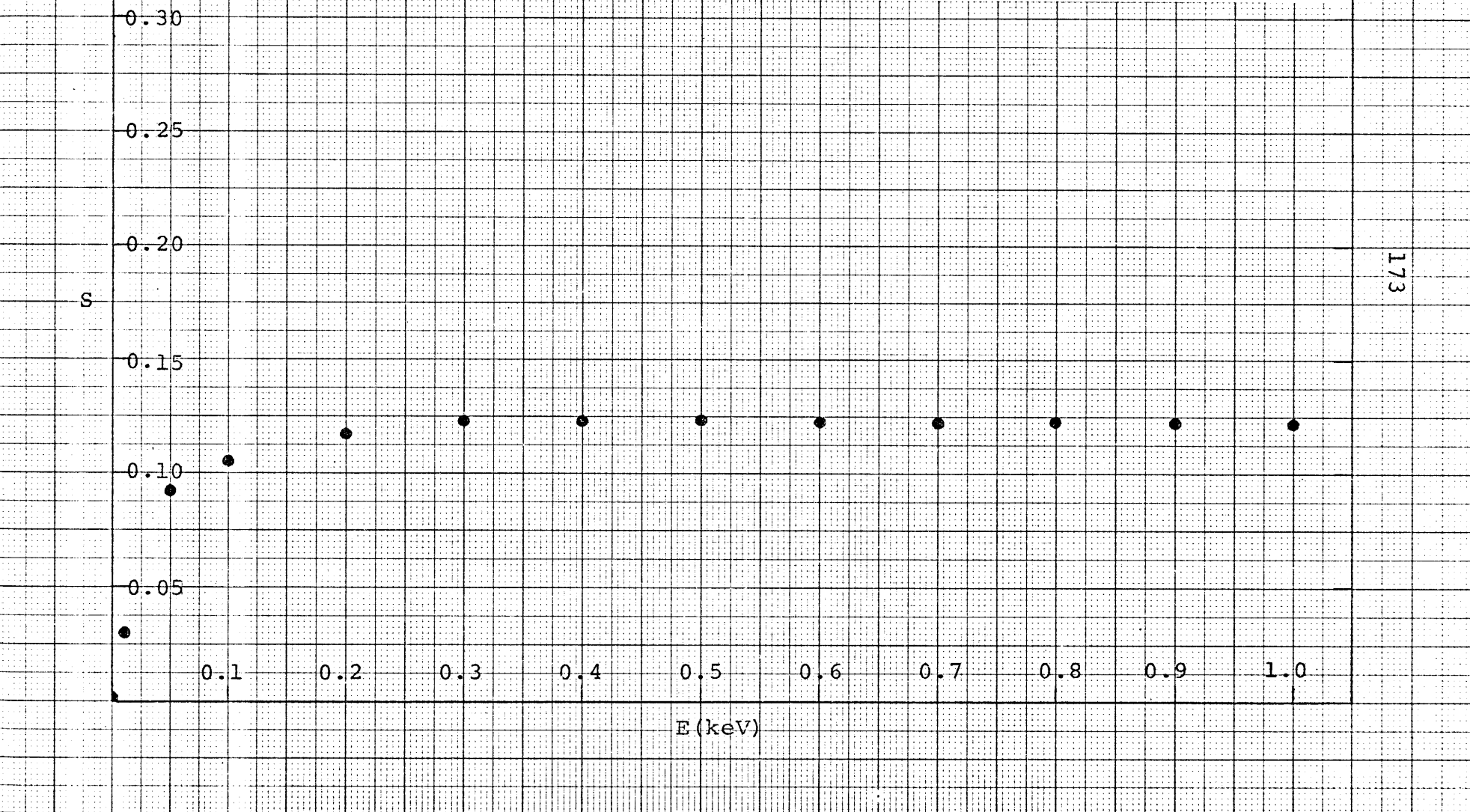


Fig. 64. Sputtering yields for H^+ ions incident on CaO [calculated from Eq.(32)].



173

Fig. 65. Sputtering yields for H^+ ions incident on FeO [calculated from Eq.(32)].

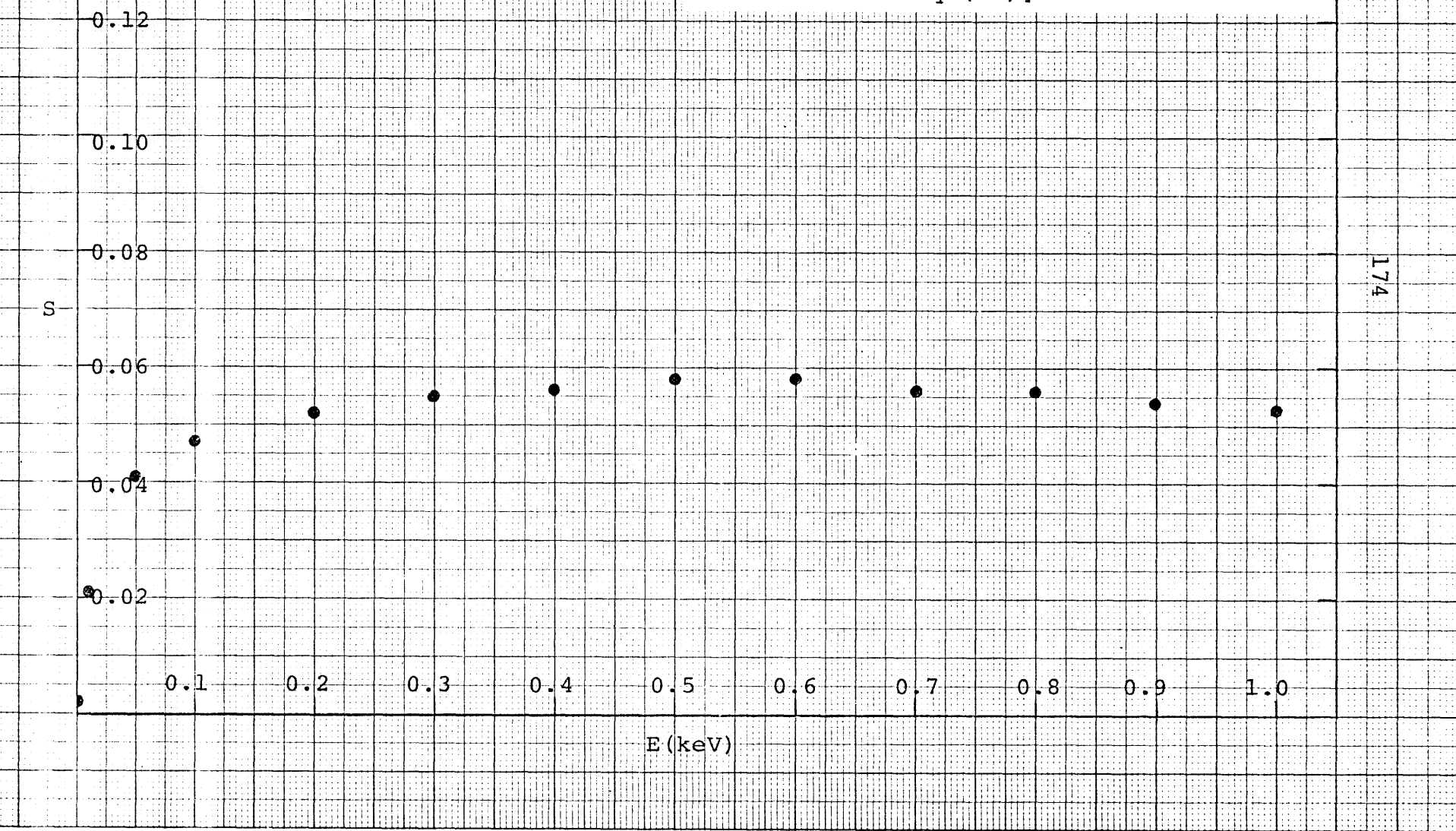


Fig. 66. Sputtering yields for H^+ ions incident on Fe_2O_3 [calculated from Eq. (32)].

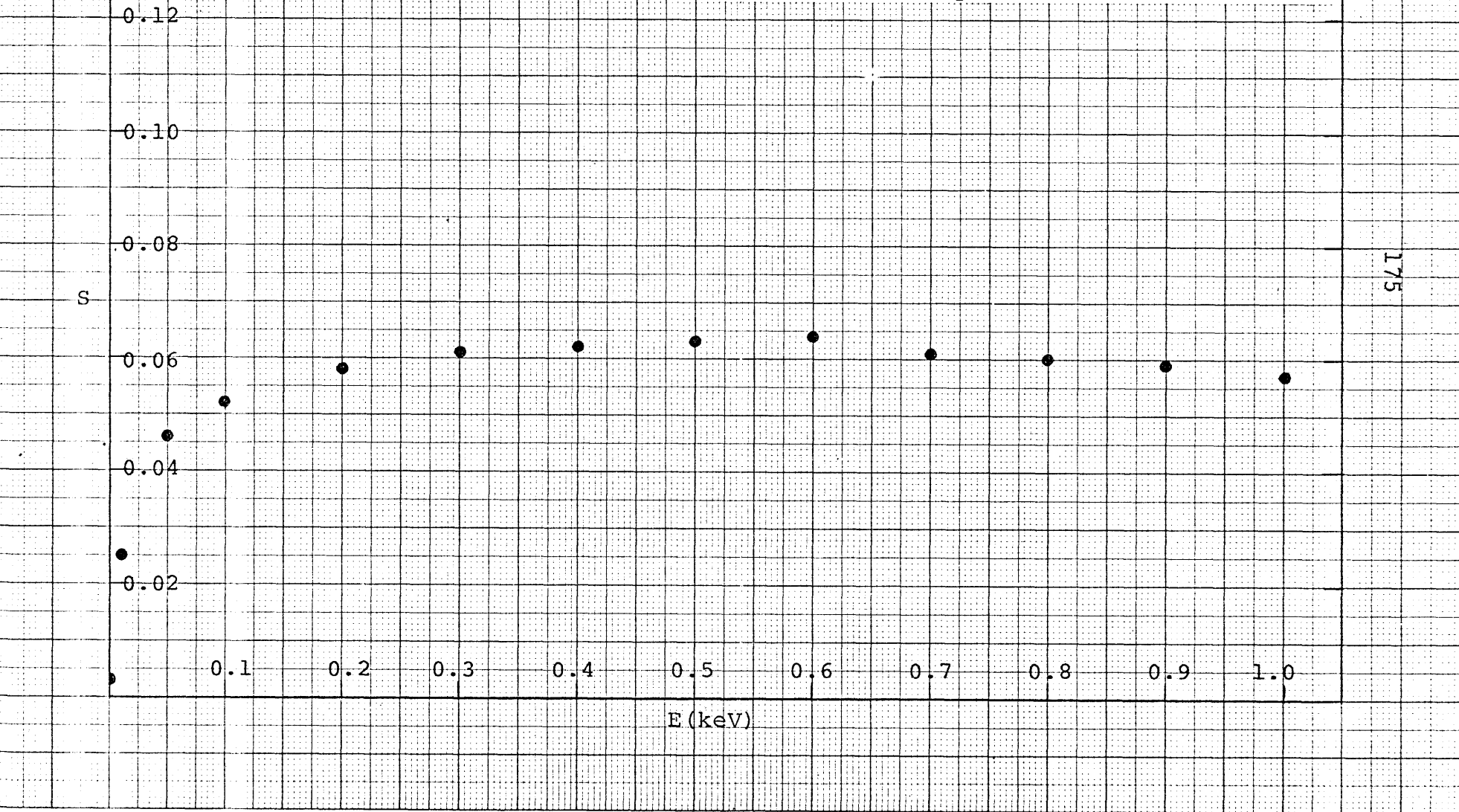


Fig. 67. Sputtering yields for H^+ ions
incident on Fe_3O_4 [calculated
from Eq.(32)].

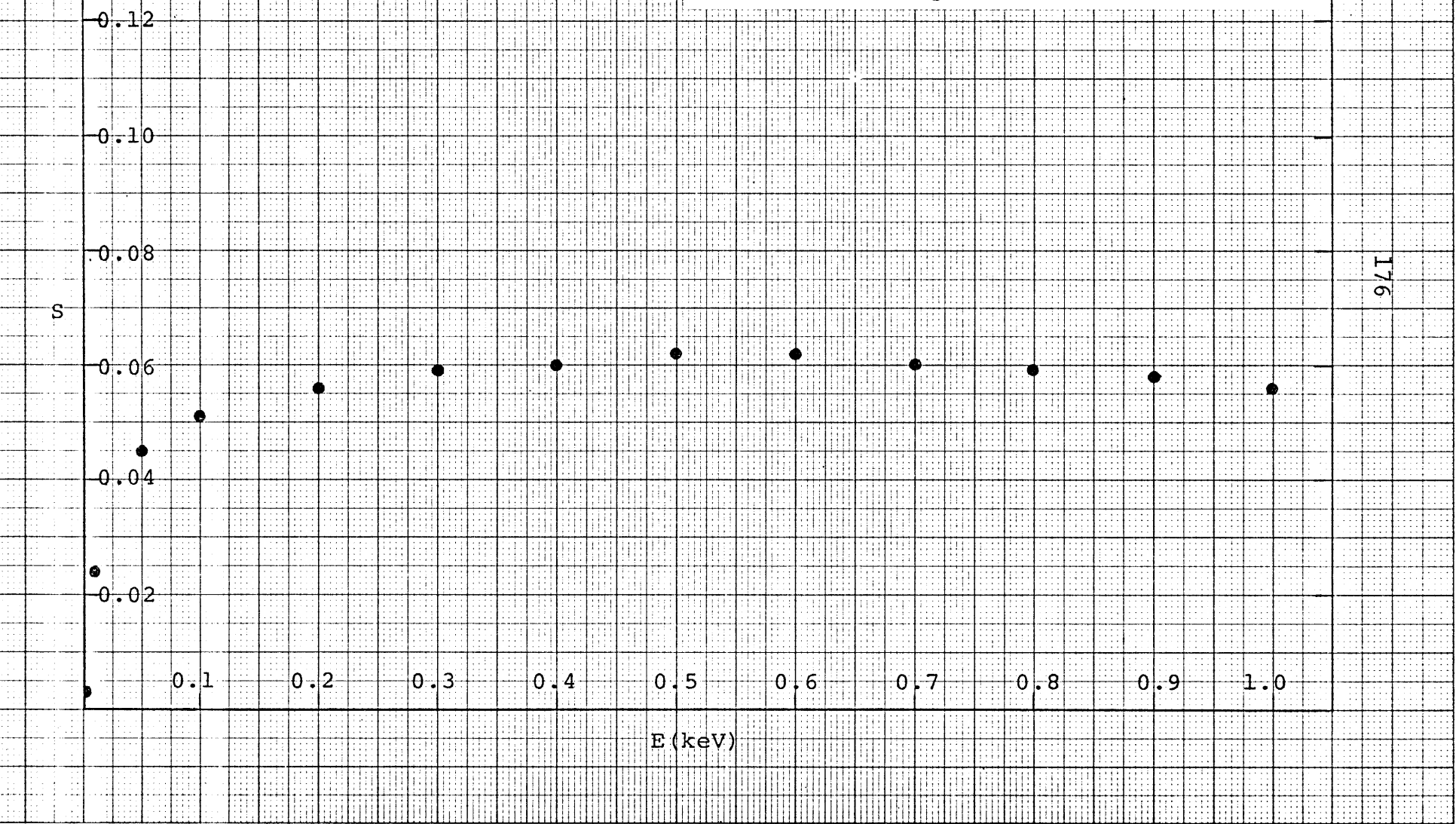


Fig. 68. Sputtering yields for H^+ ions incident on MgO [calculated from Eq.(32)].

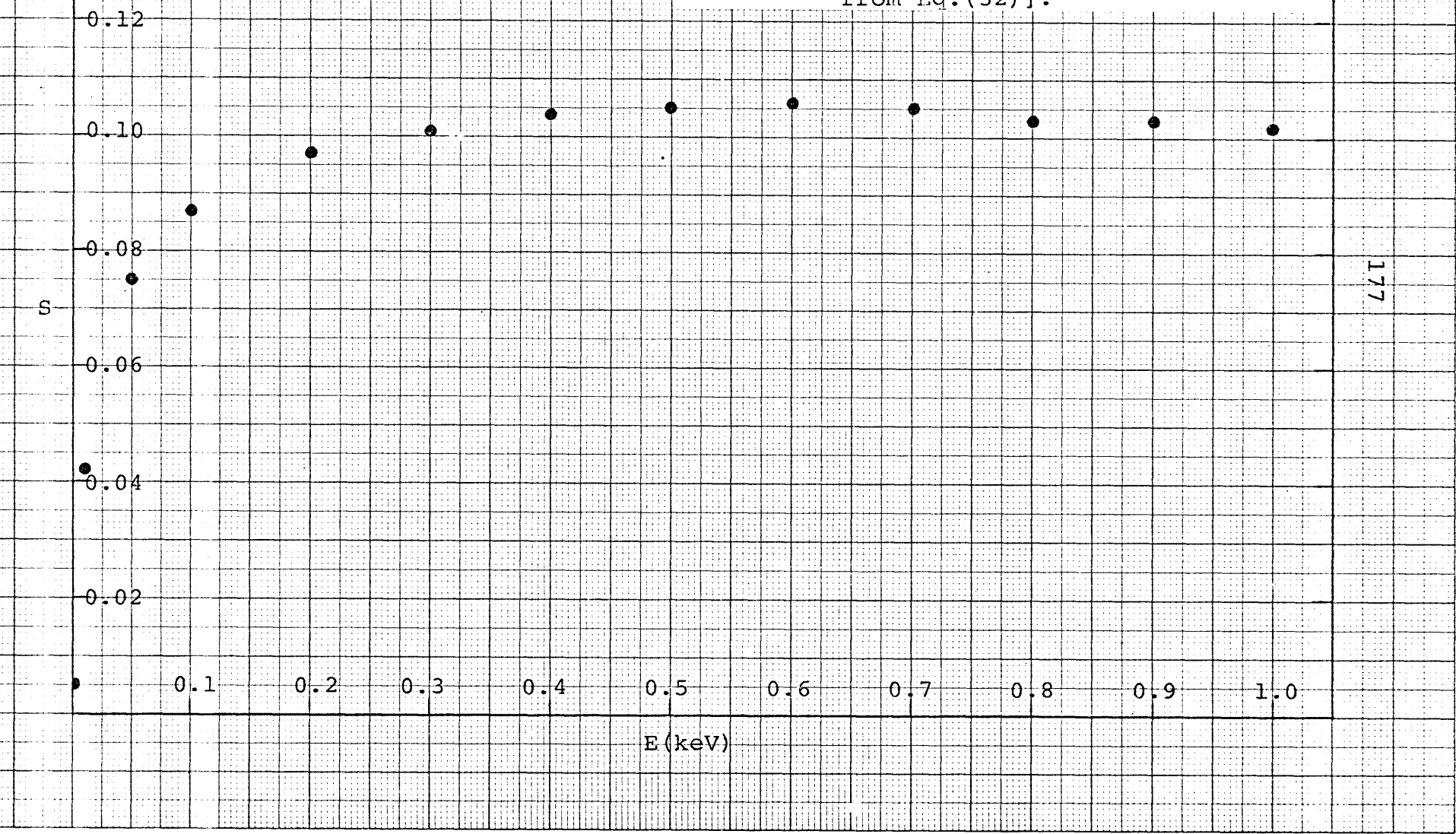


Fig. 69. Sputtering yields for H^+ ions incident on MnO [calculated from Eq.(32)].

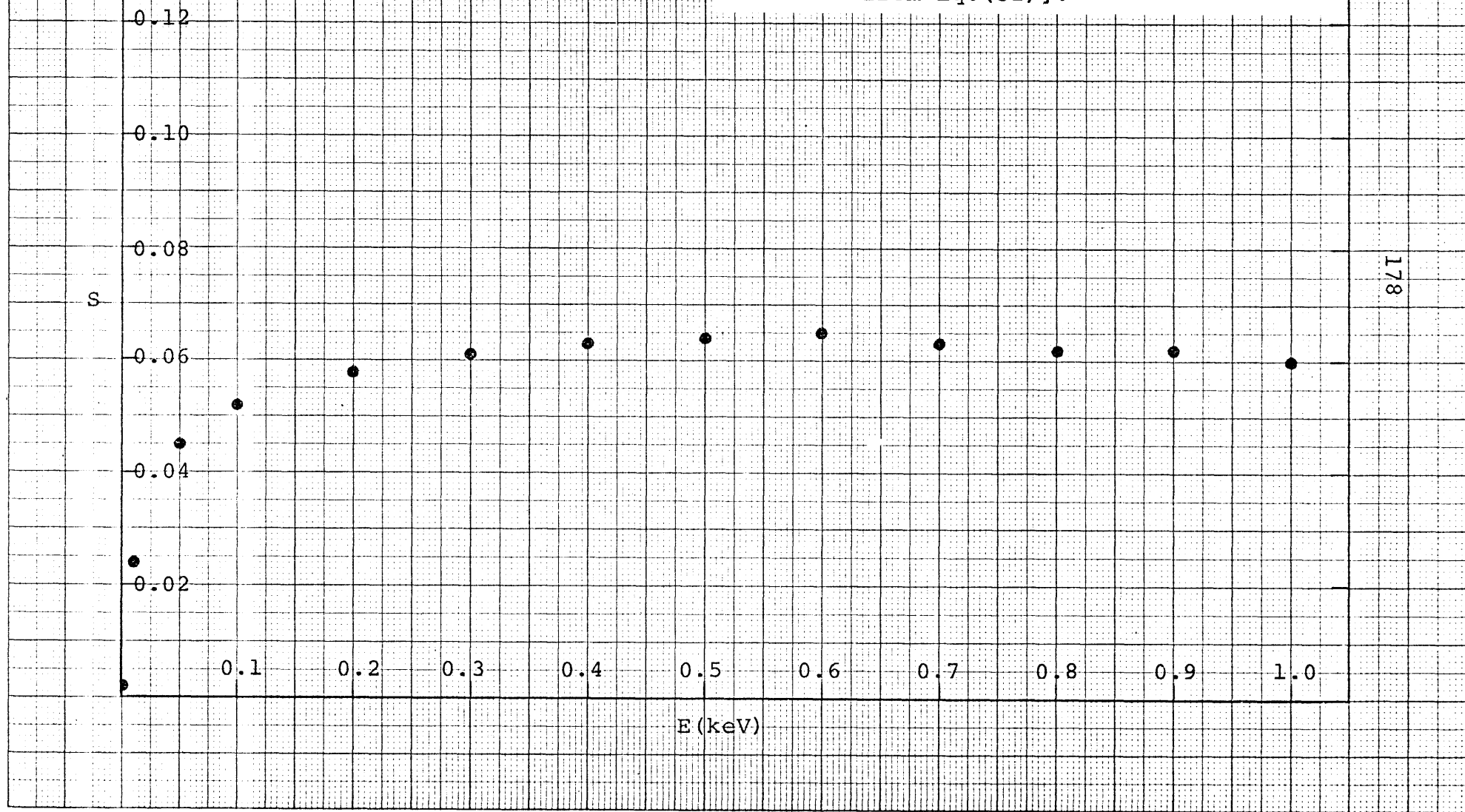


Fig. 70. Sputtering yields for H^+ ions incident on TiO_2 [calculated from Eq.(32)].

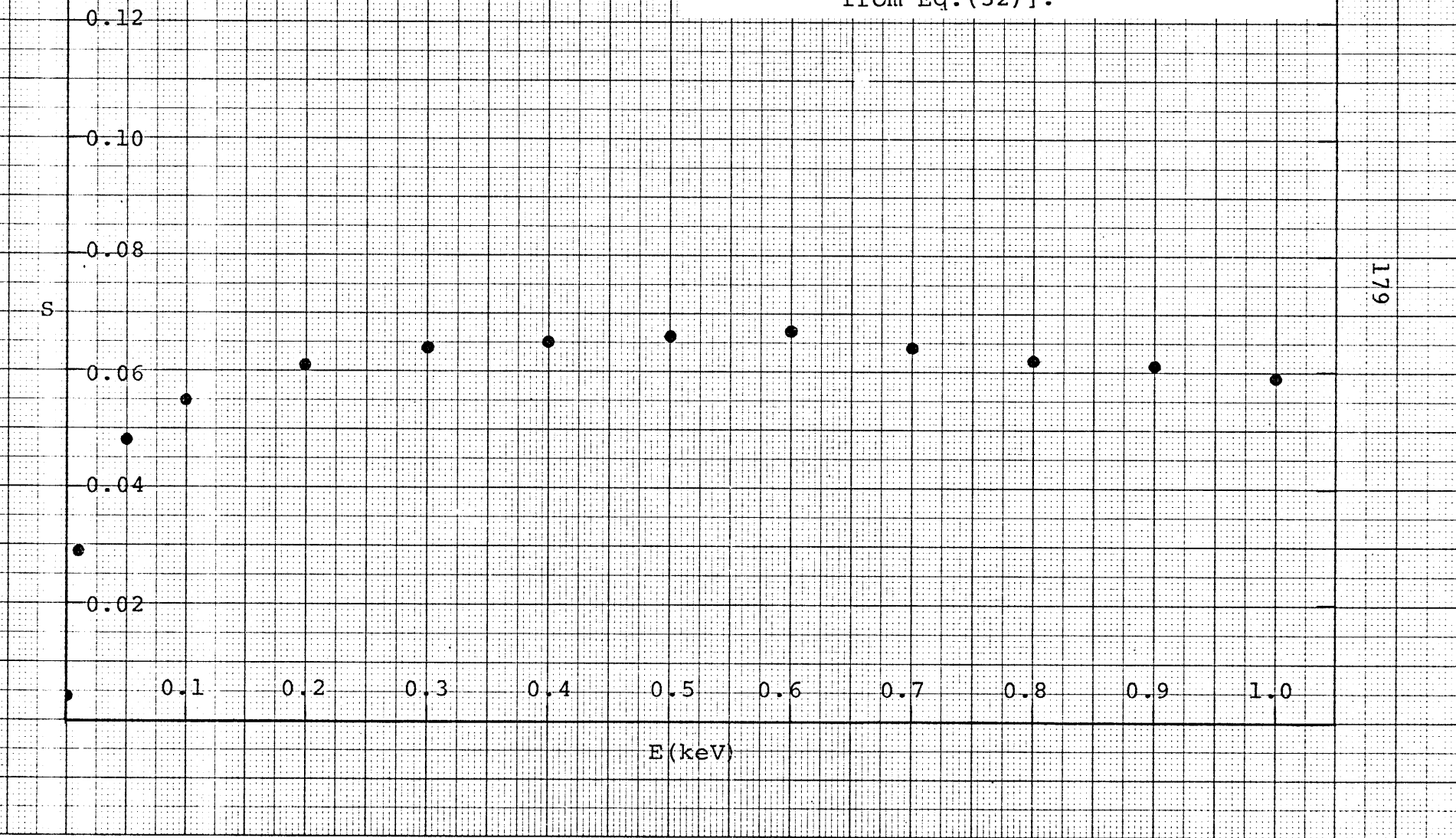


Fig. 71. Variation of the sputtering yield with angle of incidence for H^+ ions on Al_2O_3 [calculated from Eq.(26)].

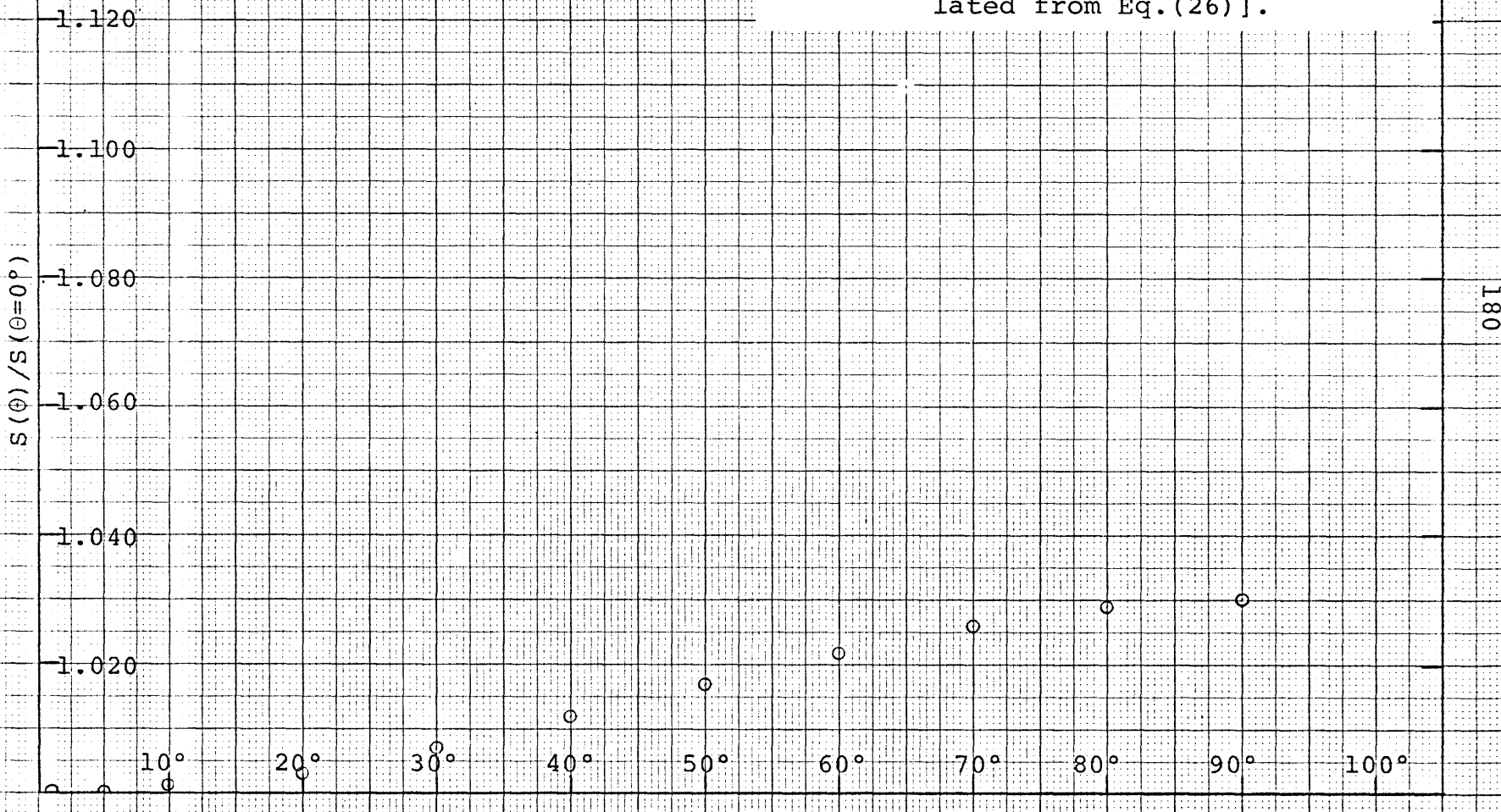
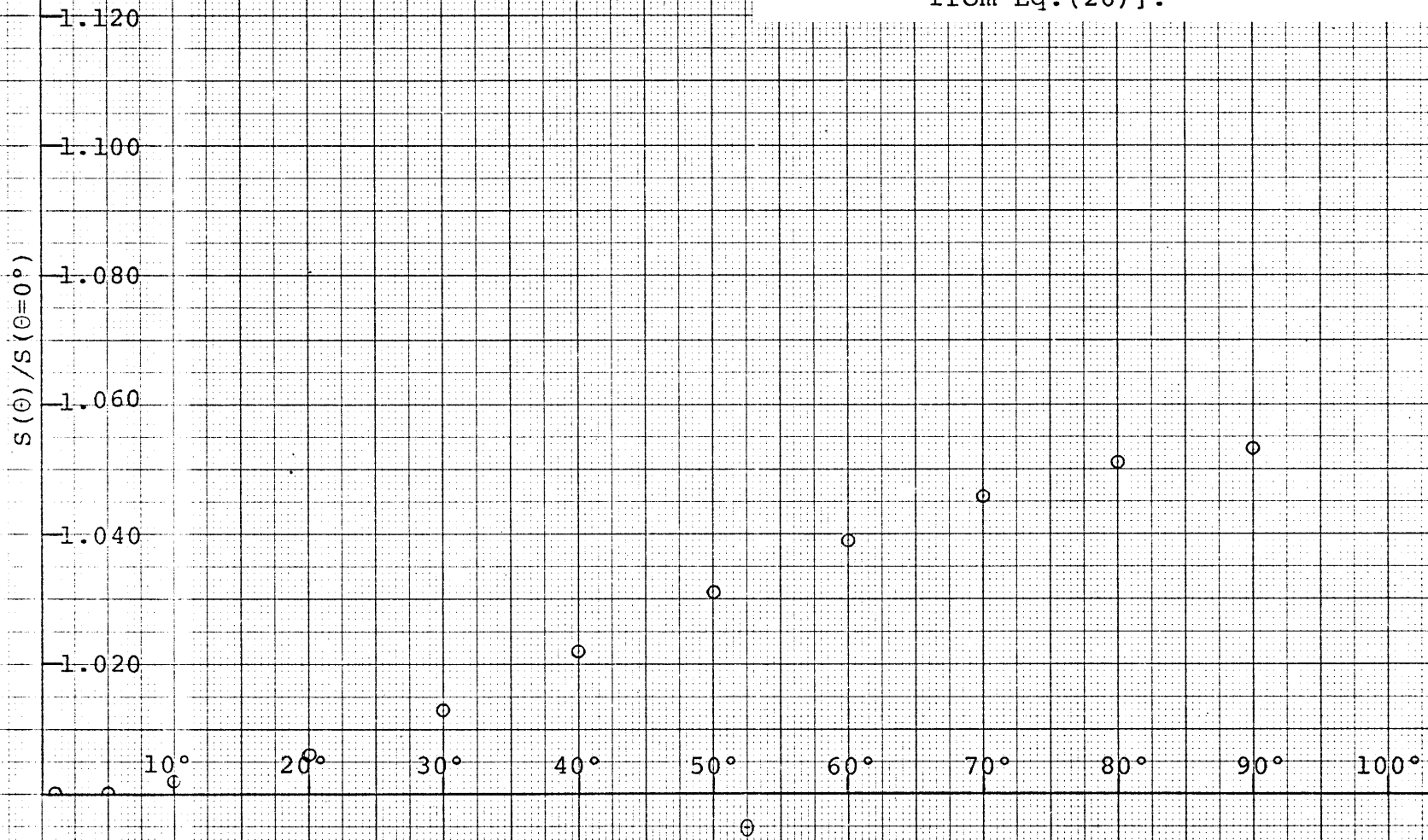


Fig. 72. Variation of the sputtering yield with angle of incidence for H^+ ions on CaO [calculated from Eq.(26)].



181

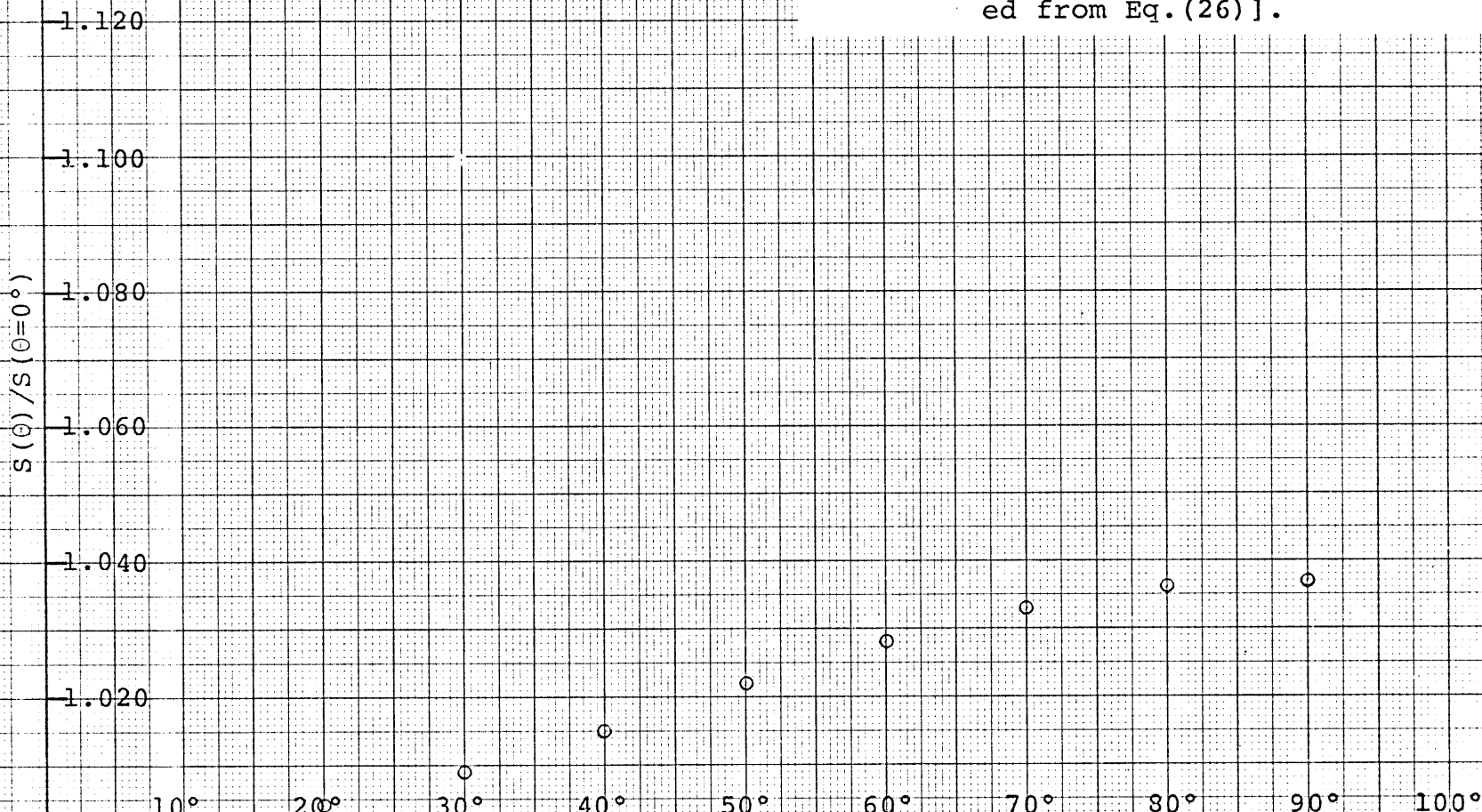


Fig. 73. Variation of the sputtering yield with angle of incidence for H^+ ions on FeO [calculated from Eq. (26)].

Fig. 74. Variation of the sputtering yield with angle of incidence for H^+ ions on Fe_2O_3 [calculated from Eq.(26)].

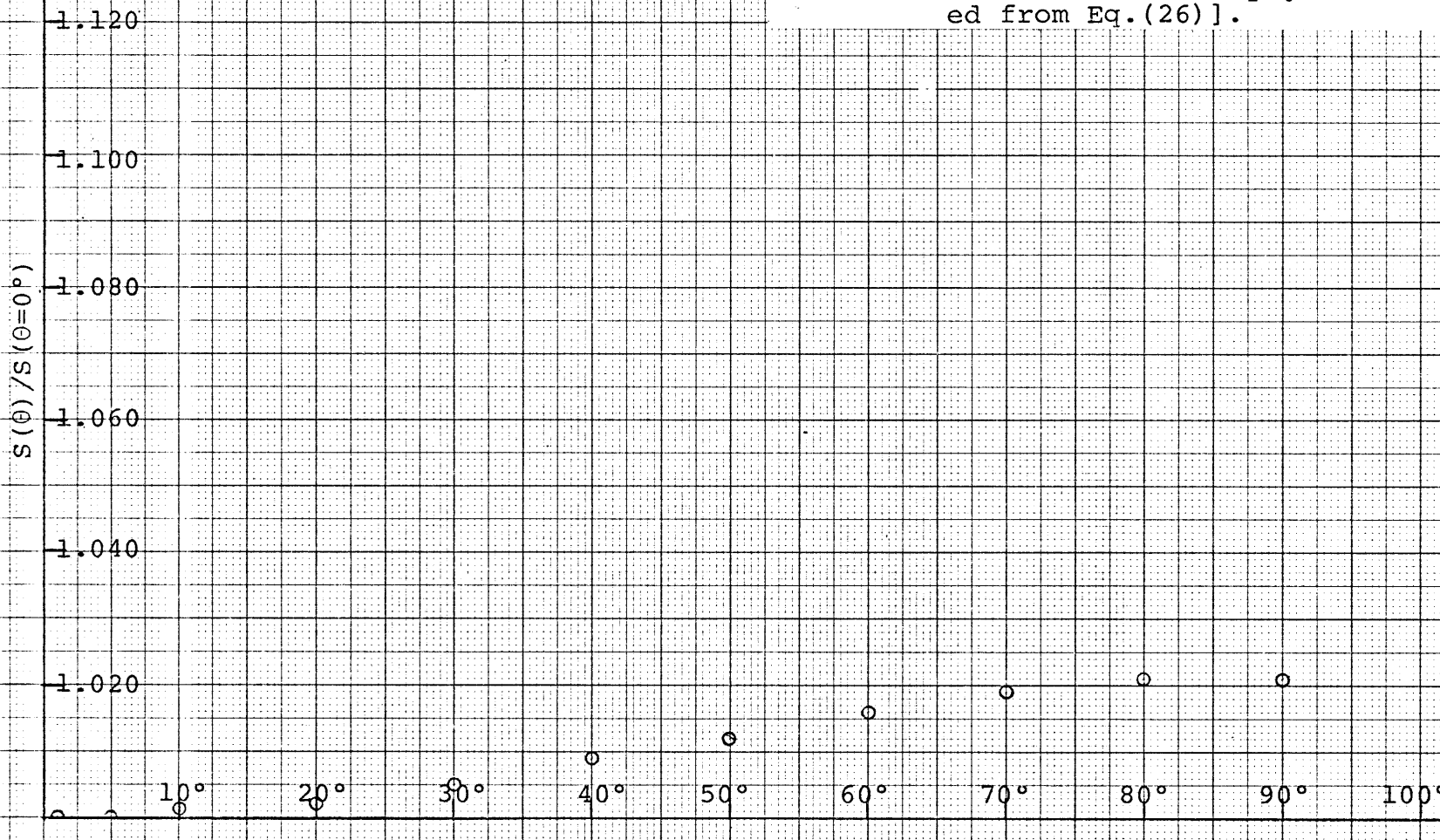
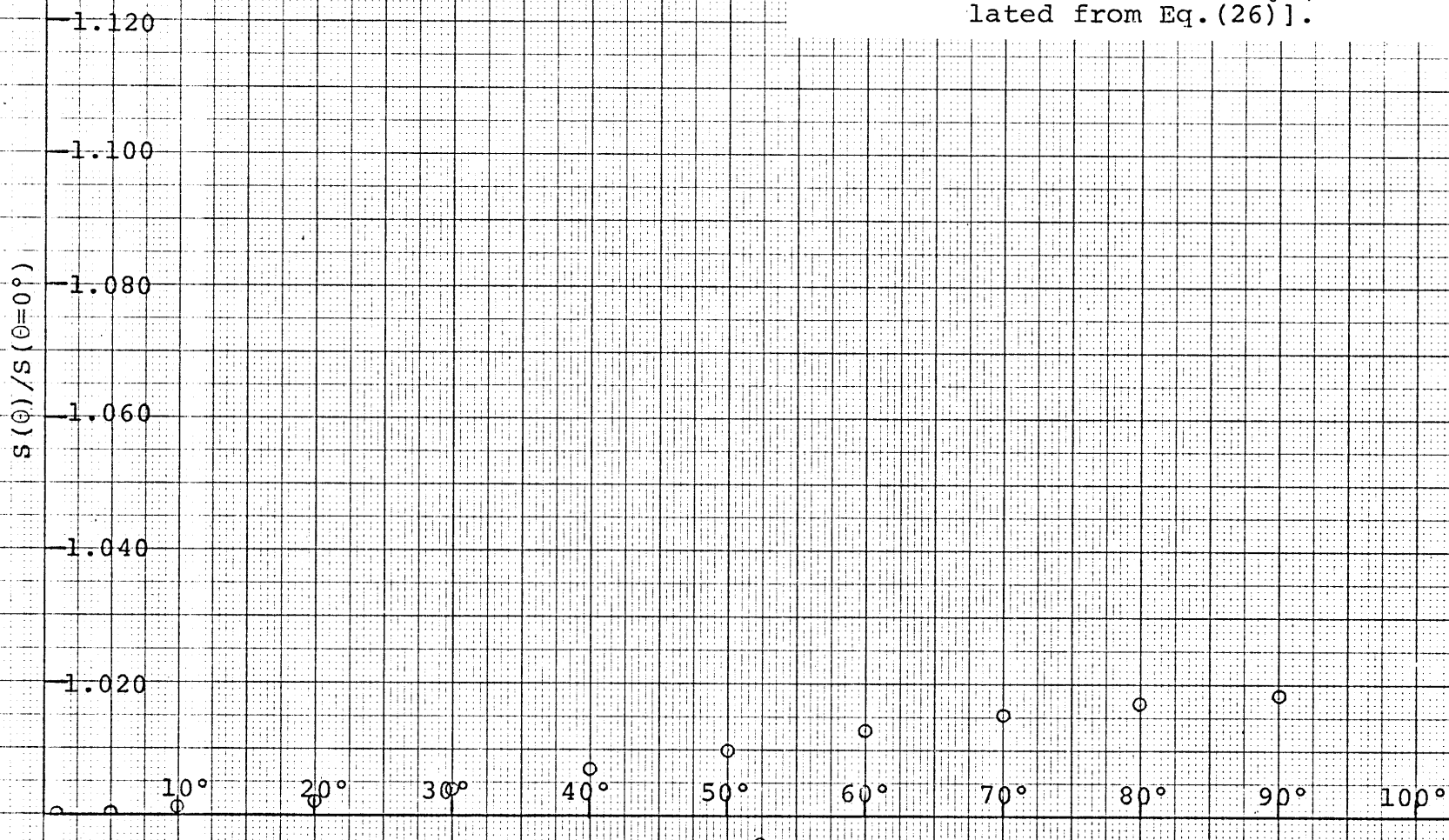
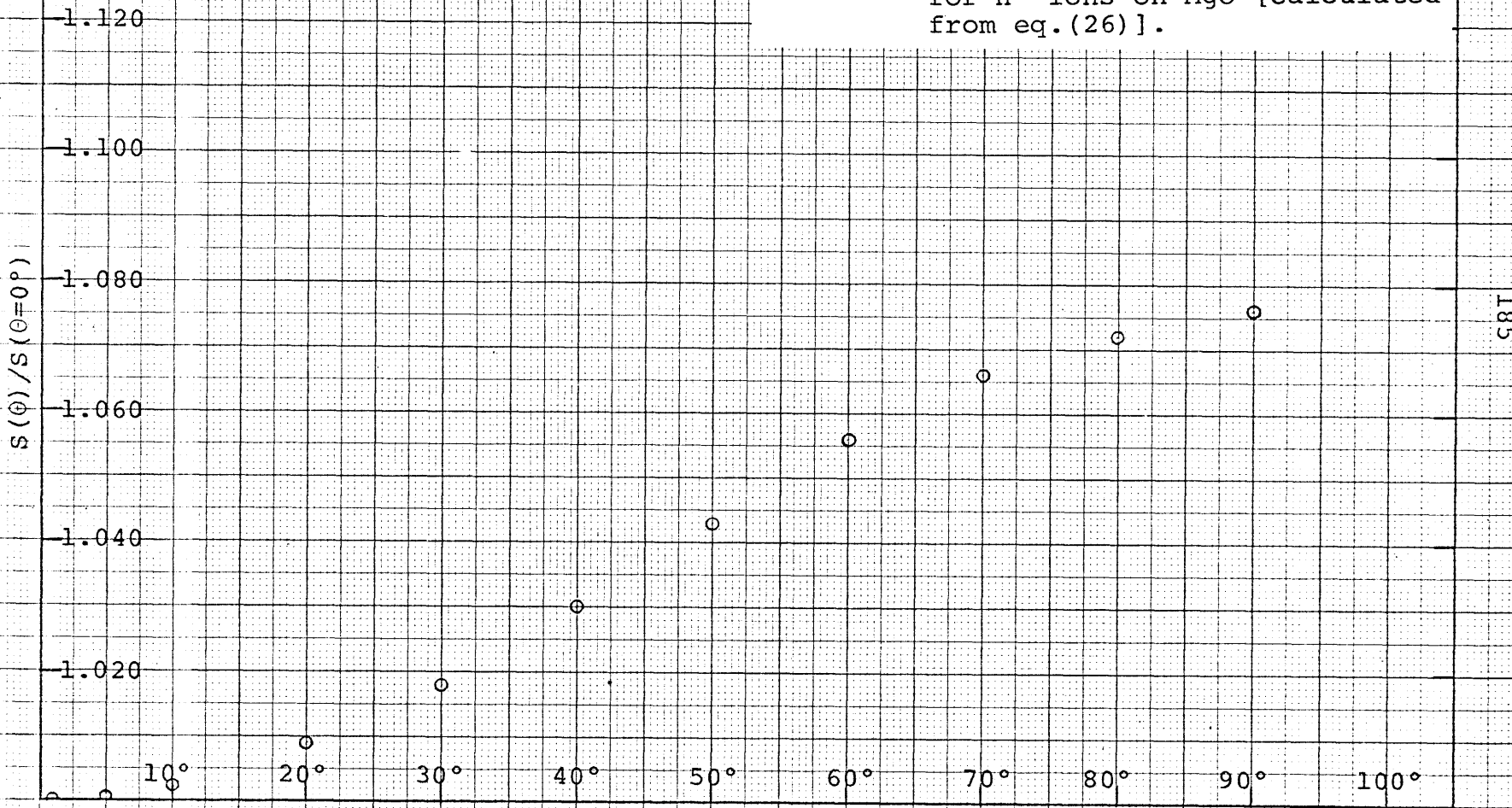


Fig. 75. Variation of the sputtering yield with angle of incidence for H^+ ions on Fe_3O_4 [calculated from Eq. (26)].



184

Fig. 76. Variation of the sputtering yield with angle of incidence for H^+ ions on MgO [calculated from eq.(26)].



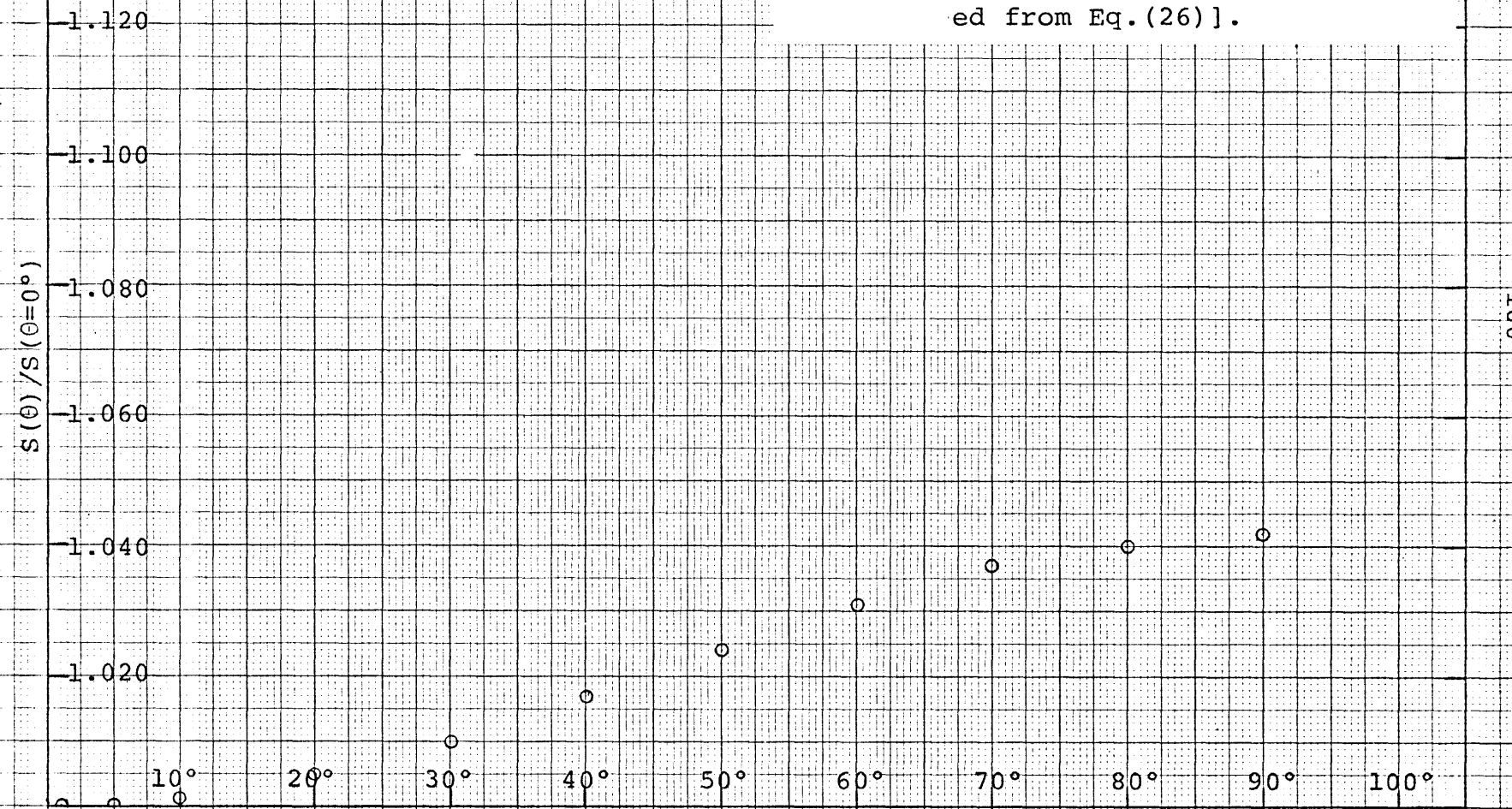
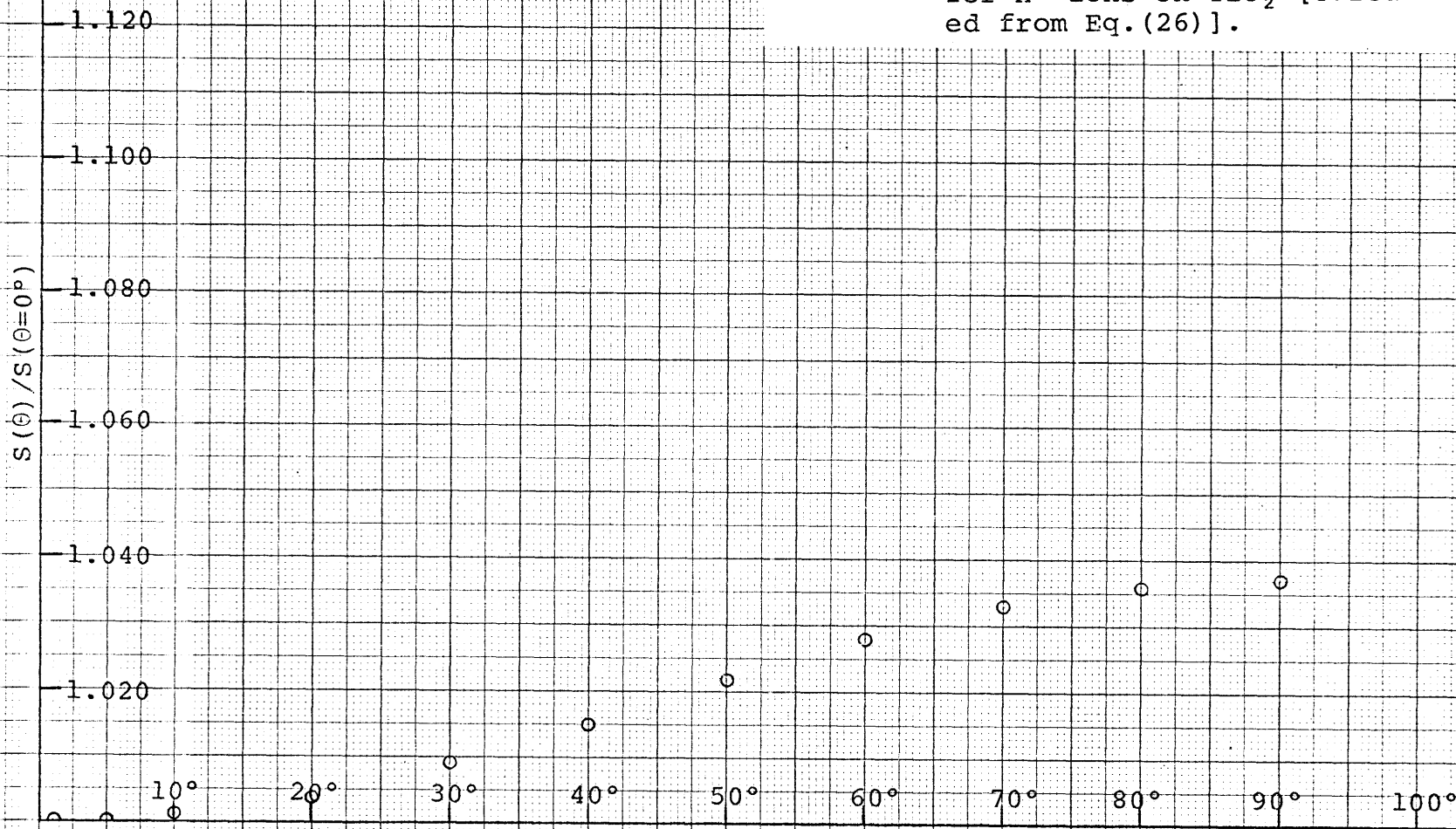
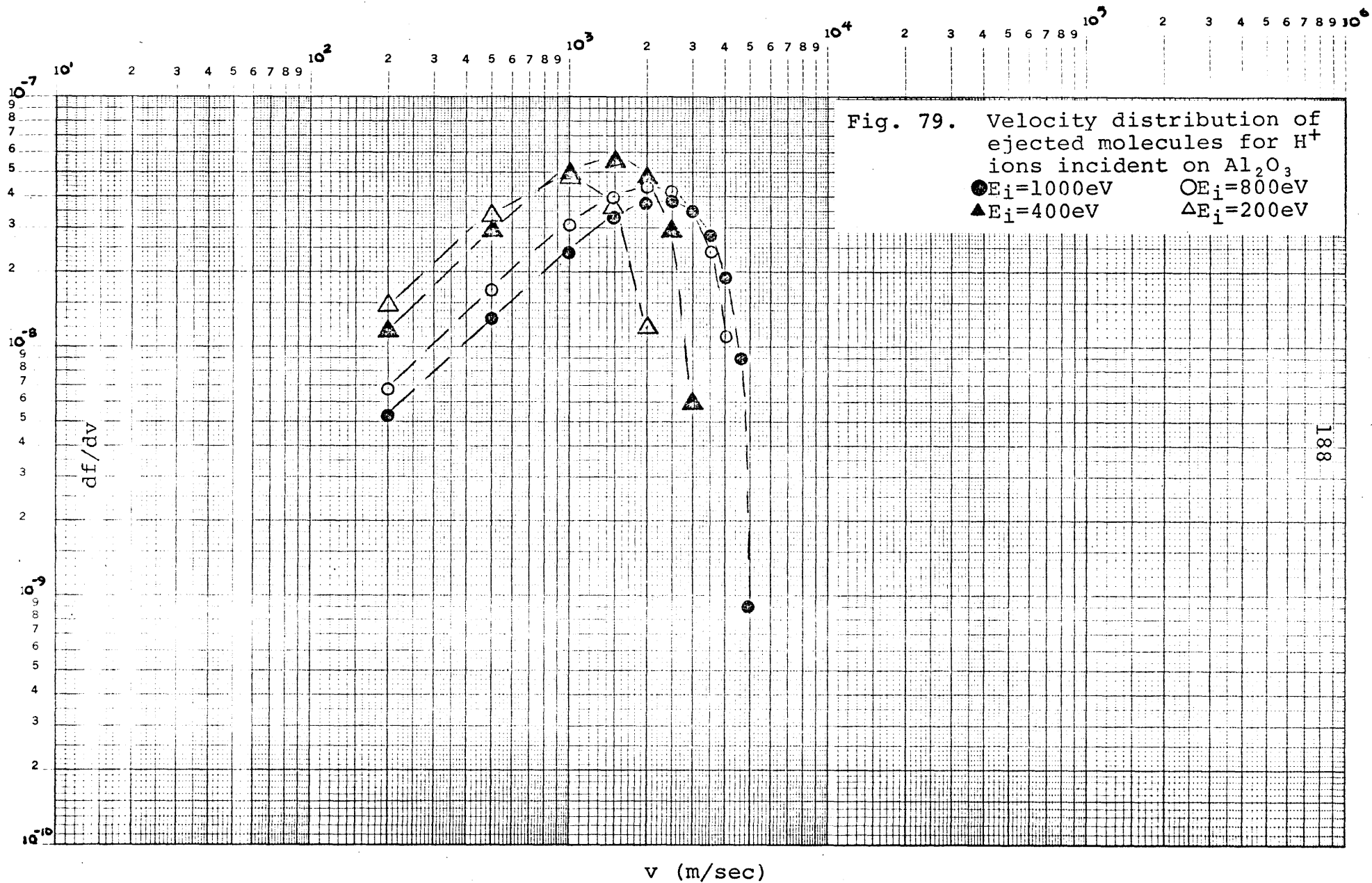
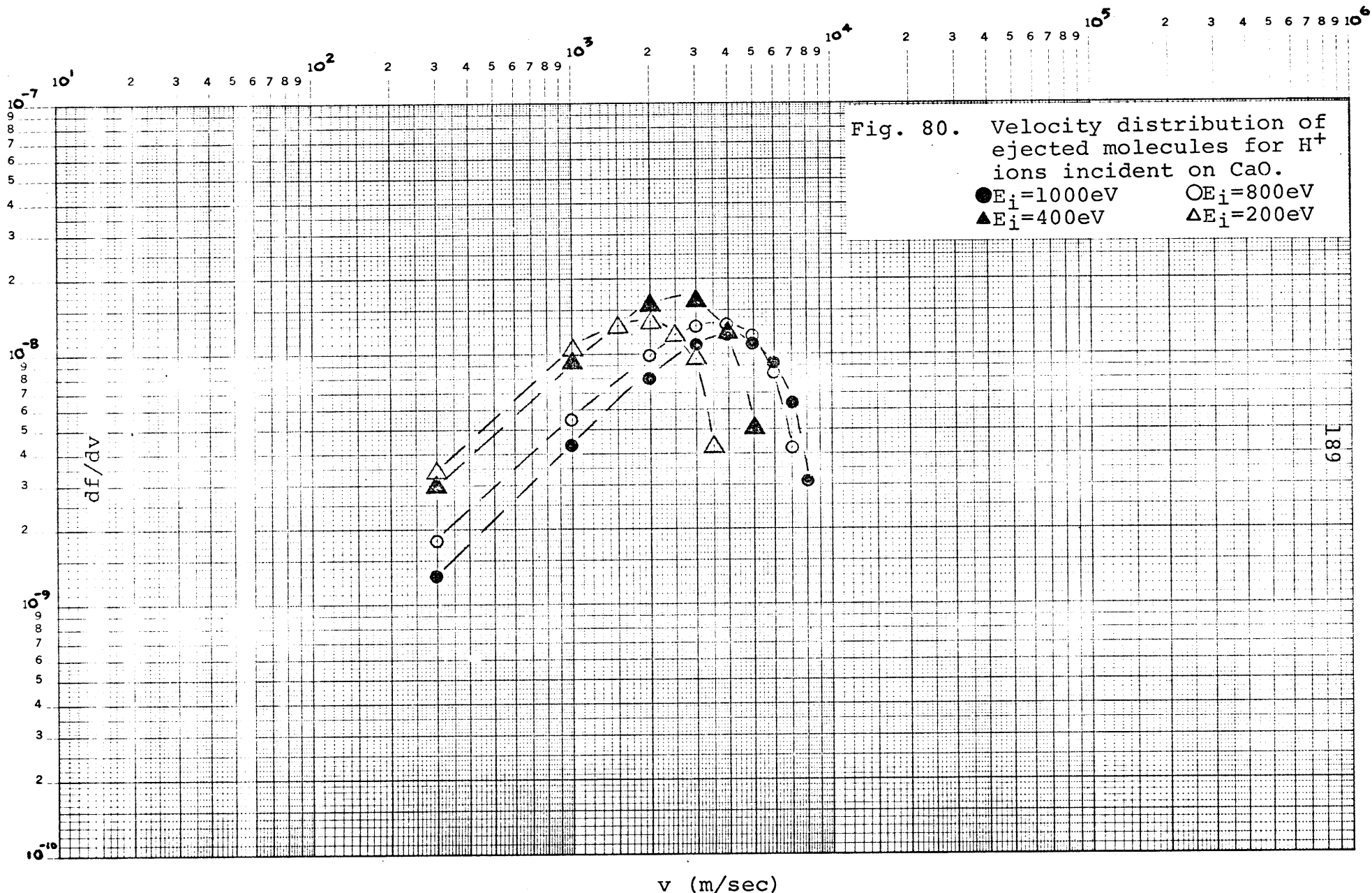


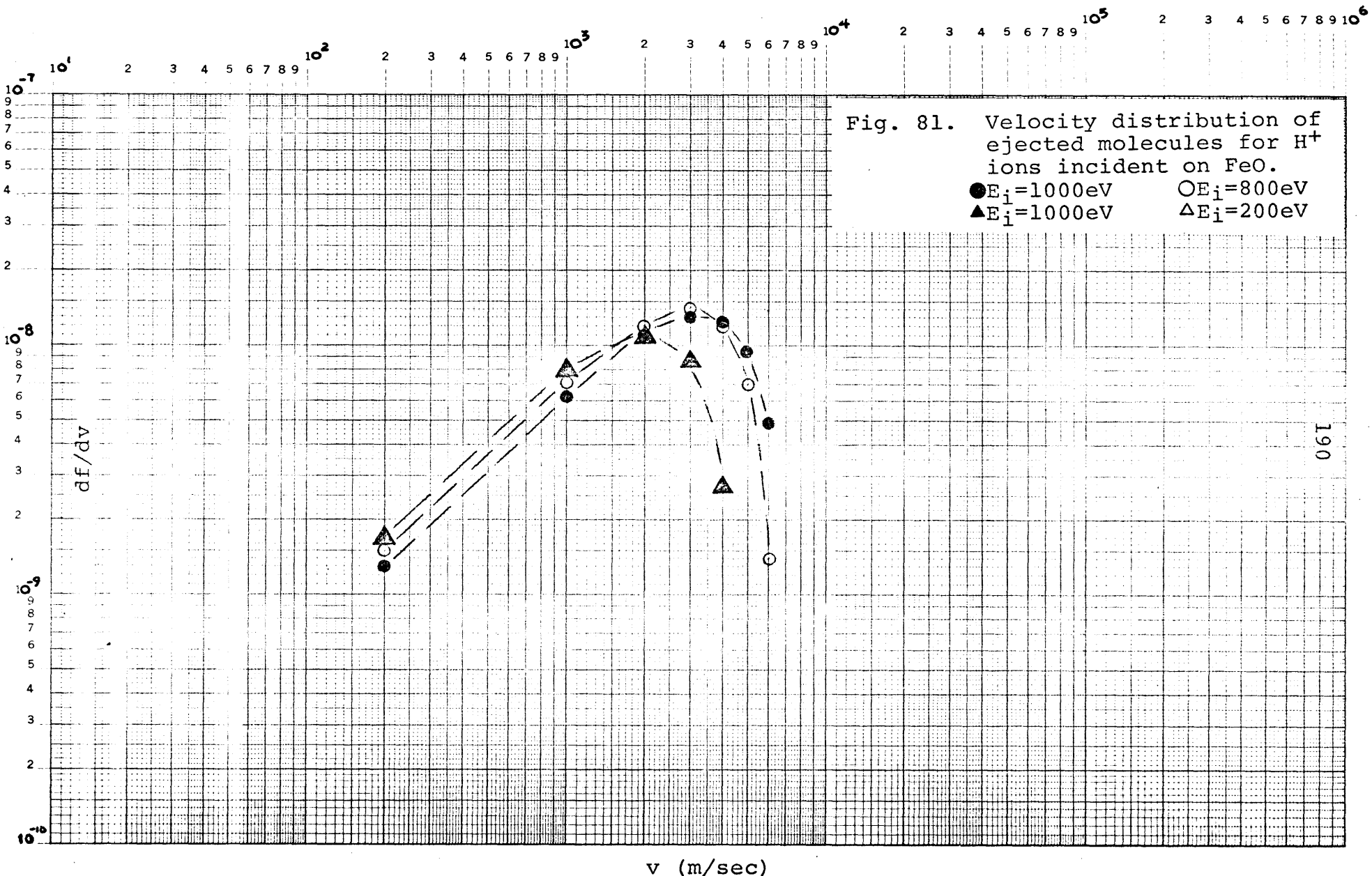
Fig. 78. Variation of the sputtering yield with angle of incidence for H^+ ions on TiO_2 [calculated from Eq.(26)].



187







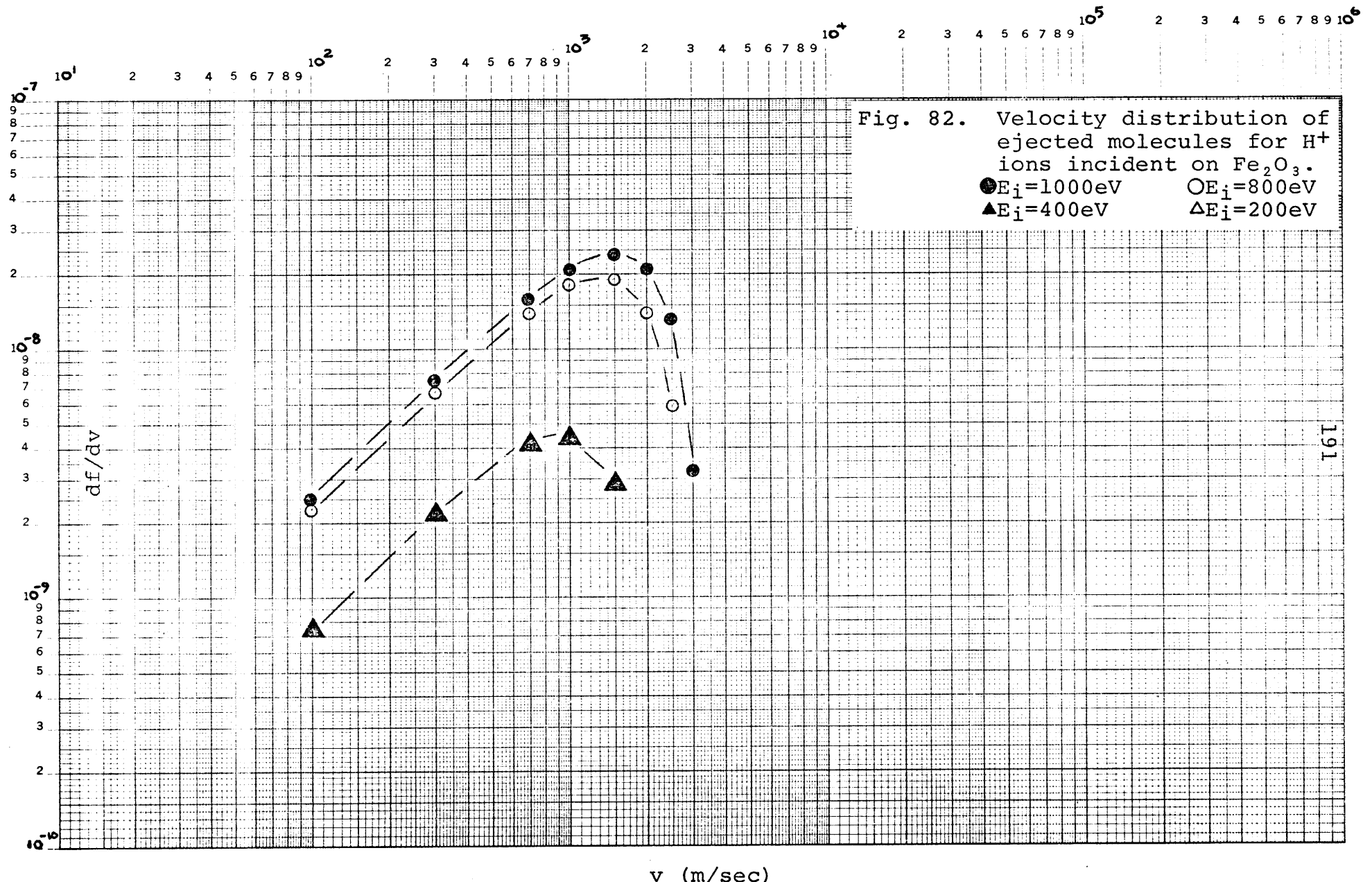


Fig. 82. Velocity distribution of ejected molecules for H^+ ions incident on Fe_2O_3 .

\bullet $E_i = 1000 \text{ eV}$ \circ $E_i = 800 \text{ eV}$
 \blacktriangle $E_i = 400 \text{ eV}$ \triangle $E_i = 200 \text{ eV}$

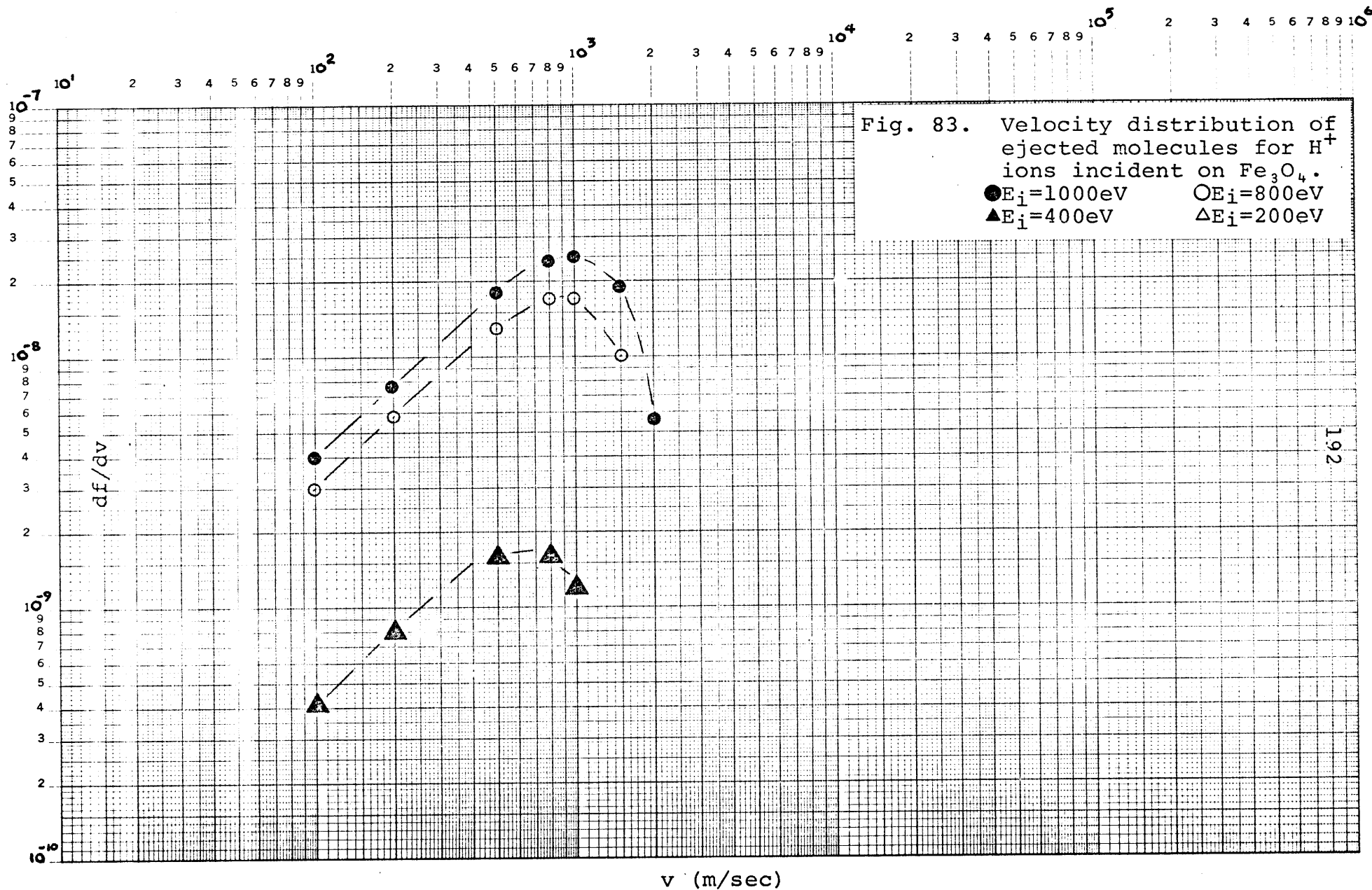


Fig. 83. Velocity distribution of ejected molecules for H^+ ions incident on Fe_3O_4 .

$\bullet E_i = 1000 \text{ eV}$	$\circ E_i = 800 \text{ eV}$
$\blacktriangle E_i = 400 \text{ eV}$	$\triangle E_i = 200 \text{ eV}$

